THE UNIVERSITY OF HULL

AN INVESTIGATION OF ALTERNATING-DIRECTION IMPLICIT FINITE-DIFFERENCE TIME-DOMAIN (ADI-FDTD) METHOD IN NUMERICAL ELECTROMAGNETICS

being a Thesis submitted for the degree of Doctor of Philosophy
at the University of Hull

by

Say Cheoh Ow M.Eng (Hons)

October 2003

ACKNOWLEDGEMENTS

I would like to thank Dr. Sunil Judah for his assistance throughout this research work, my parents for their continuous moral support and Dr. David Stubbs for his patience, support, encouragement, many useful technical discussions and for proof-reading this thesis.

CONTENTS

Acknowledgements ii

Abstract vii

List of symbols viii

CHAPTER 1 - INTRODUCTION

1.1 Introduction 1

1.2 FDTD Method 2

1.3 Finite-difference approximation to derivatives 3

1.3.1 Explicit method 4

1.3.2 Implicit method 4

1.4 Alternating-direction implicit procedure 5

CHAPTER 2 - FINITE-DIFFERENCE TIME-DOMAIN METHOD

2.1 Introduction 7

2.2 Maxwell's equations in three dimensions 7

2.3 FDTD algorithm 8

2.4 Finite difference expression of Maxwell's equations in three dimensions 9

2.5 Divergence of FDTD algorithm 10

2.6 Numerical stability of the three-dimensional FDTD algorithm 11

2.7 Numerical dispersion of the three-dimensional FDTD algorithm 15

2.8 Boundary conditions 16

2.8.1 1st order Mur boundary condition 17

2.9 Conductor boundaries 19

2.10 Dielectric boundaries 19

2.11 Excitation 20

2.12 Simulation of a line-fed rectangular microstrip patch 21

2.13 Extraction of voltage and current from the FDTD mesh 23
2.14 Extraction of S_{11} 24
2.14.1 Two runs 24
2.14.2 Single run 24
2.15 Extraction of Zin 26
2.16 Results 28
2.17 Conclusion 30

CHAPTER 3 - ALTERNATING-DIRECTION IMPLICIT FINITE-DIFFERENCE TIME-DOMAIN METHOD

3.1 Introduction 31
3.2 Three-dimensional ADI-FDTD algorithm 31
3.3 Physical interpretation of three-dimensional ADI-FDTD method 35
3.4 Divergence of ADI-FDTD algorithm 36
3.5 Numerical stability 36
3.5.1 2-dimensional ADI-FDTD 36
3.5.2 3-dimensional ADI-FDTD 39
3.6 Numerical dispersion 40
3.6.1 2-dimensional ADI-FDTD 40
3.7 Implementation of 1st order Mur absorbing boundary condition 42
3.7.1 Boundary condition within the tri-diagonal matrix 42
3.7.2 Boundary condition outside the tri-diagonal matrix 44
3.8 Simulated results 45
3.8.1 Three-dimensional cavity 46
3.8.2 Three-dimensional cavity with inhomogeneous media 48
3.8.3 Simulation of a line-fed rectangular microstrip patch 49
3.8.4 Three-dimensional cavity with a transmission line 50
3.9 Conclusion 51

CHAPTER 4 - MODIFIED ALTERNATING-DIRECTION IMPLICIT METHOD

4.1 Introduction 52

4.2 Three-dimensional modified ADI-FDTD algorithm 52

4.3 Weighting factor in the modified ADI-FDTD algorithm 55

4.4 Divergence of modified ADI-FDTD algorithm 56

4.5 Numerical stability 56

4.5.1 2-dimensional modified ADI-FDTD 56

4.5.2 3-dimensional modified ADI-FDTD 59

4.6 Numerical dispersion 61

4.6.1 2-dimensional modified ADI-FDTD 61

4.7 Simulated results 63

4.8 Relationship between attenuation and weighting factor *f* 64

4.9 Conclusion 66

CHAPTER 5 - SIMULATING COPPER LAYER IN ALTERNATING-DIRECTION IMPLICIT METHOD

5.1 Introduction 67

5.2 Three-dimensional ADI-FDTD algorithm with electric conductivity term . . . 67

5.3 Simulated results 71

5.3.1 Simulation of a line-fed rectangular microstrip patch 71

5.3.1.1 Transient response 72

5.3.1.2 Frequency response 74

5.3.1.3 Accuracy vs stability factor 77

5.3.1.4 Run-time comparison 77

5.3.1.5 Input impedance 78

5.3.2 Simulation of a line-fed rectangular microstrip patch with three parasitic patches . 81

5.3.2.1 Transient response 81

5.3.2.2 Frequency response 83

5.3.2.3 Input impedance 85

5.4 Conclusion 86

CHAPTER 6 - CONCLUSION AND FURTHER WORK

6.1 Overall Conclusion 87

6.2 Further Work 88

6.2.1 Cylindrical coordinate system 88

6.2.2 Microstrips with slots and notches 88

6.2.3 Graded mesh 89

REFERENCES

[1] Papers 90

[2] Books 94

APPENDICES

A1 2^{nd} order accuracy of central difference approximation 95

B1 Tri-diagonal matrix equations for procedures 1 and 2 in ADI-FDTD method . . . 96

B2 Tri-diagonal matrix equations for procedures 1 and 2 in modified ADI-FDTD method 98

B3 Tri-diagonal matrix equations for procedures 1 and 2 in ADI-FDTD method with electric conductivity term 100

C1 Graphical illustration of implicit/explicit ADI-FDTD method 102

ABSTRACT

In this thesis, the alternating-direction implicit method (ADI) is investigated in conjunction with the finite-difference time-domain method (FDTD) to allow crossing of the Courant-Friedrich-Levy (CFL) stability criterion while maintaining stability in the FDTD algorithm. The main reason for this is to be able to use a larger numerical time step than that governed by the CFL criterion. The desired effect is a significant reduction in numerical run-times. Although the ADI-FDTD method has been used in the literature, most analysis and application have been performed on simple three-dimensional cavities.

This work makes original contribution in two aspects. Firstly, a new modified alternating-direction implicit method for a three-dimensional FDTD algorithm has been successfully developed and implemented in this research. This new method allows correct modelling of a realistic physical structure such as a microstrip patch with the ADI scheme without causing instability even when the CFL criterion is not observed. However, due to the inherent property of this modified ADI-FDTD method, a decreasing reflection coefficient is observed using this scheme.

The second and more important contribution this research makes in the field of numerical electromagnetics is the development of a new method of simulating realistic complex structures such as geometries comprising copper patch antennas on a dielectric substrate. With this new method, for the first time, the ADI-FDTD algorithm remains stable while still in violation of the CFL criterion, even when complex structures are being modelled.

However, there is a trade-off between accuracy and computational speed in ADI-FDTD and modified ADI-FDTD methods. The larger the numerical time step, the shorter is the simulation run-time but an increase in numerical time step causes a degradation in accuracy of numerical results. Comparison between speed and accuracy is shown in this thesis and it has to be mentioned here that these values are very much dependent on the structure being modelled.

LIST OF SYMBOLS

k	propagating wave wavenumber
G	scalar Green's function
δ	dirac delta function
r	radial distance
Δt	time step in numerical algorithm
Δx	numerical space step in x-direction
Δy	numerical space step in y-direction
Δz	numerical space step in z-direction
v	wave velocity
n	nth time step
i	ith space step in x-direction
j	jth space step in y-direction
k	kth space step in z-direction
$\vec{E}$	electric field vector in volts per metre
$\vec{D}$	electric flux density in coulombs per square metre
$\vec{H}$	magnetic field vector in amperes per metre
$\vec{B}$	magnetic flux density vector in webers per square metre
$\vec{J}_e$	electric conduction current density in amperes per square metre
$\vec{J}_m$	magnetic conduction current density in volts per square metre
ρ	magnetic resistivity in ohms per metre
σ	electric conductivity in siemens per metre
μ	magnetic permeability in Henrys per metre
ε	electric permittivity in Farads per metre
Λ_t	time eigenvalues due to temporal differentiation
Λ_s	space eigenvalues due to spatial differentiation
j	complex number $\sqrt{-1}$
$\tilde{k}_x$	numerical wavenumber in x-direction
$\tilde{k}_y$	numerical wavenumber in y-direction
$\tilde{k}_z$	numerical wavenumber in z-direction
c	speed of light in metre per second
β	phase constant of propagating wave in radians per metre
ω	angular frequency in radians per second
Γ	reflection coefficient
γ	propagation constant of propagating wave

CHAPTER 1
INTRODUCTION

1.1 Introduction

Frequency domain analytical methods have been extensively used [1.1],[2.1] to solve complicated microstrip circuits. Generally, when using this approach, the thickness of the microstrip substrate is assumed to be much thinner than the shortest wavelength of interest. As a result, there is no field variation throughout the thickness of the substrate and this renders it a two-dimensional electromagnetic problem. In such a case the microstrip patch is modelled by applying a magnetic wall around it. The fringing fields, however, have to be accounted for by using empirically obtained effective patch dimensions and effective permittivities. This is also known as the cavity model. Despite these disadvantages, the cavity model is simple to implement and gives great physical insight to the circuit operation. The scalar Green's function is used to analytically solve this two-dimensional electromagnetic problem with perfect wall boundaries. In general, the scalar Green's function solves the following scalar Helmholtz equation :

$$\nabla^2 G + k^2 G = \delta(r - r_o) \tag{1.1}$$

where k is the wavenumber in the medium and the excitation is in the form of a dirac delta function at $r = r_o$. The Helmholtz equation (1.1) is solved by first expanding the solution in terms of eigenfunctions of the homogeneous Helmholtz equation for the appropriate coordinate system with the application of perfect boundary conditions. By applying the method of separable variables, an exact solution to the differential equation may be found. The solution is generally in the form of a double series Green's function for a two-dimensional problem. This method has been widely used to analyse various patch circuits [2.1]. This double series Green's function was successfully reduced to a single series summation [1.1] by applying the reduced operator method as described in [2.2]. However, this type of solution is restricted to only modelling thin substrates.

To model thick substrates and account for any fringing field effects, a full-wave electromagnetic solution is required. There are generally two categories of numerical methods for solving electromagnetic scattering problems, namely, frequency domain methods and time domain methods. Frequency domain methods include the finite-element method and the method of moments [2.3] while the transmission line matrix (TLM) [1.2] - [1.3] and the finite-difference time-domain (FDTD) [1.4] are time domain methods. Full-wave frequency domain methods have been used to model various problems, especially those with few selected frequency points of interest. This is because, in such methods, the data for the whole frequency range are calculated one frequency at a time. However, for wideband solutions, time domain methods are generally preferable as a whole spectrum of frequency response can be obtained from a single simulation run. By exciting the time domain model with a broad-band Gaussian pulse, for example,

and then applying the Fourier transform on the time-domain results, one can get the entire frequency range of interest, all in a single simulation run.

The FDTD method has been extensively used to solve two- and three-dimensional scattering problems [1.5] - [1.7]. The author has chosen the FDTD method over other time-domain methods because its implementation is straight forward, directly derived from Maxwell's equations.

1.2 FDTD Method

The finite-difference time-domain or commonly known as the FDTD method was first proposed by K.S.Yee in 1966 [1.4]. The FDTD method is formulated by discretizing the differential form of Maxwell's two curl equations over a finite volume and approximating the derivatives with centred difference approximation to obtain a second order accuracy in time and space. Appropriate boundary conditions are imposed on the source point, conductors and computational boundaries to model the real structure. Indeed, FDTD is relatively simple, flexible and easy to implement. However, over the years, FDTD applications have been restricted to solving electrically small structures. To obtain accurate results for large electrical structures, large amounts of CPU time and memory resources are required. These expensive computer resources come from two modelling constraints.

1. The spatial step, Δh, must be at least 10 to 20 times smaller than the smallest wavelength of interest for a negligible dispersion error and
2. The time step used in the algorithm must satisfy the Courant-Friedrich-Levy (CFL) stability condition stated below (and derived in Chapter 2) :

$$\Delta t \leq \frac{1}{v\sqrt{\frac{1}{\Delta x^2} + \frac{1}{\Delta y^2} + \frac{1}{\Delta z^2}}} \tag{1.2}$$

where Δx, Δy and Δz are the spatial steps, Δt the time step and v the maximum wave velocity in the media being modelled. The implications of the above two constraints are considerable.

A physical understanding of the CFL stability constraint (1.2) will be explained below with the help of Fig. 1.1 which shows an elemental three-dimensional building block in the FDTD mesh. Assume that the elemental block is a cube, that is $\Delta x = \Delta y = \Delta z = \Delta h$. In numerical FDTD, for example, when modelling a wave speed, v, the numerical wave takes 3 Δt to propagate diagonally in the cube; that is, the wave takes 3 time steps to travel a distance of $\sqrt{3}\ \Delta h$. The numerical wave speed is governed by the dielectric constant used in the simulation. Therefore, if a bigger time step is used to model wave propagating at the same speed, v, the wave will seem to have travelled further than it actually has. This gives rise to errant simulation results. Since FDTD is a time-domain method with each time-domain results feeding back to the next time-domain algorithm, this error will accumulate and eventually grow as time progresses resulting in an unstable system.

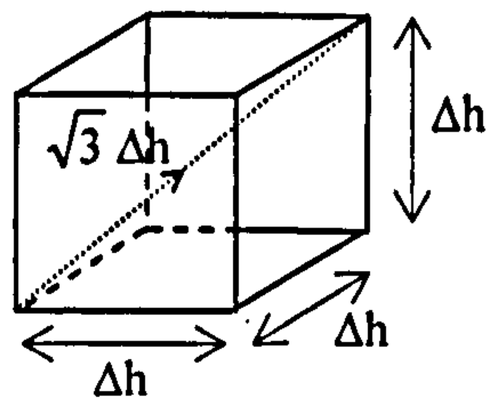

Fig.1.1 : Elemental cube in FDTD mesh

Another modelling constraint is that not only must the spatial incremental step be small relative to the smallest wavelength of interest, but, in order to model an electrically large structure which contains discontinuities accurately, the spatial step must also be made fine near the discontinuities. The constraint of equation (1.2) above means that the time step has to be small near the discontinuities in order to maintain stability in the FDTD scheme. The smaller the time step, the longer is the simulation run-time because more numerical iterations are required to represent a finite amount of real physical time. This can lead to a prohibitively long simulation run-time.

One way to model an electrically large structure with fine discontinuities without incurring intensive use of memory storage is to sub-divide the computational domain into regions, each with a different mesh size; a finer mesh size is used for regions with high irregularity and a larger mesh size for the rest of the domain [1.8] - [1.12]. The finer mesh is obtained by further meshing the larger mesh. This process is referred to as subgridding. In such a situation, to maintain stability as defined by equation (1.2), either the time step corresponding to the smallest mesh size is used for the whole computational domain, or the time steps are set separately for each mesh region. For a large object with a highly irregular structure, the first method can be computationally expensive in terms of simulation run-time. Using the second method, the mesh sizes have to be such that the time steps are integer multiples of one another. Furthermore, space and time interpolations at the interfaces of the mesh may be required for accurate simulation. Also, numerical dispersion will vary throughout the different mesh sizes. All in all, this makes the implementation of FDTD to mesh geometries that vary across a volume, a difficult and time consuming task both in implementation and execution. Despite the saving in computer storage, the overall simulation run-time will still be long due to the run-time necessary over regions with fine mesh size.

The key to modelling electrically large structures with fine discontinuities without incurring a huge computational burden in terms of simulation run-time is if the CFL stability criterion can be violated without causing instability thereby allowing the use of bigger time steps in the simulation. This is realized when the alternating-direction implicit (ADI) method is applied on the FDTD algorithm.

1.3 Finite-difference approximation to derivatives

Consider a two-dimensional parabolic equation (1.3) below :

$$\frac{\partial u}{\partial t} = \frac{\partial^2 u}{\partial x^2} + \frac{\partial^2 u}{\partial y^2} \qquad (1.3)$$

1.3.1 Explicit method

One finite-difference approximation to (1.3) is :

$$\frac{u_{i,j}^{n+1} - u_{i,j}^{n}}{\Delta t} = \frac{u_{i+1,j}^{n} - 2u_{i,j}^{n} + u_{i-1,j}^{n}}{\Delta x^2} + \frac{u_{i,j+1}^{n} - 2u_{i,j}^{n} + u_{i,j-1}^{n}}{\Delta y^2} \qquad (1.4a)$$

where $x = i\Delta x$, $y = j\Delta y$ and $t = n\Delta t$. Equation (1.4a) can be written as :

$$u_{i,j}^{n+1} = u_{i,j}^{n} + \Delta t\left(\frac{u_{i+1,j}^{n} - 2u_{i,j}^{n} + u_{i-1,j}^{n}}{\Delta x^2} + \frac{u_{i,j+1}^{n} - 2u_{i,j}^{n} + u_{i,j-1}^{n}}{\Delta y^2}\right) \qquad (1.4b)$$

and (1.4b) gives the unknown values u at time step (n+1)Δt in terms of known values u at time step nΔt. This is known as an explicit method. This explicit method is simple but can be computationally intensive because the condition for its validity [2.4], shown below, limits the time step, Δt that can be used in order to maintain stability in the system.

$$\Delta t \leq \frac{1}{2\left(\frac{1}{\Delta x^2} + \frac{1}{\Delta y^2}\right)} \qquad (1.4c)$$

1.3.2 Implicit method

Another possible finite-difference approximation to (1.3) is :

$$\begin{aligned}\frac{u_{i,j}^{n+1} - u_{i,j}^{n}}{\Delta t} = {} & \frac{1}{2}\left(\frac{u_{i+1,j}^{n+1} - 2u_{i,j}^{n+1} + u_{i-1,j}^{n+1}}{\Delta x^2} + \frac{u_{i+1,j}^{n} - 2u_{i,j}^{n} + u_{i-1,j}^{n}}{\Delta x^2}\right) \\ & + \frac{1}{2}\left(\frac{u_{i,j+1}^{n+1} - 2u_{i,j}^{n+1} + u_{i,j-1}^{n+1}}{\Delta y^2} + \frac{u_{i,j+1}^{n} - 2u_{i,j}^{n} + u_{i,j-1}^{n}}{\Delta y^2}\right)\end{aligned} \qquad (1.5)$$

The unknown values u at time step (n+1)Δt are given in terms of the known values u at time step nΔt and also the unknown values u at time step (n+1)Δt. The unknown values u at time step (n+1)Δt are then calculated by solving (M-1)(N-1) simultaneous equations comprising the known values u at time step nΔt where M is the number of Δx space steps and N the number of Δy space steps. For large values of M and N, the simultaneous equations will be solved iteratively. This method is known as the Crank-Nicolson implicit method. This implicit method is valid for all values of Δx, Δy and Δt, that is, there is no constraint on the time step used. But it takes considerably more computing power than the explicit method as the simultaneous equations may need to be solved iteratively and they involve finding the inverse of the matrices containing the equations.

1.4 Alternating-direction implicit procedure

One crucial point about the FDTD method is that it is a fully explicit method of solving differential equations. This means that the iterative field values are calculated from previously known values. As mentioned above this method is attractive as it is simple to implement but it is limited to some extent by the CFL stability criterion that limits the time step that can be used in the algorithm. Implicit methods, on the other hand, have superior stability properties [2.4] where the time step is not limited to any size. Unfortunately, an implicit method in two dimensions requires at each time step, the solution of large sets of simultaneous equations, which is not always easy to accomplish directly. Morever, when applied in conjunction with the three-dimensional FDTD algorithm, this method results in three three-dimensional matrices which have to be solved simultaneously.

The most efficient method to date that incorporates the implicit method is the one first proposed by Peaceman and Rachford in 1955 [1.13]. This method requires the line-by-line solution of small sets of simultaneous equations that can be solved by a direct, non-iterative method. This is called an alternating-direction implicit (ADI) procedure. Peaceman and Rachford tested the ADI procedure by using it to solve the heat flow equation with boundary conditions in two space dimensions and compared the solutions with known formal solution. The two solutions showed good agreement. The ADI method was also tested by Peaceman and Rachford on steady-state problems in two dimensions by solving Laplace's equation in a square. The stability of the ADI scheme was also discussed and analysed in their paper. Part of their work in the ADI method used to find solutions of an unsteady-state heat-flow in a square is described below.

$$\frac{u_{i,j}^{n+1} - u_{i,j}^{n}}{\Delta t} = \frac{u_{i+1,j}^{n+1} - 2u_{i,j}^{n+1} + u_{i-1,j}^{n+1}}{\Delta x^2} + \frac{u_{i,j+1}^{n} - 2u_{i,j}^{n} + u_{i,j-1}^{n}}{\Delta y^2} \tag{1.6a}$$

In [1.13], the second order derivative term from (1.3), $\partial^2 u/\partial x^2$ is replaced by a second order difference term evaluated in terms of the unknown values of u, that is implicit in the x-direction, while the other derivative, $\partial^2 u/\partial y^2$ is replaced by a second order difference term evaluated in terms of known values of u. This results in sets of simultaneous equations that can be solved easily without iteration. If the procedure is then repeated for a second time step of equal size to the first time step and the difference equations are set implicit in the y-direction, as shown in (1.6b), then Peaceman and Rachford showed that the overall procedure for the two time steps would be stable for any size time step. This means that the time step used is no longer restricted by the stability requirement of the system.

$$\frac{u_{i,j}^{n+2} - u_{i,j}^{n+1}}{\Delta t} = \frac{u_{i+1,j}^{n+1} - 2u_{i,j}^{n+1} + u_{i-1,j}^{n+1}}{\Delta x^2} + \frac{u_{i,j+1}^{n+2} - 2u_{i,j}^{n+2} + u_{i,j-1}^{n+2}}{\Delta y^2} \tag{1.6b}$$

Since its introduction, the ADI procedure has been broadly used to solve diffusion problems. This method was first adapted to solve wave problems in FDTD mesh by T.Namiki [1.14]. With the application of the alternating-direction implicit procedure on the FDTD method, the well-known CFL stability criterion stated in equation (1.2) can now be violated without causing instability. The physical understanding of how violation of the CFL criterion will lead to instability of the FDTD system was discussed earlier in

section 1.2 and illustrated using Fig 1.1. This means that potentially bigger time steps can be used in the simulation thereby reducing the overall simulation time.

In this thesis, the ADI-FDTD method is investigated and a new modified ADI-FDTD method is proposed and discussed. The detailed implementation of the ADI-FDTD method with respect to the structure being modelled is also presented in this thesis. Numerical simulations of a simple line-fed rectangular microstrip patch are used to verify both the ADI-FDTD and the newly proposed modified ADI-FDTD methods. A bigger patch with three parasitic patches is also simulated to verify the application of ADI-FDTD method on an electrically large object. Where possible, the simulated results are compared with results from published literature.

This thesis is organized as follows.

Chapter 2 : Discusses the theory behind the finite-difference time-domain method, the implementation procedures, and compares the simulated results obtained in this research work with those in the published literature [1.5]. A new, more efficient method of extracting the reflection coefficient from the simulated data is also presented.

Chapter 3 : Presents the theory of the alternating-direction implicit method applied on the FDTD algorithm and illustrates the physical interpretation of the ADI-FDTD method. With the help of simulated data, the problems encountered when a line-fed rectangular microstrip patch is simulated, are discussed. This chapter also explains the implementation of the absorbing boundary condition at the boundary of the computational domain which is critical for accurate and correct modelling of the structure.

Chapter 4 : Proposes a new modified ADI-FDTD method to surmount the problem of modelling the microstrip patch in chapter 3 using perfect electric wall boundary on the copper patch. The limitation of this new method is also discussed.

Chapter 5 : Shows that a different technique of implementing a boundary condition helps eliminate the problem encountered in chapter 3. Simulated results for more complex structures are also shown.

Chapter 6 : Concludes the research undertaken by the author and suggests some further work in this field of research.

CHAPTER 2
FINITE-DIFFERENCE TIME-DOMAIN METHOD

2.1 Introduction

The algorithm of finite-difference time-domain field analysis was first introduced by Kane Yee in 1966 [1.4] and has been widely used to solve electromagnetic scattering problems.

2.2 Maxwell's equations in three dimensions

In a region of space, the time dependent Maxwell's equations are given in the differential form by [2.5] :

Faraday's Law :

$$\frac{\partial \vec{B}}{\partial t} = -\nabla \times \vec{E} - \vec{J}_m \tag{2.1}$$

Ampere's Law :

$$\frac{\partial \vec{D}}{\partial t} = \nabla \times \vec{H} - \vec{J}_e \tag{2.2}$$

And the constituent relations are :

$$\nabla \cdot \vec{D} = 0 \tag{2.3}$$

$$\nabla \cdot \vec{B} = 0 \tag{2.4}$$

In linear, isotropic non-dispersive materials,

$$\vec{B} = \mu \vec{H} \tag{2.5}$$

and

$$\vec{D} = \varepsilon \vec{E} \tag{2.6}$$

In order to account for the magnetic loss in the system, the magnetic current density is given by :

$$\vec{J}_m = \rho \vec{H} \tag{2.7}$$

and similarly the electric current density is :

$$\vec{J}_e = \sigma \vec{E} \tag{2.8}$$

$\vec{E}$ is the electric field vector in volts per metre, $\vec{D}$ is the electric flux density vector in coulombs per square metre, $\vec{H}$ is the magnetic field vector in amperes per metre, $\vec{B}$ is the magnetic flux density vector in webers per square metre, $\vec{J}_e$ is the electric conduction current density in amperes per square metre, $\vec{J}_m$ is the equivalent magnetic conduction current density in volts per square metre, ρ is an equivalent magnetic resistivity in ohms per metre and σ is the electric conductivity in siemens per metre.

Combining the assumptions of (2.5) to (2.8) and substituting into Maxwell's curl equations (2.1) and (2.2), we obtain :

$$\frac{\partial \vec{H}}{\partial t} = -\frac{1}{\mu}\nabla \times \vec{E} - \frac{\rho}{\mu}\vec{H} \tag{2.9}$$

$$\frac{\partial \vec{E}}{\partial t} = \frac{1}{\varepsilon}\nabla \times \vec{H} - \frac{\sigma}{\varepsilon}\vec{E} \tag{2.10}$$

which govern the propagation of both electric and magnetic fields in any structure.

Writing out the vector components of the curl operator in (2.10) and (2.9) yields the following six coupled equations equivalent to Maxwell's curl equations in a three-dimensional Cartesian coordinate system.

$$\frac{\partial E_x}{\partial t} = \frac{1}{\varepsilon}\left(\frac{\partial H_z}{\partial y} - \frac{\partial H_y}{\partial z} - \sigma E_x\right) \tag{2.11a}$$

$$\frac{\partial E_y}{\partial t} = \frac{1}{\varepsilon}\left(\frac{\partial H_x}{\partial z} - \frac{\partial H_z}{\partial x} - \sigma E_y\right) \tag{2.11b}$$

$$\frac{\partial E_z}{\partial t} = \frac{1}{\varepsilon}\left(\frac{\partial H_y}{\partial x} - \frac{\partial H_x}{\partial y} - \sigma E_z\right) \tag{2.11c}$$

$$\frac{\partial H_x}{\partial t} = -\frac{1}{\mu}\left(\frac{\partial E_z}{\partial y} - \frac{\partial E_y}{\partial z} + \rho H_x\right) \tag{2.12a}$$

$$\frac{\partial H_y}{\partial t} = -\frac{1}{\mu}\left(\frac{\partial E_x}{\partial z} - \frac{\partial E_z}{\partial x} + \rho H_y\right) \tag{2.12b}$$

$$\frac{\partial H_z}{\partial t} = -\frac{1}{\mu}\left(\frac{\partial E_y}{\partial x} - \frac{\partial E_x}{\partial y} + \rho H_z\right) \tag{2.12c}$$

This system of six coupled partial differential equations of (2.11) and (2.12) forms the basis of the finite-difference time-domain (FDTD) numerical algorithm for electromagnetic wave interactions.

2.3 FDTD algorithm

The FDTD algorithm solves for both electric and magnetic fields in time and space by solving the six coupled Maxwell's curl equations (2.11) – (2.12). A physical model of the fields in a Cartesian grid is shown in Fig. 2.1. For programming considerations, the numbering of the spatial location of E and $\vec{H}$ fields in Fig. 2.1 differ from that in the original Yee's cell.

As illustrated in Fig. 2.1, the algorithm centres its $\vec{E}$ and $\vec{H}$ components in three-dimensional space so that every $\vec{E}$ component is surrounded by four $\vec{H}$ components and vice versa. Every component of $\vec{H}$ can now be obtained by the loop integral of $\vec{E}$ using the four surrounding $\vec{E}$ nodal values according to Maxwell's curl equation of $\vec{E}$. A similar condition holds for $\vec{H}$.

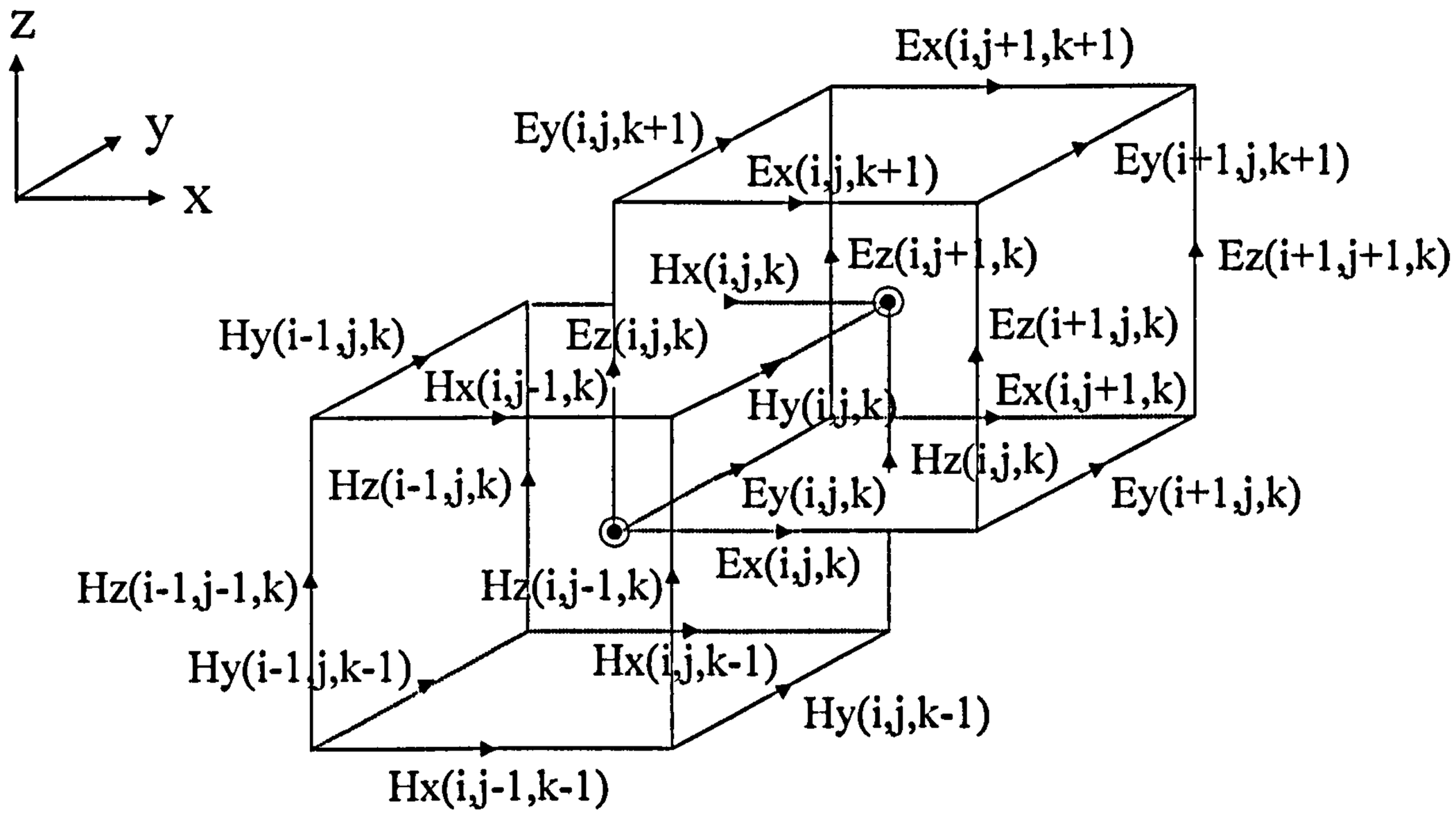

Fig. 2.1 : Yee's staggered cell

We note that in the FDTD algorithm, the $\vec{E}$ and $\vec{H}$ nodes are disjointed by half a space step. In addition, calculation of $\vec{E}$ and $\vec{H}$ fields are also disjointed by half a time step. This means that the $\vec{E}$ and $\vec{H}$ fields are calculated at alternate half time steps. For this reason, this algorithm is called the leapfrog method. The leapfrog time-stepping process is fully explicit; that is, the current field values are calculated using previously stored field values. As a consequence it is not necessary to solve sets of simultaneous equations by involving matrix inversions.

It is worth noting that continuity of the tangential $\vec{E}$ and $\vec{H}$ is automatically maintained across an interface of dissimilar materials if the interface is parallel to one of the grid coordinate axes. Change in materials is specified using the material permittivity and permeability. These are defined in the FDTD equations.

2.4 Finite difference expression of Maxwell's equations in three dimensions

Assuming lossless materials, discretizing (2.11) & (2.12) leads to the approximation of Maxwell's curl equations in three-dimensions as follows :

$$E_x^{n+1}(i,j,k) = E_x^n(i,j,k) + \frac{\Delta t}{\varepsilon}\left\{\frac{H_z^{n+1/2}(i,j,k) - H_z^{n+1/2}(i,j-1,k)}{\Delta y} - \frac{H_y^{n+1/2}(i,j,k) - H_y^{n+1/2}(i,j,k-1)}{\Delta z}\right\} \quad (2.13a)$$

$$E_y^{n+1}(i,j,k) = E_y^n(i,j,k) + \frac{\Delta t}{\varepsilon}\left\{\frac{H_x^{n+1/2}(i,j,k) - H_x^{n+1/2}(i,j,k-1)}{\Delta z} - \frac{H_z^{n+1/2}(i,j,k) - H_z^{n+1/2}(i-1,j,k)}{\Delta x}\right\} \quad (2.13b)$$

$$E_z^{n+1}(i,j,k) = E_z^n(i,j,k) + \frac{\Delta t}{\varepsilon}\left\{\frac{H_y^{n+1/2}(i,j,k) - H_y^{n+1/2}(i\text{-}1,j,k)}{\Delta x} - \frac{H_x^{n+1/2}(i,j,k) - H_x^{n+1/2}(i,j\text{-}1,k)}{\Delta y}\right\} \quad (2.13c)$$

$$H_x^{n+1/2}(i,j,k) = H_x^{n-1/2}(i,j,k) - \frac{\Delta t}{\mu}\left\{\frac{E_z^n(i,j+1,k) - E_z^n(i,j,k)}{\Delta y} - \frac{E_y^n(i,j,k+1) - E_y^n(i,j,k)}{\Delta z}\right\} \quad (2.14a)$$

$$H_y^{n+1/2}(i,j,k) = H_y^{n-1/2}(i,j,k) - \frac{\Delta t}{\mu}\left\{\frac{E_x^n(i,j,k+1) - E_x^n(i,j,k)}{\Delta z} - \frac{E_z^n(i+1,j,k) - E_z^n(i,j,k)}{\Delta x}\right\} \quad (2.14b)$$

$$H_z^{n+1/2}(i,j,k) = H_z^{n-1/2}(i,j,k) - \frac{\Delta t}{\mu}\left\{\frac{E_y^n(i+1,j,k) - E_y^n(i,j,k)}{\Delta x} - \frac{E_x^n(i,j+1,k) - E_x^n(i,j,k)}{\Delta y}\right\} \quad (2.14c)$$

where $x = i\Delta x$, $y = j\Delta y$, $z = k\Delta z$ and $t = n\Delta t$.

This FDTD algorithm has second order accuracy in both space and time because the central difference method is applied on both the space and time derivatives [A.1].

2.5 Divergence of FDTD algorithm

While the FDTD algorithm solves for both electric and magnetic fields in time and space using the coupled Maxwell's curl equations, there is no explicit enforcement of the Gauss's Law relations for both the electric and magnetic fields as stated in (2.3) and (2.4) for source free regions. It is important that the Gauss's Law is observed in the FDTD algorithm.

The time derivative of the surface integrals of the electric flux density over all the surfaces of a free-space Yee cell of Fig. 2.1 is given by [2.5] :

$$\begin{aligned}\frac{\partial}{\partial t}\oiint_S \vec{D}\cdot d\hat{S} &= \frac{\varepsilon_0\partial}{\partial t}\left[E_x(i,j,k) - E_x(i-1,j,k)\right]\Delta y\Delta z \\ &+ \frac{\varepsilon_0\partial}{\partial t}\left[E_y(i,j,k) - E_y(i,j-1,k)\right]\Delta x\Delta z \\ &+ \frac{\varepsilon_0\partial}{\partial t}\left[E_z(i,j,k) - E_z(i,j,k-1)\right]\Delta x\Delta y\end{aligned} \quad (2.15)$$

Using the finite difference expressions of the electric field (2.13a) – (2.13c), the electric field time derivatives in (2.15) can be substituted with the magnetic field spatial finite differences in each of the RHS term in (2.15) producing :

$$\frac{\partial}{\partial t}\oiint_S \vec{D}\cdot d\hat{S} = \left\{\left[\frac{H_z(i,j,k) - H_z(i,j-1,k)}{\Delta y} - \frac{H_y(i,j,k) - H_y(i,j,k-1)}{\Delta z}\right] - \left[\frac{H_z(i-1,j,k) - H_z(i-1,j-1,k)}{\Delta y} - \frac{H_y(i-1,j,k) - H_y(i-1,j,k-1)}{\Delta z}\right]\right\}\Delta y\Delta z$$

$$+\left\{\left[\frac{H_x(i,j,k) - H_x(i,j,k-1)}{\Delta z} - \frac{H_z(i,j,k) - H_z(i-1,j,k)}{\Delta x}\right] - \left[\frac{H_x(i,j-1,k) - H_x(i,j-1,k-1)}{\Delta z} - \frac{H_z(i,j-1,k) - H_z(i-1,j-1,k)}{\Delta x}\right]\right\}\Delta x\Delta z$$

$$+\left\{\left[\frac{H_y(i,j,k) - H_y(i-1,j,k)}{\Delta x} - \frac{H_x(i,j,k) - H_x(i,j-1,k)}{\Delta y}\right] - \left[\frac{H_y(i,j,k-1) - H_y(i-1,j,k-1)}{\Delta x} - \frac{H_x(i,j,k-1) - H_x(i,j-1,k-1)}{\Delta y}\right]\right\}\Delta x\Delta y \tag{2.16}$$

for all time steps. The RHS terms of (2.16) cancel each other out. Hence,

$$\frac{\partial}{\partial t}\oiint_S \vec{D}\cdot d\hat{S} = \frac{\partial}{\partial t}\iiint \nabla\cdot\vec{D}\,dV$$

$$= 0$$

$$\Rightarrow \quad \nabla\cdot\vec{D} = 0$$

Therefore, the time derivative of the net electric flux leaving the surfaces of a cubic Yee cell is zero, hence upholding Gauss's Law for the electric field in charge-free space. The same can be shown for time derivative of the net magnetic flux leaving the surfaces of a cubic Yee cell. This shows that the FDTD algorithm is divergence-free in source free regions and *implicitly* enforces Gauss's Law for both electric and magnetic fields in those regions.

2.6 Numerical stability of the three-dimensional FDTD algorithm

Numerical instability is an undesirable possibility with explicit numerical differential equation solvers that can cause the computed results to spuriously increase without limit as time-marching progresses. A standard method to analyse numerical stability was presented by von Neumann and Courant, Friedrich and Levy [the CFL condition, 2.4].

Electromagnetic waves propagating in a finite-difference grid naturally results in the generation of numerical wave modes or Fourier modes. In order to maintain stability in the finite-difference time-domain system, the spectrum of eigenvalues for these modes due to the numerical space differentiation process must be contained within the stable spectrum of eigenvalues determined by the numerical time differentiation process. The magnitude of field growth at every time step, called growth factor, is limited to a maximum value of unity. If the growth factor is greater than unity, the system will be unstable.

Without loss of generality, consider a normalised region of space with $\mu = 1$, $\varepsilon = 1$, $\sigma = 0$, $\rho = 0$ and

c = 1 where c is the normalized wave velocity in a vacuum. We can re-write Maxwell's equations in a more compact form [1.7] as :

$$j\nabla x\vec{V} = \frac{\partial\vec{V}}{\partial t} \tag{2.17}$$

where $\vec{V} = \vec{H} + j\vec{E}$

and $j = \sqrt{-1}$

Unlike compact derivations in most literature, the following derivations for time and space eigenvalues have been expanded and explained in detail by the author where necessary to ease understanding. To analyse the stability of the numerical representation of (2.17), consider the following pair of eigenvalue problems :

$$\left.\frac{\partial}{\partial t}\right|_{numerical}\vec{V} = \Lambda_t\vec{V} \tag{2.18}$$

$$j\nabla|_{numerical}\, x\vec{V} = \Lambda_s\vec{V} \tag{2.19}$$

where Λ_t represents the eigenvalues due to the numerical time differentiation process and Λ_s, the eigenvalues due to the numerical spatial differentiation process.

First, consider the time eigenvalues, from (2.18),

$$\frac{\vec{V}^{n+1/2} - \vec{V}^{n-1/2}}{\Delta t} = \Lambda_t\vec{V}^n \tag{2.20}$$

Now define a constant growth factor for the numerical solution as a function of space point i

$$q_i = \frac{\vec{V}_i^{n+1/2}}{\vec{V}_i^n} = \frac{\vec{V}_i^n}{\vec{V}_i^{n-1/2}} \quad \text{for all n time steps} \tag{2.21}$$

In order to maintain stability in the FDTD algorithm, $|q_i| \le 1$ for all possible spatial modes in the grid and for all points i. Substituting (2.21) into (2.20) yields

$$\frac{q_i\vec{V}^n - \vec{V}^n/q_i}{\Delta t} = \Lambda_t\vec{V}^n$$

or

$$\vec{V}^n\left[q_i^2 - \Lambda_t\Delta t\, q_i - 1\right] = 0$$

$$q_i = \frac{\Lambda_t\Delta t}{2} \pm \sqrt{\left(\frac{\Lambda_t\Delta t}{2}\right)^2 + 1} \tag{2.22}$$

We see that $|q_i| = 1$ if $\frac{\Lambda_i \Delta t}{2}$ is purely imaginary and has a magnitude of 1 which means

$$-j \le \frac{\Lambda_i \Delta t}{2} \le +j$$

or

$$-\frac{2}{\Delta t} \le |\mathrm{Imag}(\Lambda_i)| \le \frac{2}{\Delta t} \tag{2.23}$$

All possible spatial modes must have eigenvalues that are within this stable range to ensure stability of the algorithm. The spatial eigenvalues can be determined by analysing (2.19) as follows.

$$\nabla|_{numerical} \times \vec{V} = \begin{vmatrix} \hat{x} & \hat{y} & \hat{z} \\ \left.\frac{\partial}{\partial x}\right|_{numerical} & \left.\frac{\partial}{\partial y}\right|_{numerical} & \left.\frac{\partial}{\partial z}\right|_{numerical} \\ V_x & V_y & V_z \end{vmatrix} \tag{2.24}$$

At any time step, the instantaneous values of the electric and magnetic fields distributed in FDTD space across the grid can be Fourier-transformed with respect to the grid coordinates to provide a spectrum of sinusoidal modes, resulting in plane wave eigenmodes of the grid. Now let the following specify a typical mode of this spatial frequency spectrum having $\tilde{k}_x, \tilde{k}_y$ and $\tilde{k}_z$ as the x- , y- and z- components of its numerical wavevector respectively.

$$\vec{V} = \vec{V_o}\, e^{j(\tilde{k}_x i \Delta x + \tilde{k}_y j \Delta y + \tilde{k}_z k \Delta z)} \tag{2.25}$$

Then,

$$\left.\frac{\partial \vec{V}}{\partial x}\right|_{numerical} = \frac{\vec{V}(i+1/2, j, k) - \vec{V}(i-1/2, j, k)}{\Delta x}$$

$$= \frac{\vec{V_o}\left[e^{j(\tilde{k}_x (i+1/2)\Delta x + \tilde{k}_y j \Delta y + \tilde{k}_z k \Delta z)} - e^{j(\tilde{k}_x (i-1/2)\Delta x + \tilde{k}_y j \Delta y + \tilde{k}_z k \Delta z)} \right]}{\Delta x}$$

$$= \frac{\vec{V_o}\, e^{j(\tilde{k}_x i \Delta x + \tilde{k}_y j \Delta y + \tilde{k}_z k \Delta z)} \left[e^{j(\tilde{k}_x \Delta x/2)} - e^{-j(\tilde{k}_x \Delta x/2)} \right]}{\Delta x}$$

$$= \vec{V}\left[\frac{j2\sin(\tilde{k}_x \Delta x/2)}{\Delta x} \right] \tag{2.26}$$

Therefore,

$$\left.\frac{\partial}{\partial x}\right|_{numerical} = \frac{j2\sin(\tilde{k}_x \Delta x/2)}{\Delta x} \tag{2.27a}$$

$$\left.\frac{\partial}{\partial y}\right|_{numerical} = \frac{j2\sin(\tilde{k}_y \Delta y/2)}{\Delta y} \tag{2.27b}$$

$$\left.\frac{\partial}{\partial z}\right|_{numerical} = \frac{j2\sin(\tilde{k}_z \Delta z/2)}{\Delta z} \tag{2.27c}$$

Let $X = \dfrac{2\sin\left(\tilde{k}_x \Delta x/2\right)}{\Delta x}$, $Y = \dfrac{2\sin\left(\tilde{k}_y \Delta y/2\right)}{\Delta y}$ and $Z = \dfrac{2\sin\left(\tilde{k}_z \Delta z/2\right)}{\Delta z}$

Then combining (2.19), (2.24) and (2.27) gives,

$$\mathrm{j}\left\{\hat{x}\,\mathrm{j}\left[YV_z - ZV_y\right] - \hat{y}\,\mathrm{j}\left[XV_z - ZV_x\right] + \hat{z}\,\mathrm{j}\left[XV_y - YV_x\right]\right\} = \Lambda_s \vec{V} \tag{2.28}$$

or

$$\begin{bmatrix} 0 & Z & -Y \\ -Z & 0 & X \\ Y & -X & 0 \end{bmatrix}\begin{bmatrix} V_x \\ V_y \\ V_z \end{bmatrix} = \Lambda_s \begin{bmatrix} V_x \\ V_y \\ V_z \end{bmatrix}$$

$$\begin{bmatrix} -\Lambda_s & Z & -Y \\ -Z & -\Lambda_s & X \\ Y & -X & -\Lambda_s \end{bmatrix}\begin{bmatrix} V_x \\ V_y \\ V_z \end{bmatrix} = 0 \tag{2.29}$$

Solving for eigenvalues Λ_s gives

$$\Lambda_s^2 = -\left(X^2 + Y^2 + Z^2\right)$$

Substituting back X, Y and Z gives

$$\Lambda_s^2 = -4\left[\frac{\sin^2\left(\tilde{k}_x \Delta x/2\right)}{\Delta x^2} + \frac{\sin^2\left(\tilde{k}_y \Delta y/2\right)}{\Delta y^2} + \frac{\sin^2\left(\tilde{k}_z \Delta z/2\right)}{\Delta z^2}\right] \tag{2.30}$$

As $-1 \le \sin^2 p \le 1$, for all possible $\tilde{k}_x, \tilde{k}_y$ and $\tilde{k}_z$, we can bound the range of Λ_s:

$$\left|\mathrm{Imag}\left(\Lambda_s\right)\right| \le 2\sqrt{\frac{1}{\Delta x^2} + \frac{1}{\Delta y^2} + \frac{1}{\Delta z^2}} \tag{2.31}$$

To satisfy the stability condition (2.23) for the arbitrary lattice spatial mode, all the eigenvalues in (2.31) must lie within the range specified in (2.23) i.e.

$$2\sqrt{\frac{1}{\Delta x^2} + \frac{1}{\Delta y^2} + \frac{1}{\Delta z^2}} \le \frac{2}{\Delta t} \tag{2.32}$$

and denormalizing (2.32) by the FDTD wave velocity, where $v = 1/\sqrt{\mu\varepsilon}$

$$\Delta t \le \frac{1}{v\sqrt{\dfrac{1}{\Delta x^2} + \dfrac{1}{\Delta y^2} + \dfrac{1}{\Delta z^2}}} \tag{2.33}$$

This is generally known as the CFL (Courant-Friedrich-Levy) stability condition. In an inhomogeneous region of space, it is difficult to determine a spectrum of Λ_s equivalent to (2.31) for all possible lattice

spatial modes. For absolute algorithm stability, (2.33) will be good enough as it represents the worst case choice of time step, Δt. If Δt is selected to be larger than the bound in (2.33), the FDTD numerical algorithm will definitely be unstable. This is true as long as the FDTD algorithm is completely *explicit*. It is the aim of this work to investigate the possibility of using the time-step beyond the constraint of (2.33) while maintaining stability of the system. Chapters 3 and 4 will discuss two different methods employed to achieve this aim.

2.7 Numerical dispersion of the three-dimensional FDTD algorithm

Dispersion is defined as the variation of the propagating wave's wavenumber $k = 2\pi / \lambda$ with angular frequency $\omega = 2\pi f$. The analytical dispersion of physical wave propagation is an inherent property of the medium of propagation and is structure dependent. For example, in a microstrip patch circuit, the effective permittivity changes as a function of frequency. This gives rise to analytical dispersion. The wavenumber of the continuous physical wave, k, is different from $\tilde{k}$ which is the wavenumber of the numerical sinusoidal travelling wave of angular frequency ω that is present in the finite-difference grid. This difference between k, analytical wavenumber, and $\tilde{k}$, numerical wavenumber, gives rise to numerical phase and group velocities that are different from the exact values obtained for physical waves. This difference gives rise to numerical dispersion and consequently an errant simulation result. Whilst analytical dispersion is an inherent characteristic of the microwave structure, numerical dispersion is due to discretization of time and spatial steps in the finite-difference algorithm. The variation of the numerical wave velocity with wave propagation angle due to numerical dispersion is shown in [2.5].

Numerical dispersion can be found by analysing (2.17). Substituting the vector-field travelling-wave expression with time dependence :

$$\vec{V}^{n}(i,j,k) = \vec{V}_o \, e^{j\left(\tilde{k}_x i \Delta x + \tilde{k}_y j \Delta y + \tilde{k}_z k \Delta z - \omega n \Delta t\right)} \tag{2.33}$$

into (2.17) results in :

$$-2\left[\frac{\hat{x}}{\Delta x}\sin\left(\frac{\tilde{k}_x \Delta x}{2}\right) + \frac{\hat{y}}{\Delta y}\sin\left(\frac{\tilde{k}_y \Delta y}{2}\right) + \frac{\hat{z}}{\Delta z}\sin\left(\frac{\tilde{k}_z \Delta z}{2}\right)\right] \times \vec{V}^{n+1/2}(i,j,k) = \frac{\vec{V}^{n+1}(i,j,k) - \vec{V}^{n}(i,j,k)}{\Delta t} \tag{2.34}$$

or

$$-2\left[\frac{\hat{x}}{\Delta x}\sin\left(\frac{\tilde{k}_x \Delta x}{2}\right) + \frac{\hat{y}}{\Delta y}\sin\left(\frac{\tilde{k}_y \Delta y}{2}\right) + \frac{\hat{z}}{\Delta z}\sin\left(\frac{\tilde{k}_z \Delta z}{2}\right)\right] \times \vec{V}^{n} e^{-j\omega\Delta t/2} = \frac{2j\sin(\omega\Delta t/2)}{\Delta t}\vec{V}^{n} e^{-j\omega\Delta t/2} \tag{2.35}$$

Comparing (2.35) with (2.28) and (2.30) and denormalizing it to a non-unity wave velocity v, gives us the general form of the numerical dispersion relation for the full vector-field FDTD algorithm in three dimensions as :

$$\left[\frac{1}{v\Delta t}\sin\left(\frac{\omega\Delta t}{2}\right)\right]^2 = \left[\frac{1}{\Delta x}\sin\left(\frac{\tilde{k}_x\Delta x}{2}\right)\right]^2 + \left[\frac{1}{\Delta y}\sin\left(\frac{\tilde{k}_y\Delta y}{2}\right)\right]^2 + \left[\frac{1}{\Delta z}\sin\left(\frac{\tilde{k}_z\Delta z}{2}\right)\right]^2 \quad (2.36)$$

In contrast to the numerical dispersion relation (2.36), the analytical dispersion relation for a plane wave in a continuous lossless medium is simply :

$$\frac{\omega^2}{c^2} = k_x^2 + k_y^2 + k_z^2 \quad (2.37)$$

However, (2.36) will reduce to (2.37) in the limit as $\Delta t, \Delta x, \Delta y$ and Δz all go to zero, that is, if the FDTD grid is made very fine.

As the FDTD grid size increases with respect to the wavelength of propagating waves, the deviation of the numerical phase velocity from the exact analytical phase velocity increases until the waves eventually cease to propagate. This numerical low-pass filtering effect is inherent in the FDTD grid. Consequently, FDTD modelling of pulses with high bandwidth will result in progressive pulse distortion as the high spatial frequency components will propagate more slowly than the low spatial frequency components. In addition, the very high spatial frequency components with wavelengths less than 2 to 3 cells are completely rejected [2.5].

2.8 Boundary conditions

In a finite-difference scheme, the finite-difference mesh has to be of finite extent due to the limitation of computer storage capacity. However, in many applications, the media to be modelled are of infinite extent. Scattering problems, for example, lead to solutions of fields in an unbounded domain. Imposing boundary conditions on the finite-difference mesh boundary may give rise to reflections that are not representative of the actual physical situation. Consequently, absorbing boundary conditions are applied on the mesh boundary, also known as the computational boundary, in order to simulate infinite or very large geometries. The algorithm on the truncation planes has to simulate propagation of outgoing waves as if they were propagating to infinity. This is accomplished by enforcing an impedance match on the computational boundary so that there is no reflection of outgoing waves back into the domain.

Referring to Fig.2.1, if the finite-difference mesh terminates on the electric field cell, we can see that all components of the electric field on the boundary are tangential to the boundary while the components of the magnetic field are normal to it. While the $\vec{H}$ -field components can be calculated from the respective $\vec{E}$ -field components using equations (2.14), the $\vec{E}$ -field components cannot be evaluated in the same way as this would require $\vec{H}$ -field components that are outside the mesh. For the structures considered in this thesis, the pulses on the microstrip lines will be normally incident on the mesh boundaries. Therefore, a simple approximate continuous absorbing boundary condition, where the tangential fields on the mesh boundaries obey the one-dimensional wave equation in the direction normal to the mesh wall, will suffice.

Engquist and Majda derived a theory of one-way wave equations suitable for absorbing boundary condition in Cartesian FDTD grids [1.15]. It was further discussed by Mur in 1981 [1.16] and implemented on a finite-difference scheme.

2.8.1 1st order Mur boundary condition

To derive Mur's first approximate absorbing boundary condition, consider TEM wave propagation on a lossfree transmission line giving rise to voltage and current as follows :

$$V_x = V_l \cos\beta x + \mathrm{j} I_l Z_o \sin\beta x \tag{2.38}$$

$$I_x = I_l \cos\beta x + \mathrm{j}\frac{V_l}{Z_o}\sin\beta x \tag{2.39}$$

where x is an arbitrary point on the transmission line and l is the load end of the transmission line. In order to have no reflection at the boundary, the line must be matched at the boundary, therefore,

$$\frac{V_l}{I_l} = Z_o \tag{2.40}$$

where Z_o is the characteristic impedance of the line.

Then, (2.38) and (2.39) reduce to

$$V_x = V_l\, \mathrm{e}^{\mathrm{j}\beta x} \tag{2.41}$$

$$I_x = I_l\, \mathrm{e}^{\mathrm{j}\beta x} \tag{2.42}$$

which is a standard equation for one-dimensional propagating wave travelling towards the –x direction. Assuming sinusoidal time variation, we have,

$$V_x = V_l\, \mathrm{e}^{\mathrm{j}(\beta x + \omega t)} \tag{2.43}$$

Taking time and space derivatives of (2.43) gives

$$\frac{\partial V_x}{\partial t} = \mathrm{j}\omega V_x \quad \text{and} \quad \frac{\partial V_x}{\partial x} = \mathrm{j}\beta V_x$$

and equating the V_x terms results in

$$\frac{1}{\mathrm{j}\beta}\frac{\partial V_x}{\partial x} = \frac{1}{\mathrm{j}\omega}\frac{\partial V_x}{\partial t} \tag{2.44}$$

or

$$\frac{\partial V_x}{\partial x} - \frac{1}{v}\frac{\partial V_x}{\partial t} = 0 \tag{2.45}$$

So, for wave propagating in the –x direction, normal to the absorbing boundary wall, the Mur's first approximate boundary condition is :

$$\frac{\partial E_{\text{tangential}}}{\partial x} - \frac{1}{v}\frac{\partial E_{\text{tangential}}}{\partial t} = 0 \tag{2.46}$$

while for wave propagating in the +x direction,

$$\frac{\partial E_{\text{tangential}}}{\partial x} + \frac{1}{v}\frac{\partial E_{\text{tangential}}}{\partial t} = 0 \qquad (2.47)$$

where $E_{\text{tangential}}$ is the E field tangential to the boundary wall and v is the velocity of the propagating wave. (2.46) can be discretised so that the field components on the boundary walls are dependent on only the field components on and just inside the walls.

One way to approximate (2.46) is to use forward differencing for both space and time. This results in :

$$E_{x1}^{t} - E_{x0}^{t} = \frac{\Delta x}{v\Delta t}\left(E_{x0}^{t+1} - E_{x0}^{t}\right) \qquad (2.48)$$

where the subscript denotes the space step and the superscript, the time step. Rearranging (2.48) gives us :

$$E_{x0}^{t+1} = E_{x0}^{t}\left(1 - \frac{v\Delta t}{\Delta x}\right) + \frac{v\Delta t}{\Delta x}E_{x1}^{t} \qquad (2.49)$$

(2.49) gives 1st order accuracy in the implementation of the Mur's 1st approximate boundary condition. Another way of applying (2.46), in order to have second-order accuracy in the discretised finite-difference mesh, is to impose (2.46) at half space and time steps as follows :

$$\left.\frac{\partial E_{\text{tangential}}}{\partial x}\right|_{x=x+1/2} = \left.\frac{1}{v}\frac{\partial E_{\text{tangential}}}{\partial t}\right|_{t=t+1/2} \qquad (2.50)$$

$$\frac{1}{\Delta x}\left(E_{x1}^{t+1/2} - E_{x0}^{t+1/2}\right) = \frac{1}{v\Delta t}\left(E_{x1/2}^{t+1} - E_{x1/2}^{t}\right) \qquad (2.51)$$

Since the values at the half grid points and half time steps are not available, it is possible to use a semi-implicit approximation :

$$E_m^{n+1/2} \approx \frac{1}{2}\left(E_m^{n+1} + E_m^{n}\right) \qquad (2.52)$$

and

$$E_{m+1/2}^{n} \approx \frac{1}{2}\left(E_{m+1}^{n} + E_m^{n}\right) \qquad (2.53)$$

This is partially implicit because it uses an unknown value of E at time step $(n+1)\Delta t$.
Substituting (2.52) and (2.53) into (2.51) gives us

$$\frac{1}{\Delta x}\left[\frac{1}{2}\left(E_{x1}^{t+1} + E_{x1}^{t} - E_{x0}^{t+1} - E_{x0}^{t}\right)\right] = \frac{1}{v\Delta t}\left[\frac{1}{2}\left(E_{x1}^{t+1} + E_{x0}^{t+1} - E_{x1}^{t} - E_{x0}^{t}\right)\right] \qquad (2.54)$$

Simplifying (2.54) gives

$$E_{x0}^{t+1}\left(\frac{1}{v\Delta t}+\frac{1}{\Delta x}\right) = E_{x1}^{t}\left(\frac{1}{v\Delta t}+\frac{1}{\Delta x}\right) + E_{x1}^{t+1}\left(\frac{1}{\Delta x}-\frac{1}{v\Delta t}\right) - E_{x0}^{t}\left(\frac{1}{\Delta x}-\frac{1}{v\Delta t}\right)$$

or

$$E_{x0}^{t+1} = E_{x1}^{t} + \left(\frac{v\Delta t - \Delta x}{v\Delta t + \Delta x}\right)\left(E_{x1}^{t+1} - E_{x0}^{t}\right) \qquad (2.55)$$

where E_{x0} represents the tangential electric field components on the mesh wall and E_{x1}, the tangential electric field components one node inside the mesh wall. Strictly, (2.55) is the absorbing boundary condition for wave propagating in the –x direction, i.e. for use on the boundary wall at x=0. In this case, E_{x0}, electric field on the x=0 wall is to the *left* of E_{x1}, the electric field one node inside the x=0 wall. For a wave propagating in the +x direction, although (2.47) shows a change in sign in the one-way wave equation, (2.55) can still be applied as the absorbing boundary condition at the boundary wall x=h simply because the change in sign in equation (2.47) is equivalent to swapping the electric field positions on the boundary wall; in this case, E_{x0} is the electric field on the wall which is to the *right* of E_{x1}, the electric field one node inside the x=h wall. Similar expressions can be derived for other absorbing boundaries, i.e. normal to y and z directions.

Even after applying the absorbing boundary condition, there is some reflection because true wave propagation is not one-dimensional and also the wave velocity is not constant but a function of frequency. Besides, the normal incidence assumption is not valid for the fringing fields, therefore the side walls should be far enough away so that the effects are negligible on the walls.

2.9 Conductor boundaries

Conducting ground plane and copper metallization layer can be modelled as perfect electric conductors where the tangential electric fields are forced to be zero. It is usual to assume that these layers have zero thickness. In order to model the edge of a conductor, tangential $\vec{E}$ fields are positioned exactly on the edge of the conductor.

2.10 Dielectric boundaries

The $\vec{E}$ and $\vec{H}$ fields in a dielectric region are calculated using equations (2.13) and (2.14) with the dielectric constant, ε, set to that of the dielectric instead of unity. The field components which lie on a dielectric-air interface are the tangential $\vec{E}$ and the perpendicular $\vec{H}$ components. To calculate E_x and E_y at the dielectric-air interface, the average value of ε is used in (2.13) [1.6], i.e.

$$\varepsilon = \frac{\varepsilon_1 + \varepsilon_2}{2} \qquad (2.56)$$

where ε_1 is the permittivity of the dielectric

and $\varepsilon_2 = 1$, permittivity of air.

Generally, in order to account for fringing field effects at the edge of microstrip patch, the dielectric constant to be used is dependent on the relative permittivity of the dielectric as compared to that of air and the relation between the width and height of the dielectric below the microstrip patch being modelled. Since the fringing field effects are automatically considered in the FDTD simulation, equation (2.56) is suffice for use only at the dielectric-air interface.

(2.14) is still used to calculate normal $\vec{H}$, as the value of μ does not change across the dielectric-air boundary.

2.11 Excitation

A Gaussian pulse has been chosen as the excitation pulse in all investigations in this thesis. This is mainly because a Gaussian pulse has a smooth waveform in time and its Fourier transform is also Gaussian in shape and centred at zero frequency. This means that by adjusting the width of the Gaussian pulse, the frequency response can be obtained from dc to the frequency of interest. An ideal Gaussian pulse will have the following expression :

$$g(t) = e^{-\left(\frac{t - t_o}{T}\right)^2} \tag{2.57}$$

and the pulse will be at its maximum at $t = t_o$. Fig. 2.2 shows a typical Gaussian pulse.

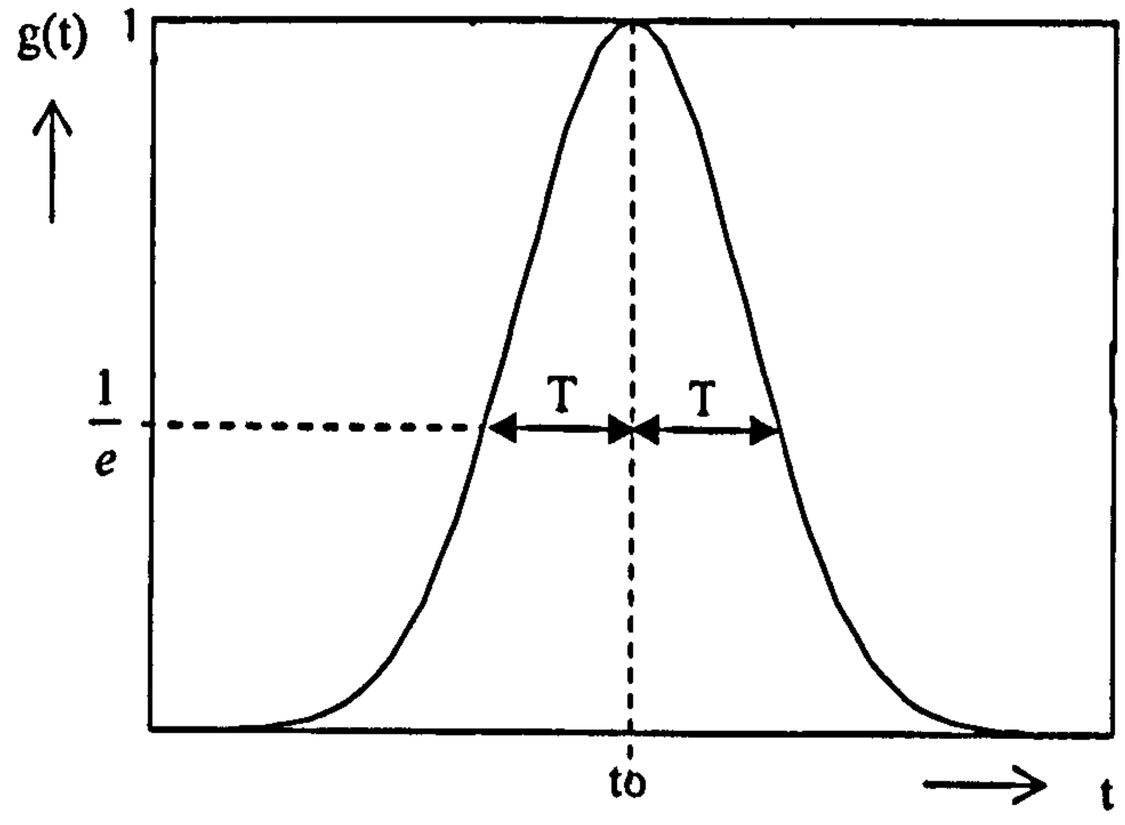

Fig. 2.2 : Gaussian pulse

The choices of T and t_o are subject to two requirements. Firstly, the FDTD grid size, Δx, Δy and Δz are chosen to be fine enough to model the smallest dimension of the structure. Also, in order to have a good spatial or mesh resolution, the grid size is set such that it is at least 1/20 of the shortest wavelength of interest. Δt is then calculated from the CFL stability criterion as given by the bound in (2.33). The Gaussian half-width is given by :

$$g(t) = e^{-\left(\frac{t - to}{T}\right)^2} = e^{-1}$$

$$\left(\frac{t - t_o}{T}\right)^2 = 1$$

or
$$t = t_o \pm T \tag{2.58}$$

that is, T is the symmetric point from the centre t_o point when $g(t)$ drops to 1/e of its maximum value. The Gaussian half-width in time is then 2T. We know from Fourier Transform method that the relationship between the highest frequency of interest, f_{max}, and T in the Gaussian pulse is given by :

$$T = \frac{1}{2f_{max}} \tag{2.59}$$

Knowing the highest frequency of interest, T is calculated from (2.59). This is to ensure that the Gaussian pulse is narrow enough to have a wide spectrum in order to maintain a substantial value within the frequency range of interest. At the same time, the Gaussian pulse has to be wide enough to contain enough number of time steps for a good time resolution. More importantly, in order to minimize numerical dispersion error, we have found that, the Gaussian half-width, derived in (2.58), must contain at least 20 space steps in the direction of propagation. If the Gaussian pulse travels at a speed, v, in the direction of propagation, then the equivalent spatial half-width, W, of the pulse is given by :

$$W = 2Tv \tag{2.60}$$

Therefore, to have 20 space steps, $\frac{2Tv}{\Delta h} \geq 20$

or
$$T \geq \frac{10\Delta h}{v} \tag{2.61}$$

where Δh is the space step in the direction of propagation. If the half width of the pulse, calculated from (2.59) is not wide enough to contain 20 space steps then, the space step has to be reduced. The time step Δt will then have to be re-calculated to ensure that the CFL stability criterion is still satisfied.

Secondly, t_o must be chosen such that the initial 'turn on' of the excitation will be small and smooth to avoid exciting high order modes. In order to have a smooth 'turn on', t_o in all simulations in this thesis is set to three times the value of T.

2.12 Simulation of a line-fed rectangular microstrip patch

The finite-difference time-domain equations (2.13) & (2.14) are used with the 1st order Mur absorbing boundary condition to simulate the propagation of a broad-band Gaussian pulse on a line-fed rectangular microstrip patch as shown in Fig. 2.3. This microstrip patch circuit was chosen from a paper published by Abouzahra et al [1.5]. The finite-difference mesh parameters are chosen to be the same as in that paper to allow direct comparison of results.

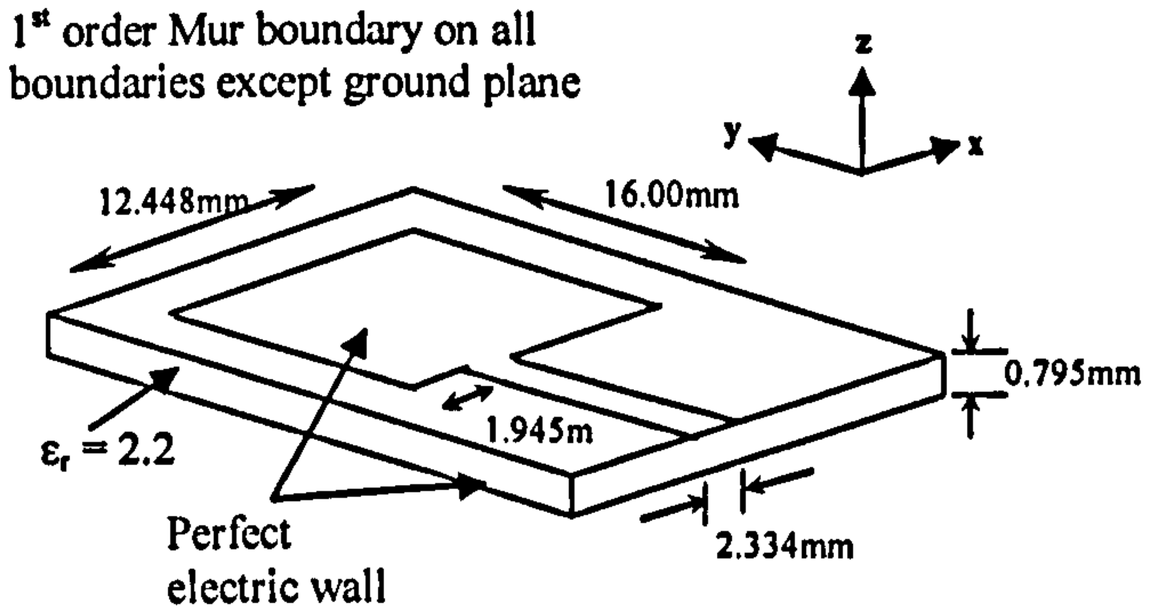

Fig. 2.3 : Line-fed rectangular microstrip patch

Mesh parameters :

Δx = 0.389 mm

Δy = 0.400 mm

Δz = 0.265 mm

Thickness of substrate : 3 Δz

Air space above substrate : 13 Δz

Rectangular microstrip patch : 32 Δx x 40Δy

Source plane to edge of rectangular patch : 50 Δy

Monitored reference plane to edge of rectangular patch : 10 Δy

Microstrip line width : 6 Δx

Total mesh dimensions : 60 x 100 x 16 in $\hat{x}, \hat{y}$ and $\hat{z}$ directions respectively

Time step Δt = 0.441ps

Gaussian half-width T = 15ps

Time delay t_o = 3T

Δf = 0.2 GHz

Since the substrate thickness is relatively small compared to the wavelength of interest, up to 20GHz, we can assume that there is no variation of electric field in the vertical direction. Then, to excite the dominant mode, a Gaussian pulse in time is launched into the source plane, setting off the vertical electric field, E_z, of the individual cell, Δz, throughout the dielectric thickness and across the width of the feed line, 6 Δx.

In [1.6], an electric wall source is used for the remaining nodes on the source plane. An unwanted side effect of this is that a sharp magnetic field is induced due to the high value of the space derivative of the electric field. This results in the distortion of the pulse. To overcome this problem, a magnetic wall is simulated on the source plane as was done in [1.5]. Applying image theory, the tangential $\vec{H}$, a node inside the source plane is set to be the negative value of the tangential $\vec{H}$, a node outside the source plane. Then the remaining $\vec{E}$ field components on the source plane may be calculated from the finite difference equations. However, when waves are reflected back to the source from the microstrip patch, the source plane has to be transparent to the waves. To simulate this, the 1st order Mur absorbing boundary condition is *switched on once the excitation is completed.* This means that the source plane has

to be a reasonable distance away from the edge of the microstrip patch such that the reflected pulse does not arrive back at the source plane while the source is still turned on.

Initially, all fields in the computational domain are set to zero. As time-marching progresses, the sequence of the algorithm implemented is as follows :

- vertical electric field is excited with Gaussian pulse below the strip
- $\vec{H}$ fields are calculated using (2.14)
- magnetic wall is applied on the source plane on nodes other than the source points
- electric field values are stored for later use in absorbing boundary condition calculation
- $\vec{E}$ fields are calculated using (2.13)
- tangential $\vec{E}$ fields are set to zero on the metallized copper patch
- tangential $\vec{E}$ fields on the computational boundaries are calculated using the Mur's first approximate absorbing boundary condition (2.55)

The iteration proceeds till the response is close to zero or until there are enough data to meet the frequency resolution.

2.13 Extraction of voltage and current from the FDTD mesh

In the FDTD simulation, excitation is in the form of the electric field and subsequently, the electric and magnetic fields are calculated on the finite-difference mesh using equations (2.13) and (2.14). To extract the voltage at the reference plane (electric field reference plane), firstly the vertical electric field underneath the microstrip feed-line for each cell is multiplied by the Δz to get the voltage for each cell; this is repeated throughout the thickness of the dielectric and all these voltages added together give the total voltage at the reference plane at a specific x location. In order to get a more accurate result, an average total voltage is obtained for the width of the strip.

To extract the current, the magnetic field is integrated with respect to the mesh size along the dotted path as shown in Fig.2.4. However, the magnetic field reference plane is shifted by half Δy from the electric field reference plane. So, to get the current at the same reference plane as the voltage reference plane (electric field reference plane), the magnetic field is integrated twice, first along the path of H-reference plane and then along the path Δy behind the H-reference plane (see Fig.2.4). Assuming linearity, the average of the two integrations gives the current at the E-reference plane.

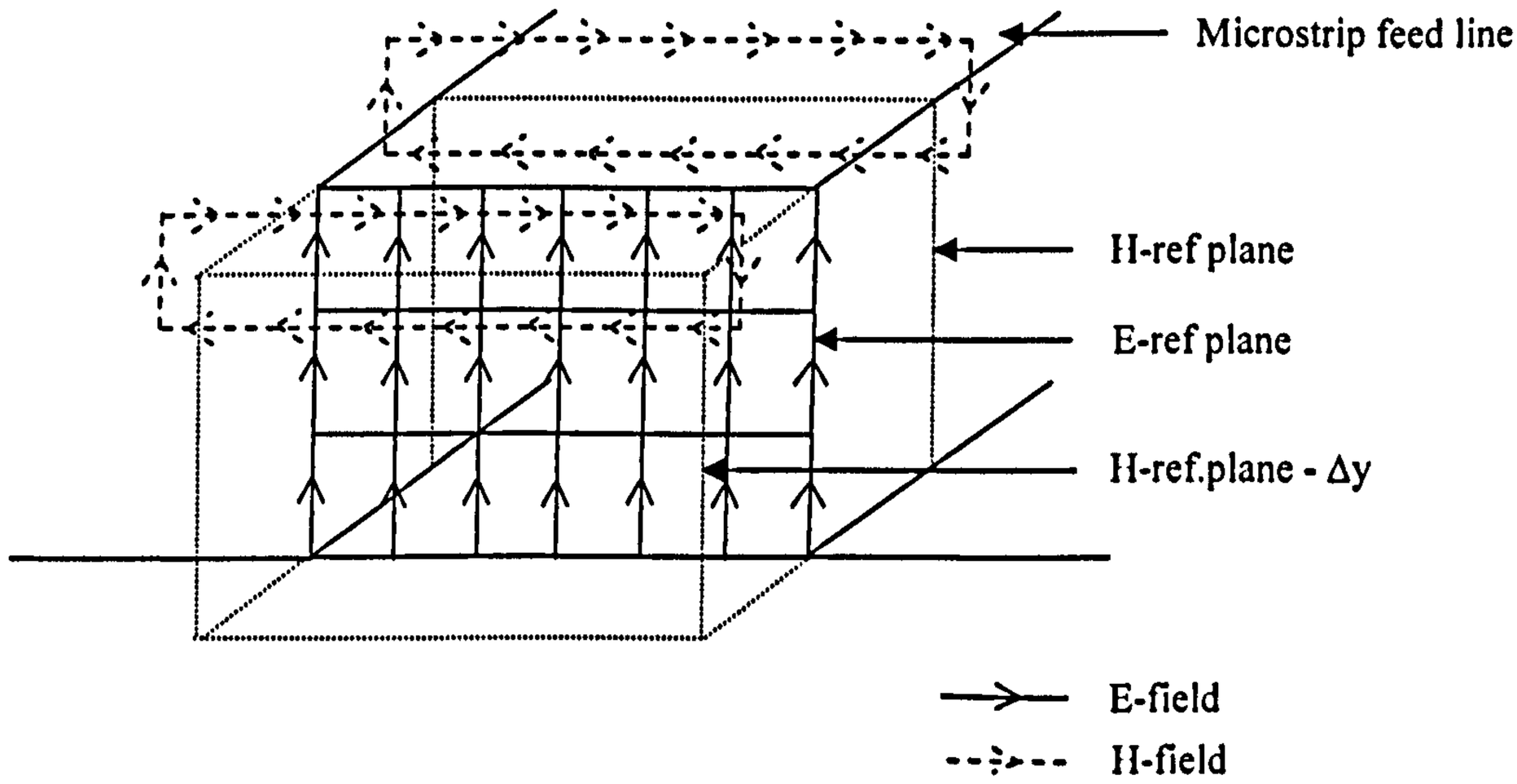

Fig.2.4 : Extraction of electric and magnetic fields

2.14 Extraction of S_{11}

2.14.1 Two runs

The microstrip patch is a one-port device and therefore its scattering matrix has only one element S_{11} which is the reflection coefficient. The reflection coefficient is given by :

$$\Gamma = \frac{E_{reflected}}{E_{incident}} \tag{2.62}$$

In order to obtain the reflection coefficient, the incident and reflected waves must be known. In FDTD simulation, however, the calculated electric fields are the total electric fields. One way to obtain the fields separately is to obtain the incident waveform, $E_{incident}$, by simulating only the microstrip feed-line which *extends right through to the absorbing boundary*. This incident waveform can now be subtracted from the total waveform, E_{total} , obtained when simulating the rectangular microstrip patch to yield the reflected waveform. The reflection coefficient is then calculated using :

$$\Gamma = \frac{E_{reflected}}{E_{incident}} = \frac{E_{total} - E_{incident}}{E_{incident}} \tag{2.63}$$

This means that two runs of the FDTD routine are required in order to obtain the reflection coefficient of the circuit. This is inefficient and time-consuming.

2.14.2 Single run

It is found in this research that by extracting four parameters instead of one from the FDTD simulation of the circuit, only a single run is necessary to calculate the reflection coefficient of the circuit.

Consider the voltage and current at any point on a transmission line :

$$V_x = V_l \cosh \gamma x + I_l Z_o \sinh \gamma x \tag{2.64}$$

$$I_x = I_l \cosh \gamma x + \frac{V_l}{Z_o} \sinh \gamma x \tag{2.65}$$

then
$$\frac{V_x}{I_x} = Z_o \left(\frac{Z_l + Z_o \tanh \gamma x}{Z_o + Z_l \tanh \gamma x} \right) \tag{2.66}$$

also
$$\frac{\partial V_x}{\partial x} = (V_l \sinh \gamma x + I_l Z_o \cosh \gamma x) \gamma \tag{2.67}$$

$$\frac{\partial I_x}{\partial x} = \left(I_l \sinh \gamma x + \frac{V_l}{Z_o} \cosh \gamma x \right) \gamma \tag{2.68}$$

then at $x = 0$, set as the reference plane at the monitoring point, dividing (2.67) by (2.68) gives

$$\frac{\partial V_x / \partial x}{\partial I_x / \partial x} = \frac{I_l Z_o}{V_l / Z_o} = \frac{Z_o^2}{Z_l} \tag{2.69}$$

and from (2.64) and (2.65), with $x = 0$,

$$\frac{V_x}{I_x} = Z_l \tag{2.70}$$

Note that Z_l is not the load impedance in the conventional sense but the load impedance at the monitoring point as $x = 0$ has been set as the reference plane at the monitoring point. So, Z_l is the input impedance at the monitoring point and the reflection coefficient at the monitoring point is given by :

$$\Gamma = \frac{Z_l - Z_o}{Z_l + Z_o} \tag{2.71}$$

or
$$\Gamma = \frac{\sqrt{Z_l^2 / Z_o^2} - 1}{\sqrt{Z_l^2 / Z_o^2} + 1} \tag{2.72}$$

Representing (2.72) in the form of (2.69) and (2.70) gives us

$$\Gamma = \frac{\sqrt{\dfrac{V_x / I_x}{\partial V_x / \partial x \,/\, \partial I_x / \partial x}} - 1}{\sqrt{\dfrac{V_x / I_x}{\partial V_x / \partial x \,/\, \partial I_x / \partial x}} + 1} \tag{2.73}$$

It can be seen from (2.73) that the reflection coefficient of the circuit can be calculated from a single run of the FDTD routine if four parameters, namely, V_x, I_x, $\partial V_x / \partial x$ and $\partial I_x / \partial x$ are extracted from the FDTD simulation.

The derivation above is done for wave propagation in the *x*-direction. It can be applied to any direction of propagation as long as appropriate parameters are extracted. In all simulations in this thesis the direction of propagation is in the *y*-direction while the excited tangential electric field is in the z-direction. Therefore, the required parameters are V_z, I_y, $\partial V_z/\partial y$ and $\partial I_y/\partial y$.

2.15 Extraction of Zin

The input impedance, Zin, of the microstrip patch antenna at the edge of the patch can be calculated from the $S_{11}(\omega)$ extracted in section 2.14 by transforming the reference plane from the monitoring point to the edge of the antenna and applying the equation below.

$$Z_{in} = Z_o\left(\frac{1 + S_{11}e^{j2\beta l}}{1-S_{11}e^{j2\beta l}}\right) \tag{2.74}$$

where β is the phase constant on the microstrip and *l* is the length from the monitoring point to the edge of the patch antenna and Z_o is the characteristic impedance of the microstrip line.

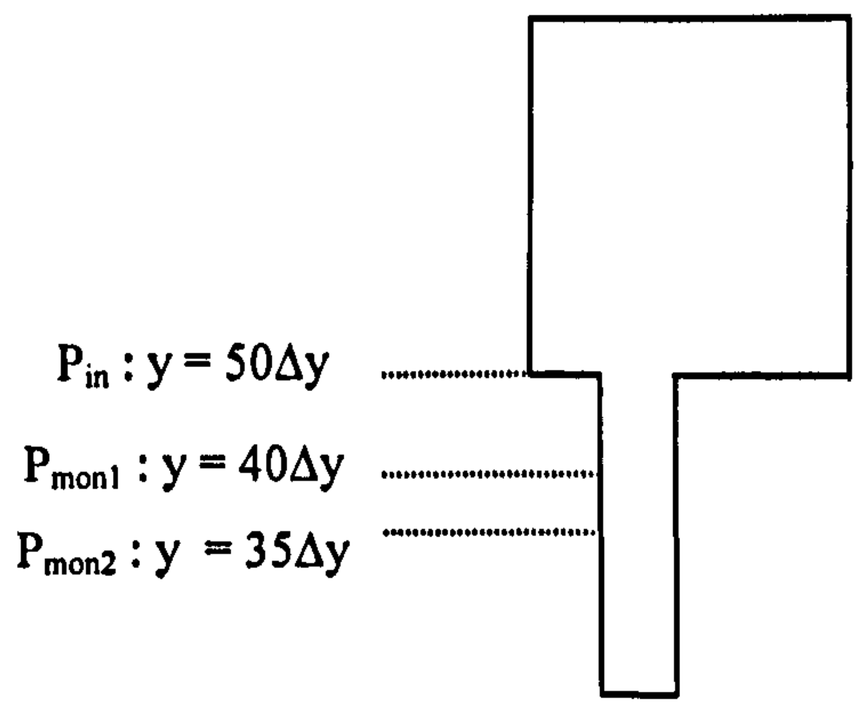

Fig.2.5 : Plan view of the microstrip patch antenna

Fig. 2.5 shows the plan view of the simulated microstrip patch antenna where the monitoring point is at P_{mon1} and the input impedance to be calculated is at P_{in}. By applying equations (2.70) and (2.73), we have the input impedance, Z_{in_mon1} and reflection coefficient, S_{11_mon1} at the monitoring point, P_{mon1}. In order to apply (2.74) to find Z_{in} at P_{in}, we need to calculate β, the phase constant on the microstrip and Z_o the characteristic impedance of the microstrip line. Re-arranging (2.74), we get

$$Z_o = Z_{in\_mon1}\left(\frac{1 - S_{11\_mon1}}{1+S_{11\_mon1}}\right) \tag{2.75}$$

which gives us the characteristic impedance of the microstrip line. In order to calculate β, the phase constant, V_z, I_y, $\partial V_z/\partial y$ and $\partial I_y/\partial y$ are monitored at another point P_{mon2} in addition to point P_{mon1}. Again, applying (2.73) to the data extracted from point P_{mon2}, we obtain the reflection coefficient, S_{11_mon2}.

Let

$$S_{11\_mon1} = \frac{E_{reflected}}{E_{incident}} \tag{2.76}$$

then

$$S_{11\_mon2} = \frac{E_{reflected}\, e^{-j\beta L_1}}{E_{incident}\, e^{j\beta L_1}} = S_{11\_mon1}\, e^{-j2\beta L_1} \tag{2.77}$$

since the reflected wave at P_{mon2} is delayed from P_{mon1} by a phase length $\beta L1$ and the incident wave at P_{mon2} is ahead of P_{mon1} by the same amount where $L1$ is the length from P_{mon1} to P_{mon2} which is set at $5\Delta y$. Let θ_1 be the phase of S_{11} at P_{mon1} and θ_2 the phase of S_{11} at P_{mon2}, then (2.77) becomes

$$\left|S_{11\_mon2}\right| e^{j\theta_2} = \left|S_{11\_mon1}\right| e^{j\theta_1} e^{-j2\beta L_1} \tag{2.78}$$

then

$$\beta = \frac{\theta_1 - \theta_2}{2L_1} \tag{2.79}$$

Substituting β and Z_o back into (2.74), we get the input impedance of the patch antenna as

$$Z_{in} = Z_{in\_mon1}\left(\frac{1 - S_{11\_mon1}}{1+S_{11\_mon1}}\right)\left(\frac{1 + S_{11\_mon1}\, e^{j\frac{\theta_1 - \theta_2}{L_1}L_2}}{1-S_{11\_mon1}\, e^{j\frac{\theta_1 - \theta_2}{L_1}L_2}}\right) \tag{2.80}$$

Since the monitoring points chosen are at P_{mon1} and P_{mon2}, $L_1 = 5\Delta y$ and $L_2 = 10\Delta y$, then (2.80) reduces to

$$Z_{in} = Z_{in\_mon1}\left(\frac{1 - S_{11\_mon1}}{1+S_{11\_mon1}}\right)\left(\frac{1 + S_{11\_mon1}\, e^{j2(\theta_1 - \theta_2)}}{1-S_{11\_mon1}\, e^{j2(\theta_1 - \theta_2)}}\right) \tag{2.81}$$

Equation (2.81) is used to calculate Z_{in} in one simulation.

2.16 Results

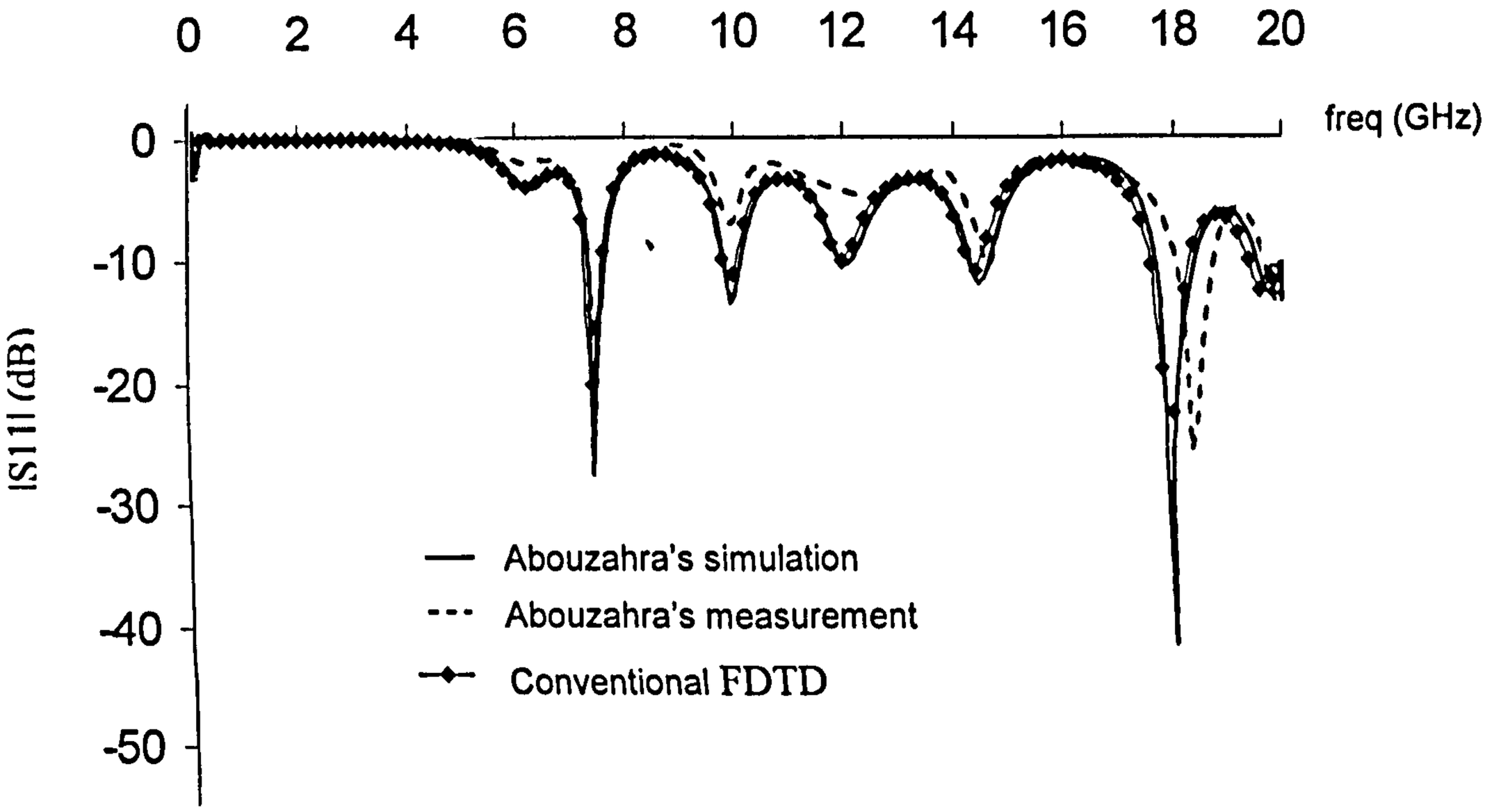

Fig. 2.6 : Comparison between simulated and Abouzahra's published results for $|S_{11}|$

M.D.Abouzahra et al [1.5] discussed the application of the three-dimensional FDTD method to the analysis of planar microstrip circuits, one of which was the line-fed rectangular microstrip patch shown in Fig.2.3. In order to validate the FDTD program, the patch in Fig.2.3 is simulated using the same mesh parameters as in the published paper [1.5] to allow exact comparison. Fig. 2.6 above shows a comparison between the published data and the data generated. The simulated result agrees well with Abouzahra's simulated results. However, at high frequencies, both Abouzahra's simulated results and the simulated results generated in this work shifted slightly towards the lower frequency. The discrepancy between the simulated and measured data may be due to an increase in numerical dispersion at high frequencies. Furthermore, the results have been obtained in the time-domain and then converted into frequency domain by applying Fourier Transform method on the time-domain data. Consequently, a small error in the form of truncation error in the time-domain will result in a more significant error in the frequency domain. Besides, the experimental data here are assumed to be error-free which may not be a sound assumption. The discrepancy between the simulated data and Abouzahra's measurement may well be due to measurement error. The simulated result in Fig. 2.6 was obtained using a single run FDTD method as described in 2.15.2

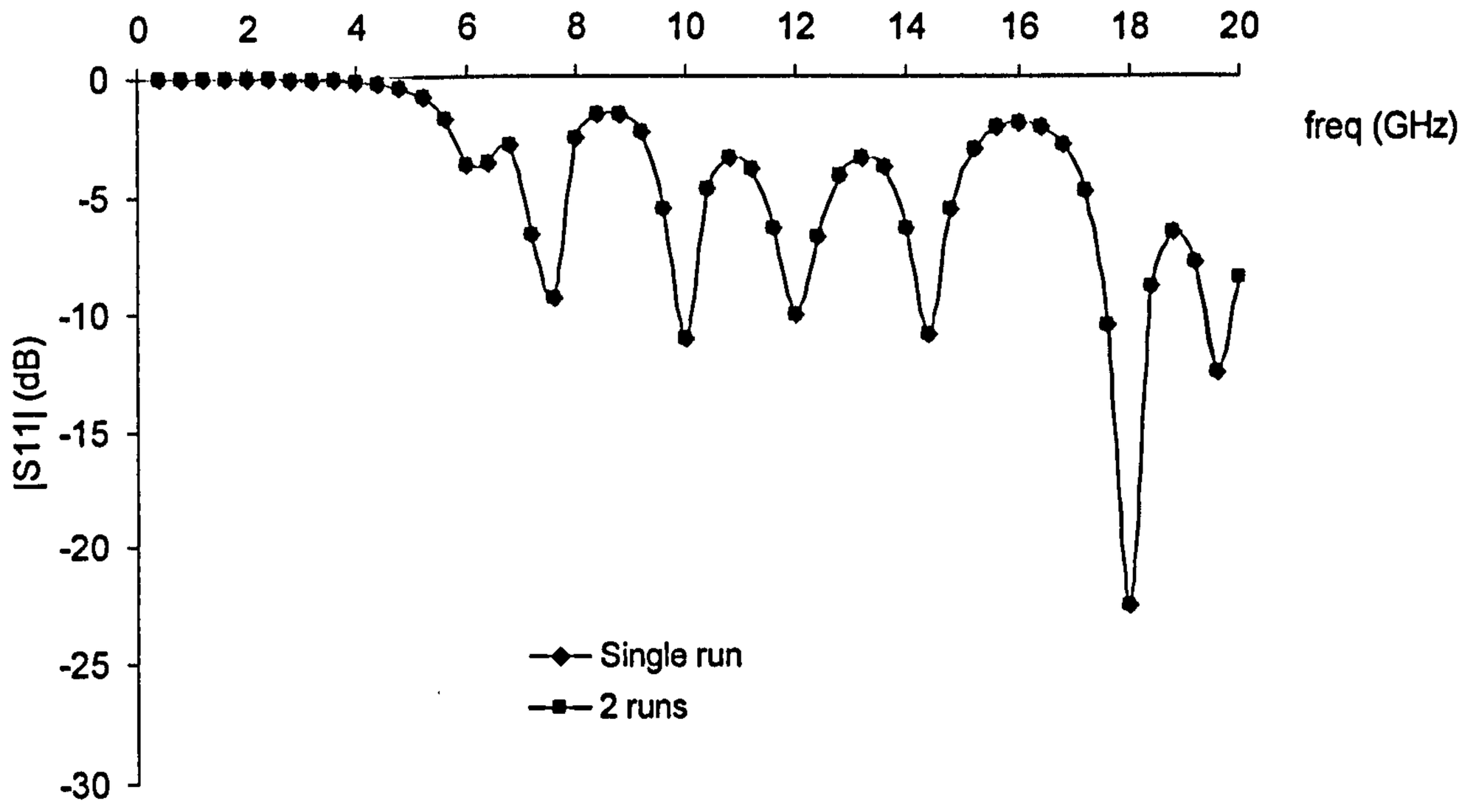

Fig 2.7 : Comparison between two-run and single run simulated results

In order to validate the single run method of obtaining the reflection coefficient for the microstrip patch circuit as derived in section 2.14.2, two sets of data are generated, one using the single run method and the other using the double-run method. Fig. 2.7 shows a comparison between both sets of reflection coefficients. They show exact agreement. Since the single run method is more efficient, all subsequent results from this point onwards have been generated using the single run method.

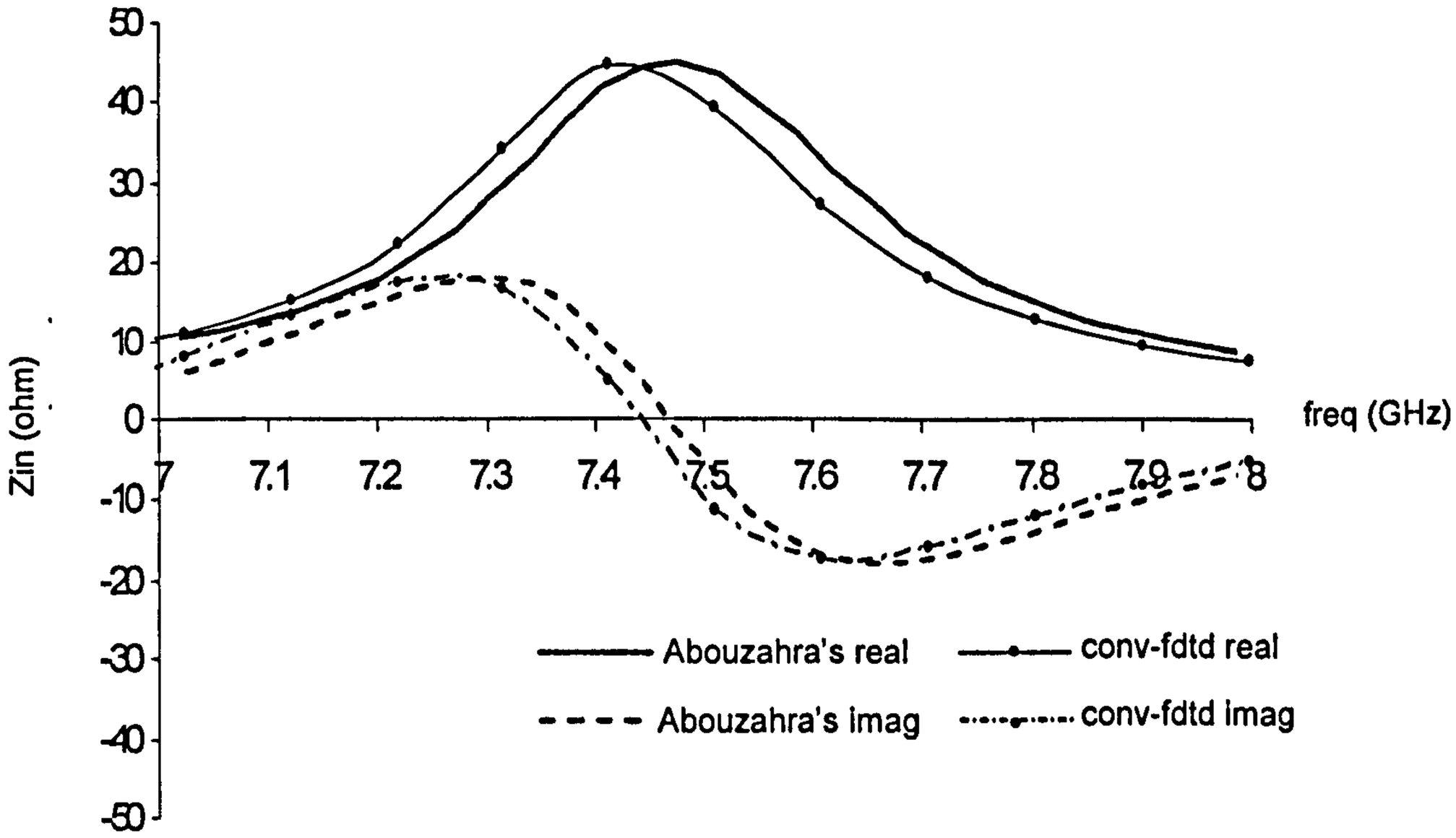

Fig. 2.8 : Comparison between simulated and Abouzahra's published results for Z_{in}

Fig.2.8 above shows a comparison of real and imaginary parts of the patch antenna input impedance between the simulated and Abouzahra's published results. In Abouzahra's published paper, the microstrip is assumed to have a constant characteristic impedance, Z_o of 50 Ω and an effective permittivity of 1.9 is used to calculate the wavenumber, β. In this research work, these values have been calculated using the simulation data as discussed in section 2.15. Due to an inherent dispersive characteristic of the microstrip, the effective permittivity is no longer static but changes as a function of frequency. Since a Gaussian pulse which contains all the frequencies of interest is used as an excitation, the dispersive nature of the microstrip patch due to the inhomogeneous media is automatically incorporated in the full-wave time-domain solution provided by FDTD. The variation of the characteristic impedance in the frequency range of interest is also accounted for in the simulated data. It is therefore not surprising to see the discrepancy between the calculated input impedance and that presented in the published literature [1.5].

2.17 Conclusion

The three-dimensional finite-difference time-domain algorithm for solving numerical electromagnetic problems has been introduced in this chapter. The salient features and key considerations in the implementation have been discussed. Following this, the FDTD algorithm in this work has been shown to produce results that agree with published results using a new more efficient technique of extracting the reflection coefficient. This method of data extraction has been shown to give identical results to the conventional approach and removes the necessity of performing two separate simulation runs, therefore saving simulation run-time. Another important point is that the input impedance has been calculated directly from simulated data which automatically incorporate the dispersive characteristic of the microstrip; this removes the need for a-priori knowledge of the line characteristic impedance and effective permittivity. Unlike in [1.5], there is no need to assume the characteristic impedance of the line and use an effective permittivity to calculate the wavenumber.

CHAPTER 3
ALTERNATING-DIRECTION IMPLICIT FINITE-DIFFERENCE TIME-DOMAIN METHOD

3.1 Introduction

The FDTD method has been widely used in solving a broad range of electromagnetic problems. The accuracy of the simulation can be greatly improved with the use of finer spatial increments, especially where there are discontinuities in the structure. This though leads to the requirement of having fine mesh sizes in localized areas. In the past, to maintain stability, as defined by the Courant-Friedrich-Levy (CFL) criterion in (2.33), the time step used would have to be small. This would lead to a prohibitively long simulation run-time if the object was electrically large but had small localized discontinuities.

In this chapter, the author shows that with the application of the alternating-direction implicit (ADI) method on the FDTD, the CFL stability constraint is eliminated [1.14] and therefore a single time step, larger than the one allowed by the CFL criterion, can be used for all mesh sizes throughout the model. The time step is no longer governed by the stability but by the accuracy required for the simulation. This is particularly useful, for example, when modelling a probe-fed circular patch where the probe is extremely narrow compared to the diameter of the patch. In order to represent the effective input impedance of the probe-fed circular patch accurately, a high FDTD mesh density is applied in the vicinity of the probe and the mesh density decreases gradually away from the probe. Another area where the ADI-FDTD may be useful is in the modelling of a structure comprising narrow slots or notches. Here, fine meshes are required around the slots and notches with a consequent increase in computation time.

This chapter will discuss the key features in implementation of ADI-FDTD with particular emphasis on absorption boundaries. Note that all the finite-difference algorithms from this chapter onwards will be expressed such that the electric and magnetic terms are staggered by half a space step as depicted in the original Yee cell to enable the derivation of numerical dispersions for the ADI methods.

3.2 Three-dimensional ADI-FDTD algorithm

The conventional ADI method has been widely used to solve many diffusion problems. As stated in equations (1.6a) and (1.6b) in chapter one, the conventional ADI finite difference equations are split into two procedures for a two-dimensional ADI scheme. Correspondingly, a three-dimensional conventional ADI method will require the finite difference equations to be split into three procedures, each one replacing a spatial derivative with an implicit difference approximation [2.4]. However, unlike in the conventional ADI method, in this three-dimensional ADI-FDTD method, the formulation is split into only two procedures, each one replacing each spatial derivative in the Maxwell's curl equations with an

implicit difference approximation. Procedure 1 is applied for advancement from $n\Delta t$ to $(n+\frac{1}{2})\Delta t$ while procedure 2 is used for advancement from $(n+\frac{1}{2})\Delta t$ to $(n+1)\Delta t$.

Equations (3.1) – (3.2) show the numerical formulation for procedure 1 of the ADI-FDTD method. The electric and magnetic fields are spatially staggered as in the conventional FDTD. Examining equation (3.1a), one notes that it has a form which is reminiscent of the conventional FDTD as in (2.13a). However, whilst all the H-field terms in the RHS of (2.13a) in the conventional FDTD are explicit, i.e. all values are known, the H-fields on the RHS of (3.1a) in the ADI-FDTD have two implicit terms which are yet to be calculated. The same form runs through all subsequent equations from (3.1a) to (3.2c), i.e. there are two implicit terms in each equation.

Procedure 1

$$E_x^{n+1/2}(i+1/2,j,k) = E_x^n(i+1/2,j,k) + \frac{\Delta t}{2\varepsilon}\left\{\frac{H_z^{n+1/2}(i+1/2,j+1/2,k) - H_z^{n+1/2}(i+1/2,j-1/2,k)}{\Delta y} - \frac{H_y^n(i+1/2,j,k+1/2) - H_y^n(i+1/2,j,k-1/2)}{\Delta z}\right\} \tag{3.1a}$$

$$E_y^{n+1/2}(i,j+1/2,k) = E_y^n(i,j+1/2,k) + \frac{\Delta t}{2\varepsilon}\left\{\frac{H_x^{n+1/2}(i,j+1/2,k+1/2) - H_x^{n+1/2}(i,j+1/2,k-1/2)}{\Delta z} - \frac{H_z^n(i+1/2,j+1/2,k) - H_z^n(i-1/2,j+1/2,k)}{\Delta x}\right\} \tag{3.1b}$$

$$E_z^{n+1/2}(i,j,k+1/2) = E_z^n(i,j,k+1/2) + \frac{\Delta t}{2\varepsilon}\left\{\frac{H_y^{n+1/2}(i+1/2,j,k+1/2) - H_y^{n+1/2}(i-1/2,j,k+1/2)}{\Delta x} - \frac{H_x^n(i,j+1/2,k+1/2) - H_x^n(i,j-1/2,k+1/2)}{\Delta y}\right\} \tag{3.1c}$$

$$H_x^{n+1/2}(i,j+1/2,k+1/2) = H_x^n(i,j+1/2,k+1/2) - \frac{\Delta t}{2\mu}\left\{\frac{E_z^n(i,j+1,k+1/2) - E_z^n(i,j,k+1/2)}{\Delta y} - \frac{E_y^{n+1/2}(i,j+1/2,k+1) - E_y^{n+1/2}(i,j+1/2,k)}{\Delta z}\right\} \tag{3.2a}$$

$$H_y^{n+1/2}(i+1/2,j,k+1/2) = H_y^n(i+1/2,j,k+1/2) - \frac{\Delta t}{2\mu}\left\{\frac{E_x^n(i+1/2,j,k+1) - E_x^n(i+1/2,j,k)}{\Delta z} - \frac{E_z^{n+1/2}(i+1,j,k+1/2) - E_z^{n+1/2}(i,j,k+1/2)}{\Delta x}\right\} \tag{3.2b}$$

$$H_z^{n+1/2}(i+1/2,j+1/2,k) = H_z^n(i+1/2,j+1/2,k) - \frac{\Delta t}{2\mu}\left\{\frac{E_y^n(i+1,j+1/2,k) - E_y^n(i,j+1/2,k)}{\Delta x} - \frac{E_x^{n+1/2}(i+1/2,j+1,k) - E_x^{n+1/2}(i+1/2,j,k)}{\Delta y}\right\} \tag{3.2c}$$

Because of the unknown implicit terms on the RHS, equations (3.1) cannot be solved directly as in the conventional FDTD. To solve equations (3.1), the LHS electric fields have to be expressed such that the RHS terms are all known values. In other words, the RHS terms have to be in the form of previously calculated values. This can be accomplished by substituting equations (3.2) into (3.1) appropriately; specifically, substituting (3.2c) into (3.1a) results in (3.3) below. In equation (3.3), the LHS forms a tri-diagonal matrix of E_x when E_x is scanned in the $\hat{y}$ direction. The RHS of (3.3) now consists of only explicit, known terms. This tri-diagonal matrix is a sparse matrix that can be solved efficiently [2.6].

$$E_x^{n+1/2}(i+1/2,j-1,k) - E_x^{n+1/2}(i+1/2,j,k)\left[2 + \left(\frac{\sqrt{\mu\varepsilon}\,\Delta y}{\Delta t}\right)^2\right] + E_x^{n+1/2}(i+1/2,j+1,k)$$

$$= -E_x^n(i+1/2,j,k)\left(\frac{\sqrt{\mu\varepsilon}\,\Delta y}{\Delta t}\right)^2 + \left(\frac{\Delta y}{\Delta x}\right)\left[E_y^n(i+1,j+1/2,k) - E_y^n(i,j+1/2,k) - E_y^n(i+1,j-1/2,k) + E_y^n(i,j-1/2,k)\right]$$

$$-\left(\frac{\mu\Delta y}{\Delta t}\right)\left[H_z^n(i+1/2,j+1/2,k) - H_z^n(i+1/2,j-1/2,k)\right] + \left(\frac{\mu\Delta y^2}{\Delta t\Delta z}\right)\left[H_y^n(i+1/2,j,k+1/2) - H_y^n(i+1/2,j,k-1/2)\right] \tag{3.3}$$

E_y and E_z can be solved in a similar manner with the former resulting in a tri-diagonal matrix when scanned in the direction of $\hat{z}$ and the latter in $\hat{x}$ in procedure 1. Once all the electric fields are computed, the magnetic fields can be computed directly using (3.2a) – (3.2c).

Equations (3.4) – (3.5) show the numerical formulation for procedure 2 of the ADI-FDTD method. Those partial derivatives that were replaced with implicit approximations in procedure 1 are expressed in explicit approximations in procedure 2 and vice versa. The switching between the implicit and explicit expressions in the two half time steps gives rise to the name alternating-direction.

Procedure 2

$$E_x^{n+1}(i+1/2,j,k) = E_x^{n+1/2}(i+1/2,j,k) + \frac{\Delta t}{2\varepsilon}\left\{\frac{H_z^{n+1/2}(i+1/2,j+1/2,k) - H_z^{n+1/2}(i+1/2,j-1/2,k)}{\Delta y} - \frac{H_y^{n+1}(i+1/2,j,k+1/2) - H_y^{n+1}(i+1/2,j,k-1/2)}{\Delta z}\right\} \tag{3.4a}$$

$$E_y^{n+1}(i,j+1/2,k) = E_y^{n+1/2}(i,j+1/2,k) + \frac{\Delta t}{2\varepsilon}\left\{\frac{H_x^{n+1/2}(i,j+1/2,k+1/2) - H_x^{n+1/2}(i,j+1/2,k-1/2)}{\Delta z} - \frac{H_z^{n+1}(i+1/2,j+1/2,k) - H_z^{n+1}(i-1/2,j+1/2,k)}{\Delta x}\right\} \tag{3.4b}$$

$$E_z^{n+1}(i,j,k+1/2) = E_z^{n+1/2}(i,j,k+1/2) + \frac{\Delta t}{2\varepsilon}\left\{\frac{H_y^{n+1/2}(i+1/2,j,k+1/2) - H_y^{n+1/2}(i-1/2,j,k+1/2)}{\Delta x} - \frac{H_x^{n+1}(i,j+1/2,k+1/2) - H_x^{n+1}(i,j-1/2,k+1/2)}{\Delta y}\right\} \tag{3.4c}$$

$$H_x^{n+1}(i,j+1/2,k+1/2) = H_x^{n+1/2}(i,j+1/2,k+1/2) - \frac{\Delta t}{2\mu}\left\{\frac{E_z^{n+1}(i,j+1,k+1/2) - E_z^{n+1}(i,j,k+1/2)}{\Delta y} - \frac{E_y^{n+1/2}(i,j+1/2,k+1) - E_y^{n+1/2}(i,j+1/2,k)}{\Delta z}\right\} \tag{3.5a}$$

$$H_y^{n+1}(i+1/2,j,k+1/2) = H_y^{n+1/2}(i+1/2,j,k+1/2) - \frac{\Delta t}{2\mu}\left\{\frac{E_x^{n+1}(i+1/2,j,k+1) - E_x^{n+1}(i+1/2,j,k)}{\Delta z} - \frac{E_z^{n+1/2}(i+1,j,k+1/2) - E_z^{n+1/2}(i,j,k+1/2)}{\Delta x}\right\} \tag{3.5b}$$

$$H_z^{n+1}(i+1/2,j+1/2,k) = H_z^{n+1/2}(i+1/2,j+1/2,k) - \frac{\Delta t}{2\mu}\left\{\frac{E_y^{n+1}(i+1,j+1/2,k) - E_y^{n+1}(i,j+1/2,k)}{\Delta x} - \frac{E_x^{n+1/2}(i+1/2,j+1,k) - E_x^{n+1/2}(i+1/2,j,k)}{\Delta y}\right\} \tag{3.5c}$$

Again, substituting equation (3.5b) into (3.4a) and collecting the E_x terms on the left give rise to equation (3.6) below where all the RHS terms are explicit terms, i.e. known values. Repeating the same process over equations (3.4) leads to tri-diagonal matrices for E_x, E_y and E_z when the fields are scanned in the $\hat{z}$, $\hat{x}$ and $\hat{y}$ directions respectively. The full formulation of electric fields in both procedures 1 and 2 are in Appendix B1.

$$E_x^{n+1}(i+1/2,j,k-1) - E_x^{n+1}(i+1/2,j,k)\left[2 + \left(\frac{\sqrt{\mu\varepsilon}\Delta z}{\Delta t}\right)^2\right] + E_x^{n+1}(i+1/2,j,k+1)$$

$$= -E_x^{n+1/2}(i+1/2,j,k)\left(\frac{\sqrt{\mu\varepsilon}\Delta z}{\Delta t}\right)^2 + \left(\frac{\Delta z}{\Delta x}\right)\left[E_z^{n+1/2}(i+1,j,k+1/2) - E_z^{n+1/2}(i,j,k+1/2) - E_z^{n+1/2}(i+1,j,k-1/2) + E_z^{n+1/2}(i,j,k-1/2)\right]$$

$$-\left(\frac{\mu\Delta z}{\Delta t}\right)\left[H_y^{n+1/2}(i+1/2,j,k+1/2) - H_y^{n+1/2}(i+1/2,j,k-1/2)\right] + \left(\frac{\mu\Delta z^2}{\Delta t\Delta y}\right)\left[H_z^{n+1/2}(i+1/2,j+1/2,k) - H_z^{n+1/2}(i+1/2,j-1/2,k)\right] \tag{3.6}$$

3.3 Physical interpretation of three-dimensional ADI-FDTD method

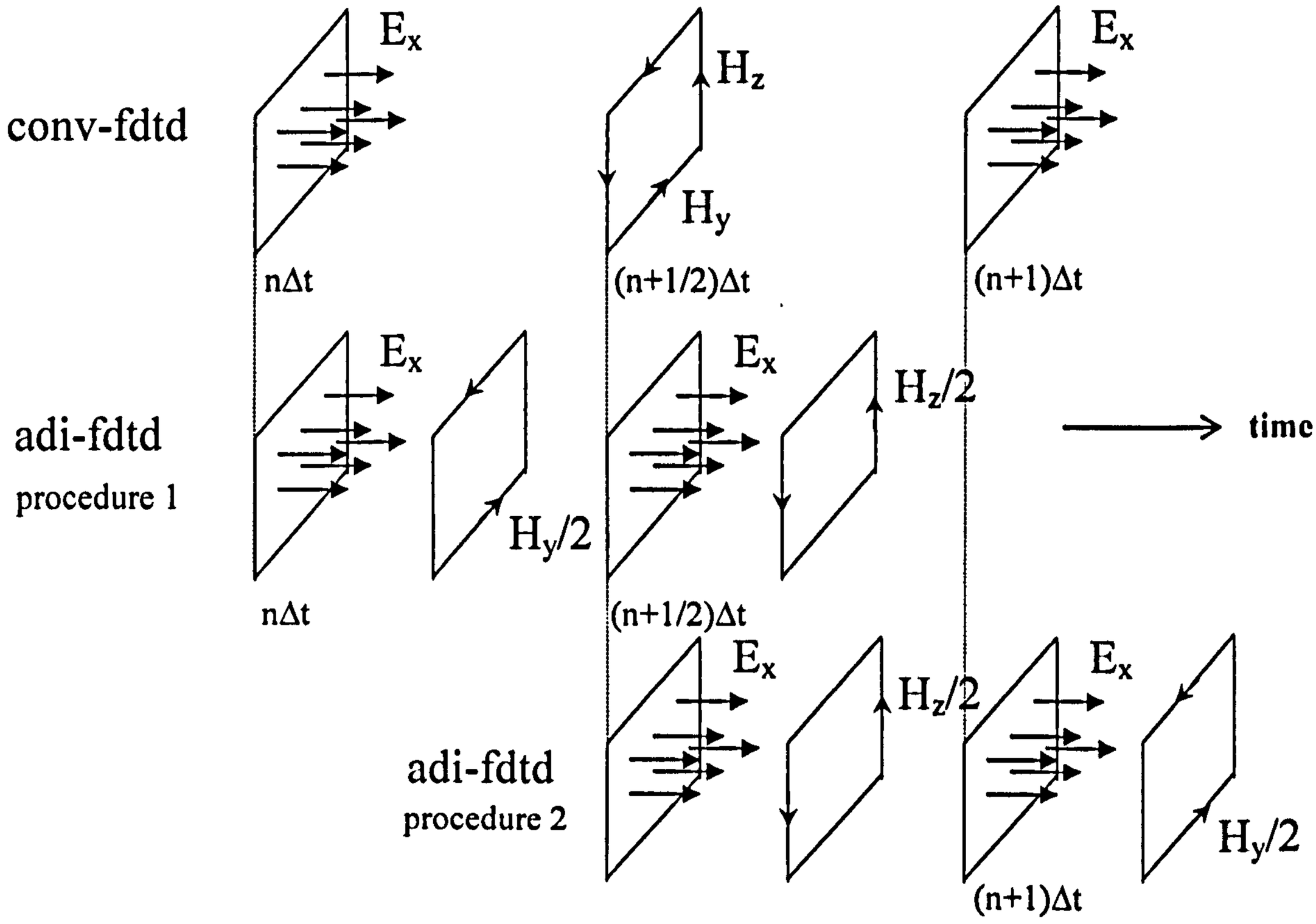

Fig. 3.1 : Comparison between conventional FDTD and ADI-FDTD

Fig. 3.1 above illustrates a physical representation of the ADI-FDTD formulation in comparison to its conventional FDTD counterpart. The diagram shows that in the conventional FDTD method, the electric field at time step $(n+1)\Delta t$ is calculated using the previously calculated electric field at time step $n\Delta t$ and the curl of the known (hence explicit) magnetic fields, H_y and H_z, at time step $(n+ \frac{1}{2})\Delta t$. In the ADI-FDTD method, an intermediate electric field is calculated at time step $(n+ \frac{1}{2})\Delta t$. In procedure 1 of the ADI-FDTD method, the electric field at time step $(n+ \frac{1}{2})\Delta t$ is calculated using, again, the previously calculated electric field at time step $n\Delta t$ and the curl of the magnetic fields. However, this time, half the curl is performed on the known (explicit) value, i.e. H_y at time step $n\Delta t$, and the other half of the curl is performed on the unknown (implicit) value, i.e. H_z at time step $(n+ \frac{1}{2})\Delta t$. This is immediately followed on by procedure 2 of the ADI-FDTD method; now the known (explicit) value of H_z at time step $(n+ \frac{1}{2})\Delta t$ and the unknown (implicit) value of H_y at time step $(n+1)\Delta t$ are used in the curl formulation. The total magnetic field over a full time step remains unchanged. Note that although the curl at each half time step is separated into two different time instances, it is still performed at a same point in space.

A further graphical illustration comparing implicit, explicit and ADI-FDTD methods with reference to the Runga-Kutta method is shown in Appendix C1.

3.4 Divergence of ADI-FDTD algorithm

As in the conventional FDTD algorithm, there is no explicit enforcement of the Gauss's Law relations for both the electric and magnetic fields as stated in (2.3) and (2.4) for source free regions in the ADI-FDTD algorithm. It is important that Gauss's Law is also observed in the ADI-FDTD algorithm. Although the curl operation of the magnetic fields is performed over two half time steps, the total magnetic field over a full time step remains unchanged in the ADI-FDTD scheme. Therefore, the ADI-FDTD algorithm will still satisfy equation (2.16), i.e. the time derivative of the net electric flux leaving the surfaces of a cubic Yee cell is zero, hence upholding the Gauss's Law for the electric field in charge-free space in the ADI-FDTD scheme.

3.5 Numerical stability

As in chapter two, numerical stability of the ADI-FDTD can be analysed using the standard von Neumann and Courant, Friedrich and Levy (CFL) method. Assuming the spatial frequency to be $\tilde{k}_x, \tilde{k}_y$ and $\tilde{k}_z$ as the x- , y- and z- components of its numerical wavevector respectively, the field components can be written as follows.

$$E_x^n(i+1/2, j, k) = E_x^n \exp\left\{-\mathrm{j}\left[\tilde{k}_x(i+1/2)\Delta x + \tilde{k}_y j\Delta y + \tilde{k}_z k\Delta z\right]\right\} \tag{3.7a}$$

$$E_y^n(i, j+1/2, k) = E_y^n \exp\left\{-\mathrm{j}\left[\tilde{k}_x i\Delta x + \tilde{k}_y(j+1/2)\Delta y + \tilde{k}_z k\Delta z\right]\right\} \tag{3.7b}$$

$$E_z^n(i, j, k+1/2) = E_z^n \exp\left\{-\mathrm{j}\left[\tilde{k}_x i\Delta x + \tilde{k}_y j\Delta y + \tilde{k}_z(k+1/2)\Delta z\right]\right\} \tag{3.7c}$$

$$H_x^n(i, j+1/2, k+1/2) = H_x^n \exp\left\{-\mathrm{j}\left[\tilde{k}_x i\Delta x + \tilde{k}_y(j+1/2)\Delta y + \tilde{k}_z(k+1/2)\Delta z\right]\right\} \tag{3.8a}$$

$$H_y^n(i+1/2, j, k+1/2) = H_y^n \exp\left\{-\mathrm{j}\left[\tilde{k}_x(i+1/2)\Delta x + \tilde{k}_y j\Delta y + \tilde{k}_z(k+1/2)\Delta z\right]\right\} \tag{3.8b}$$

$$H_z^n(i+1/2, j+1/2, k) = H_z^n \exp\left\{-\mathrm{j}\left[\tilde{k}_x(i+1/2)\Delta x + \tilde{k}_y(j+1/2)\Delta y + \tilde{k}_z k\Delta z\right]\right\} \tag{3.8c}$$

where n, i, j, k, Δx, Δy and Δz all have their usual meanings as defined earlier in chapter one.

3.5.1 2-dimensional ADI-FDTD

For the sake of simplicity, we consider first the numerical stability of a 2-dimensional TE wave consisting of the following fields :

Procedure 1

$$E_x^{n+1/2}(i+1/2, j) = E_x^n(i+1/2, j) + \frac{\Delta t}{2\varepsilon}\left\{\frac{H_z^{n+1/2}(i+1/2, j+1/2) - H_z^{n+1/2}(i+1/2, j-1/2)}{\Delta y}\right\} \tag{3.9a}$$

$$E_y^{n+1/2}(i, j+1/2) = E_y^n(i, j+1/2) - \frac{\Delta t}{2\varepsilon}\left\{\frac{H_z^n(i+1/2, j+1/2) - H_z^n(i-1/2, j+1/2)}{\Delta x}\right\} \tag{3.9b}$$

$$H_z^{n+1/2}(i+1/2, j+1/2) = H_z^n(i+1/2, j+1/2) - \frac{\Delta t}{2\mu}\left\{\begin{array}{l}\dfrac{E_y^n(i+1/2, j+1/2) - E_y^n(i, j+1/2)}{\Delta x} \\ -\dfrac{E_x^{n+1/2}(i+1/2, j+1) - E_x^{n+1/2}(i+1/2, j)}{\Delta y}\end{array}\right\} \tag{3.9c}$$

Substituting (3.7a), (3.7b) and (3.8c) into (3.9) yields the following :

$$E_x * GF1 = E_x - GF1 * H_z \frac{\Delta t}{2\varepsilon\Delta y} 2j \sin\left(\frac{\tilde{k}_y \Delta y}{2}\right) \tag{3.10a}$$

$$E_y * GF1 = E_y + H_z \frac{\Delta t}{2\varepsilon\Delta x} 2j \sin\left(\frac{\tilde{k}_x \Delta x}{2}\right) \tag{3.10b}$$

$$H_z * GF1 = H_z + E_y \frac{\Delta t}{2\mu\Delta x} 2j \sin\left(\frac{\tilde{k}_x \Delta x}{2}\right) - GF1 * E_x \frac{\Delta t}{2\mu\Delta y} 2j \sin\left(\frac{\tilde{k}_y \Delta y}{2}\right) \tag{3.10c}$$

where *GF1* is the growth factor in procedure 1. Substituting (3.10a) and (3.10b) into (3.10c) gives :

$$H_z * GF1 = H_z + \frac{H_z \frac{\Delta t}{2\varepsilon\Delta x} 2j \sin\left(\frac{\tilde{k}_x \Delta x}{2}\right) \frac{\Delta t}{2\mu\Delta x} 2j \sin\left(\frac{\tilde{k}_x \Delta x}{2}\right)}{GF1 - 1} + \frac{GF1 * GF1 * H_z \frac{\Delta t}{2\varepsilon\Delta y} 2j \sin\left(\frac{\tilde{k}_y \Delta y}{2}\right) \frac{\Delta t}{2\mu\Delta y} 2j \sin\left(\frac{\tilde{k}_y \Delta y}{2}\right)}{GF1 - 1} \tag{3.11}$$

$$H_z(GF1-1)^2 = -H_z\left(\frac{1}{\mu\varepsilon}\right)\left[\frac{\Delta t}{\Delta x}\sin\left(\frac{\tilde{k}_x \Delta x}{2}\right)\right]^2 - GF1^2 H_z\left(\frac{1}{\mu\varepsilon}\right)\left[\frac{\Delta t}{\Delta y}\sin\left(\frac{\tilde{k}_y \Delta y}{2}\right)\right]^2 \tag{3.12}$$

Let $M_x = \frac{\Delta t}{\Delta x}\sin\left(\frac{\tilde{k}_x \Delta x}{2}\right)$ and $M_y = \frac{\Delta t}{\Delta y}\sin\left(\frac{\tilde{k}_y \Delta y}{2}\right)$

and dividing (3.12) by H_z

$$GF1^2\left(1+\frac{M_y^2}{\mu\varepsilon}\right) - 2GF1 + \left(1+\frac{M_x^2}{\mu\varepsilon}\right) = 0 \tag{3.13}$$

Let $a = \left(1+\frac{M_y^2}{\mu\varepsilon}\right)$ and $c = \left(1+\frac{M_x^2}{\mu\varepsilon}\right)$

then (3.13) becomes

$$a\,GF1^2 - 2\,GF1 + c = 0 \tag{3.14}$$

$$GF1 = \frac{1 \pm \sqrt{1-ac}}{a}$$

and since $0 \leq \sin^2 p \leq 1$, then $ac \geq 1$

$$\therefore \quad GF1 = \frac{1 \pm j\sqrt{ac-1}}{a} \tag{3.15}$$

Procedure 2

$$E_x^{n+1}(i+1/2, j) = E_x^{n+1/2}(i+1/2, j) + \frac{\Delta t}{2\varepsilon}\left\{\frac{H_z^{n+1/2}(i+1/2, j+1/2) - H_z^{n+1/2}(i+1/2, j-1/2)}{\Delta y}\right\} \tag{3.16a}$$

$$E_y^{n+1}(i, j+1/2) = E_y^{n+1/2}(i, j+1/2) - \frac{\Delta t}{2\varepsilon}\left\{\frac{H_z^{n+1}(i+1/2, j+1/2) - H_z^{n+1}(i-1/2, j+1/2)}{\Delta x}\right\} \tag{3.16b}$$

$$H_z^{n+1}(i+1/2, j+1/2) = H_z^{n+1/2}(i+1/2, j+1/2) - \frac{\Delta t}{2\mu}\left\{\begin{array}{l}\dfrac{E_y^{n+1}(i+1/2, j+1/2) - E_y^{n+1}(i, j+1/2)}{\Delta x} \\ -\dfrac{E_x^{n+1/2}(i+1/2, j+1) - E_x^{n+1/2}(i+1/2, j)}{\Delta y}\end{array}\right\} \tag{3.16c}$$

Again, substituting (3.7a), (3.7b) and (3.8c) into (3.16) will yield the following :

$$E_x * GF2 = E_x - H_z \frac{\Delta t}{2\varepsilon \Delta y} 2j \sin\left(\frac{\tilde{k}_y \Delta y}{2}\right) \tag{3.17a}$$

$$E_y * GF2 = E_y + GF2 * H_z \frac{\Delta t}{2\varepsilon \Delta x} 2j \sin\left(\frac{\tilde{k}_x \Delta x}{2}\right) \tag{3.17b}$$

$$H_z * GF2 = H_z + GF2 * E_y \frac{\Delta t}{2\mu \Delta x} 2j \sin\left(\frac{\tilde{k}_x \Delta x}{2}\right) - E_x \frac{\Delta t}{2\mu \Delta y} 2j \sin\left(\frac{\tilde{k}_y \Delta y}{2}\right) \tag{3.17c}$$

where *GF2* is the growth factor in procedure 2. Applying the same technique on procedure 2, we get,

$$GF1^2\left(1 + \frac{M_x^2}{\mu\varepsilon}\right) - 2GF1 + \left(1 + \frac{M_y^2}{\mu\varepsilon}\right) = 0 \tag{3.18}$$

$$\therefore \quad GF2 = \frac{1 \pm j\sqrt{ac-1}}{c} \tag{3.19}$$

Therefore, the total growth factor of procedures 1 and 2 combined is given by :

$$\begin{aligned} GF &= |GF1| * |GF2| \\ &= \sqrt{\frac{c}{a}} * \sqrt{\frac{a}{c}} \\ &= 1 \end{aligned} \tag{3.20}$$

Since the overall growth factor of the 2-dimensional ADI-FDTD is unity, the system is said to be unconditionally stable [1.14]. However, if we note carefully, the growth factor (3.20) or the gain of the ADI-FDTD system, is exactly unity; potentially any slight increase in the growth factor due to any truncation errors may cause the system to go unstable. This 'exact' phenomenon is discussed in more detail in [1.17].

3.5.2 3-dimensional ADI-FDTD

To analyse the numerical stability of a three dimensional ADI-FDTD, we apply von Neumann method again on the three dimensional ADI-FDTD formulations (3.1) – (3.4). Denoting all the electric and magnetic fields as X matrix, procedure 1 can be written in the form :

$$X^{n+1/2} = GF1 * X^{n} \tag{3.21}$$

and procedure 2 as

$$X^{n+1} = GF2 * X^{n+1/2} \tag{3.22}$$

The overall growth factor for the proposed scheme is then given by :

$$GF = |GF1| * |GF2| \tag{3.23}$$

where

$$GF1 = \begin{bmatrix} \frac{1}{Ny} & \frac{Mx\cdot My}{Ny\cdot\mu\cdot\varepsilon} & 0 & 0 & \frac{-j\cdot Mz}{Ny\cdot\varepsilon} & \frac{j\cdot My}{Ny\cdot\varepsilon} \\ 0 & \frac{1}{Nz} & \frac{My\cdot Mz}{Nz\cdot\mu\cdot\varepsilon} & \frac{j\cdot Mz}{Nz\cdot\varepsilon} & 0 & \frac{-j\cdot Mx}{Nz\cdot\varepsilon} \\ \frac{Mx\cdot Mz}{Nx\cdot\mu\cdot\varepsilon} & 0 & \frac{1}{Nx} & \frac{-j\cdot My}{Nx\cdot\varepsilon} & \frac{j\cdot Mx}{Nx\cdot\varepsilon} & 0 \\ 0 & \frac{j\cdot Mz}{Nz\cdot\mu} & \frac{-j\cdot My}{Nz\cdot\mu} & \frac{1}{Nz} & 0 & \frac{Mx\cdot Mz}{Nz\cdot\mu\cdot\varepsilon} \\ \frac{-j\cdot Mz}{Nx\cdot\mu} & 0 & \frac{j\cdot Mx}{Nx\cdot\mu} & \frac{Mx\cdot My}{Nx\cdot\mu\cdot\varepsilon} & \frac{1}{Nx} & 0 \\ \frac{j\cdot My}{Ny\cdot\mu} & \frac{-j\cdot Mx}{Ny\cdot\mu} & 0 & 0 & \frac{My\cdot Mz}{Ny\cdot\mu\cdot\varepsilon} & \frac{1}{Ny} \end{bmatrix} \tag{3.24}$$

and

$$GF2 = \begin{bmatrix} \frac{1}{Nz} & 0 & \frac{Mx\cdot Mz}{Nz\cdot\mu\cdot\varepsilon} & 0 & \frac{-j\cdot Mz}{Nz\cdot\varepsilon} & \frac{j\cdot My}{Nz\cdot\varepsilon} \\ \frac{Mx\cdot My}{Nx\cdot\mu\cdot\varepsilon} & \frac{1}{Nx} & 0 & \frac{j\cdot Mz}{Nz\cdot\varepsilon} & 0 & \frac{-j\cdot Mx}{Nz\cdot\varepsilon} \\ 0 & \frac{My\cdot Mz}{Ny\cdot\mu\cdot\varepsilon} & \frac{1}{Ny} & \frac{-j\cdot My}{Ny\cdot\varepsilon} & \frac{j\cdot Mx}{Ny\cdot\varepsilon} & 0 \\ 0 & \frac{j\cdot Mz}{Ny\cdot\mu} & \frac{-j\cdot My}{Ny\cdot\mu} & \frac{1}{Ny} & \frac{Mx\cdot My}{Ny\cdot\mu\cdot\varepsilon} & 0 \\ \frac{-j\cdot Mz}{Nz\cdot\mu} & 0 & \frac{j\cdot Mx}{Nz\cdot\mu} & 0 & \frac{1}{Nz} & \frac{My\cdot Mz}{Nz\cdot\mu\cdot\varepsilon} \\ \frac{j\cdot My}{Nx\cdot\mu} & \frac{-j\cdot Mx}{Nx\cdot\mu} & 0 & 0 & \frac{Mx\cdot Mz}{Nx\cdot\mu\cdot\varepsilon} & \frac{1}{Nx} \end{bmatrix} \tag{3.25}$$

where

$$M_h = \frac{\Delta t}{\Delta h}\sin\left(\frac{k_h \Delta h}{2}\right) \qquad \text{and} \qquad N_h = 1 + \frac{M_h^2}{\mu\varepsilon} \qquad h = x, y, z \tag{3.26}$$

It has been shown [1.18] that the eigenvalues of GF all have magnitudes of unity. Again, with the theoretical gain of unity, the three dimensional ADI-FDTD is said to be unconditionally stable.

3.6 Numerical dispersion

The numerical dispersion for the ADI-FDTD method can be found by substituting the vector-field travelling-wave expression with time dependence shown below into the ADI-FDTD finite-difference equations .

$$E_x^n(i+1/2, j, k) = E_x \exp\left\{j\omega n\Delta t - j\left[\tilde{k}_x(i+1/2)\Delta x + \tilde{k}_y j\Delta y + \tilde{k}_z k\Delta z\right]\right\} \tag{3.27a}$$

$$E_y^n(i, j+1/2, k) = E_y \exp\left\{j\omega n\Delta t - j\left[\tilde{k}_x i\Delta x + \tilde{k}_y(j+1/2)\Delta y + \tilde{k}_z k\Delta z\right]\right\} \tag{3.27b}$$

$$H_z^n(i+1/2, j+1/2, k) = H_z \exp\left\{j\omega n\Delta t - j\left[\tilde{k}_x(i+1/2)\Delta x + \tilde{k}_y(j+1/2)\Delta y + \tilde{k}_z k\Delta z\right]\right\} \tag{3.27c}$$

3.6.1 2-dimensional ADI-FDTD

Again, for simplicity, we investigate the numerical dispersion of a 2-dimensional TE wave [1.19].

Substituting (3.27) into (3.9) (procedure 1) gives :

$$(e^{j\omega\Delta t/2} - 1)\, E_x^n = -j\left(\frac{\Delta t}{\varepsilon\,\Delta y}\right)\sin\left(\frac{\tilde{k}_y\Delta y}{2}\right) e^{j\omega\Delta t/2}\, H_z^n \tag{3.28a}$$

$$(e^{j\omega\Delta t/2} - 1)\, E_y^n = j\left(\frac{\Delta t}{\varepsilon\,\Delta x}\right)\sin\left(\frac{\tilde{k}_x\Delta x}{2}\right) H_z^n \tag{3.28b}$$

$$(e^{j\omega\Delta t/2} - 1)\, H_z^n = j\left(\frac{\Delta t}{\mu\,\Delta x}\right)\sin\left(\frac{\tilde{k}_x\Delta x}{2}\right) E_y^n - j\left(\frac{\Delta t}{\mu\,\Delta y}\right)\sin\left(\frac{\tilde{k}_y\Delta y}{2}\right) e^{j\omega\Delta t/2}\, E_x^n \tag{3.28c}$$

and into (3.16) (procedure 2) gives :

$$(e^{j\omega\Delta t} - e^{j\omega\Delta t/2})\, E_x^n = -j\left(\frac{\Delta t}{\varepsilon\,\Delta y}\right)\sin\left(\frac{\tilde{k}_y\Delta y}{2}\right) e^{j\omega\Delta t/2}\, H_z^n \tag{3.29a}$$

$$(e^{j\omega\Delta t} - e^{j\omega\Delta t/2})\, E_y^n = j\left(\frac{\Delta t}{\varepsilon\,\Delta x}\right)\sin\left(\frac{\tilde{k}_x\Delta x}{2}\right) e^{j\omega\Delta t}\, H_z^n \tag{3.29b}$$

$$(e^{j\omega\Delta t} - e^{j\omega\Delta t/2})\, H_z^n = j\left(\frac{\Delta t}{\mu\,\Delta x}\right)\sin\left(\frac{\tilde{k}_x\Delta x}{2}\right) e^{j\omega\Delta t}\, E_y^n - j\left(\frac{\Delta t}{\mu\,\Delta y}\right)\sin\left(\frac{\tilde{k}_y\Delta y}{2}\right) e^{j\omega\Delta t/2}\, E_x^n \tag{3.29c}$$

Combining (3.28a) & (3.29a), (3.28b) & (3.29b) and (3.28c) & (3.29c) gives rise to the following :

$$(e^{j\omega\Delta t} - 1)\, E_x^n = -2j\left(\frac{\Delta t}{\varepsilon\,\Delta y}\right)\sin\left(\frac{\tilde{k}_y \Delta y}{2}\right) e^{j\omega\Delta t/2}\, H_z^n \tag{3.30a}$$

$$(e^{j\omega\Delta t} - 1)\, E_y^n = j\left(\frac{\Delta t}{\varepsilon\,\Delta x}\right)\sin\left(\frac{\tilde{k}_x \Delta x}{2}\right)\left(e^{j\omega\Delta t} + 1\right) H_z^n \tag{3.30b}$$

$$(e^{j\omega\Delta t} - 1)\, H_z^n = j\left(\frac{\Delta t}{\mu\,\Delta x}\right)\sin\left(\frac{\tilde{k}_x \Delta x}{2}\right)\left(e^{j\omega\Delta t} + 1\right) E_y^n - 2j\left(\frac{\Delta t}{\mu\,\Delta y}\right)\sin\left(\frac{\tilde{k}_y \Delta y}{2}\right) e^{j\omega\Delta t/2}\, E_x^n \tag{3.30c}$$

(3.30) can be simplified to :

$$\sin\left(\frac{\omega\Delta t}{2}\right) E_x^n = -\left(\frac{\Delta t}{\varepsilon\,\Delta y}\right)\sin\left(\frac{\tilde{k}_y \Delta y}{2}\right) H_z^n \tag{3.31a}$$

$$\sin\left(\frac{\omega\Delta t}{2}\right) E_y^n = \left(\frac{\Delta t}{\varepsilon\,\Delta x}\right)\sin\left(\frac{\tilde{k}_x \Delta x}{2}\right)\cos\left(\frac{\omega\Delta t}{2}\right) H_z^n \tag{3.31b}$$

$$\sin\left(\frac{\omega\Delta t}{2}\right) H_z^n = \left(\frac{\Delta t}{\mu\,\Delta x}\right)\sin\left(\frac{\tilde{k}_x \Delta x}{2}\right)\cos\left(\frac{\omega\Delta t}{2}\right) E_y^n - \left(\frac{\Delta t}{\mu\,\Delta y}\right)\sin\left(\frac{\tilde{k}_y \Delta y}{2}\right) E_x^n \tag{3.31c}$$

or

$$\begin{bmatrix} \sin\left(\frac{\omega\Delta t}{2}\right) & 0 & \left(\frac{\Delta t}{\varepsilon\,\Delta y}\right)\sin\left(\frac{\tilde{k}_y \Delta y}{2}\right) \\ 0 & \sin\left(\frac{\omega\Delta t}{2}\right) & -\left(\frac{\Delta t}{\varepsilon\,\Delta x}\right)\sin\left(\frac{\tilde{k}_x \Delta x}{2}\right)\cos\left(\frac{\omega\Delta t}{2}\right) \\ \left(\frac{\Delta t}{\mu\,\Delta y}\right)\sin\left(\frac{\tilde{k}_y \Delta y}{2}\right) & -\left(\frac{\Delta t}{\mu\,\Delta x}\right)\sin\left(\frac{\tilde{k}_x \Delta x}{2}\right)\cos\left(\frac{\omega\Delta t}{2}\right) & \sin\left(\frac{\omega\Delta t}{2}\right) \end{bmatrix} \begin{bmatrix} E_x^n \\ E_y^n \\ H_z^n \end{bmatrix} = 0 \tag{3.32}$$

Thus the numerical dispersion relation for a 2-dimensional TE wave is given by making the determinant of the matrix zero, i.e.

$$\begin{aligned} \sin\left(\frac{\omega\Delta t}{2}\right)\left\{\sin^2\left(\frac{\omega\Delta t}{2}\right) - \frac{1}{\mu\varepsilon}\left(\frac{\Delta t}{\Delta x}\right)^2 \sin^2\left(\frac{\tilde{k}_x \Delta x}{2}\right)\cos^2\left(\frac{\omega\Delta t}{2}\right)\right\} \\ + \sin\left(\frac{\omega\Delta t}{2}\right)\left\{-\frac{1}{\mu\varepsilon}\left(\frac{\Delta t}{\Delta y}\right)^2 \sin^2\left(\frac{\tilde{k}_y \Delta y}{2}\right)\right\} = 0 \end{aligned} \tag{3.33}$$

or

$$\left(\frac{1}{\Delta x}\right)^2 \sin^2\left(\frac{\tilde{k}_x \Delta x}{2}\right)\cos^2\left(\frac{\omega\Delta t}{2}\right) + \left(\frac{1}{\Delta y}\right)^2 \sin^2\left(\frac{\tilde{k}_y \Delta y}{2}\right) = \left(\frac{1}{c\Delta t}\right)^2 \sin^2\left(\frac{\omega\Delta t}{2}\right) \tag{3.34}$$

where $c = 1/\sqrt{\mu\,\varepsilon}$.

Comparing (3.34), the dispersion relation for a 2-dimensional ADI-FDTD with the known numerical dispersion relation for a 2-dimensional FDTD :

$$\left(\frac{1}{\Delta x}\right)^2 \sin^2\left(\frac{\tilde{k}_x \Delta x}{2}\right) + \left(\frac{1}{\Delta y}\right)^2 \sin^2\left(\frac{\tilde{k}_y \Delta y}{2}\right) = \left(\frac{1}{c\Delta t}\right)^2 \sin^2\left(\frac{\omega \Delta t}{2}\right) \tag{3.35}$$

it can be seen that there is a difference of a factor of $\cos^2\left(\frac{\omega \Delta t}{2}\right)$ in one of the left-hand-side terms, i.e. the term with numerical wavenumber $\tilde{k}_x$. The dispersion equation (3.34) was derived from the 2D ADI-FDTD equations of (3.9) & (3.16). In procedure 1, (3.9), the H_z field was calculated using explicit E_y and implicit E_x while in procedure 2, (3.16) the H_z field was calculated from implicit E_y and explicit E_x. According to Peaceman and Rachford [1.13], the ADI method remains unconditionally stable so long as the two procedures are repeated over the same time step, one after another. Indeed, there is nothing to stop us writing out the 2D ADI-FDTD equations with the implicit and explicit terms interchanged. In such a case, the factor $\cos^2\left(\frac{\omega \Delta t}{2}\right)$ will be imposed on the numerical wavenumber $\tilde{k}_y$ rather than $\tilde{k}_x$.

The additional factor in (3.34) means that the variation in the numerical phase velocity due to numerical dispersion for the ADI-FDTD scheme changes in a non-uniform manner, depending on the direction of wave propagation, as the time-step, Δt, is increased. Consider (3.34), where the $\cos^2\left(\frac{\omega \Delta t}{2}\right)$ factor is imposed on $\tilde{k}_x$. For wave propagating in the direction of x, $\tilde{k}_y = 0$, then the numerical wave velocity is reduced from that of the standard FDTD scheme due to the factor $\cos^2\left(\frac{\omega \Delta t}{2}\right)$. On the other hand, for wave propagating in the direction of y, $\tilde{k}_x = 0$, then the numerical wave velocity in the ADI-FDTD scheme is the same as that of the standard FDTD scheme [1.19].

3.7 Implementation of 1st order Mur absorbing boundary condition

The second approximation of the 1st order Mur absorbing boundary condition (2.55) is applied to the ADI-FDTD algorithm. The implementation of the absorbing boundary condition is shown here in two ways. The first way is to implement the absorbing boundary condition simultaneously within the tri-diagonal matrix when the rest of the fields are calculated and the second way is to implement the absorbing boundary condition recursively after the other internal fields are found by solving the tri-diagonal matrix. Although the first way may seem easier to implement, it is indeed an incomplete way. Despite this, the author feels it is necessary to describe this incomplete approach and explain why it can lead to incorrect results.

3.7.1 Boundary condition within the tri-diagonal matrix

The first method is to apply the boundary condition as part of the tri-diagonal matrix so that all fields within the computational boundary are computed when the matrix is scanned through in each direction.

To illustrate the implementation of the absorbing boundary condition with the tri-diagonal matrix, the tri-diagonal matrix of (3.5) and the 1st order Mur absorbing boundary equation (2.55) are repeated below.

$$E_x^{n+1/2}(i+1/2,j-1,k) - E_x^{n+1/2}(i+1/2,j,k)\left[2+\left(\frac{\sqrt{\mu\varepsilon}\,\Delta y}{\Delta t}\right)^2\right] + E_x^{n+1/2}(i+1/2,j+1,k)$$

$$= -E_x^n(i+1/2,j,k)\left(\frac{\sqrt{\mu\varepsilon}\,\Delta y}{\Delta t}\right)^2 + \left(\frac{\Delta y}{\Delta x}\right)\left[E_y^n(i+1,j+1/2,k) - E_y^n(i,j+1/2,k) - E_y^n(i+1,j-1/2,k) + E_y^n(i,j-1/2,k)\right]$$

$$-\left(\frac{\mu\Delta y}{\Delta t}\right)\left[H_z^n(i+1/2,j+1/2,k) - H_z^n(i+1/2,j-1/2,k)\right] + \left(\frac{\mu\Delta y^2}{\Delta t\Delta z}\right)\left[H_y^n(i+1/2,j,k+1/2) - H_y^n(i+1/2,j,k-1/2)\right] \quad (3.36)$$

Let $$b = -\left[2+\left(\frac{\sqrt{\mu\varepsilon}\,\Delta y}{\Delta t}\right)^2\right]$$

1st order Mur absorbing boundary equation is given by :

$$E_0^{n+1} = E_1^n + \left(\frac{v\Delta t - \Delta x}{v\Delta t + \Delta x}\right)\left(E_1^{n+1} - E_0^n\right) \quad (3.37)$$

Now, let $$\text{Mur\_x} = \left(\frac{v\Delta t - \Delta x}{v\Delta t + \Delta x}\right)$$

and re-arranging (3.37), we get

$$E_0^{n+1} - (\text{Mur\_x} \,.\, E_1^{n+1}) = E_1^n - (\text{Mur\_x} \,.\, E_0^n) \quad (3.38)$$

Let all the terms on the right hand side of (3.36) be known as 'rhs' and for the purpose of this illustration, we shall consider only six spatial steps in the y-direction. Now, incorporating (3.38) into the tri-diagonal matrix (3.36) gives us a tri-diagonal matrix of the form below.

$$\begin{bmatrix} 1 & -\text{Mur\_x} & 0 & 0 & 0 & 0 \\ 1 & b & 1 & 0 & 0 & 0 \\ 0 & 1 & b & 1 & 0 & 0 \\ 0 & 0 & 1 & b & 1 & 0 \\ 0 & 0 & 0 & 1 & b & 1 \\ 0 & 0 & 0 & 0 & -\text{Mur\_x} & 1 \end{bmatrix} \begin{bmatrix} E_x^{n+1/2}(i+1/2,0,k) \\ E_x^{n+1/2}(i+1/2,1,k) \\ E_x^{n+1/2}(i+1/2,2,k) \\ E_x^{n+1/2}(i+1/2,3,k) \\ E_x^{n+1/2}(i+1/2,4,k) \\ E_x^{n+1/2}(i+1/2,5,k) \end{bmatrix} = \begin{bmatrix} E_1^n - (\text{Mur\_x} \,.\, E_0^n) \\ \text{rhs at j} = 1 \\ \text{rhs at j} = 2 \\ \text{rhs at j} = 3 \\ \text{rhs at j} = 4 \\ E_4^n - (\text{Mur\_x} \,.\, E_5^n) \end{bmatrix} \quad (3.39)$$

The same can be applied for E_y & E_z in procedure 1 and then all the electric fields in procedure 2. However, upon close observation of the matrices, one can identify a problem with this method of implementation. In procedure 1, only one out of the two normal incident fields at each boundary is implemented as a one-way wave equation. In procedure 1, E_x, sees absorbing boundaries at the y-direction boundaries, E_y at the z-direction boundaries and E_z at the x-direction boundaries. Then in procedure 2, E_x is 'absorbed' at z-direction boundaries, E_y at x-direction boundaries and E_z at y-direction boundaries. This is an incomplete implementation as all normal incident fields should see the appropriate absorbing boundaries for both procedures 1 and 2 at each half time step. Therefore, although at first sight it may seem simpler to implement the absorbing boundary condition simultaneously within the tri-diagonal

matrix, this method can in fact lead to incorrect results. This problem can be resolved if the other half of the normal incident fields that are not implemented as a one-way wave equation within the tri-diagonal matrix are recursively calculated separately from the tri-diagonal matrix.

3.7.2 Boundary condition outside the tri-diagonal matrix

The second method is to initially solve the tri-diagonal matrix for all the fields in the computational domain except for those at the boundaries. The field values at the absorbing boundaries are then calculated recursively using the field values found from solving the tri-diagonal matrix. These boundary field terms, however, have to be taken into account within the tri-diagonal matrix. For consistency, six spatial steps in the y-direction are used. This gives rise to only four internal fields excluding the fields at the absorbing boundaries. First, we write the tri-diagonal matrix for the four internal fields.

$$\begin{bmatrix} b & 1 & 0 & 0 \\ 1 & b & 1 & 0 \\ 0 & 1 & b & 1 \\ 0 & 0 & 1 & b \end{bmatrix} \begin{bmatrix} E_x^{n+1/2}(i+1/2,1,k) \\ E_x^{n+1/2}(i+1/2,2,k) \\ E_x^{n+1/2}(i+1/2,3,k) \\ E_x^{n+1/2}(i+1/2,4,k) \end{bmatrix} = \begin{bmatrix} \text{rhs at j} = 1 \\ \text{rhs at j} = 2 \\ \text{rhs at j} = 3 \\ \text{rhs at j} = 4 \end{bmatrix} \tag{3.40}$$

Incidentally, (3.40) is the final tri-diagonal matrix to be solved if the computational boundary is a perfect electric wall boundary.

To include the fields at the absorbing boundaries, we re-write (3.40) to give :

$$\begin{bmatrix} b & 1 & 0 & 0 \\ 1 & b & 1 & 0 \\ 0 & 1 & b & 1 \\ 0 & 0 & 1 & b \end{bmatrix} \begin{bmatrix} E_x^{n+1/2}(i+1/2,1,k) \\ E_x^{n+1/2}(i+1/2,2,k) \\ E_x^{n+1/2}(i+1/2,3,k) \\ E_x^{n+1/2}(i+1/2,4,k) \end{bmatrix} = \begin{bmatrix} (\text{rhs at j} = 1) - E_x^{n+1/2}(i+1/2,0,k) \\ \text{rhs at j} = 2 \\ \text{rhs at j} = 3 \\ (\text{rhs at j} = 4) - E_x^{n+1/2}(i+1/2,5,k) \end{bmatrix} \tag{3.41}$$

Now, re-arranging the 1st order Mur absorbing boundary condition,

$$E_0^{n+1/2} = E_1^n - (\text{Mur\_x} \cdot E_0^n) - (\text{Mur\_x} \cdot E_1^{n+1/2}) \tag{3.42}$$

Substituting (3.42) into (3.41) and re-arranging (3.41) to have the n+1/2 terms on the LHS gives us :

$$\begin{bmatrix} b+\text{Mur\_x} & 1 & 0 & 0 \\ 1 & b & 1 & 0 \\ 0 & 1 & b & 1 \\ 0 & 0 & 1 & b+\text{Mur\_x} \end{bmatrix} \begin{bmatrix} E_x^{n+1/2}(i+1/2,1,k) \\ E_x^{n+1/2}(i+1/2,2,k) \\ E_x^{n+1/2}(i+1/2,3,k) \\ E_x^{n+1/2}(i+1/2,4,k) \end{bmatrix} = \begin{bmatrix} (\text{rhs at j} = 1) - E_1^n + (\text{Mur\_x}.E_0^n) \\ \text{rhs at j} = 2 \\ \text{rhs at j} = 3 \\ (\text{rhs at j} = 4) - E_4^n + (\text{Mur\_x}.E_5^n) \end{bmatrix} \tag{3.43}$$

The same can be applied for E_y & E_z in procedure 1 and then all the electric fields in procedure 2. With this method of implementation, the fields at the absorbing boundaries have to be calculated separately from the tri-diagonal matrix. This can be done recursively after the internal fields of the computational

domain are obtained. In all simulations using the ADI-FDTD method, the 1st order Mur absorbing boundary condition is implemented using this technique.

3.8 Simulated results

Several different models were simulated to show the application of the ADI-FDTD method. Even though the ADI-FDTD method will see its time-saving benefit most in a model where there is a variety of mesh sizes, for the purpose of showing the application of the ADI-FDTD method, a regular finite-difference mesh has been used in all the following models. This means that the worst case has been modelled when the stability factor is increased beyond the CFL constraint. Since in the ADI-FDTD method the time step is no longer restricted by the CFL criterion (2.33), the time step Δt, can be set to be greater than the maximum allowed by the CFL criterion modified below by including the stability factor term.

$$\Delta t = \frac{\text{stability factor}}{v\sqrt{\frac{1}{\Delta x^2} + \frac{1}{\Delta y^2} + \frac{1}{\Delta z^2}}} \tag{3.44}$$

where a stability factor of 1.0 implies the maximum Δt as allowed by the CFL constraint.

In all structures simulated below, the conductor is treated as a perfect electric wall boundary. The dielectric is modelled in the same way as in the conventional FDTD method described in chapter 2 and a Gaussian source is used for excitation.

Initially all fields are set to zero. As time-marching progresses, the sequence of the implemented algorithm is as follows :

Procedure 1:

- $\vec{E}$ fields are calculated by solving the tri-diagonal matrices, one of which is (3.5)
- tangential $\vec{E}$ fields are set to zero on the metallized patch
- tangential $\vec{E}$ fields on the computational boundaries are calculated using the Mur's 1st order absorbing boundary condition (2.55)
- the vertical electric field is excited with Gaussian pulse below the strip
- $\vec{H}$ fields are calculated using (3.2)
- electric and magnetic field values are stored for later use in absorbing boundary condition calculation and for field calculations in procedure 2
- the time step is incremented by half Δt

Procedure 2:

- $\vec{E}$ fields are calculated by solving the tri-diagonal matrices, one of which is (3.6)
- tangential $\vec{E}$ fields are set to zero on the metallized patch

- tangential $\vec{E}$ fields on the computational boundaries are calculated using the Mur's 1st order absorbing boundary condition (2.55)
- $\vec{H}$ fields are calculated using (3.4)
- electric and magnetic field values are stored for later use in absorbing boundary condition calculation and for field calculations in procedure 1
- the time step is incremented by half Δt

To model a cavity, the calculation of the tangential $\vec{E}$ fields on the computational boundaries is left out because by solving the tri-diagonal matrix in the form of (3.40), a perfect electric wall boundary on the computational domain is automatically assumed.

3.8.1 Three-dimensional cavity

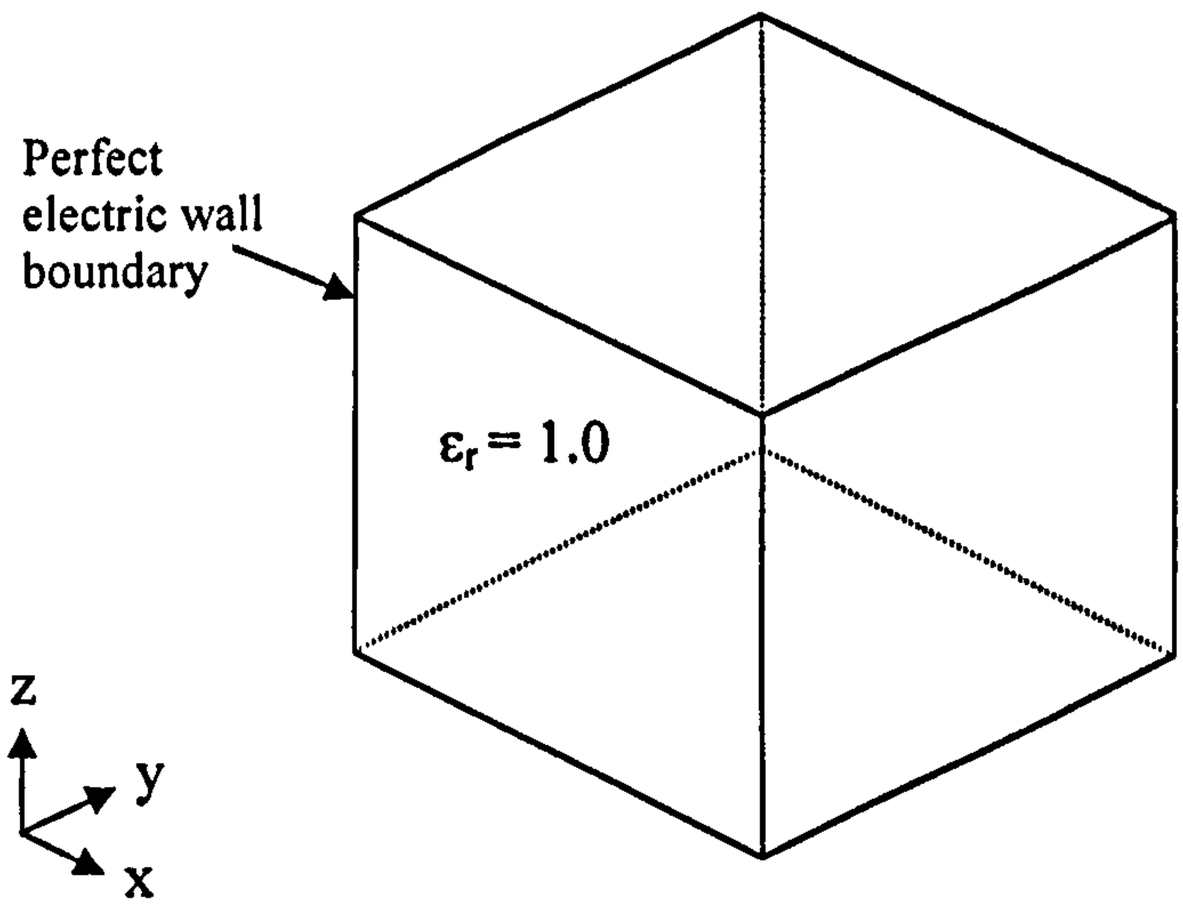

Fig.3.2 : Three-dimensional cavity

A simple three-dimensional cavity, filled with air, and bounded by a perfect electric wall boundary, shown above in Fig.3.2 is used to validate the ADI-FDTD method.

Mesh parameters :

Δx = 0.2mm Δy = 0.2mm Δz = 0.2mm

Total mesh dimensions : 60 x 60 x 60 in $\hat{x}, \hat{y}$ and $\hat{z}$ directions respectively

Critical time step Δt = 0.3851626 ps

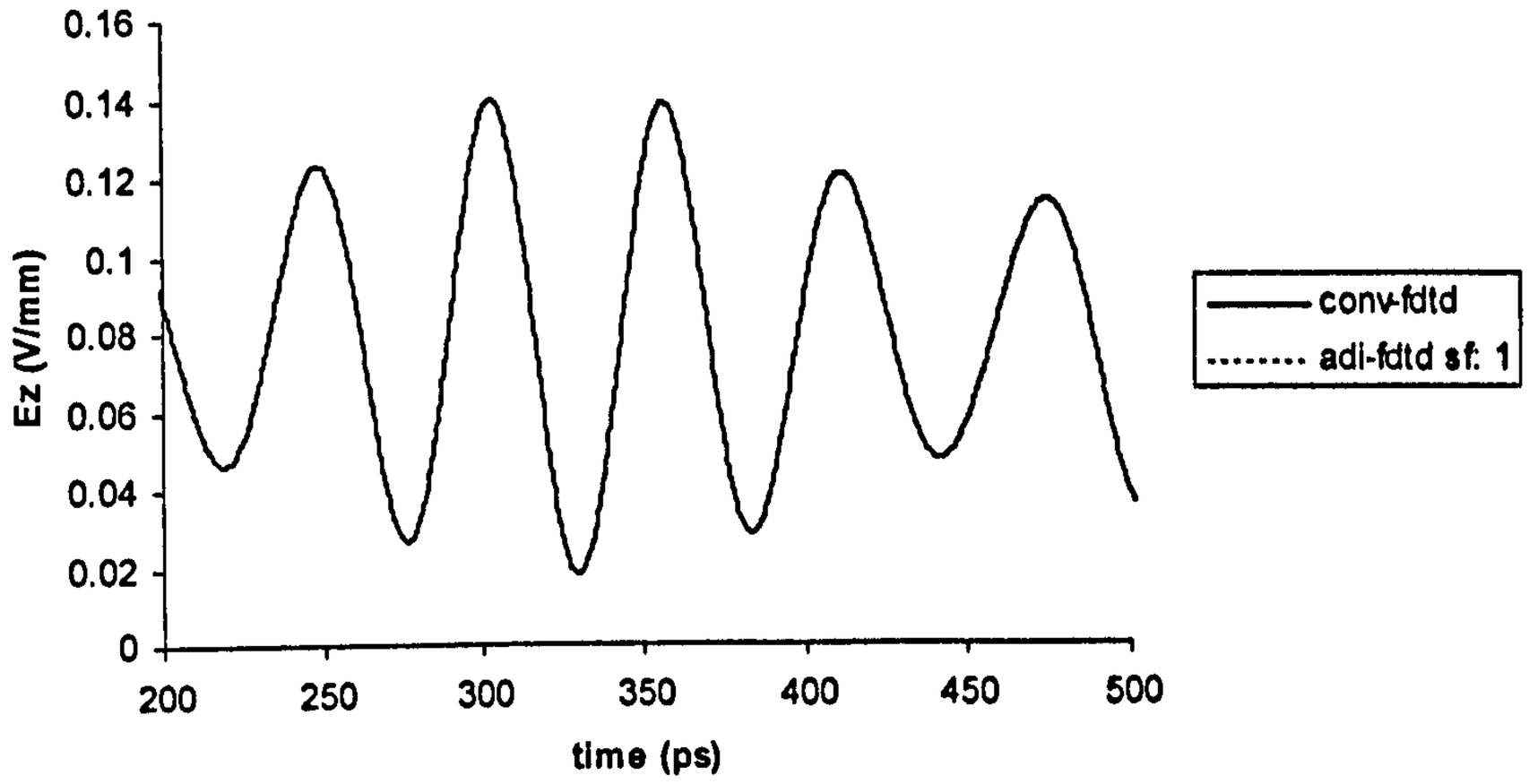

Fig. 3.3 : Comparison between conventional FDTD and ADI-FDTD results with stability factor 1 for a three-dimensional cavity

Fig. 3.3 shows the time-domain results for wave propagation in a three-dimensional cavity with perfect electric wall boundary. The stability factor used here is 1.0; that is the time step used is the critical time step. It shows good agreement between the results using the conventional FDTD and the ADI-FDTD methods. Fig.3.4 shows that the results from the ADI-FDTD are still stable with stability factors 2, 5 and 10 although the effect of numerical dispersion begins to show when stability 5 and 10 are used. However, Fig. 3.5 shows that using the conventional FDTD method, increasing the stability factor to 2.0, thus violating the CFL stability criterion, immediately causes the results to go unstable. In all cases above, the position of the monitoring point is not important as the main aim of these simulations is to show that unlike the conventional FDTD method, with ADI-FDTD method, the results remain stable even when CFL criterion is not observed. More detailed results showing the accuracy of ADI-FDTD results against the stability factors used will be shown and discussed in chapter 5.

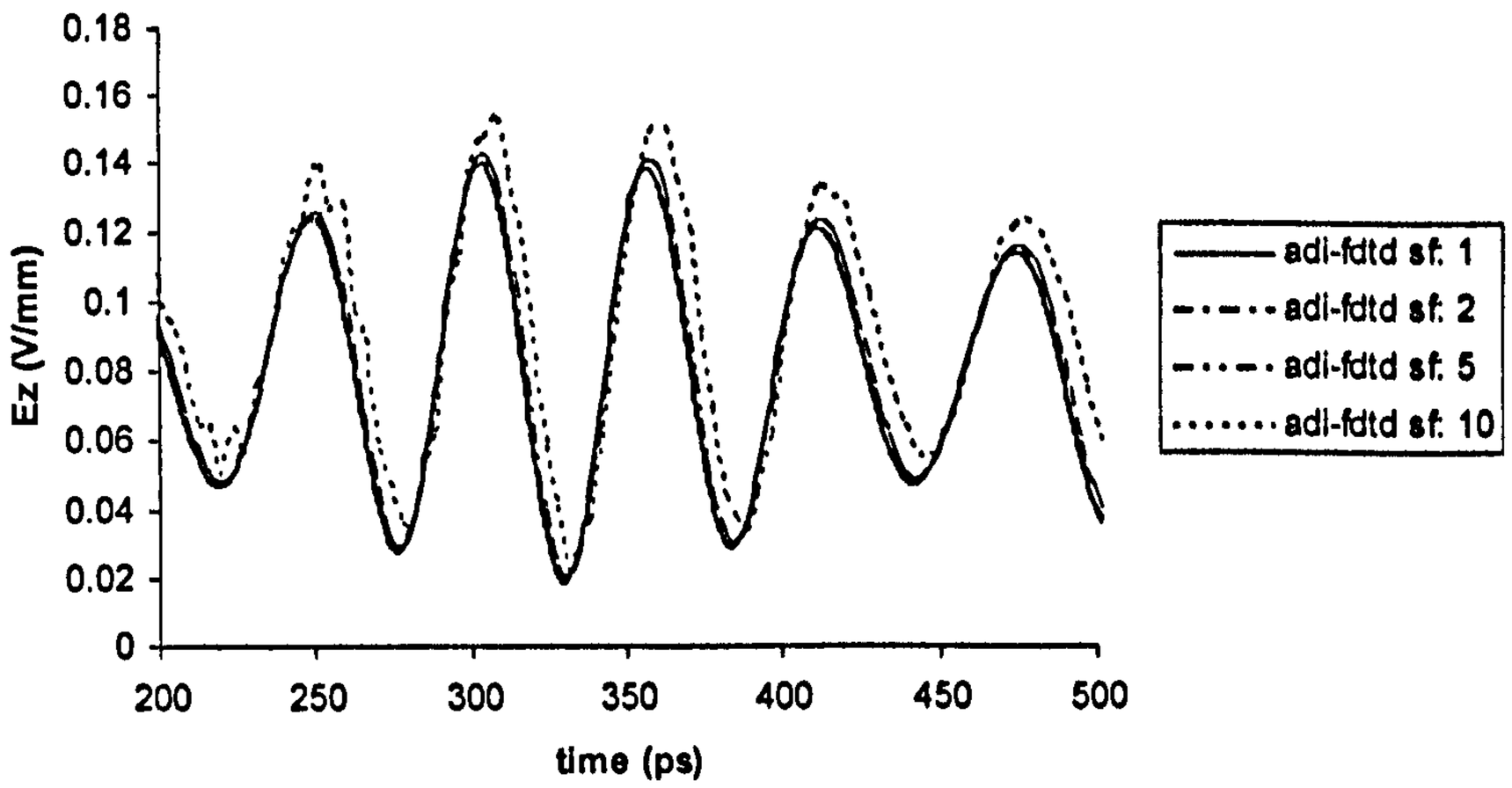

Fig. 3.4 : ADI-FDTD results with stability factors 1, 2, 5 and 10 for a three-dimensional cavity

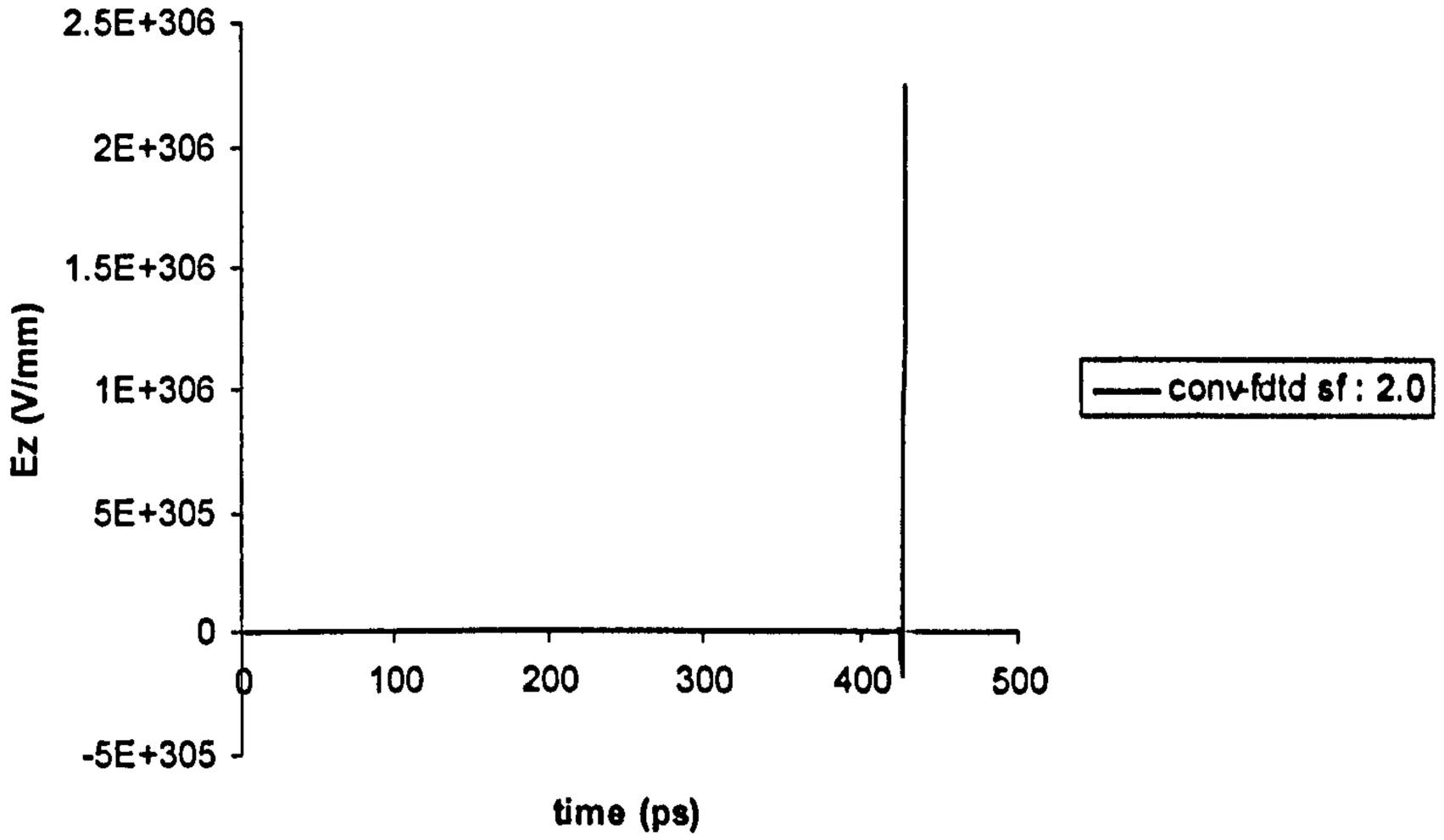

Fig. 3.5 : Conventional FDTD results with stability factor 2.0 for a three-dimensional cavity

3.8.2 Three-dimensional cavity with inhomogeneous media

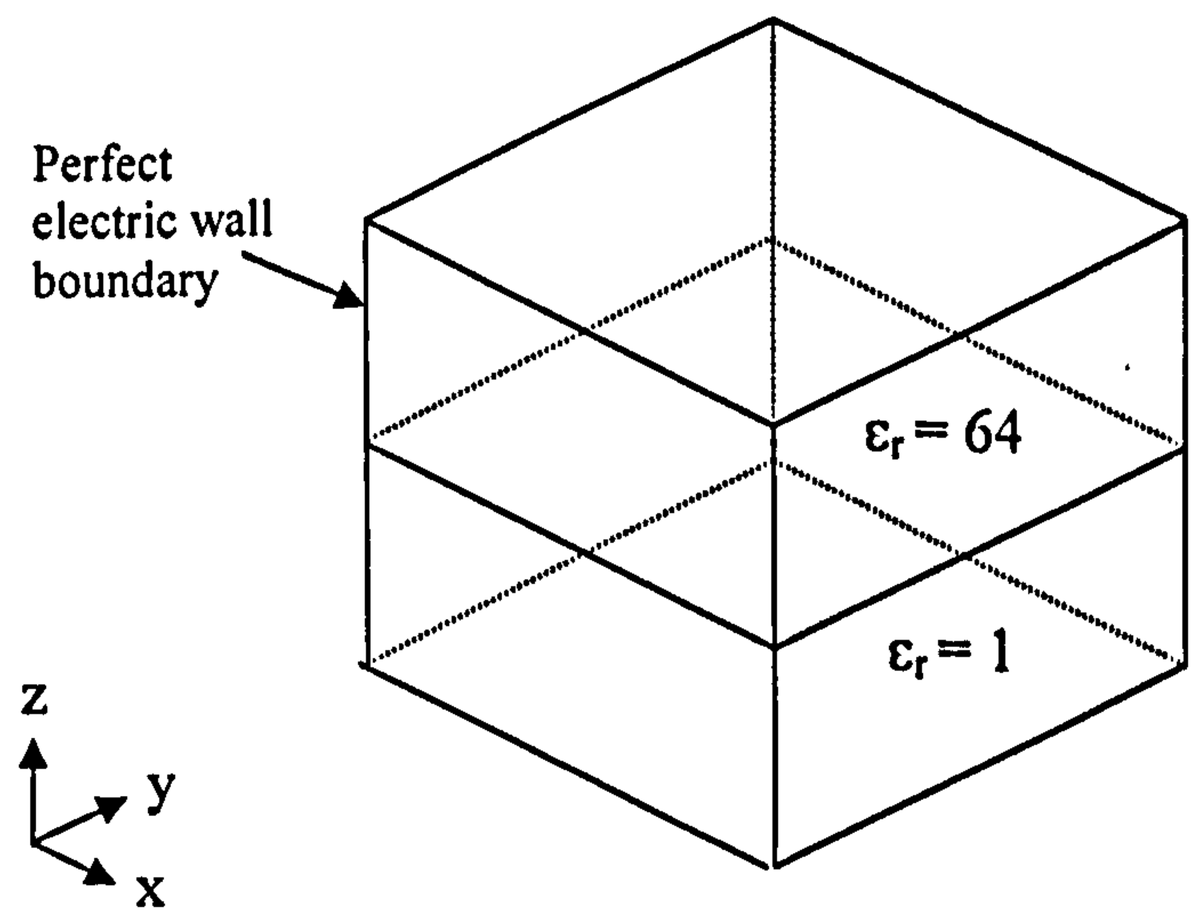

Fig.3.6 : Three-dimensional cavity with inhomogeneous media

In order to model inhomogeneous media, the three-dimensional cavity is partitioned into two sections, one with its permittivity set to 64 and the other set to 1 as shown above in Fig.3.6.

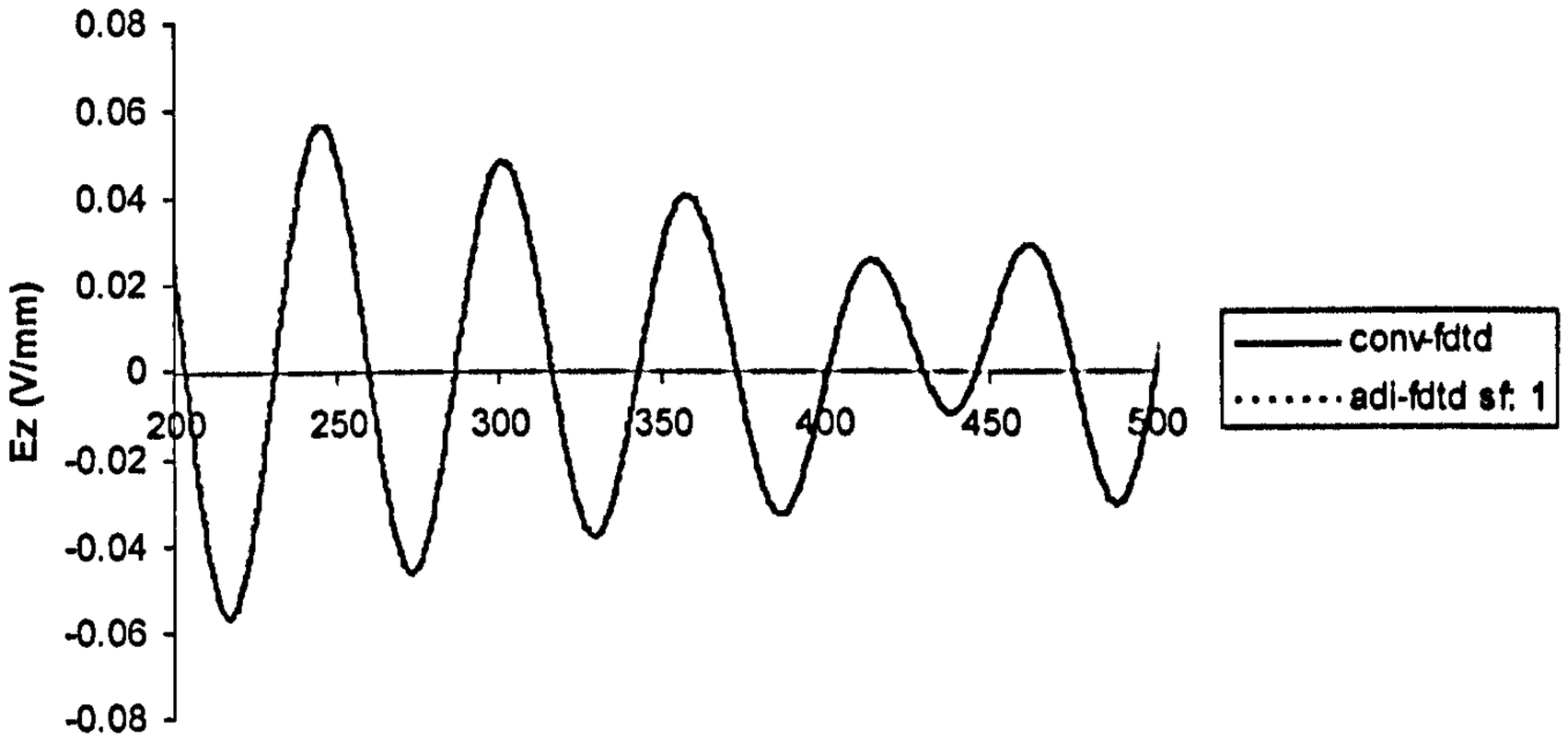

Fig. 3.7 : Comparison between conventional FDTD and ADI-FDTD results with stability factor 1 for a three-dimensional cavity with inhomogeneous media

A comparison between the results generated using the ADI-FDTD algorithm and those generated using the conventional FDTD method is shown in Fig. 3.7. Again, the results show very good agreement. Fig.3.8 shows that the results are still stable when using stability factors 2, 5 and 10 with the ADI-FDTD algorithm. Again, the effects of numerical dispersion begin to appear when the stability factor is increased beyond 5

.

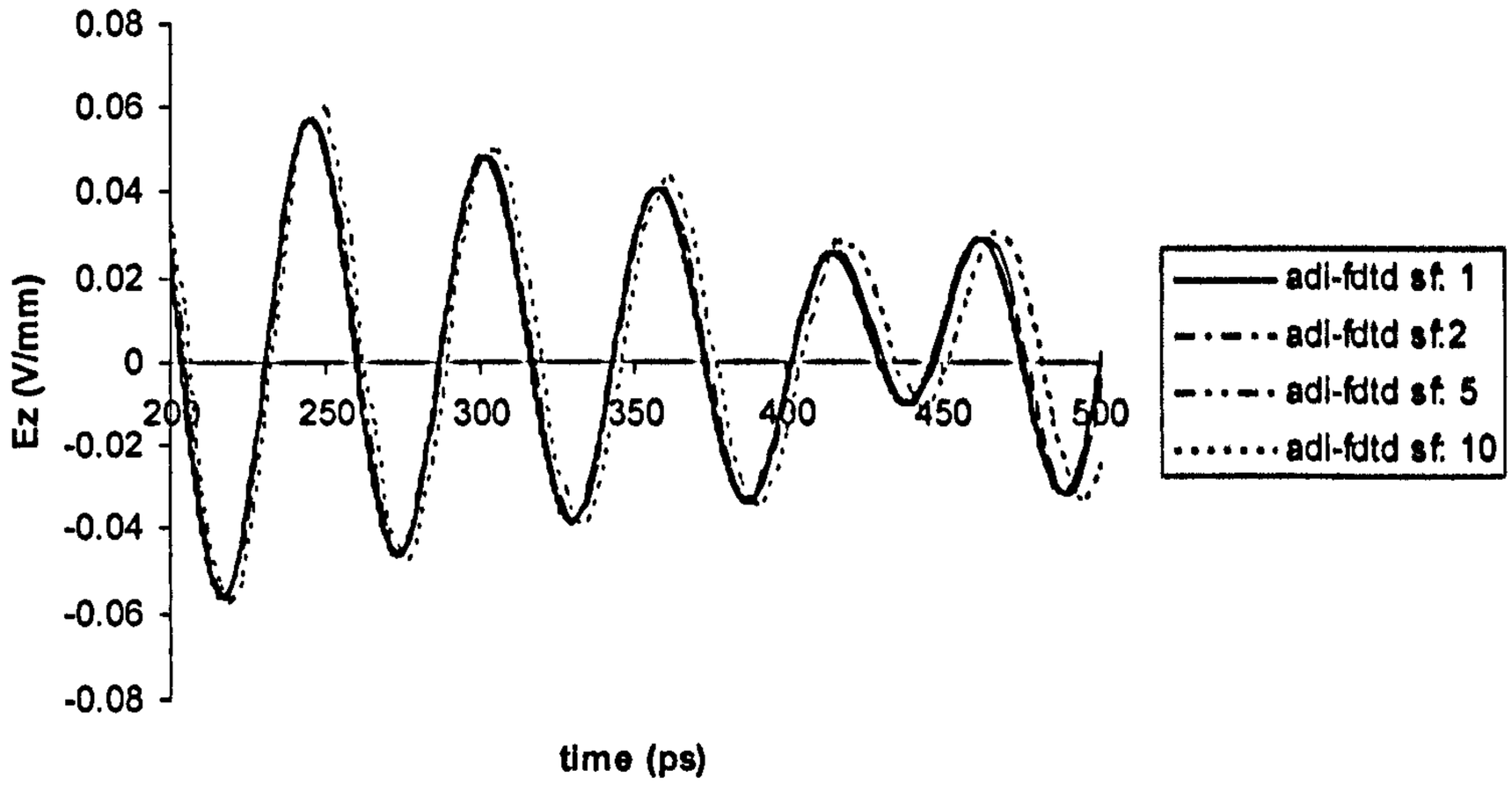

Fig. 3.8 : ADI-FDTD results for stability factors 1.0, 2.0,5.0 and 10.0

3.8.3 Simulation of a line-fed rectangular microstrip patch

In order to validate the ADI-FDTD scheme on a more complex structure, a line-fed rectangular microstrip patch as shown in Fig.2.3 is modelled. As can be seen, the results shown here in Fig. 3.9 eventually became unstable. This happens even when a stability factor of 1.0 is used in the ADI-FDTD algorithm. Since the three-dimensional ADI-FDTD has been validated in homogeneous and inhomogeneous media

with different dielectric constants, it was suspected that the introduction of the copper strip in the model caused the instability.

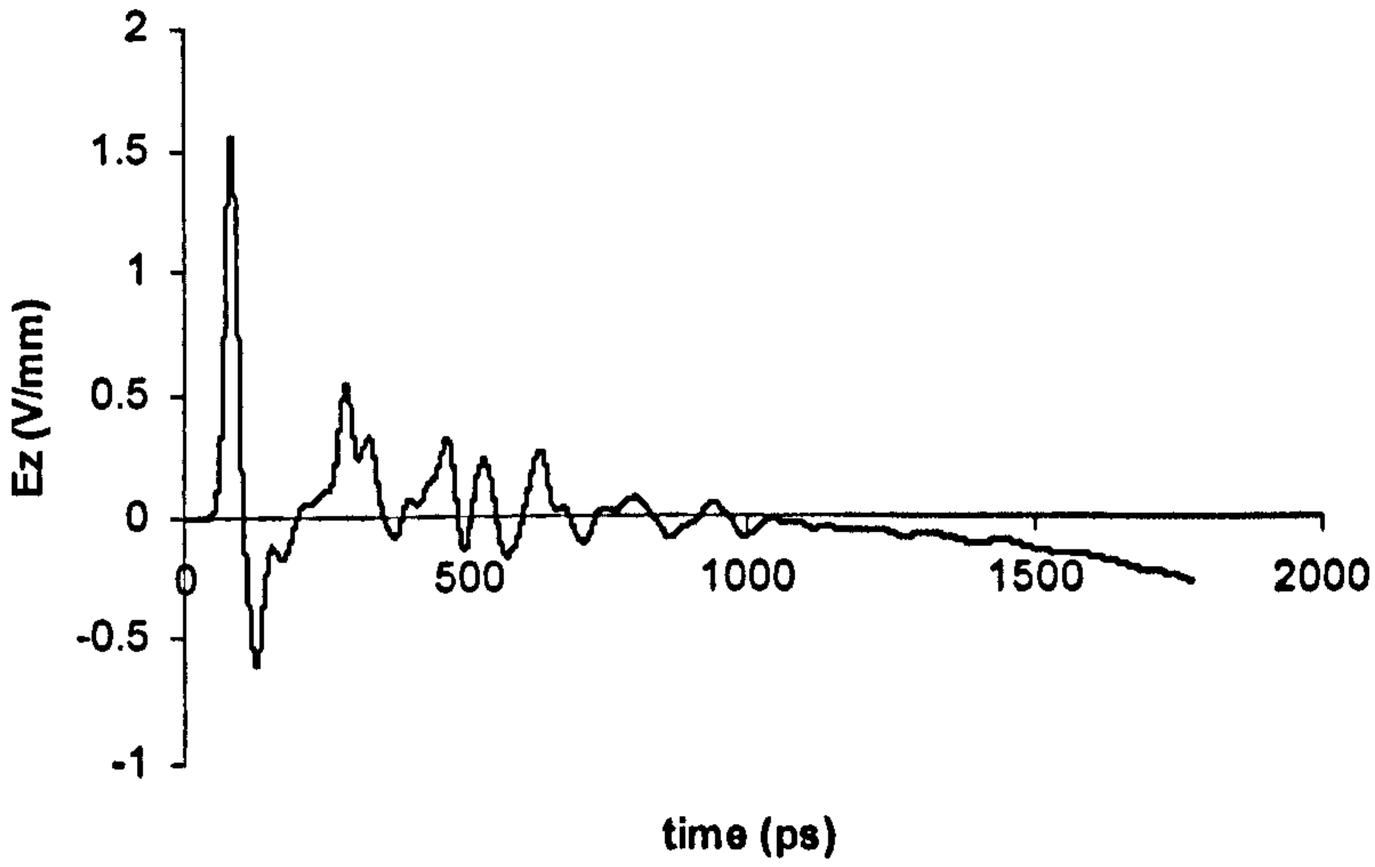

Fig. 3.9 : Line-fed rectangular microstrip patch using ADI-FDTD method with stability factor 1.0

3.8.4 Three-dimensional cavity with a transmission line

To further examine the stability problem encountered here, the three-dimensional air-filled rectangular cavity shown in Fig.3.2 is simulated again. This time, a transmission line that extends between two of the computational boundaries is introduced in the cavity, as shown in Fig. 3.10. The transmission line is implemented as a perfect electric wall boundary where all the tangential electric fields are set to zero.

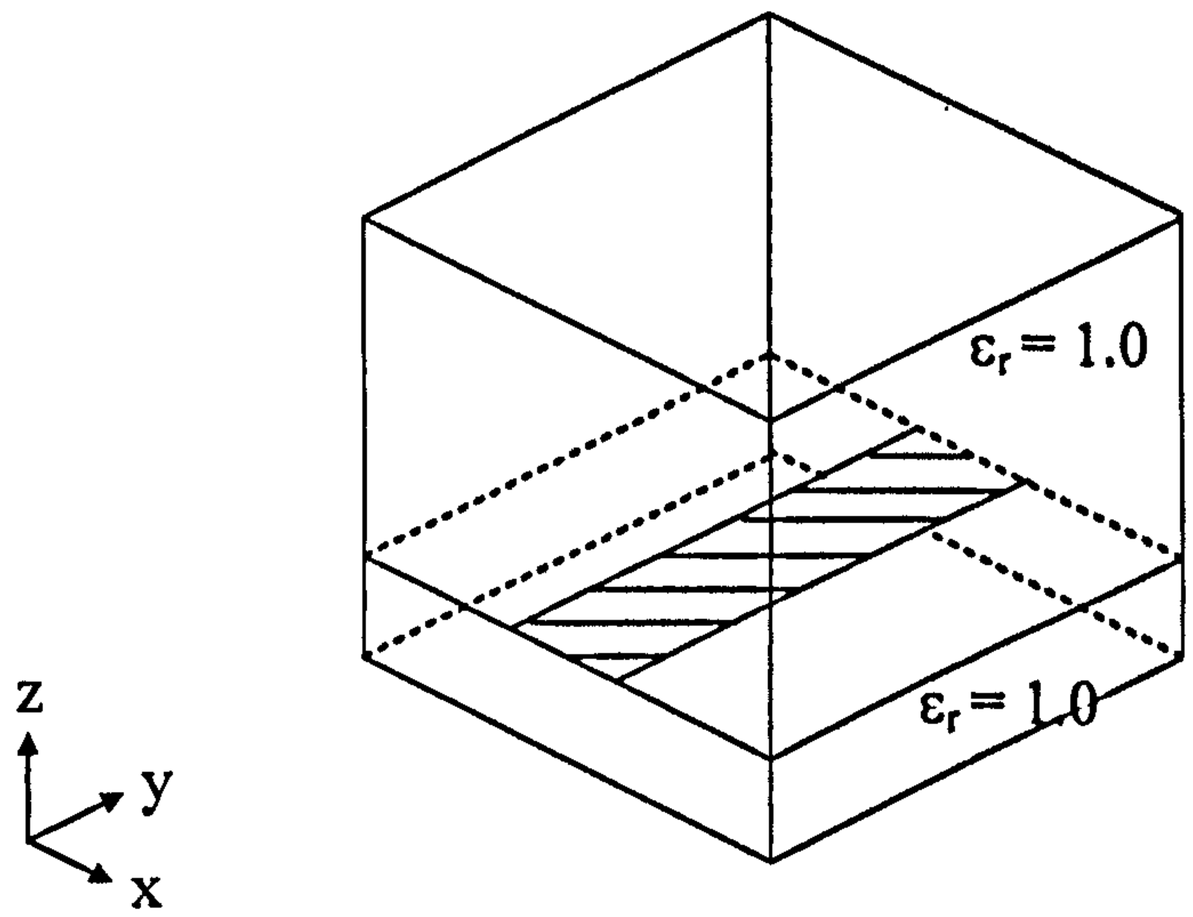

Fig.3.10 : Three-dimensional cavity with a transmission line

Fig. 3.11 shows that the ADI-FDTD results are unstable even when a stability factor of 1.0 is used thus confirming our initial guess. The fact that this model has all the same parameters as that which produced the results in Fig. 3.2 except for the inclusion of a transmission line in the cavity is an indication that the transmission line, i.e. a perfect electric wall boundary within the computation domain, has to be treated with care.

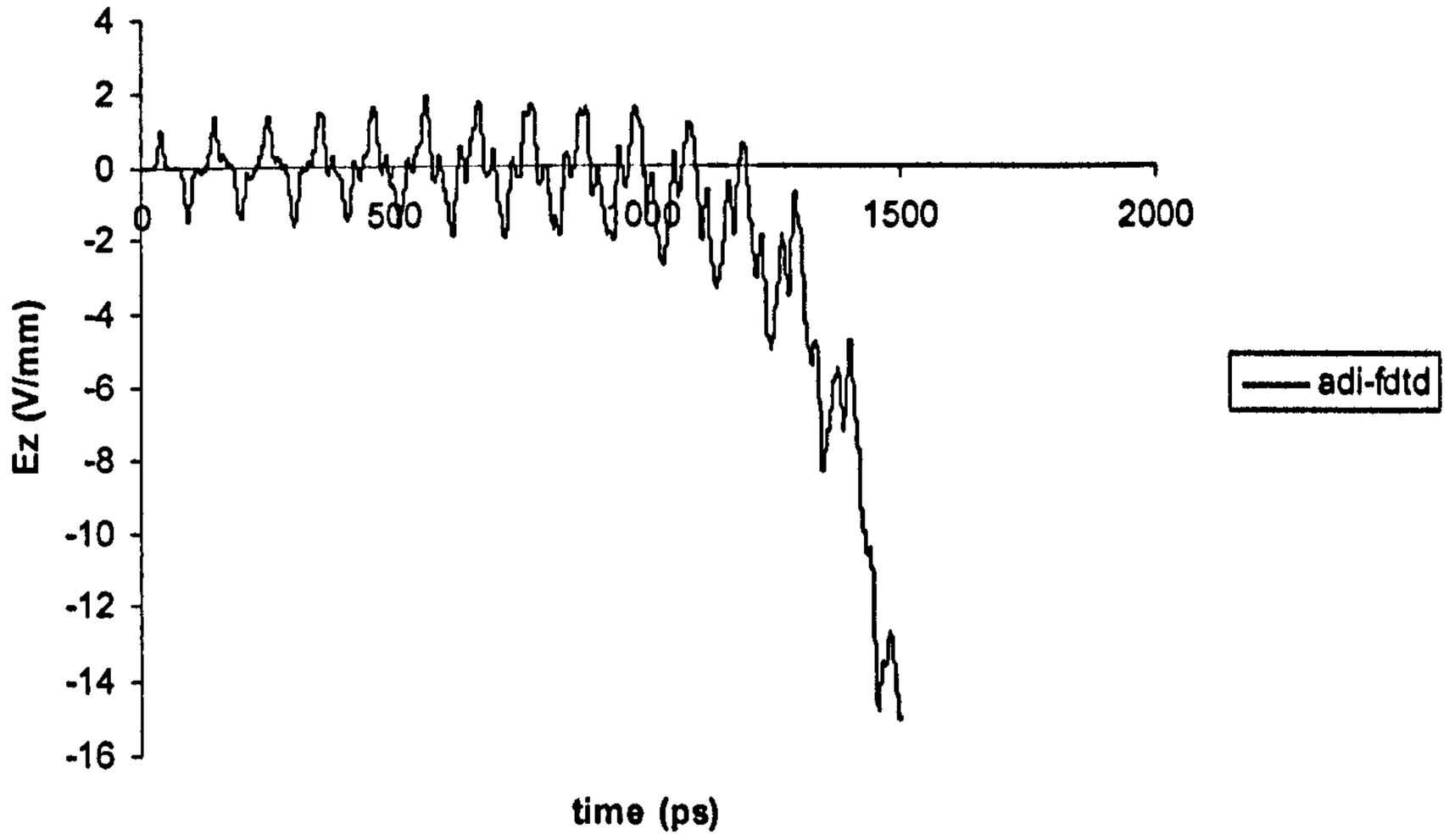

Fig. 3.11 : Three-dimensional cavity with a transmission line with stability factor 1.0

3.9 Conclusion

The two- and three-dimensional ADI-FDTD algorithms for solving numerical electromagnetic problems have been introduced in this chapter. The important aspects of this method have also been discussed. The detailed technique of implementing the 1st order Mur absorbing boundary condition in conjunction with the ADI-FDTD scheme has been discussed.

Following this, the ADI-FDTD with the time steps 2, 5 and 10 times the maximum allowed by the CFL stability criterion have been successfully implemented on an air-filled three-dimensional rectangular cavity and on a three-dimensional rectangular cavity with inhomogeneous media. Both sets of results are stable and agree reasonably well with that produced using the conventional FDTD method. This shows that in the ADI-FDTD scheme, the time step used is no longer restricted by the CFL stability criterion but by the accuracy required in the model. This is a significant advancement in the field of numerical electromagnetics as simulation run-time can now be reduced without causing instability.

Nevertheless, there are still some teething problems with regard to implementing ADI-FDTD on complex structures as seen when the ADI-FDTD method is applied on a microstrip patch, where the tangential electric field on the copper patch is forced to be zero at each time step. Instability occurs even when the time step is within the CFL constraint. This happens when a cavity with a transmission line is simulated with stability factor 1.0. This shows that the implementation of the transmission line as a perfect electric wall boundary causes the instability.

In the next two chapters, chapters 4 and 5, we examine this in greater detail and propose two approaches of overcoming this problem.

CHAPTER 4
MODIFIED ALTERNATING-DIRECTION IMPLICIT METHOD

4.1 Introduction

The introduction of the ADI-FDTD method has had a great impact in numerical electromagnetics. For the first time, simulation run-times can be speeded up by using a bigger time step in the FDTD algorithm. The time step in the numerical algorithm is no longer governed by the CFL stability criterion. In fact, the upper most limit of the time step used is restricted only by the Nyquist sampling theory which states that sampling must be carried out at a frequency of at least twice the maximum frequency of interest in order to avoid aliasing. Therefore, the upper limit of the time step is an inverse of twice the maximum frequency of interest.

However, as explained in chapter 3, there is a difficulty when the ADI-FDTD scheme is used to model a more realistic problem. Initially, as discussed in chapter 3, the ADI-FDTD method was applied to a rectangular cavity and the simulated result agreed with that obtained by applying conventional FDTD method even when the CFL condition was violated in the ADI-FDTD algorithm. But when the ADI-FDTD scheme was used to model a complex geometry such as a microstrip patch antenna, the result went unstable even when the time step used was within the constraint of the CFL stability criterion. To overcome this problem, the author proposes a new modified ADI-FDTD method [1.48].

In order to exploit the advantageous feature of the ADI method without suffering from instability in a three-dimensional model, a factor f, where $0 < f < 1$, is introduced [1.20] in the ADI-FDTD routine. A very important characteristic of this modification is that it is consistent with physical considerations. This will be illustrated section 4.3 later in this chapter. The modified ADI-FDTD allows us to violate the CFL stability constraint in a complex three-dimensional model without causing instability. Furthermore, no graded mesh is necessary to maintain stability of the overall system.

In this chapter, the ADI-FDTD scheme is modified whereby a factor f is introduced as a direct weighting factor on the implicit-explicit terms of the ADI-FDTD equations. This method is applied to the Yee's staggered cell to solve Maxwell's equations. The growth factor of this method is derived for a three-dimensional modified ADI-FDTD. This modified ADI-FDTD method is then used to model a line-fed rectangular patch antenna and the results are discussed.

4.2 Three-dimensional modified ADI-FDTD algorithm

Equations (4.1) – (4.4) show the numerical formulation for the modified ADI-FDTD method. The electric and magnetic fields are spatially staggered as in the conventional FDTD. Without loss of generality, the formulation is carried out for lossless media. The formulations are split into two procedures, procedure 1 is applied for advancement from $n\Delta t$ to $(n+\frac{1}{2})\Delta t$ while procedure 2 is used for advancement from

(n+ ½)Δt to (n+1)Δt.

Procedure 1

$$E_x^{n+1/2}(i+1/2,j,k)=E_x^n(i+1/2,j,k)+\frac{\Delta t}{2\varepsilon}\left\{\begin{array}{l}(2-f)\left[\dfrac{H_z^{n+1/2}(i+1/2,j+1/2,k)-H_z^{n+1/2}(i+1/2,j-1/2,k)}{\Delta y}\right]\\ -\ (f)\left[\dfrac{H_y^n(i+1/2,j,k+1/2)-H_y^n(i+1/2,j,k-1/2)}{\Delta z}\right]\end{array}\right\} \quad (4.1a)$$

$$E_y^{n+1/2}(i,j+1/2,k)=E_y^n(i,j+1/2,k)+\frac{\Delta t}{2\varepsilon}\left\{\begin{array}{l}(2-f)\left[\dfrac{H_x^{n+1/2}(i,j+1/2,k+1/2)-H_x^{n+1/2}(i,j+1/2,k-1/2)}{\Delta z}\right]\\ -\ (f)\left[\dfrac{H_z^n(i+1/2,j+1/2,k)-H_z^n(i-1/2,j+1/2,k)}{\Delta x}\right]\end{array}\right\} \quad (4.1b)$$

$$E_z^{n+1/2}(i,j,k+1/2)=E_z^n(i,j,k+1/2)+\frac{\Delta t}{2\varepsilon}\left\{\begin{array}{l}(2-f)\left[\dfrac{H_y^{n+1/2}(i+1/2,j,k+1/2)-H_y^{n+1/2}(i-1/2,j,k+1/2)}{\Delta x}\right]\\ -\ (f)\left[\dfrac{H_x^n(i,j+1/2,k+1/2)-H_x^n(i,j-1/2,k+1/2)}{\Delta y}\right]\end{array}\right\} \quad (4.1c)$$

$$H_x^{n+1/2}(i,j+1/2,k+1/2)=H_x^n(i,j+1/2,k+1/2)-\frac{\Delta t}{2\mu}\left\{\begin{array}{l}(f)\left[\dfrac{E_z^n(i,j+1,k+1/2)-E_z^n(i,j,k+1/2)}{\Delta y}\right]\\ -\ (2-f)\left[\dfrac{E_y^{n+1/2}(i,j+1/2,k+1)-E_y^{n+1/2}(i,j+1/2,k)}{\Delta z}\right]\end{array}\right\} \quad (4.2a)$$

$$H_y^{n+1/2}(i+1/2,j,k+1/2)=H_y^n(i+1/2,j,k+1/2)-\frac{\Delta t}{2\mu}\left\{\begin{array}{l}(f)\left[\dfrac{E_x^n(i+1/2,j,k+1)-E_x^n(i+1/2,j,k)}{\Delta z}\right]\\ -\ (2-f)\left[\dfrac{E_z^{n+1/2}(i+1,j,k+1/2)-E_z^{n+1/2}(i,j,k+1/2)}{\Delta x}\right]\end{array}\right\} \quad (4.2b)$$

$$H_z^{n+1/2}(+1/2i,j+1/2,k)=H_z^n(i+1/2,j+1/2,k)-\frac{\Delta t}{2\mu}\left\{\begin{array}{l}(f)\left[\dfrac{E_y^n(i+1,j+1/2,k)-E_y^n(i,j+1/2,k)}{\Delta x}\right]\\ -\ (2-f)\left[\dfrac{E_x^{n+1/2}(i+1/2,j+1,k)-E_x^{n+1/2}(i+1/2,j,k)}{\Delta y}\right]\end{array}\right\} \quad (4.2c)$$

Referring to the equations (4.1), for the electric field terms, in procedure 1, the implicit terms have the weighting factor of $(2-f)$ while the explicit terms have f. The same applies for the magnetic fields terms in procedure 1, the implicit terms are weighted by $(2-f)$ while the explicit terms by f. This is repeated

for procedure 2 in equations (4.3) and (4.4). As in the ADI-FDTD, the implicit and explicit terms are switched between procedures 1 and 2.

Procedure 2

$$E_x^{n+1}(i+1/2,j,k) = E_x^{n+1/2}(i+1/2,j,k) + \frac{\Delta t}{2\varepsilon}\left\{\begin{array}{l}(f)\left[\dfrac{H_z^{n+1/2}(i+1/2,j+1/2,k) - H_z^{n+1/2}(i+1/2,j-1/2,k)}{\Delta y}\right] \\ -(2-f)\left[\dfrac{H_y^{n+1}(i+1/2,j,k+1/2) - H_y^{n+1}(i+1/2,j,k-1/2)}{\Delta z}\right]\end{array}\right\} \tag{4.3a}$$

$$E_y^{n+1}(i,j+1/2,k) = E_y^{n+1/2}(i,j+1/2,k) + \frac{\Delta t}{2\varepsilon}\left\{\begin{array}{l}(f)\left[\dfrac{H_x^{n+1/2}(i,j+1/2,k+1/2) - H_x^{n+1/2}(i,j+1/2,k-1/2)}{\Delta z}\right] \\ -(2-f)\left[\dfrac{H_z^{n+1}(i+1/2,j+1/2,k) - H_z^{n+1}(i-1/2,j+1/2,k)}{\Delta x}\right]\end{array}\right\} \tag{4.3b}$$

$$E_z^{n+1}(i,j,k+1/2) = E_z^{n+1/2}(i,j,k+1/2) + \frac{\Delta t}{2\varepsilon}\left\{\begin{array}{l}(f)\left[\dfrac{H_y^{n+1/2}(i+1/2,j,k+1/2) - H_y^{n+1/2}(i-1/2,j,k+1/2)}{\Delta x}\right] \\ -(2-f)\left[\dfrac{H_x^{n+1}(i,j+1/2,k+1/2) - H_x^{n+1}(i,j-1/2,k+1/2)}{\Delta y}\right]\end{array}\right\} \tag{4.3c}$$

$$H_x^{n+1}(i,j+1/2,k+1/2) = H_x^{n+1/2}(i,j+1/2,k+1/2) - \frac{\Delta t}{2\mu}\left\{\begin{array}{l}(2-f)\left[\dfrac{E_z^{n+1}(i,j+1,k+1/2) - E_z^{n+1}(i,j,k+1/2)}{\Delta y}\right] \\ -(f)\left[\dfrac{E_y^{n+1/2}(i,j+1/2,k+1) - E_y^{n+1/2}(i,j+1/2,k)}{\Delta z}\right]\end{array}\right\} \tag{4.4a}$$

$$H_y^{n+1}(i+1/2,j,k+1/2) = H_y^{n+1/2}(i+1/2,j,k+1/2) - \frac{\Delta t}{2\mu}\left\{\begin{array}{l}(2-f)\left[\dfrac{E_x^{n+1}(i+1/2,j,k+1) - E_x^{n}+1(i+1/2,j,k)}{\Delta z}\right] \\ -(f)\left[\dfrac{E_z^{n+1/2}(i+1,j,k+1/2) - E_z^{n+1/2}(i,j,k+1/2)}{\Delta x}\right]\end{array}\right\} \tag{4.4b}$$

$$H_z^{n+1}(+1/2i,j+1/2,k) = H_z^{n+1/2}(i+1/2,j+1/2,k) - \frac{\Delta t}{2\mu}\left\{\begin{array}{l}(2-f)\left[\dfrac{E_y^{n+1}(i+1,j+1/2,k) - E_y^{n+1}(i,j+1/2,k)}{\Delta x}\right] \\ -(f)\left[\dfrac{E_x^{n+1/2}(i+1/2,j+1,k) - E_x^{n+1/2}(i+1/2,j,k)}{\Delta y}\right]\end{array}\right\} \tag{4.4c}$$

Again, as in the ADI-FDTD method equations (4.1) cannot be solved directly due to the implicit terms involved on the RHS. To solve equations (4.1), the LHS electric fields have to be expressed such that the RHS terms are all explicit. This is accomplished by substituting equations (4.2) into (4.1) appropriately; specifically, substituting (4.2c) into (4.1a) results in (4.5) below, where the LHS forms a tri-diagonal matrix of E_x when E_x is scanned in the $\hat{y}$ direction. The RHS of (4.5) now consists of only explicit terms.

$$E_x^{n+1/2}(i+1/2,j-1,k) - E_x^{n+1/2}(i+1/2,j,k)\left[2+\left(\frac{\sqrt{\mu\varepsilon}\Delta y}{\Delta t}\right)^2\left(\frac{1}{(2-f)^2}\right)\right] + E_x^{n+1/2}(i+1/2,j+1,k)$$

$$= -E_x^{n}(i+1/2,j,k)\left(\frac{\sqrt{\mu\varepsilon}\Delta y}{\Delta t}\right)^2\left(\frac{1}{(2-f)^2}\right) + \left(\frac{\Delta y}{\Delta x}\right)\left(\frac{f}{2-f}\right)\left[E_y^{n}(i+1,j+1/2,k) - E_y^{n}(i,j+1/2,k) - E_y^{n}(i+1,j-1/2,k) + E_y^{n}(i,j-1/2,k)\right]$$

$$-\left(\frac{\mu\Delta y}{\Delta t}\right)\left(\frac{1}{2-f}\right)\left[H_z^{n}(i+1/2,j+1/2,k) - H_z^{n}(i+1/2,j-1/2,k)\right] + \left(\frac{\mu\Delta y^2}{\Delta t\Delta z}\right)\left(\frac{f}{(2-f)^2}\right)\left[H_y^{n}(i+1/2,j,k+1/2) - H_y^{n}(i+1/2,j,k-1/2)\right]$$

(4.5)

Similarly, E_y and E_z can be solved in this manner. Once all the electric fields are computed, the magnetic fields can be computed directly using (4.2a) – (4.2c). The same approach can be applied for procedure 2. Equation (4.6) shows the tri-diagonal matrix for E_x in procedure 2. The full formulation of electric fields in both procedures 1 and 2 are given in Appendix B2

$$E_x^{n+1}(i+1/2,j,k-1) - E_x^{n+1}(i+1/2,j,k)\left[2+\left(\frac{\sqrt{\mu\varepsilon}\Delta z}{\Delta t}\right)^2\left(\frac{1}{(2-f)^2}\right)\right] + E_x^{n+1}(i+1/2,j,k+1)$$

$$= -E_x^{n+1/2}(i+1/2,j,k)\left(\frac{\sqrt{\mu\varepsilon}\Delta z}{\Delta t}\right)^2\left(\frac{1}{(2-f)^2}\right) + \left(\frac{\Delta z}{\Delta x}\right)\left(\frac{f}{2-f}\right)\left[E_z^{n+1/2}(i+1,j,k+1/2) - E_z^{n+1/2}(i,j,k+1/2) - E_z^{n+1/2}(i+1,j,k-1/2) + E_z^{n}(i,j,k-1/2)\right]$$

$$-\left(\frac{\mu\Delta z}{\Delta t}\right)\left(\frac{1}{2-f}\right)\left[H_y^{n+1/2}(i+1/2,j,k+1/2) - H_y^{n+1/2}(i+1/2,j,k-1/2)\right] + \left(\frac{\mu\Delta z^2}{\Delta t\Delta y}\right)\left(\frac{f}{(2-f)^2}\right)\left[H_z^{n+1/2}(i+1/2,j+1/2,k) - H_z^{n+1/2}(i+1/2,j-1/2,k)\right]$$

(4.6)

4.3 Weighting factor in the modified ADI-FDTD algorithm

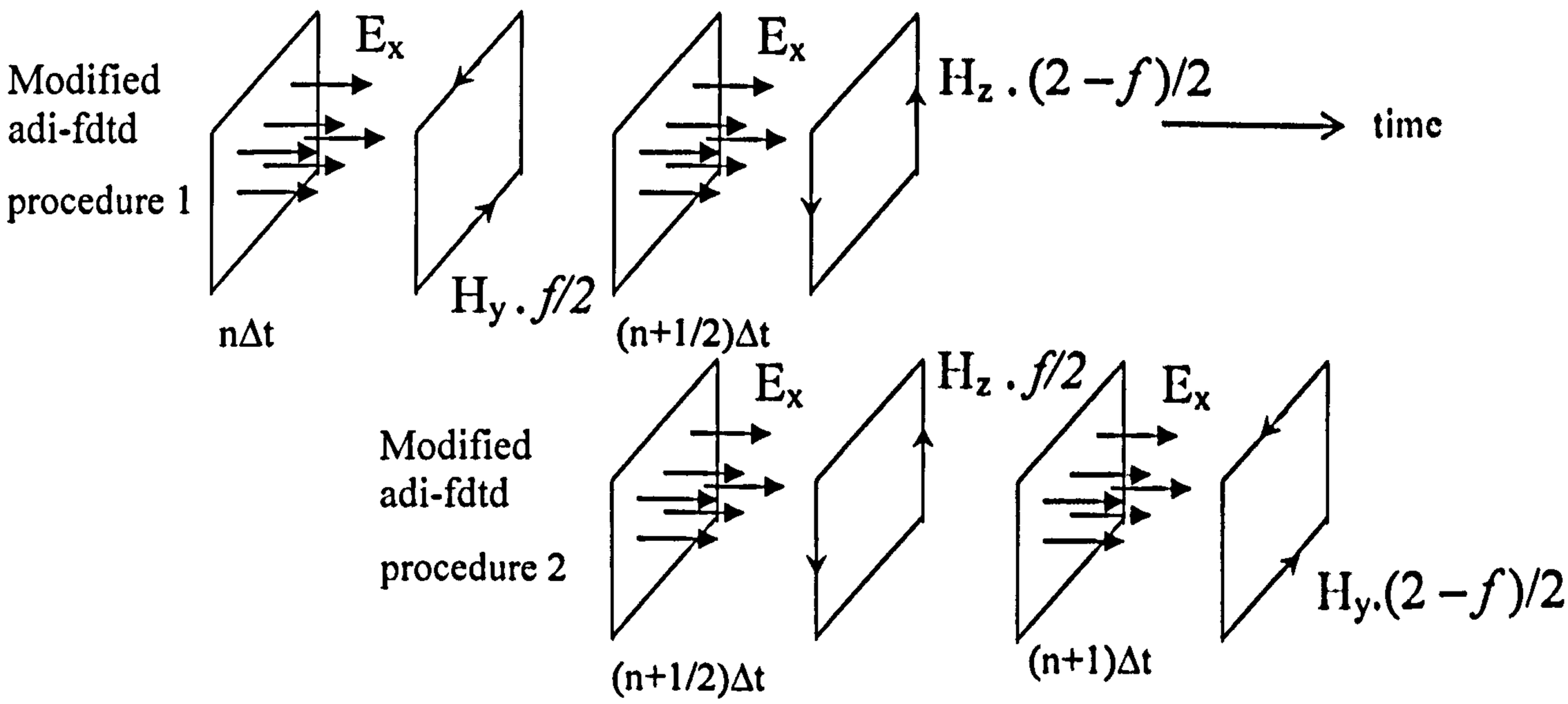

Fig 4.1 : Physical representation of modified ADI-FDTD algorithm

Fig. 4.1 above illustrates the physical representation of the modified ADI-FDTD formulation. In the modified ADI-FDTD method, an intermediate electric field is calculated at time step (n+ ½)Δt. As in the ADI-FDTD method explained in chapter 3, in procedure 1 of the ADI-FDTD method, the electric field at time step (n+ ½)Δt is calculated using the previously calculated electric field at time step nΔt and the curl of the magnetic fields, part implicit and part explicit. In the ADI-FDTD method, the weighting factors for the magnetic fields, implicit H_z and explicit H_y are the same, i.e. ½ for both of them. However, in the modified ADI-FDTD the implicit term H_z at time step (n+ ½)Δt is weighted by $(2-f)/2$ and the explicit term H_y at time step nΔt by $f/2$ where $0 < f < 1$. This is immediately followed on by procedure 2; now the known (explicit) value of H_z at time step (n+ ½)Δt is weighted by $f/2$ and the unknown (implicit) value of H_y at time step (n+1)Δt is weighted by $(2-f)/2$. The total magnetic field over a full time step remains unchanged.

4.4 Divergence of modified ADI-FDTD algorithm

As in the ADI-FDTD algorithm, there is no explicit enforcement of the Gauss's Law relations for both the electric and magnetic fields in the modified ADI-FDTD algorithm. Although the curl operation of the magnetic fields is performed over two half time steps and the magnetic fields are weighted differently at each half time step, the total magnetic field over a full time step remains unchanged in the modified ADI-FDTD scheme. Therefore, the modified ADI-FDTD algorithm will still result in zero divergence for both electric and magnetic flux i.e. the time derivative of the net magnetic/electric flux leaving the surfaces of a cubic Yee cell is zero, thus upholding the Gauss's Law for the magnetic/electric field in charge-free space in the modified ADI-FDTD scheme.

4.5 Numerical stability

The numerical stability of the modified ADI-FDTD can be carried out in the same way as in the ADI-FDTD. Assume the spatial frequency to be $\tilde{k}_x, \tilde{k}_y$ and $\tilde{k}_z$ as the x- , y- and z- components of its numerical wavevector respectively as in equations (3.7) & (3.8).

4.5.1 2-dimensional modified ADI-FDTD

For the sake of simplicity, we shall consider first the numerical stability of a 2-dimensional TE wave consisting of the following fields :

Procedure 1

$$E_x^{n+1/2}(i+1/2, j) = E_x^n(i+1/2, j) + \frac{\Delta t}{2\varepsilon}\left\{(2-f)\left[\frac{H_z^{n+1/2}(i+1/2, j+1/2) - H_z^{n+1/2}(i+1/2, j-1/2)}{\Delta y}\right]\right\} \quad (4.7a)$$

$$E_y^{n+1/2}(i, j+1/2) = E_y^n(i, j+1/2) - \frac{\Delta t}{2\varepsilon}\left\{(f)\left[\frac{H_z^n(i+1/2, j+1/2) - H_z^n(i-1/2, j+1/2)}{\Delta x}\right]\right\} \quad (4.7b)$$

$$H_z^{n+1/2}(i+1/2, j+1/2) = H_z^n(i+1/2, j+1/2) - \frac{\Delta t}{2\mu}\left\{ \begin{array}{c} (f)\left[\frac{E_y^n(i+1/2, j+1/2) - E_y^n(i, j+1/2)}{\Delta x}\right] \\ -(2-f)\left[\frac{E_x^{n+1/2}(i+1/2, j+1) - E_x^{n+1/2}(i+1/2, j)}{\Delta y}\right] \end{array} \right\} \tag{4.7c}$$

Substituting the field components in spectral forms, (3.7a), (3.7b) and (3.8c) into (4.7) will yield the following :

$$E_x * GF1 = E_x - GF1 * (2-f) * H_z \frac{\Delta t}{2\varepsilon \Delta y} 2j \sin\left(\frac{\tilde{k}_y \Delta y}{2}\right) \tag{4.8a}$$

$$E_y * GF1 = E_y + f * H_z \frac{\Delta t}{2\varepsilon \Delta x} 2j \sin\left(\frac{\tilde{k}_x \Delta x}{2}\right) \tag{4.8b}$$

$$H_z * GF1 = H_z + E_y * f * \frac{\Delta t}{2\mu \Delta x} 2j \sin\left(\frac{\tilde{k}_x \Delta x}{2}\right) - GF1 * (2-f) * E_x \frac{\Delta t}{2\mu \Delta y} 2j \sin\left(\frac{\tilde{k}_y \Delta y}{2}\right) \tag{4.8c}$$

where *GF1* is the growth factor in procedure 1. Substituting (4.8a) and (4.8b) into (4.8c) gives :

$$\begin{aligned} H_z * GF1 = H_z &+ \frac{f^2 H_z \frac{\Delta t}{2\varepsilon \Delta x} 2j \sin\left(\frac{\tilde{k}_x \Delta x}{2}\right) \frac{\Delta t}{2\mu \Delta x} 2j \sin\left(\frac{\tilde{k}_x \Delta x}{2}\right)}{GF1 - 1} \\ &+ \frac{(2-f)^2 GF1 * GF1 * H_z \frac{\Delta t}{2\varepsilon \Delta y} 2j \sin\left(\frac{\tilde{k}_y \Delta y}{2}\right) \frac{\Delta t}{2\mu \Delta y} 2j \sin\left(\frac{\tilde{k}_y \Delta y}{2}\right)}{GF1 - 1} \end{aligned} \tag{4.9}$$

$$H_z(GF1-1)^2 = -f^2 H_z\left(\frac{1}{\mu \varepsilon}\right)\left[\frac{\Delta t}{\Delta x}\sin\left(\frac{\tilde{k}_x \Delta x}{2}\right)\right]^2 - (2-f)^2 GF1^2 H_z\left(\frac{1}{\mu \varepsilon}\right)\left[\frac{\Delta t}{\Delta y}\sin\left(\frac{\tilde{k}_y \Delta y}{2}\right)\right]^2 \tag{4.10}$$

let $\quad M_x = \frac{\Delta t}{\Delta x}\sin\left(\frac{\tilde{k}_x \Delta x}{2}\right) \quad$ and $\quad M_y = \frac{\Delta t}{\Delta y}\sin\left(\frac{\tilde{k}_y \Delta y}{2}\right)$

and dividing (4.9) by H_z

$$GF1^2\left(1+\frac{M_y^2}{\mu \varepsilon}(2-f)^2\right) - 2GF1 + \left(1+\frac{M_x^2}{\mu \varepsilon} f^2\right) = 0 \tag{4.11}$$

Let $\quad a = \left(1+\frac{M_y^2}{\mu \varepsilon}(2-f)^2\right) \quad$ and $\quad c = \left(1+\frac{M_x^2}{\mu \varepsilon} f^2\right)$

then (4.11) becomes

$$a\,GF1^2 - 2\,GF1 + c = 0 \tag{4.12}$$

$$GF1 = \frac{1 \pm \sqrt{1-ac}}{a}$$

and since $ac \geq 1$ $\quad\therefore\quad$ $$GF1 = \frac{1 \pm j\sqrt{ac-1}}{a} \tag{4.13}$$

Procedure 2

$$E_x^{n+1}(i+1/2, j) = E_x^{n+1/2}(i+1/2, j) + \frac{\Delta t}{2\varepsilon}\left\{(f)\left[\frac{H_z^{n+1/2}(i+1/2, j+1/2) - H_z^{n+1/2}(i+1/2, j-1/2)}{\Delta y}\right]\right\} \tag{4.14a}$$

$$E_y^{n+1}(i, j+1/2) = E_y^{n+1/2}(i, j+1/2) - \frac{\Delta t}{2\varepsilon}\left\{(2-f)\left[\frac{H_z^{n+1}(i+1/2, j+1/2) - H_z^{n+1}(i-1/2, j+1/2)}{\Delta x}\right]\right\} \tag{4.14b}$$

$$H_z^{n+1}(i+1/2, j+1/2) = H_z^{n+1/2}(i+1/2, j+1/2) - \frac{\Delta t}{2\mu}\left\{\begin{array}{l}(2-f)\left[\dfrac{E_y^{n+1}(i+1/2, j+1/2) - E_y^{n+1}(i, j+1/2)}{\Delta x}\right] \\ -(f)\left[\dfrac{E_x^{n+1/2}(i+1/2, j+1) - E_x^{n+1/2}(i+1/2, j)}{\Delta y}\right]\end{array}\right\} \tag{4.14c}$$

Again, substituting (3.7a), (3.7b) and (3.8c) into (4.14) will yield the following :

$$E_x * GF2 = E_x - f * H_z \frac{\Delta t}{2\varepsilon \Delta y} 2j \sin\left(\frac{\tilde{k}_y \Delta y}{2}\right) \tag{4.15a}$$

$$E_y * GF2 = E_y + GF2 * (2-f) * H_z \frac{\Delta t}{2\varepsilon \Delta x} 2j \sin\left(\frac{\tilde{k}_x \Delta x}{2}\right) \tag{4.15b}$$

$$H_z * GF2 = H_z + GF2 * (2-f) * E_y \frac{\Delta t}{2\mu \Delta x} 2j \sin\left(\frac{\tilde{k}_x \Delta x}{2}\right) - f * E_x \frac{\Delta t}{2\mu \Delta y} 2j \sin\left(\frac{\tilde{k}_y \Delta y}{2}\right) \tag{4.15c}$$

where *GF2* is the growth factor in procedure 2. Applying the same technique on procedure 2, we get,

$$GF2^2\left(1+\frac{M_x^2}{\mu\varepsilon}(2-f)^2\right) - 2\,GF2 + \left(1+\frac{M_y^2}{\mu\varepsilon}f^2\right) = 0 \tag{4.16}$$

Let $\quad b = \left(1+\dfrac{M_x^2}{\mu\varepsilon}(2-f)^2\right)$ $\quad$ and $\quad$ $d = \left(1+\dfrac{M_y^2}{\mu\varepsilon}f^2\right)$

then (4.16) becomes

$$b\,GF2^2 - 2\,GF2 + d = 0 \tag{4.17}$$

$$GF2 = \frac{1 \pm \sqrt{1 - bd}}{b}$$

and since $bd \geq 1$ $\therefore$ $$GF2 = \frac{1 \pm j\sqrt{bd - 1}}{b} \qquad (4.18)$$

Now,

$$GF1 = \frac{1 \pm j\sqrt{ac - 1}}{a} \quad \text{and} \quad GF2 = \frac{1 \pm j\sqrt{bd - 1}}{b}$$

where

$$a = \left(1 + \frac{M_y^2}{\mu\varepsilon}(2-f)^2\right) \quad \text{and} \quad c = \left(1 + \frac{M_x^2}{\mu\varepsilon}f^2\right)$$

$$b = \left(1 + \frac{M_x^2}{\mu\varepsilon}(2-f)^2\right) \quad \text{and} \quad d = \left(1 + \frac{M_y^2}{\mu\varepsilon}f^2\right)$$

Examining M_x and M_y, we see that

$$\frac{M_x^2}{\mu\varepsilon} = \left(\frac{\Delta t}{\Delta x}\right)^2\left(\frac{1}{\mu\varepsilon}\right)\sin^2\left(\frac{\tilde{k}_x\Delta x}{2}\right) = \left(\frac{v^2}{v_x^2}\right)\sin^2\left(\frac{\tilde{k}_x\Delta x}{2}\right)$$

Therefore, the total growth factor of procedures 1 and 2 combined is given by :

$$\begin{aligned} GF &= |GF1| * |GF2| \\ &= \sqrt{\frac{c}{a}} * \sqrt{\frac{d}{b}} \\ &= \sqrt{\frac{\left[1 + \frac{v^2}{v_x^2}\sin^2\left(\frac{\tilde{k}_x\Delta x}{2}\right)f^2\right]\left[1 + \frac{v^2}{v_y^2}\sin^2\left(\frac{\tilde{k}_y\Delta y}{2}\right)f^2\right]}{\left[1 + \frac{v^2}{v_x^2}\sin^2\left(\frac{\tilde{k}_x\Delta x}{2}\right)(2-f)^2\right]\left[1 + \frac{v^2}{v_y^2}\sin^2\left(\frac{\tilde{k}_y\Delta y}{2}\right)(2-f)^2\right]}} \end{aligned} \qquad (4.19)$$

As $0 < f < 1$, then $1 < (2-f) < 2$

Therefore (4.19) or the overall growth factor of the modified ADI-FDTD algorithm will always be less than unity. Consequently, the newly proposed two-dimensional modified ADI-FDTD method is always stable for $0 < f < 1$.

4.5.2 3-dimensional modified ADI-FDTD

To analyse the numerical stability of a three-dimensional modified ADI-FDTD, we apply the von Neumann method again on the three-dimensional modified ADI-FDTD formulations (4.1) – (4.4).

Following the same method as in chapter 3 we get GF1 and GF2 as shown below :

GF1 =

$$\begin{bmatrix} \frac{1}{Ny} & \frac{Mx\cdot My\cdot(2-f)\cdot f}{Ny\cdot\mu\cdot\varepsilon} & 0 & 0 & \frac{-j\cdot Mz\cdot f}{Ny\cdot\varepsilon} & \frac{j\cdot My\cdot(2-f)}{Ny\cdot\varepsilon} \\ 0 & \frac{1}{Nz} & \frac{My\cdot Mz\cdot(2-f)\cdot f}{Nz\cdot\mu\cdot\varepsilon} & \frac{j\cdot Mz\cdot(2-f)}{Nz\cdot\varepsilon} & 0 & \frac{-j\cdot Mx\cdot f}{Nz\cdot\varepsilon} \\ \frac{Mx\cdot Mz\cdot(2-f)\cdot f}{Nx\cdot\mu\cdot\varepsilon} & 0 & \frac{1}{Nx} & \frac{-j\cdot My\cdot f}{Nx\cdot\varepsilon} & \frac{j\cdot Mx\cdot(2-f)}{Nx\cdot\varepsilon} & 0 \\ 0 & \frac{j\cdot Mz\cdot(2-f)}{Nz\cdot\mu} & \frac{-j\cdot My\cdot f}{Nz\cdot\mu} & \frac{1}{Nz} & 0 & \frac{Mx\cdot Mz\cdot(2-f)\cdot f}{Nz\cdot\mu\cdot\varepsilon} \\ \frac{-j\cdot Mz\cdot f}{Nx\cdot\mu} & 0 & \frac{j\cdot Mx\cdot(2-f)}{Nx\cdot\mu} & \frac{Mx\cdot My\cdot(2-f)\cdot f}{Nx\cdot\mu\cdot\varepsilon} & \frac{1}{Nx} & 0 \\ \frac{j\cdot My\cdot(2-f)}{Ny\cdot\mu} & \frac{-j\cdot Mx\cdot f}{Ny\cdot\mu} & 0 & 0 & \frac{My\cdot Mz\cdot(2-f)\cdot f}{Ny\cdot\mu\cdot\varepsilon} & \frac{1}{Ny} \end{bmatrix} \tag{4.20}$$

GF2 =

$$\begin{bmatrix} \frac{1}{Nz} & 0 & \frac{Mx\cdot Mz\cdot(2-f)\cdot f}{Nz\cdot\mu\cdot\varepsilon} & 0 & \frac{-j\cdot Mz\cdot(2-f)}{Nz\cdot\varepsilon} & \frac{j\cdot My\cdot f}{Nz\cdot\varepsilon} \\ \frac{Mx\cdot My\cdot(2-f)\cdot f}{Nx\cdot\mu\cdot\varepsilon} & \frac{1}{Nx} & 0 & \frac{j\cdot Mz\cdot f}{Nx\cdot\varepsilon} & 0 & \frac{j\cdot Mx\cdot(2-f)}{Nx\cdot\varepsilon} \\ 0 & \frac{My\cdot Mz\cdot(2-f)\cdot f}{Ny\cdot\mu\cdot\varepsilon} & \frac{1}{Ny} & \frac{-j\cdot My\cdot(2-f)}{Ny\cdot\varepsilon} & \frac{j\cdot Mx\cdot f}{Ny\cdot\varepsilon} & 0 \\ 0 & \frac{j\cdot Mz\cdot f}{Ny\cdot\mu} & \frac{-j\cdot My\cdot(2-f)}{Ny\cdot\mu} & \frac{1}{Ny} & \frac{Mx\cdot My\cdot(2-f)\cdot f}{Ny\cdot\mu\cdot\varepsilon} & 0 \\ \frac{-j\cdot Mz\cdot(2-f)}{Nz\cdot\mu} & 0 & \frac{j\cdot Mx\cdot f}{Nz\cdot\mu} & 0 & \frac{1}{Nz} & \frac{My\cdot Mz\cdot(2-f)\cdot f}{Nz\cdot\mu\cdot\varepsilon} \\ \frac{j\cdot My\cdot f}{Nx\cdot\mu} & \frac{-j\cdot Mx\cdot(2-f)}{Nx\cdot\mu} & 0 & \frac{Mx\cdot Mz\cdot(2-f)\cdot f}{Nx\cdot\mu\cdot\varepsilon} & 0 & \frac{1}{Nx} \end{bmatrix} \tag{4.21}$$

where

$$M_h = \frac{\Delta t}{\Delta h}\sin\left(\frac{k_h \Delta h}{2}\right) \quad \text{and} \quad N_h = 1+\frac{M_h^2}{\mu\varepsilon} \quad h = x, y, z \tag{4.22}$$

In order to solve the overall growth factor for the three-dimensional modified ADI-FDTD, the following assumption is made.

$$\text{Overall growth factor, GF} = \text{GF1*GF2} = \text{GF2*GF1} \tag{4.23}$$

The assumption is sound because the procedures are commutative.

Solving (4.20) and (4.21) using (4.23), we get

$$GF = \left(\frac{f}{2-f}\right)^2 \tag{4.24}$$

Therefore, the newly proposed three-dimensional modified ADI-FDTD is always stable for $0 < f < 1$.

4.6 Numerical dispersion

The numerical dispersion for the modified ADI-FDTD method can be found by substituting the vector-field travelling-wave expression with time dependence (3.27) into the modified ADI-FDTD finite difference equations .

4.6.1 2-dimensional modified ADI-FDTD

Again, for simplicity, we investigate the numerical dispersion of a 2-dimensional TE wave [1.19].

Substituting (3.27) into (4.4) (procedure 1) gives :

$$(e^{j\omega\Delta t/2} - 1)\,E_x^n = -j\left(\frac{\Delta t}{\varepsilon\,\Delta y}\right)\sin\left(\frac{\tilde{k}_y\Delta y}{2}\right)e^{j\omega\Delta t/2}\,H_z^n\,(2-f) \tag{4.25a}$$

$$(e^{j\omega\Delta t/2} - 1)\,E_y^n = j\left(\frac{\Delta t}{\varepsilon\,\Delta x}\right)\sin\left(\frac{\tilde{k}_x\Delta x}{2}\right)H_z^n\,f \tag{4.25b}$$

$$(e^{j\omega\Delta t/2} - 1)\,H_z^n = j\left(\frac{\Delta t}{\mu\,\Delta x}\right)\sin\left(\frac{\tilde{k}_x\Delta x}{2}\right)E_y^n\,f - j\left(\frac{\Delta t}{\mu\,\Delta y}\right)\sin\left(\frac{\tilde{k}_y\Delta y}{2}\right)e^{j\omega\Delta t/2}\,E_x^n\,(2-f) \tag{4.25c}$$

and into (3.14) (procedure 2) gives :

$$(e^{j\omega\Delta t} - e^{j\omega\Delta t/2})\,E_x^n = -j\left(\frac{\Delta t}{\varepsilon\,\Delta y}\right)\sin\left(\frac{\tilde{k}_y\Delta y}{2}\right)e^{j\omega\Delta t/2}\,H_z^n\,f \tag{4.26a}$$

$$(e^{j\omega\Delta t} - e^{j\omega\Delta t/2})\,E_y^n = j\left(\frac{\Delta t}{\varepsilon\,\Delta x}\right)\sin\left(\frac{\tilde{k}_x\Delta x}{2}\right)e^{j\omega\Delta t}\,H_z^n\,(2-f) \tag{4.26b}$$

$$(e^{j\omega\Delta t} - e^{j\omega\Delta t/2})\,H_z^n = j\left(\frac{\Delta t}{\mu\,\Delta x}\right)\sin\left(\frac{\tilde{k}_x\Delta x}{2}\right)e^{j\omega\Delta t}\,E_y^n\,(2-f) - j\left(\frac{\Delta t}{\mu\,\Delta y}\right)\sin\left(\frac{\tilde{k}_y\Delta y}{2}\right)e^{j\omega\Delta t/2}\,E_x^n\,f \tag{4.26c}$$

Combining (4.25a) & (4.26a), (4.25b) & (4.26b) and (4.25c) & (4.26c) gives rise to the following :

$$(e^{j\omega\Delta t} - 1)\,E_x^n = -2j\left(\frac{\Delta t}{\varepsilon\,\Delta y}\right)\sin\left(\frac{\tilde{k}_y\Delta y}{2}\right)e^{j\omega\Delta t/2}\,H_z^n \tag{4.27a}$$

$$(e^{j\omega\Delta t} - 1)\,E_y^n = j\left(\frac{\Delta t}{\varepsilon\,\Delta x}\right)\sin\left(\frac{\tilde{k}_x\Delta x}{2}\right)H_z^n\left(e^{j\omega\Delta t}(2-f)+f\right) \tag{4.27b}$$

$$(e^{j\omega\Delta t} - 1)\,H_z^n = j\left(\frac{\Delta t}{\mu\,\Delta x}\right)\sin\left(\frac{\tilde{k}_x\Delta x}{2}\right)E_y^n\left(e^{j\omega\Delta t}(2-f)+f\right) - 2j\left(\frac{\Delta t}{\mu\,\Delta y}\right)\sin\left(\frac{\tilde{k}_y\Delta y}{2}\right)e^{j\omega\Delta t/2}\,E_x^n \tag{4.27c}$$

(4.27) can be simplified to :

$$\sin\left(\frac{\omega\Delta t}{2}\right)E_x^n = -\left(\frac{\Delta t}{\varepsilon\,\Delta y}\right)\sin\left(\frac{\tilde{k}_y\Delta y}{2}\right)H_z^n \tag{4.28a}$$

$$\sin\left(\frac{\omega\Delta t}{2}\right)E_y^n = f\left(\frac{\Delta t}{\varepsilon\Delta x}\right)\sin\left(\frac{\tilde{k}_x\Delta x}{2}\right)H_z^n\left[\cos\left(\frac{\omega\Delta t}{2}\right) + (1-f)\,e^{j\omega\Delta t/2}\right] \tag{4.28b}$$

$$\sin\left(\frac{\omega\Delta t}{2}\right)H_z^n = f\left(\frac{\Delta t}{\mu\Delta x}\right)\sin\left(\frac{\tilde{k}_x\Delta x}{2}\right)E_y^n\left[\cos\left(\frac{\omega\Delta t}{2}\right) + (1-f)\,e^{j\omega\Delta t/2}\right] - \left(\frac{\Delta t}{\mu\Delta y}\right)\sin\left(\frac{\tilde{k}_y\Delta y}{2}\right)E_x^n \tag{4.28c}$$

or

$$\begin{bmatrix} \sin\left(\frac{\omega\Delta t}{2}\right) & 0 & \frac{M_y}{\varepsilon} \\ 0 & \sin\left(\frac{\omega\Delta t}{2}\right) & -f\frac{M_x}{\varepsilon}\left[\cos\left(\frac{\omega\Delta t}{2}\right) + (1-f)\,e^{j\omega\Delta t/2}\right] \\ \frac{M_y}{\mu} & -f\frac{M_x}{\mu}\left[\cos\left(\frac{\omega\Delta t}{2}\right) + (1-f)\,e^{j\omega\Delta t/2}\right] & \sin\left(\frac{\omega\Delta t}{2}\right) \end{bmatrix}\begin{bmatrix} E_x^n \\ E_y^n \\ H_z^n \end{bmatrix} = 0 \tag{4.29}$$

Thus the numerical dispersion relation for a 2-dimensional TE wave is given by making the determinant of the matrix zero, i.e.

$$\sin\left(\frac{\omega\Delta t}{2}\right)\left\{\sin^2\left(\frac{\omega\Delta t}{2}\right) - f^2\frac{1}{\mu\varepsilon}\left(\frac{\Delta t}{\Delta x}\right)^2\sin^2\left(\frac{\tilde{k}_x\Delta x}{2}\right)\left[\cos\left(\frac{\omega\Delta t}{2}\right) + (1-f)\,e^{j\omega\Delta t/2}\right]^2\right\}$$
$$+ \sin\left(\frac{\omega\Delta t}{2}\right)\left\{-\frac{1}{\mu\varepsilon}\left(\frac{\Delta t}{\Delta y}\right)^2\sin^2\left(\frac{\tilde{k}_y\Delta y}{2}\right)\right\} = 0 \tag{4.30}$$

or

$$f^2\left(\frac{1}{\Delta x}\right)^2\sin^2\left(\frac{\tilde{k}_x\Delta x}{2}\right)\left[\cos\left(\frac{\omega\Delta t}{2}\right) + (1-f)\,e^{j\omega\Delta t/2}\right]^2 + \left(\frac{1}{\Delta y}\right)^2\sin^2\left(\frac{\tilde{k}_y\Delta y}{2}\right) = \left(\frac{1}{c\Delta t}\right)^2\sin^2\left(\frac{\omega\Delta t}{2}\right) \tag{4.31}$$

where $c = 1/\sqrt{\mu\varepsilon}$.

Equation (4.31) reverts to the numerical dispersion relation for 2-dimensional ADI-FDTD (3.34) when $f = 1$ as expected. Following the same argument as for (3.34), the implication of (4.31) is that numerical wave velocity for wave propagating in the direction of x, i.e. $\tilde{k}_y = 0$, is scaled from that of the standard FDTD scheme by the factor $\left[\cos\left(\frac{\omega\Delta t}{2}\right) + (1-f)\,e^{j\omega\Delta t/2}\right]^2$, which is larger (for $0 < f < 1$) than the factor $\cos^2\left(\frac{\omega\Delta t}{2}\right)$ in the ADI-FDTD method. On the other hand, for wave propagating in the direction of y, $\tilde{k}_x = 0$, the numerical wave velocity in the modified ADI-FDTD scheme is the same as that of the standard FDTD scheme.

4.7 Simulated results

The newly proposed modified ADI-FDTD method is used to simulate the line-fed rectangular microstrip patch. The physical dimension of the patch simulated is shown in Fig. 2.3 in chapter 2. The space steps used are $\Delta x = 0.389mm$, $\Delta y = 0.400mm$ and $\Delta z = 0.265mm$ and the total mesh dimension is 60 x 100 x 16 in the x, y and z directions respectively. The patch is excited with a Gaussian pulse. A 1st order Mur absorbing boundary condition is applied on all the five surrounding walls. A perfect electric wall boundary is applied on the ground plane and the copper patch; this is done by forcing the tangential electric fields on the copper patch to be zero at all time steps. The dielectric constant, ε_r, is set to 2.2. Fig.4.2 shows the comparison of results from the published literature [1.5] with that from the proposed modified ADI-FDTD with stability factor of 2.0, i.e. the time step is twice that allowed by the CFL criterion. For this case *f* is set to 0.9. Fig 4.3 shows another comparison of results, this time a stability factor of 3.0 is used and *f* is set to 0.8.

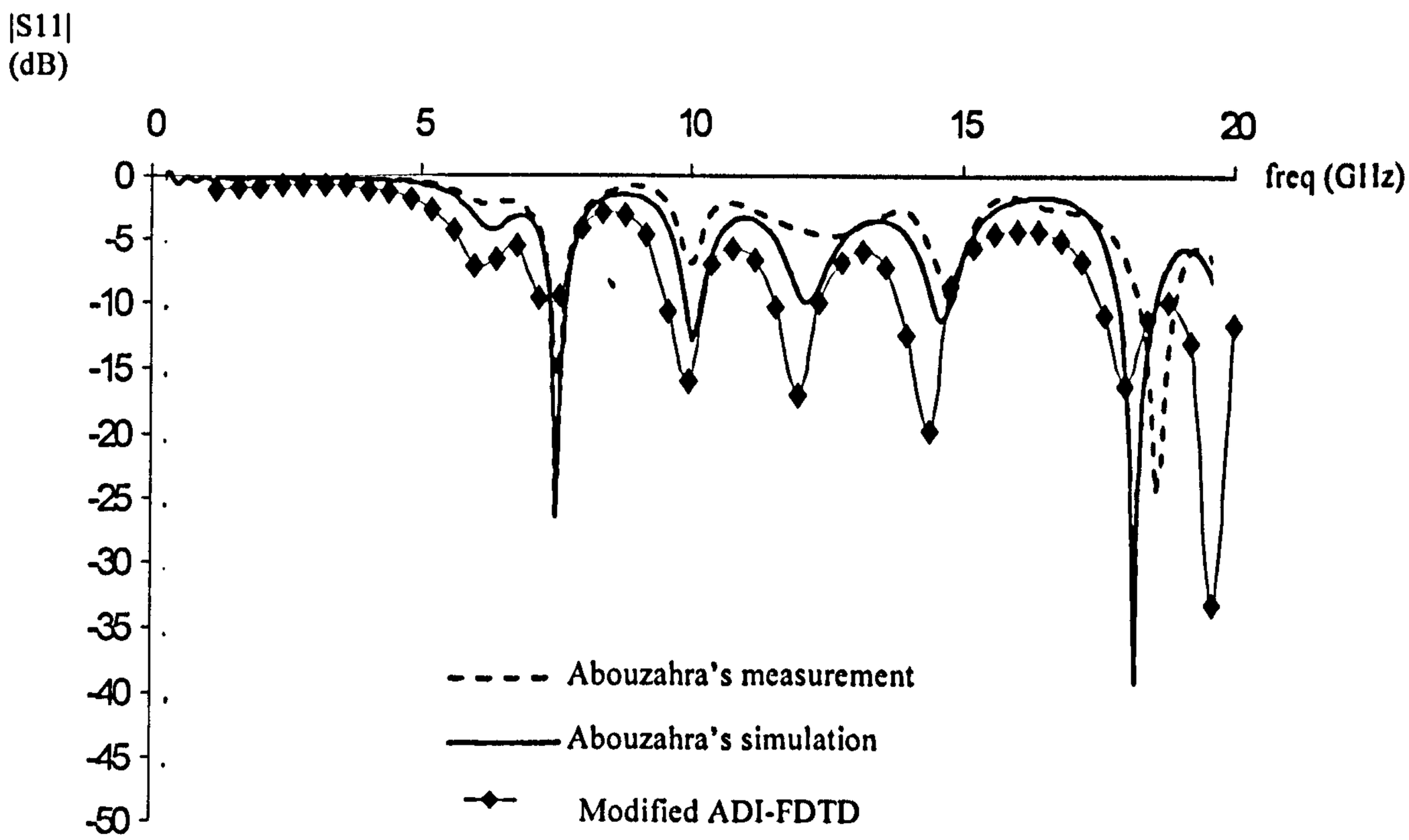

Fig. 4.2 : Modified ADI-FDTD with $\Delta t = 2 * \Delta t$ critical and $f = 0.9$

From Fig. 4.2, it can be seen that the magnitude of reflection coefficient, S_{11}, decreases from that when the conventional FDTD method is used. As explained in chapter 3, when ADI-FDTD is used to model a conductor using perfect electric wall boundary, the simulation results grow exponentially as time progresses until eventually the system becomes unstable. Unlike in the ADI-FDTD method, in modified ADI-FDTD scheme, the implicit and explicit terms are not weighted equally as shown in (4.1)-(4.4). Effectively, ADI-FDTD method is in the form of a predictor-corrector method, the explicit term being the predictor term and implicit term the corrector term. The fact that ADI-FDTD result becomes unstable in chapter 3 implies that there is a gain in the system. By introducing a weighting factor greater than unity on the implicit term in modified ADI-FDTD method, the corrector term is weighted more heavily than the predictor term. This 'corrects' the results and maintain stability in the system but the side effect of this is a reduction in the magnitude of S_{11} as expected due to the corrector term being greater than unity.

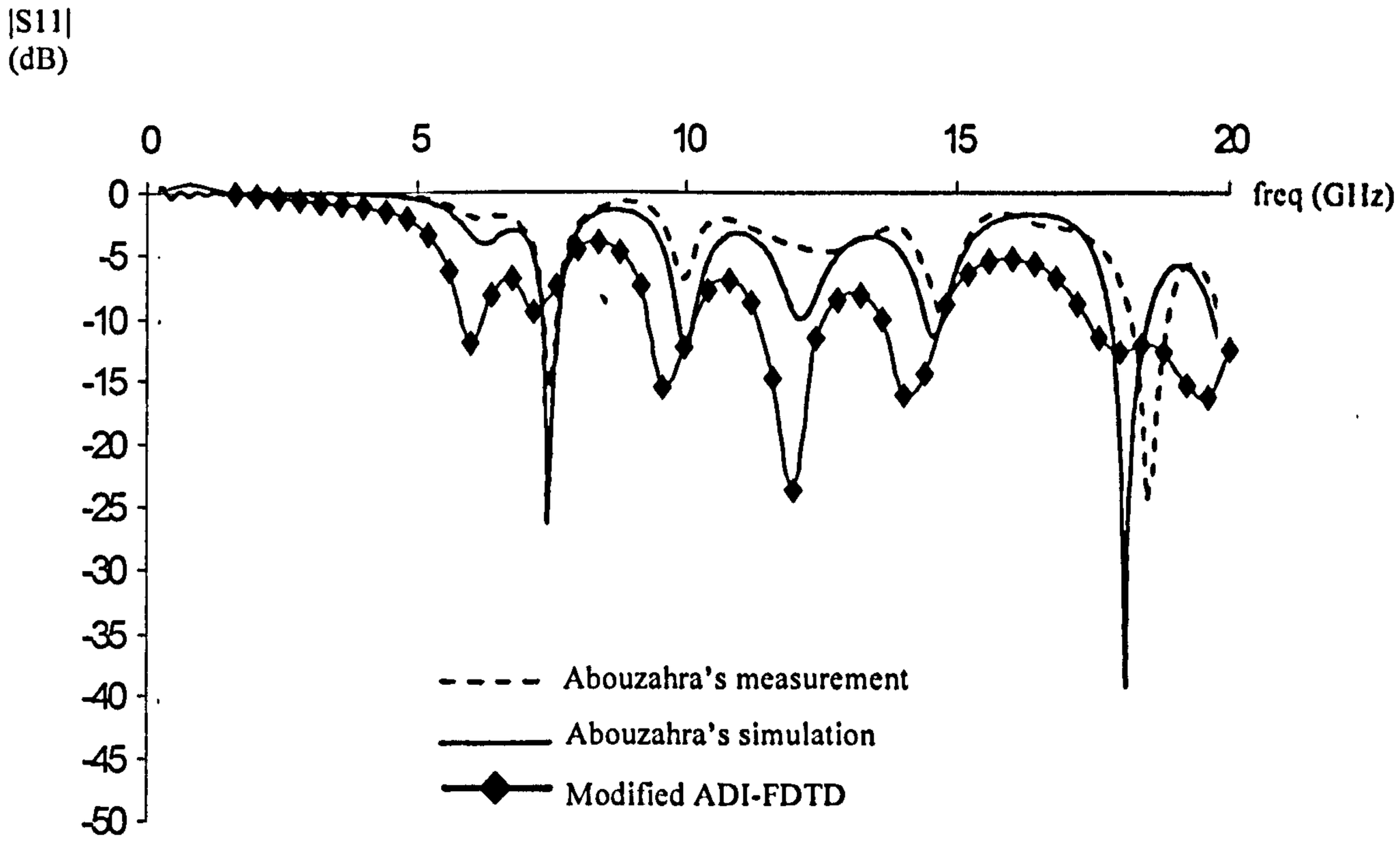

Fig. 4.3 : Modified ADI-FDTD with $\Delta t = 3 * \Delta t$ critical and $f = 0.8$

4.8 Relationship between attenuation and weighting factor *f*

To understand the relationship between the decreasing of S_{11} magnitude and the weighting factor, *f*, used, the simulation for the line-fed rectangular microstrip patch was run with several different weighting factors and the S11 plots are as shown below.

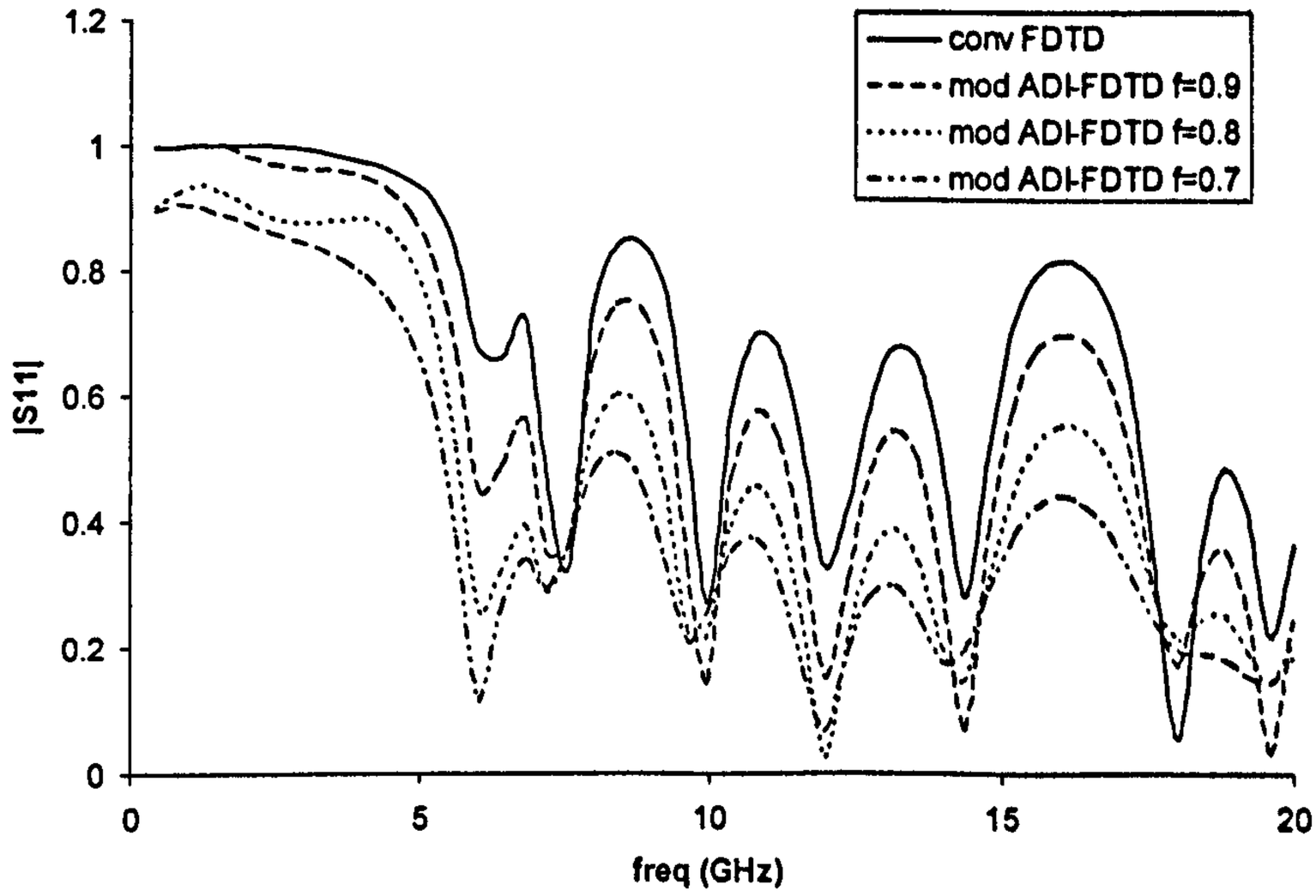

Fig. 4.4 : Comparison between conventional FDTD and modified ADI-FDTD results with $\Delta t = 2 * \Delta t$ critical and *f* set at 0.9, 0.8 & 0.7. Δt critical is used with conventional FDTD.

The results in Fig.4.4 show that the attenuation increases as the weighting factor of the explicit term on the modified ADI-FDTD, *f*, is reduced.

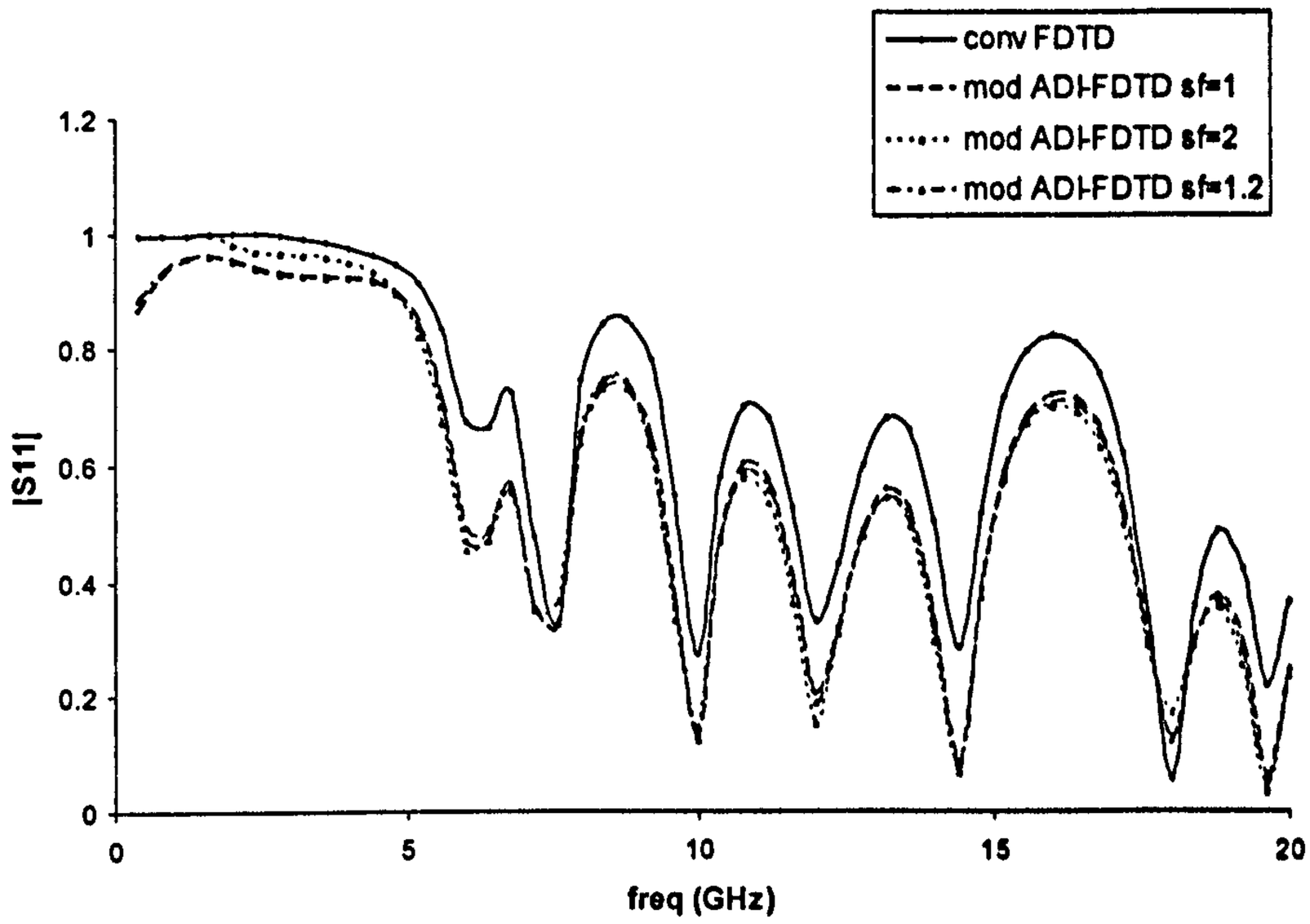

Fig. 4.5 : Modified ADI-FDTD results with *f* set at 0.9

Fig. 4.5 above shows the |S11| of the line-fed rectangular micrctrip patch simulated with the modified ADI-FDTD method with the weighting factor, *f*, set to 0.9. Fig. 4.6 below shows the results for the same patch with the weighting factor set to 0.8. Changing the stability factor and therefore the time-step used in the algorithm does not change the attenuation significantly for a particular weighting factor.

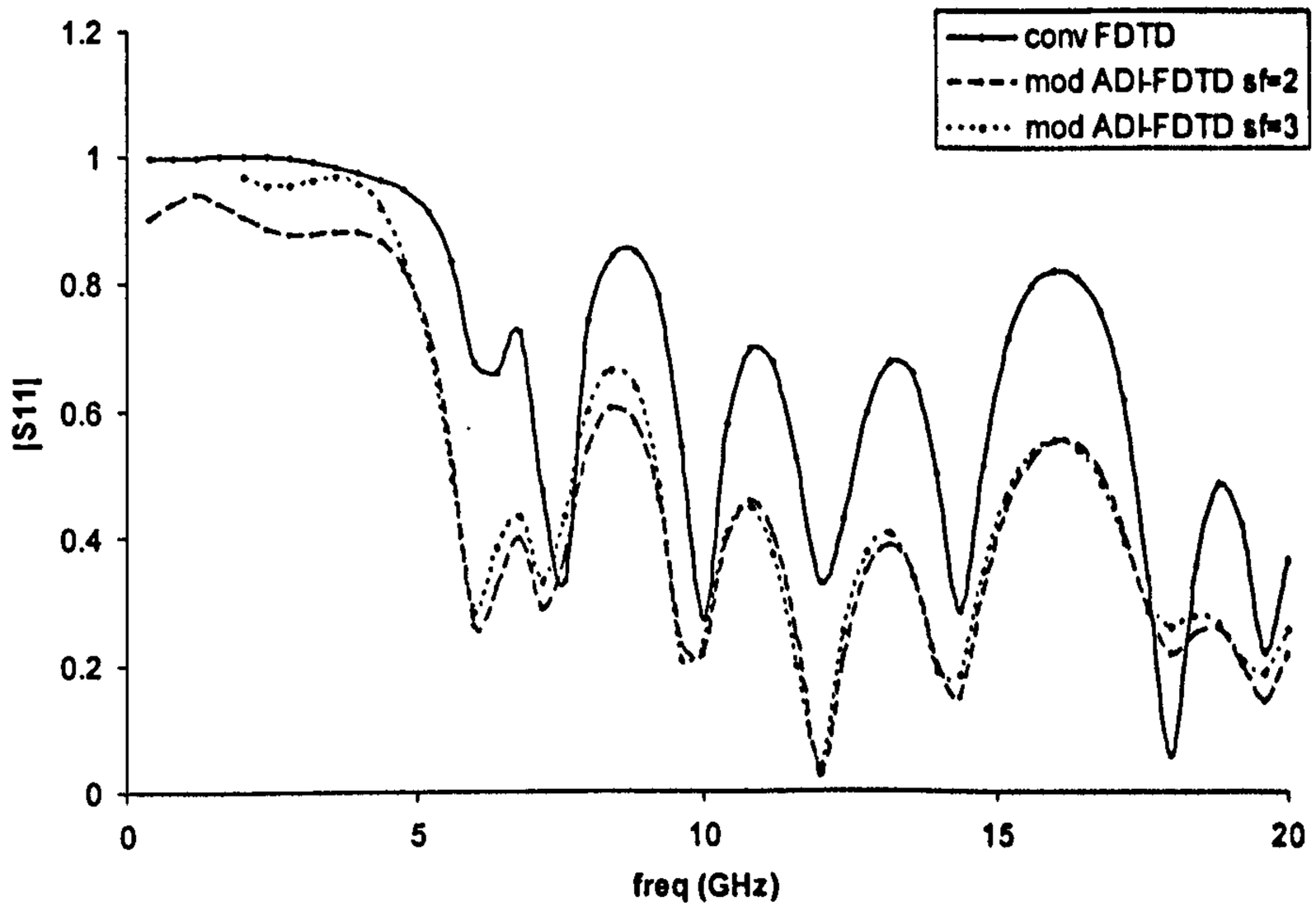

Fig. 4.6 : Modified ADI-FDTD results with *f* set at 0.8

4.9 Conclusion

A new modified ADI-FDTD method with the introduction of a factor f has been theoretically derived and numerically simulated. From the study of the numerical stability of the scheme, both two- and three-dimensional modified ADI-FDTD algorithms are shown to be permanently stable as long as $0 < f < 1$. The results for a three-dimensional model of a patch antenna are stable even though the CFL criterion has not been observed and they compare reasonably well with the published results in terms of the resonant frequency points. The copper patch in the modified ADI-FDTD scheme has been modelled as a perfect electric wall boundary where the tangential electric fields on the patch are set to zero at each time step. The same structure, when modelled using the ADI-FDTD where the copper patch is modelled also as a perfect electric wall boundary, showed instability. Although the results from the modified ADI-FDTD show a decrease in its S_{11} amplitude, this technique is easy to implement and it is useful as a quick method to obtain accurate resonant frequencies.

In Chapter 5 we propose a new implementation method of the ADI-FDTD in order to overcome the problem of instability without compromising the amplitude of the response.

CHAPTER 5
SIMULATING COPPER LAYER IN ALTERNATING-DIRECTION IMPLICIT METHOD

5.1 Introduction

The introduction of the ADI-FDTD technique has made it possible to speed up simulation run-time of large electrical objects even when there are small discontinuities in the model without compromising the stability of the system. In this research work, the ADI-FDTD method has been shown to work numerically on an air-filled three-dimensional rectangular cavity and on a three-dimensional rectangular cavity with inhomogeneous media. To model a transmission line as a perfect electric wall boundary, the modified ADI-FDTD has to be implemented instead of the ADI-FDTD to maintain stability. The modified ADI-FDTD gives reasonably accurate resonant frequency points although the amplitudes are attenuated due to the inherent property of the algorithm. Although the newly proposed modified ADI-FDTD scheme is useful for quick numerical analysis of microstrip circuits, for the ADI-FDTD scheme to be generically useful, it must be able to model more complex structures including microstrip patches with reasonable accuracy both in amplitude and frequency points without going unstable. Indeed, a method of modelling a copper patch in conjunction with the ADI-FDTD technique without causing either instability or attenuation is desirable.

In this chapter, a copper patch is modelled in the ADI-FDTD algorithm as a layer of material with a finite electric conductivity. The finite-difference equations which include the electric conductivity term are presented and results for several simulations are shown and compared with published results and results obtained from conventional FDTD method.

5.2 Three-dimensional ADI-FDTD algorithm with electric conductivity term

Consider the Maxwell's curl equation for electric field shown in (2.12a) – (2.12c) which include the electric conductivity term, σ, to account for electric current loss in materials. Equation (2.12a) is repeated below for convenience.

$$\frac{\partial E_x}{\partial t} = \frac{1}{\varepsilon}\left(\frac{\partial H_z}{\partial y} - \frac{\partial H_y}{\partial z} - \sigma E_x\right) \tag{5.1}$$

The centred-difference finite-difference approximation of (5.1) is given by :

$$E_x^{n+1}(i,j,k) = E_x^n(i,j,k) + \frac{\Delta t}{\varepsilon}\left\{\frac{H_z^{n+1/2}(i,j,k) - H_z^{n+1/2}(i,j-1,k)}{\Delta y} - \frac{H_y^{n+1/2}(i,j,k) - H_y^{n+1/2}(i,j,k-1)}{\Delta z} - \sigma(i,j,k)\, E_x^{n+1/2}(i,j,k)\right.$$

(5.2)

Note that all the fields within the bracket on the right-hand side are evaluated at time step n+ ½ Δt. Since the electric at n+ ½ Δt is not readily available, it is calculated using the semi-implicit approximation below.

$$E_x^{n+1/2}(i,j,k) = \frac{E_x^n(i,j,k) + E_x^{n+1}(i,j,k)}{2} \tag{5.3}$$

Substituting (5.3) into (5.1) gives the following :

$$E_x^{n+1}(i,j,k) = E_x^n(i,j,k)\left(\frac{1 - \frac{\sigma(i,j,k)\,\Delta t}{2\varepsilon}}{1 + \frac{\sigma(i,j,k)\,\Delta t}{2\varepsilon}}\right) + \left(\frac{\frac{\Delta t}{\varepsilon}}{1 + \frac{\sigma(i,j,k)\,\Delta t}{2\varepsilon}}\right)\left\{\frac{H_z^{n+1/2}(i,j,k) - H_z^{n+1/2}(i,j-1,k)}{\Delta y} - \frac{H_y^{n+1/2}(i,j,k) - H_y^{n+1/2}(i,j,k-1)}{\Delta z}\right\} \tag{5.4}$$

Applying the same technique on all the electric field calculations in the ADI-FDTD method produces the following equations. Note that the Δt is replaced with Δt/2 in both procedures 1 and 2 in the ADI-FDTD equations. Also, since magnetic loss is not considered here, the magnetic field equations remain the same as in the ADI-FDTD method discussed in chapter 3.

Procedure 1

$$E_x^{n+1/2}(i+1/2,j,k) = E_x^n(i+1/2,j,k)\left(\frac{1 - \frac{\sigma(i+1/2,j,k)\,\Delta t}{4\varepsilon}}{1 + \frac{\sigma(i+1/2,j,k)\,\Delta t}{4\varepsilon}}\right) + \left(\frac{\frac{\Delta t}{2\varepsilon}}{1 + \frac{\sigma(i+1/2,j,k)\,\Delta t}{4\varepsilon}}\right)\left\{\frac{H_z^{n+1/2}(i+1/2,j+1/2,k) - H_z^{n+1/2}(i+1/2,j-1/2,k)}{\Delta y} - \frac{H_y^n(i+1/2,j,k+1/2) - H_y^n(i+1/2,j,k-1/2)}{\Delta z}\right\} \tag{5.5a}$$

$$E_y^{n+1/2}(i,j+1/2,k) = E_y^n(i,j+1/2,k)\left(\frac{1 - \frac{\sigma(i,j+1/2,k)\,\Delta t}{4\varepsilon}}{1 + \frac{\sigma(i,j+1/2,k)\,\Delta t}{4\varepsilon}}\right) + \left(\frac{\frac{\Delta t}{2\varepsilon}}{1 + \frac{\sigma(i,j+1/2,k)\,\Delta t}{4\varepsilon}}\right)\left\{\frac{H_x^{n+1/2}(i,j+1/2,k+1/2) - H_x^{n+1/2}(i,j+1/2,k-1/2)}{\Delta z} - \frac{H_z^n(i+1/2,j+1/2,k) - H_z^n(i-1/2,j+1/2,k)}{\Delta x}\right\} \tag{5.5b}$$

$$E_z^{n+1/2}(i,j,k+1/2) = E_z^n(i,j,k+1/2)\left(\frac{1-\frac{\sigma(i,j,k+1/2)\,\Delta t}{4\varepsilon}}{1+\frac{\sigma(i,j,k+1/2)\,\Delta t}{4\varepsilon}}\right) + \left(\frac{\frac{\Delta t}{2\varepsilon}}{1+\frac{\sigma(i,j,k+1/2)\,\Delta t}{4\varepsilon}}\right)\left\{\frac{H_y^{n+1/2}(i+1/2,j,k+1/2)-H_y^{n+1/2}(i-1/2,j,k+1/2)}{\Delta x} - \frac{H_x^n(i,j+1/2,k+1/2)-H_x^n(i,j-1/2,k+1/2)}{\Delta y}\right\} \quad (5.5c)$$

$$H_x^{n+1/2}(i,j+1/2,k+1/2) = H_x^n(i,j+1/2,k+1/2) - \frac{\Delta t}{2\mu}\left\{\frac{E_z^n(i,j+1,k+1/2)-E_z^n(i,j,k+1/2)}{\Delta y} - \frac{E_y^{n+1/2}(i,j+1/2,k+1)-E_y^{n+1/2}(i,j+1/2,k)}{\Delta z}\right\} \quad (5.6a)$$

$$H_y^{n+1/2}(i+1/2,j,k+1/2) = H_y^n(i+1/2,j,k+1/2) - \frac{\Delta t}{2\mu}\left\{\frac{E_x^n(i+1/2,j,k+1)-E_x^n(i+1/2,j,k)}{\Delta z} - \frac{E_z^{n+1/2}(i+1,j,k+1/2)-E_z^{n+1/2}(i,j,k+1/2)}{\Delta x}\right\} \quad (5.6b)$$

$$H_z^{n+1/2}(i+1/2,j+1/2,k) = H_z^n(i+1/2,j+1/2,k) - \frac{\Delta t}{2\mu}\left\{\frac{E_y^n(i+1,j+1/2,k)-E_y^n(i,j+1/2,k)}{\Delta x} - \frac{E_x^{n+1/2}(i+1/2,j+1,k)-E_x^{n+1/2}(i+1/2,j,k)}{\Delta y}\right\} \quad (5.6c)$$

Substituting equations (5.6) into (5.5) appropriately result in tri-diagonal matrices of E_x, E_y and E_z. Tri-diagonal for E_x for procedure 1 is shown below, the rest are shown in Appendix B3

$$E_x^{n+1}(i+1/2,j,k-1) - E_x^{n+1}(i+1/2,j,k)\left[2+\left(\frac{\sqrt{\mu\varepsilon}\Delta z}{\Delta t}\right)^2\left(1+\frac{\sigma(i+1/2,j,k)\,\Delta t}{4\varepsilon}\right)\right] + E_x^{n+1}(i+1/2,j,k+1)$$

$$= -E_x^{n+1/2}(i+1/2,j,k)\left(\frac{\sqrt{\mu\varepsilon}\Delta z}{\Delta t}\right)^2\left(1-\frac{\sigma(i+1/2,j,k)\,\Delta t}{4\varepsilon}\right)$$

$$+\left(\frac{\Delta z}{\Delta x}\right)\left[E_z^{n+1/2}(i+1,j,k+1/2) - E_z^{n+1/2}(i,j,k+1/2) - E_z^{n+1/2}(i+1,j,k-1/2) + E_z^{n+1/2}(i,j,k-1/2)\right]$$

$$-\left(\frac{\mu\Delta z}{\Delta t}\right)\left[H_y^{n+1/2}(i+1/2,j,k+1/2) - H_y^{n+1/2}(i+1/2,j,k-1/2)\right] + \left(\frac{\mu\Delta z^2}{\Delta t\Delta y}\right)\left[H_z^{n+1/2}(i+1/2,j+1/2,k) - H_z^{n+1/2}(i+1/2,j-1/2,k)\right] \quad (5.7)$$

Procedure 2

$$E_x^{n+1}(i+1/2,j,k) = E_x^{n+1/2}(i+1/2,j,k)\left(\frac{1-\frac{\sigma(i+1/2,j,k)\,\Delta t}{4\varepsilon}}{1+\frac{\sigma\,\Delta t}{4\varepsilon}}\right) + \left(\frac{\frac{\Delta t}{2\varepsilon}}{1+\frac{\sigma(i+1/2,j,k)\Delta t}{4\varepsilon}}\right)\left\{\frac{H_z^{n+1/2}(i+1/2,j+1/2,k)-H_z^{n+1/2}(i+1/2,j-1/2,k)}{\Delta y} - \frac{H_y^{n+1}(i+1/2,j,k+1/2)-H_y^{n+1}(i+1/2,j,k-1/2)}{\Delta z}\right\} \quad (5.8a)$$

$$E_y^{n+1}(i,j+1/2,k) = E_y^{n+1/2}(i,j+1/2,k)\left(\frac{1-\frac{\sigma(i,j+1/2,k)\,\Delta t}{4\varepsilon}}{1+\frac{\sigma(i,j+1/2,k)\,\Delta t}{4\varepsilon}}\right) + \left(\frac{\frac{\Delta t}{2\varepsilon}}{1+\frac{\sigma(i,j+1/2,k)\Delta t}{4\varepsilon}}\right)\left\{\frac{H_x^{n+1/2}(i,j+1/2,k+1/2)-H_x^{n+1/2}(i,j+1/2,k-1/2)}{\Delta z} - \frac{H_z^{n+1}(i+1/2,j+1/2,k)-H_z^{n+1}(i-1/2,j+1/2,k)}{\Delta x}\right\} \quad (5.8b)$$

$$E_z^{n+1}(i,j,k+1/2) = E_z^{n+1/2}(i,j,k+1/2)\left(\frac{1-\frac{\sigma(i,j,k+1/2)\,\Delta t}{4\varepsilon}}{1+\frac{\sigma(i,j,k+1/2)\,\Delta t}{4\varepsilon}}\right) + \left(\frac{\frac{\Delta t}{2\varepsilon}}{1+\frac{\sigma(i,j,k+1/2)\Delta t}{4\varepsilon}}\right)\left\{\frac{H_y^{n+1/2}(i+1/2,j,k+1/2)-H_y^{n+1/2}(i-1/2,j,k+1/2)}{\Delta x} - \frac{H_x^{n+1}(i,j+1/2,k+1/2)-H_x^{n+1}(i,j-1/2,k+1/2)}{\Delta y}\right\} \quad (5.8c)$$

$$H_x^{n+1}(i,j+1/2,k+1/2) = H_x^{n+1/2}(i,j+1/2,k+1/2) - \frac{\Delta t}{2\mu}\left\{\frac{E_z^{n+1}(i,j+1,k+1/2)-E_z^{n+1}(i,j,k+1/2)}{\Delta y} - \frac{E_y^{n+1/2}(i,j+1/2,k+1)-E_y^{n+1/2}(i,j+1/2,k)}{\Delta z}\right\} \quad (5.9a)$$

$$H_y^{n+1}(i+1/2,j,k+1/2) = H_y^{n+1/2}(i+1/2,j,k+1/2) - \frac{\Delta t}{2\mu}\left\{\frac{E_x^{n+1}(i+1/2,j,k+1)-E_x^{n+1}(i+1/2,j,k)}{\Delta z} - \frac{E_z^{n+1/2}(i+1,j,k+1/2)-E_z^{n+1/2}(i,j,k+1/2)}{\Delta x}\right\} \quad (5.9b)$$

$$H_z^{n+1}(i+1/2,j+1/2,k) = H_z^{n+1/2}(i+1/2,j+1/2,k) - \frac{\Delta t}{2\mu}\left\{\frac{E_y^{n+1}(i+1,j+1/2,k)-E_y^{n+1}(i,j+1/2,k)}{\Delta x} - \frac{E_x^{n+1/2}(i+1/2,j+1,k)-E_x^{n+1/2}(i+1/2,j,k)}{\Delta y}\right\} \quad (5.9c)$$

Again, substituting equations (5.9) into (5.8) appropriately result in tri-diagonal matrices of E_x, E_y and E_z. Tri-diagonal for E_x for procedure 2 is shown below, the rest are shown in Appendix B3.

$$E_x^{n+1}(i+1/2,j,k-1) - E_x^{n+1}(i+1/2,j,k)\left[2+\left(\frac{\sqrt{\mu\varepsilon}\Delta z}{\Delta t}\right)^2\left(1+\frac{\sigma(i+1/2,j,k)\,\Delta t}{4\,\varepsilon}\right)\right] + E_x^{n+1}(i+1/2,j,k+1)$$

$$= -E_x^{n+1/2}(i+1/2,j,k)\left(\frac{\sqrt{\mu\varepsilon}\Delta z}{\Delta t}\right)^2\left(1-\frac{\sigma(i+1/2,j,k)\;\Delta t}{4\,\varepsilon}\right)$$

$$+\left(\frac{\Delta z}{\Delta x}\right)\left[E_z^{n+1/2}(i+1,j,k+1/2) - E_z^{n+1/2}(i,j,k+1/2) - E_z^{n+1/2}(i+1,j,k-1/2) + E_z^{n+1/2}(i,j,k-1/2)\right]$$

$$-\left(\frac{\mu\Delta z}{\Delta t}\right)\left[H_y^{n+1/2}(i+1/2,j,k+1/2) - H_y^{n+1/2}(i+1/2,j,k-1/2)\right] + \left(\frac{\mu\Delta z^2}{\Delta t\Delta y}\right)\left[H_z^{n+1/2}(i+1/2,j+1/2,k) - H_z^{n+1/2}(i+1/2,j-1/2,k)\right] \tag{5.10}$$

5.3 Simulated results

5.3.1 Simulation of a line-fed rectangular microstrip patch

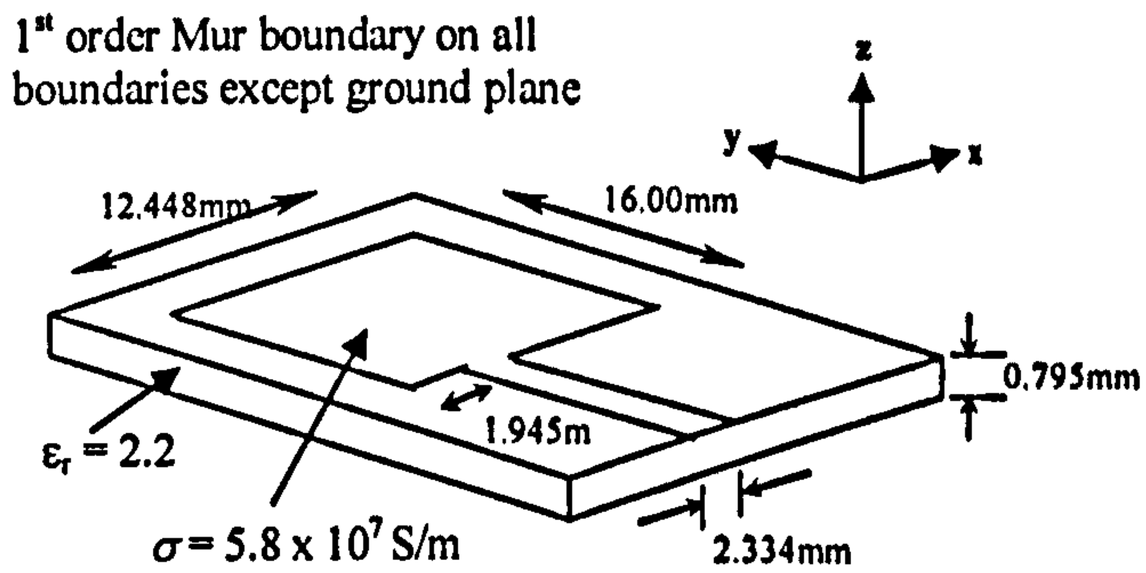

Fig. 5.1 : Line-fed rectangular microstrip patch

In chapters 3 and 4, the microstrip is modelled as a perfect electric wall boundary where the tangential electric fields on the microstrip are forced to be zero at each half time step. This models the copper on the microstrip as an ideal conductor with an infinite conductivity. In reality, the copper layer has a finite conductivity taken as 5.8×10^7 S/m which contributes to its finite electric loss in the form of conduction current on the copper layer.

In order to validate the ADI-FDTD program with the added electric conductivity term, the finite-difference time-domain equations (5.5) - (5.6) and (5.8) - (5.9) are used with the 1st order Mur boundary condition to simulate the propagation of a broad-band Gaussian pulse on a line-fed rectangular microstrip patch as shown in Fig. 5.1. As in chapter 3, the finite-difference mesh parameters are chosen to be the same as in the published paper [1.5] to allow direct comparison of results.

Fig. 5.2 shows a comparison of the time-domain response between the ADI-FDTD and the conventional FDTD method when stability factor of 1 is used in the ADI-FDTD program. With the copper layer modelled as a layer of material with finite copper conductivity, σ, of 5.8×10^7 S/m, the results are stable when stability factors of up to 8 are used in the ADI-FDTD program.

5.3.1.1 Transient response

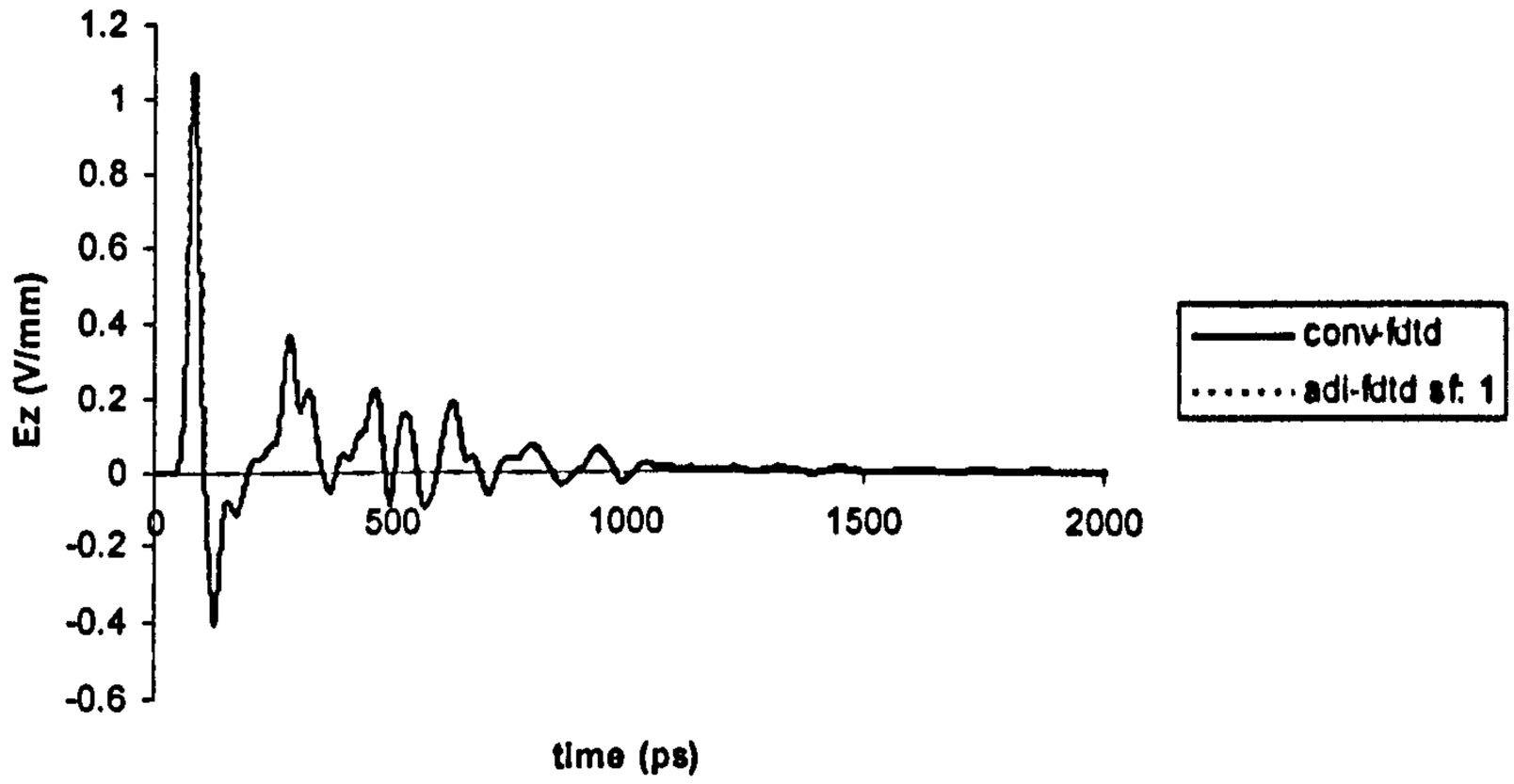

Fig.5.2 : Comparison between conventional FDTD and ADI-FDTD with stability factor 1

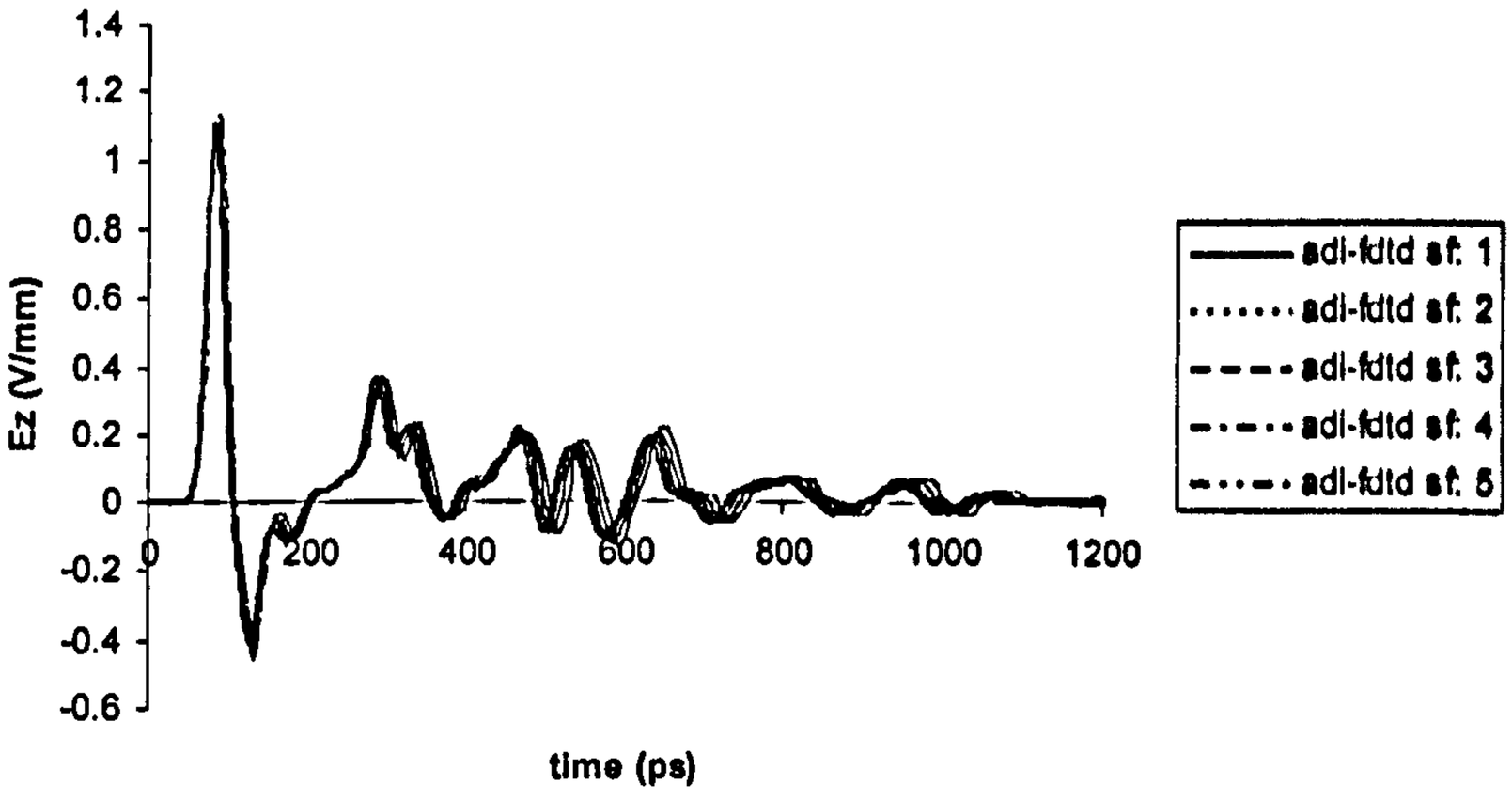

Fig.5.3 : Comparison between conventional FDTD and ADI-FDTD with stability factors 1 to 5 in steps of 1

Fig. 5.3 shows the comparison between FDTD and ADI-FDTD with stability factors 1 to 5 in steps of 1. The results are completely stable. As the stability factor is increased, the effect of numerical dispersion begins to appear in the results as the Gaussian pulse begins to broaden. This effect is shown more clearly in Figs. 5.5 and 5.6 where the time responses are magnified for a clearer view of the transient response. It can be seen from Fig.5.6 that the Gaussian pulse broadens as the time step used is increased. Fig.5.4 shows a good agreement between the conventional FDTD and ADI-FDTD with stability factor 1.

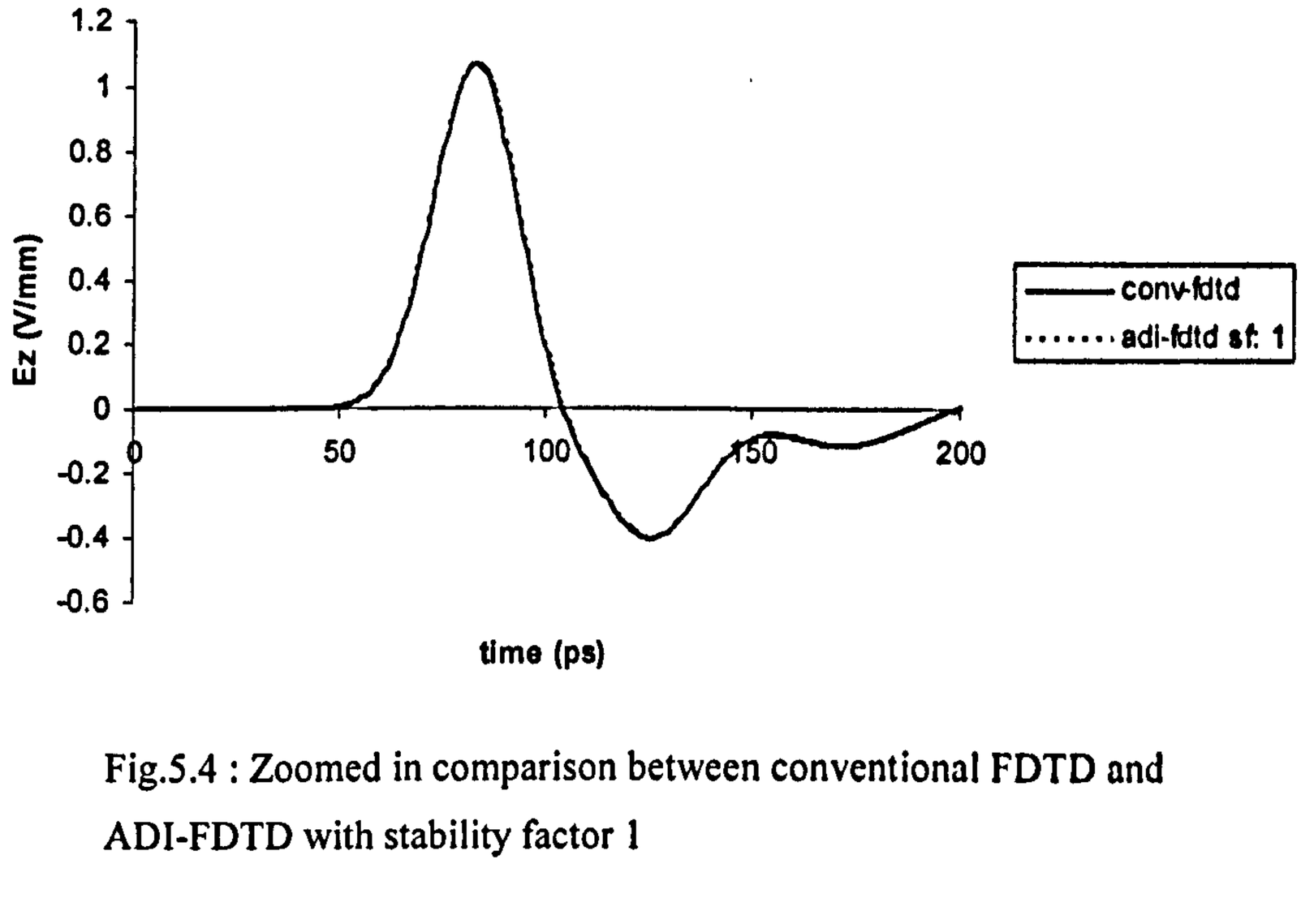

Fig.5.4 : Zoomed in comparison between conventional FDTD and ADI-FDTD with stability factor 1

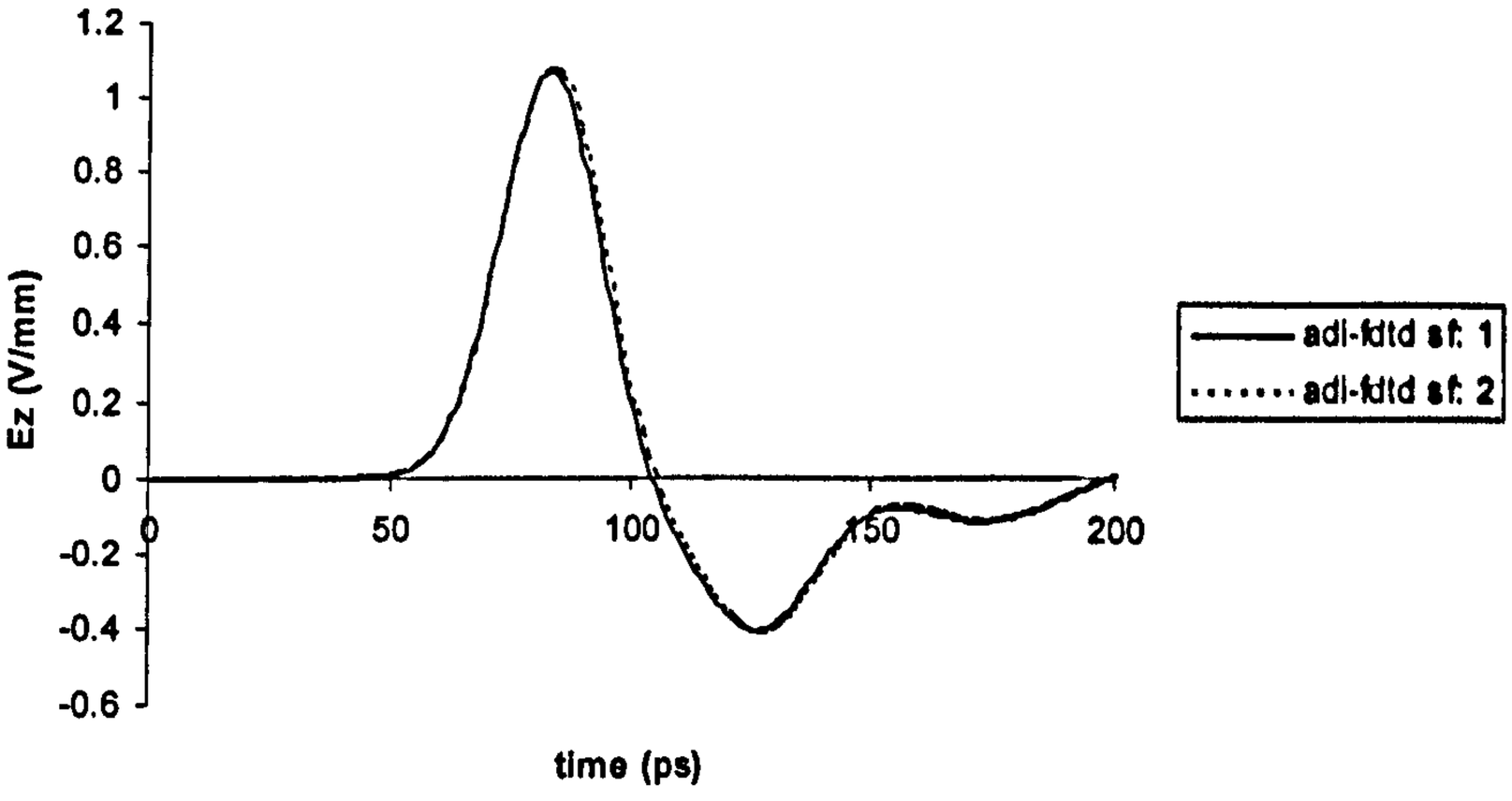

Fig.5.5 : Slight broadening of pulse in ADI-FDTD with stability factor 2

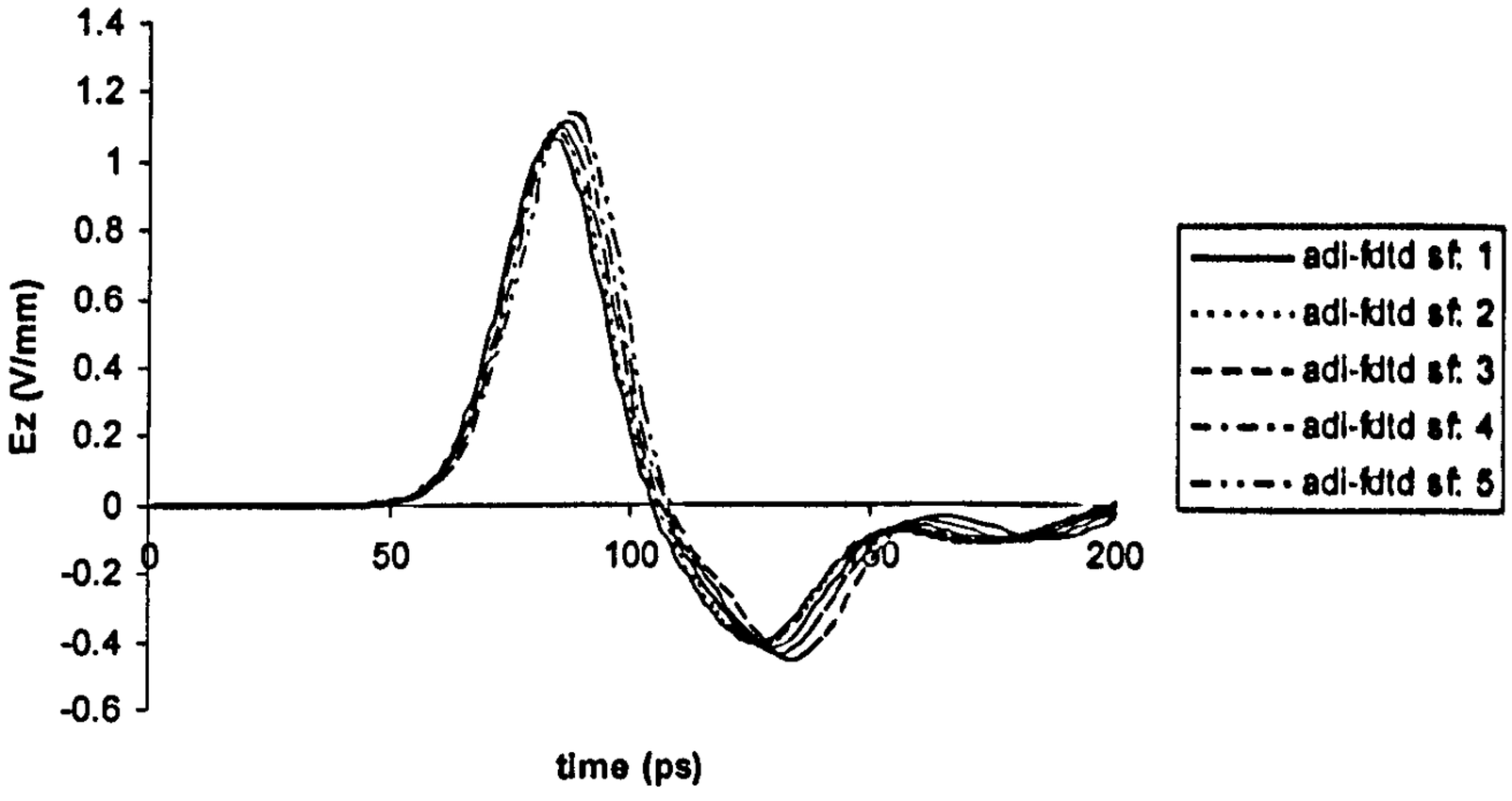

Fig. 5.6 : Effect of numerical dispersion in ADI-FDTD with stability factors 3,4 and 5

5.3.1.2 Frequency response

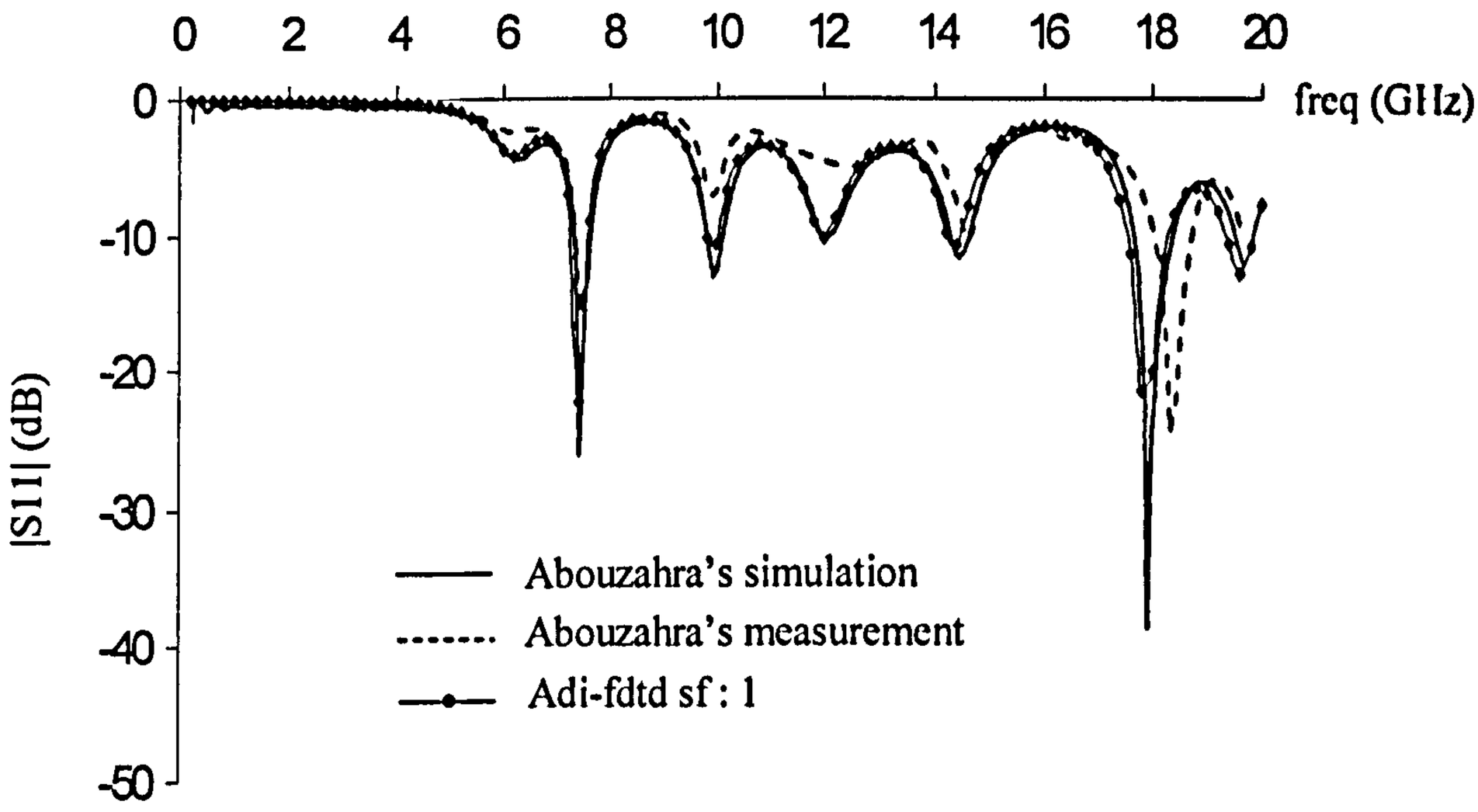

Fig.5.7 : Comparison of ADI-FDTD with stability 1 with Abouzahra [1.5]

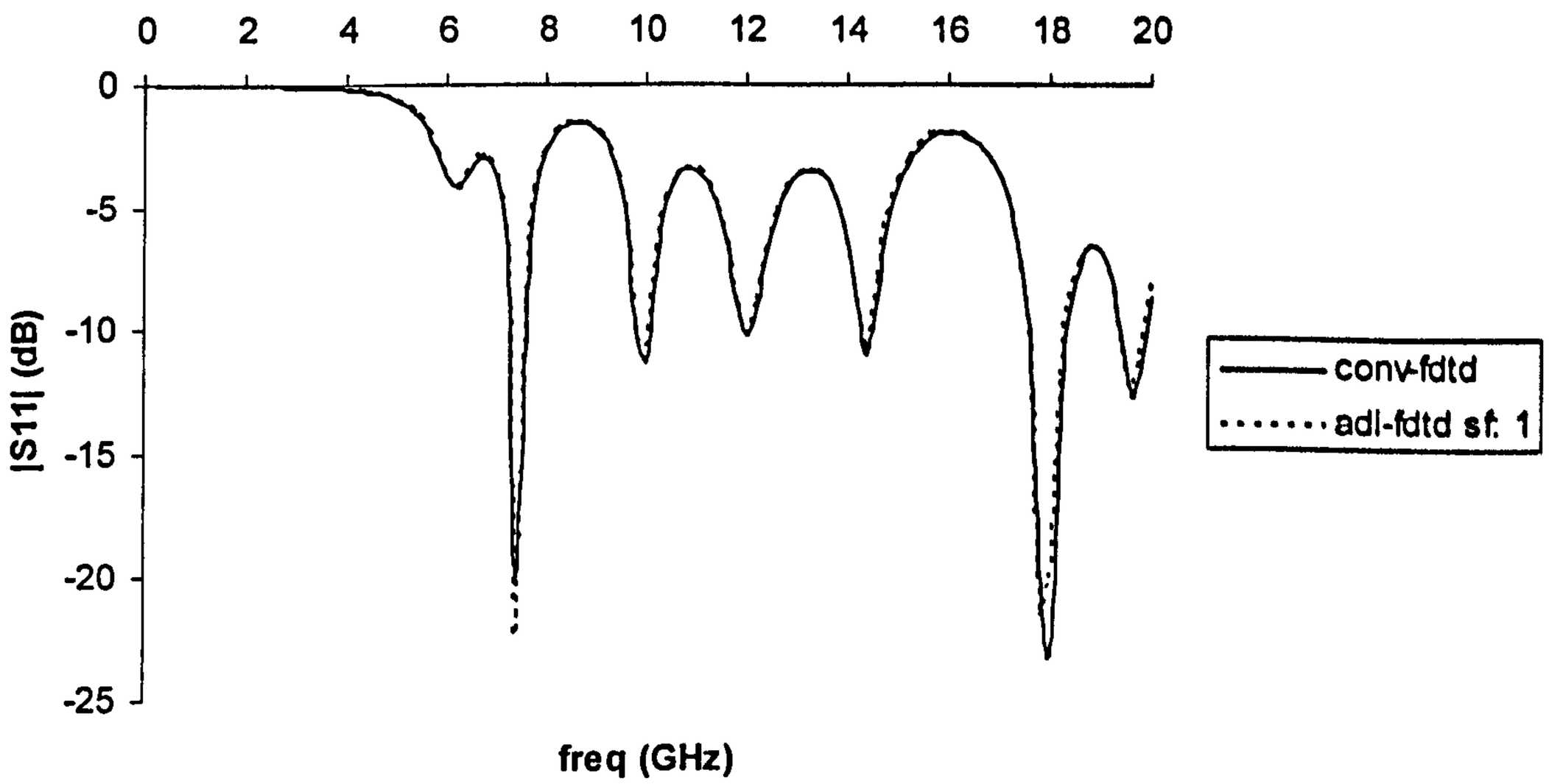

Fig. 5.8 : Comparison of conventional FDTD with ADI-FDTD with stability factor 1

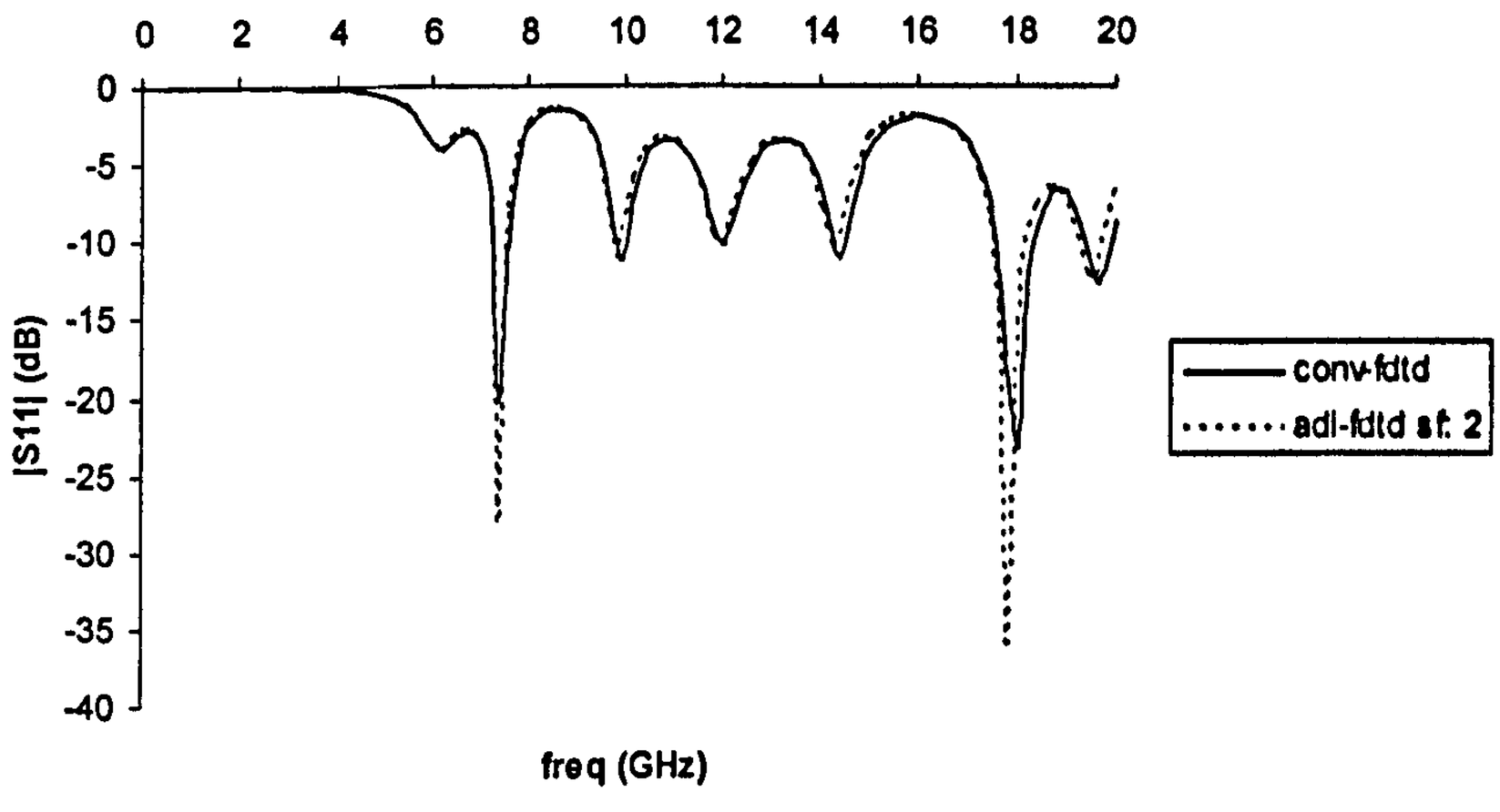

Fig. 5.9 : Comparison of conventional FDTD with ADI-FDTD with stability factor 2

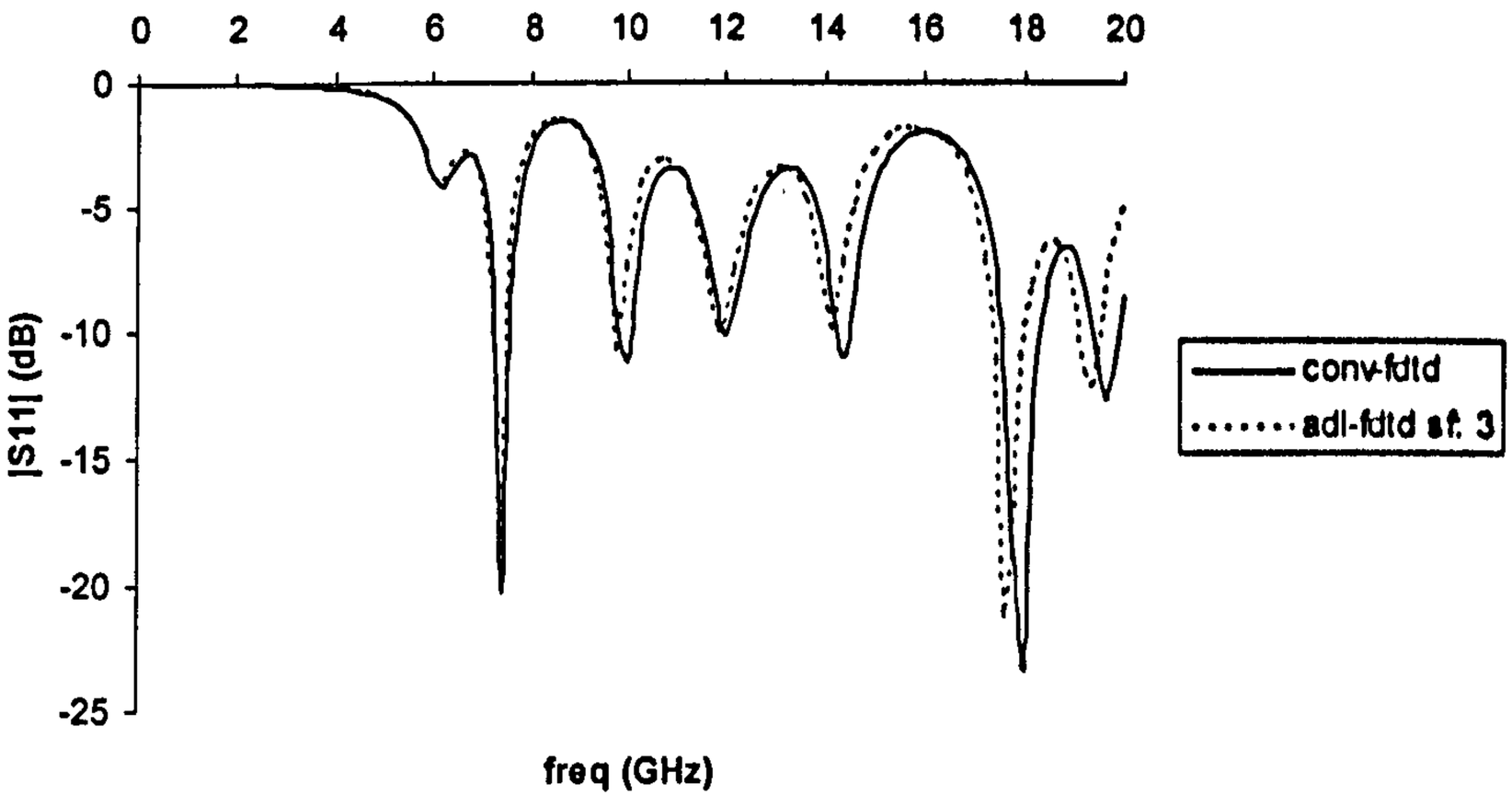

Fig. 5.10 : Comparison of conventional FDTD with ADI-FDTD with stability factor 3

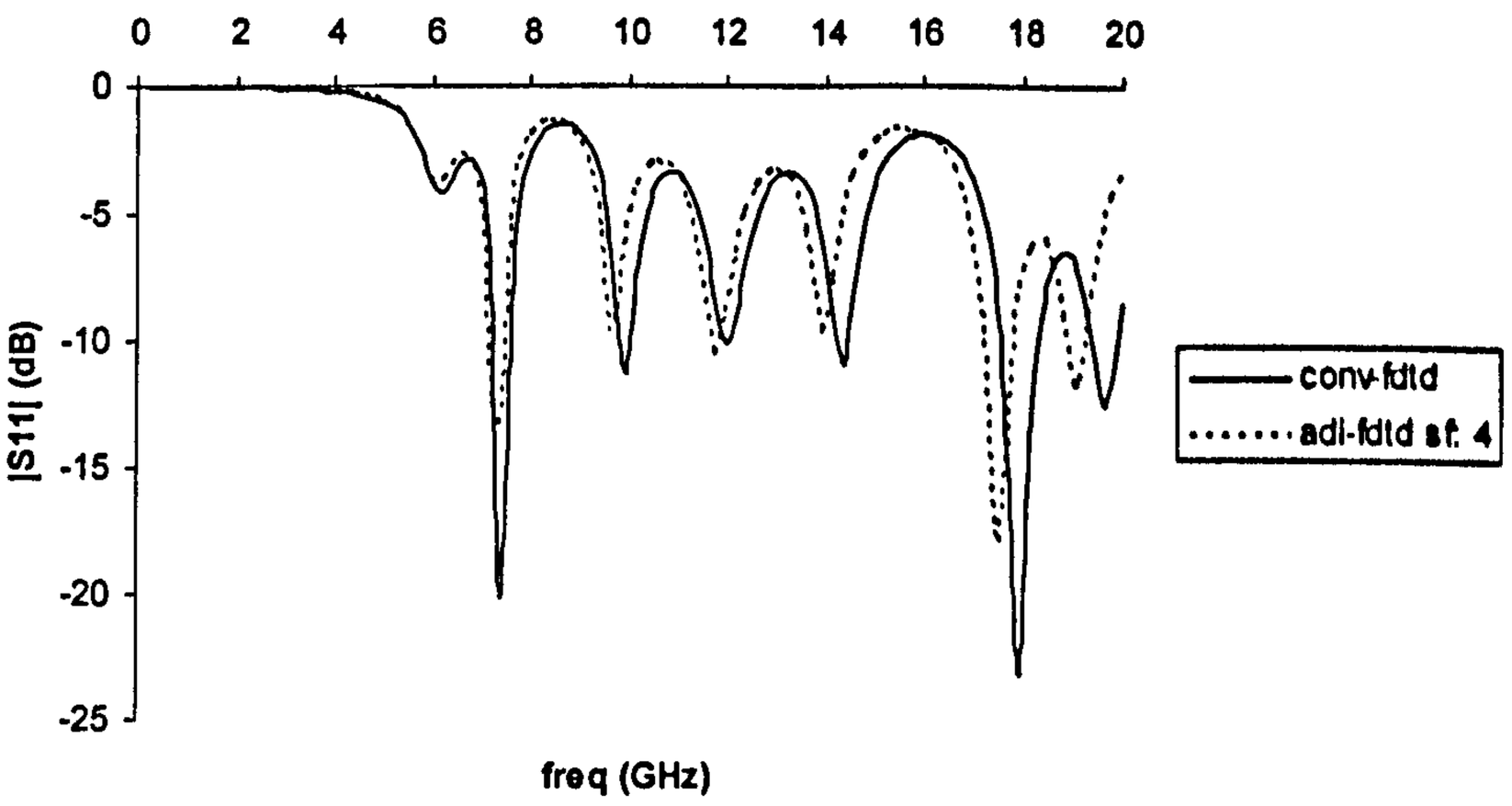

Fig. 5.11 : Comparison of conventional FDTD with ADI-FDTD with stability factor 4

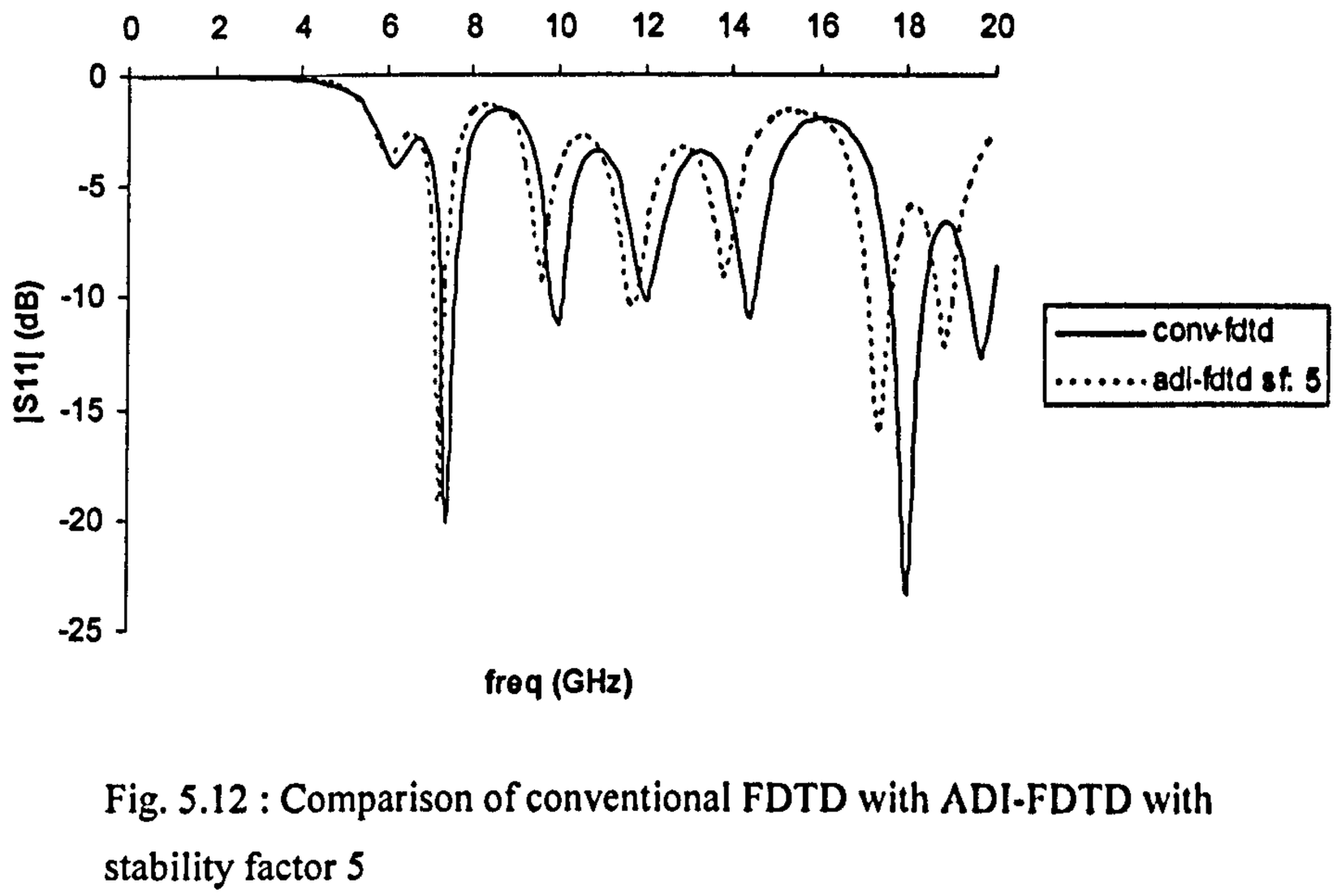

Fig. 5.12 : Comparison of conventional FDTD with ADI-FDTD with stability factor 5

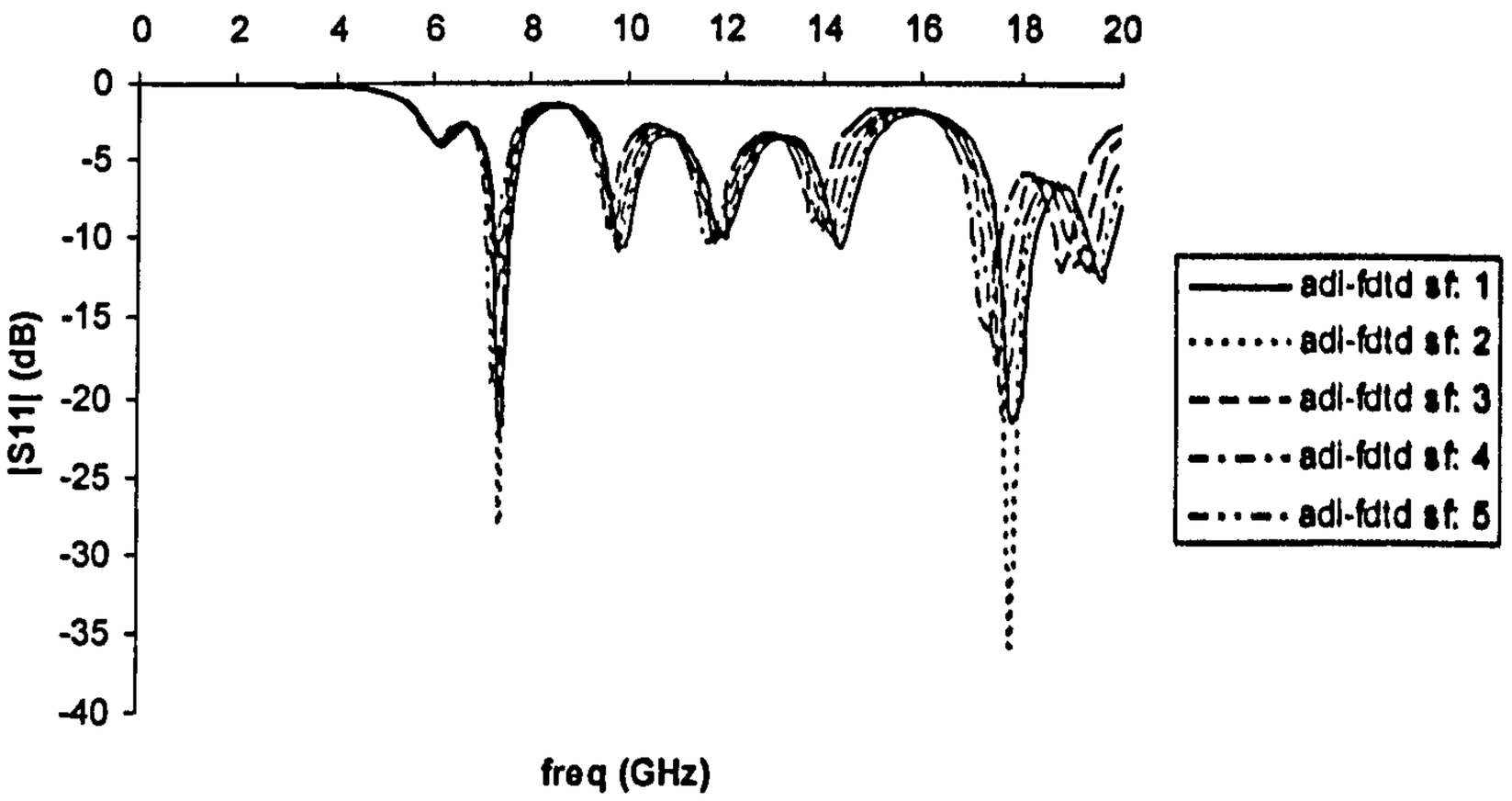

Fig.5.13 : Comparison of ADI-FDTD with stability factors 1 to 5

Fig.5.7 shows a good agreement between Abouzahra [1.5] simulated data and the ADI-FDTD result using stability factor 1. Fig. 5.8 shows very good agreement between the results generated using the conventional FDTD and the ADI-FDTD method with stability factor 1. Fig.5.9 shows that with stability factor 2 the frequency response results still agree reasonably well with the conventional FDTD results but for frequency higher than 14GHz, the response begins to shift slightly towards the lower frequency. This effect of numerical dispersion increases with the increase of the stability factor and it is greater at the high frequency range. The broadening of the pulse in time-domain causes a compression of the response in the frequency domain. Figs. 5.10, 5.11 and 5.12 show the comparison between conventional FDTD and ADI-FDTD with stability factors 3,4 and 5 respectively. Fig. 5.13 shows the comparison of ADI-FDTD results with stability factors 1 to 5. The effect of numerical dispersion can be seen clearly.

5.3.1.3 Accuracy vs stability factor

stability factor	resonance at 7.4GHz	%error	resonance at 12.0GHz	%error	resonance at 18.0GHz	%error
1	7.4	0	12	0	17.9	0.56
2	7.4	0	12	0	17.8	1.11
3	7.4	0	11.8	1.67	17.6	2.22
4	7.35	0.67	11.8	1.6	17.5	2.78
5	7.2	2.7	11.6	3.33	17.3	3.89

Table 5.1 : Percentage errors at resonances 7.4GHz, 12.0GHz and 18.0GHz using ADI-FDTD method with stability factors 1,2,3,4 and 5 as compared to the respective resonances using the conventional FDTD method.

5.3.1.4 Run-time comparison

	Computational run-time in minutes		
Stability factor	conv-FDTD	ADI-FDTD	time steps
1	25.75	58.35	8000
2	-	29.283	4000
3	-	19.45	2667
4	-	14.683	2000
5	-	11.67	1600

Table 5.2 : Run-time comparison using computer with Athlon 1.2GHz processor

Table 5.2 above shows that for the microstrip patch circuit, a stability factor greater than 2.0 in ADI-FDTD scheme is required to have any time-saving as far as computational run-time is concerned. Referring to table 5.1, by using stability factor of 3.0 in the ADI-FDTD, the errors are 1.67% and 2.22% at resonant frequencies 12GHz and 18GHz respectively. This allows a time-saving of 24%. Although a time-saving of 6.3 minutes in this example may not be significant, a 24% time-saving from 2 days, i.e. saving of about half a day of simulation run-time when more complex structures such as a human body or a huge aircraft are modelled will prove to be quite beneficial.

In reality, the % errors for stability factors greater than 3 as shown in table 5.1 may not be tolerable when it comes to designing a microstrip patch. It is, however, important to emphasize here that the accuracy of the ADI-FDTD method is very much dependent on the structure being modelled. Therefore, when applied to other structures, a stability factor of greater than 3 may be used whilst maintaining the accuracy within a tolerable range.

Note that the saving in computational run-time is not directly proportional to the stability factor used as computation in the ADI-FDTD method is much more complex than the conventional FDTD and involves matrix inversions.

5.3.1.5 Input impedance

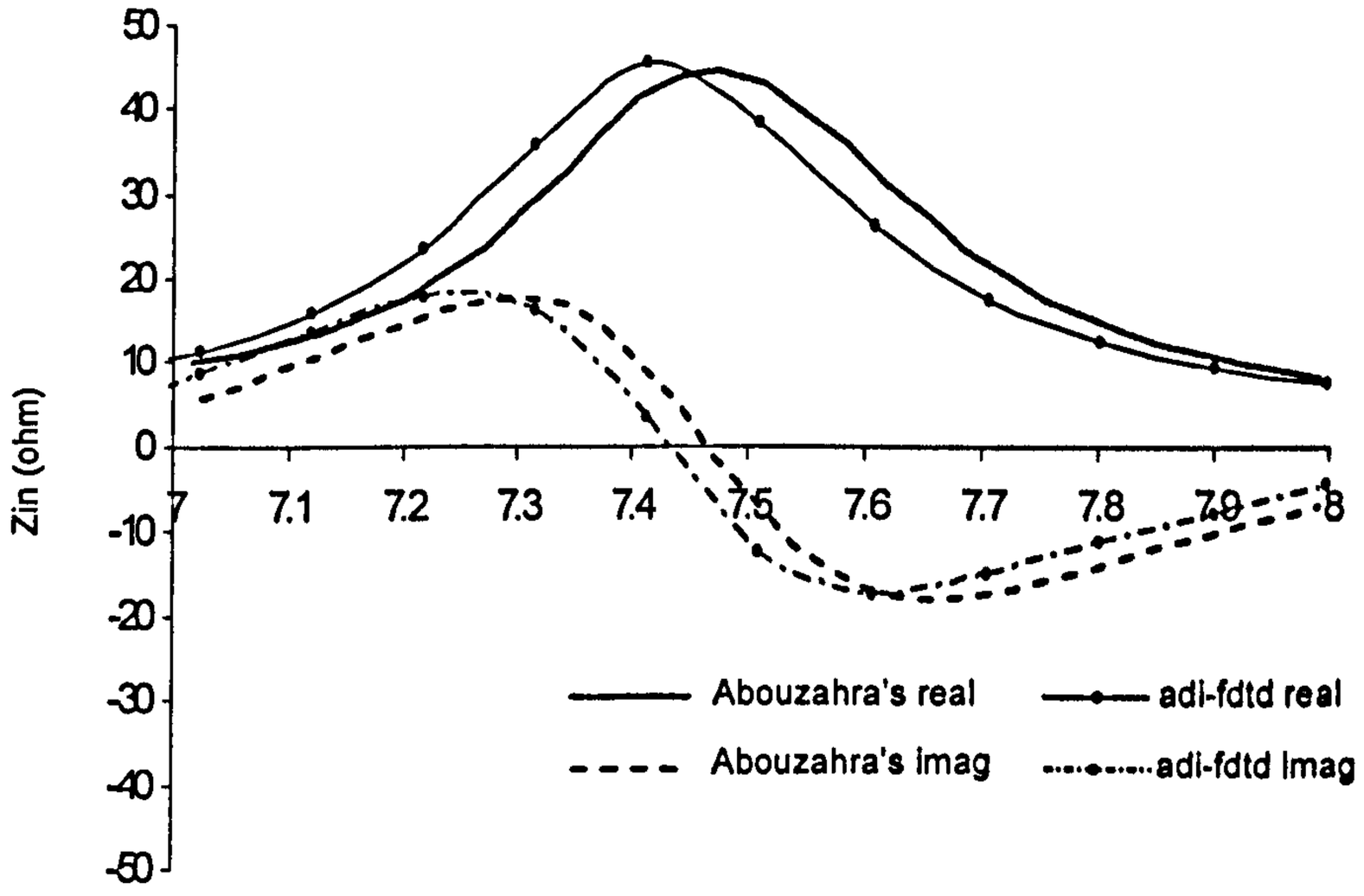

Fig.5.14 : Comparison between Abouzahra's result and ADI-FDTD with stability factor 1 for real and imaginary parts of input impedance of the patch antenna

Fig.5.14 shows the comparison between Abouzahra's results and the ADI-FDTD with stability factor 1 for real and imaginary parts of the input impedance of the patch antenna. As discussed in chapter 2, the discrepancy between both sets of data is due to the fact that in the published paper, the microstrip is assumed to have a constant characteristic impedance, Z_o of 50 Ω and an effective permittivity of 1.9 is used to calculate the wavenumber, β, whereas in this research work, these values have been calculated using data obtained from the simulation. In this way, the dispersive nature of the microstrip is accounted for in the simulated data.

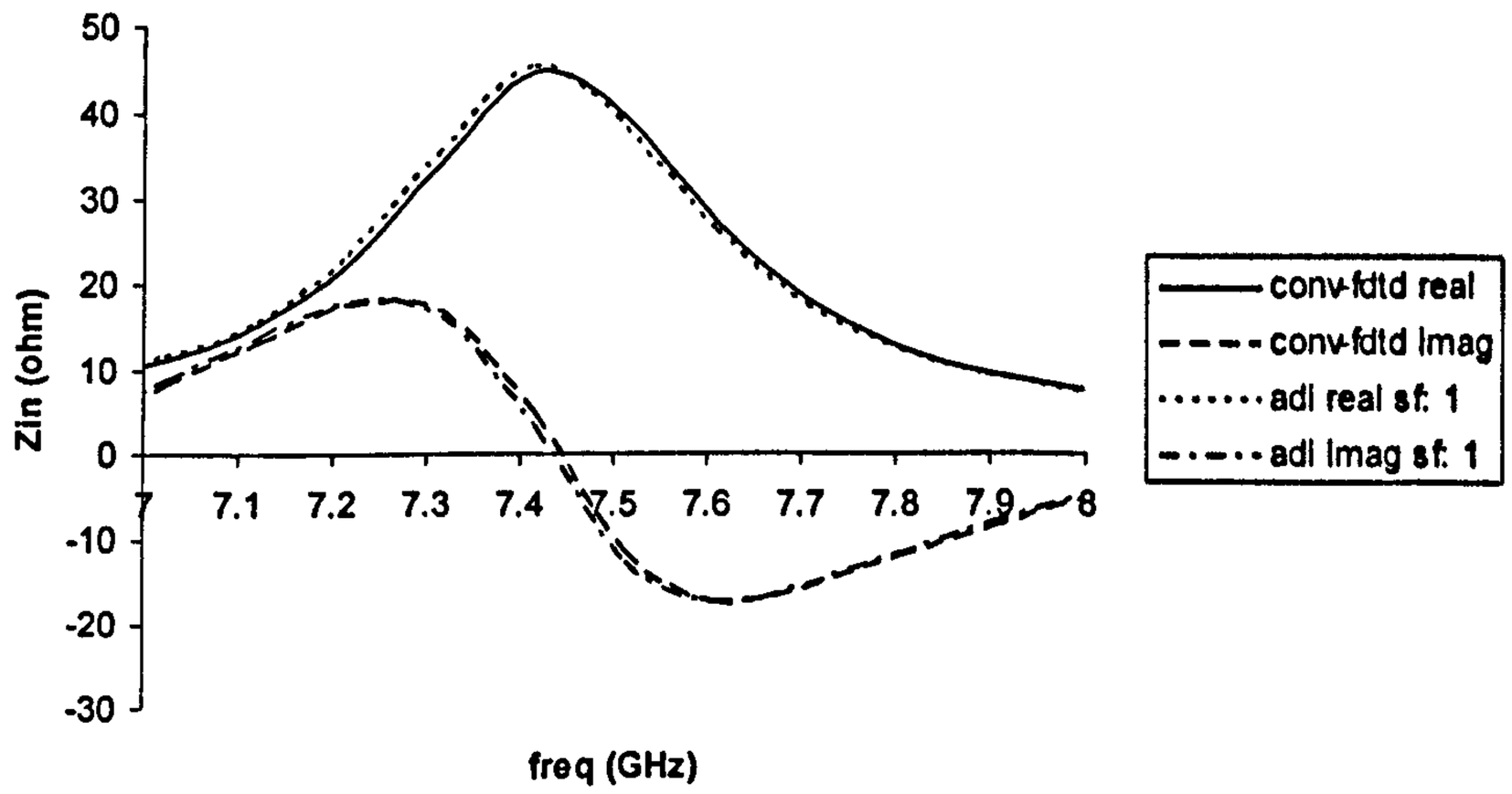

Fig.5.15 : Comparison between conventional FDTD and ADI-FDTD with stability factor 1 for real and imaginary parts of input impedance of the patch antenna

Fig.5.15 shows a good agreement between the results generated using the conventional FDTD and the ADI-FDTD with stability factor 1. Figs. 5.16 shows a comparison between conventional FDTD and ADI-FDTD results with stability factors 2. Again, when stability factor 2 and above are used, the data shift towards the lower frequency as can be seen in Figs. 5.17, 5.18 and 5.19.

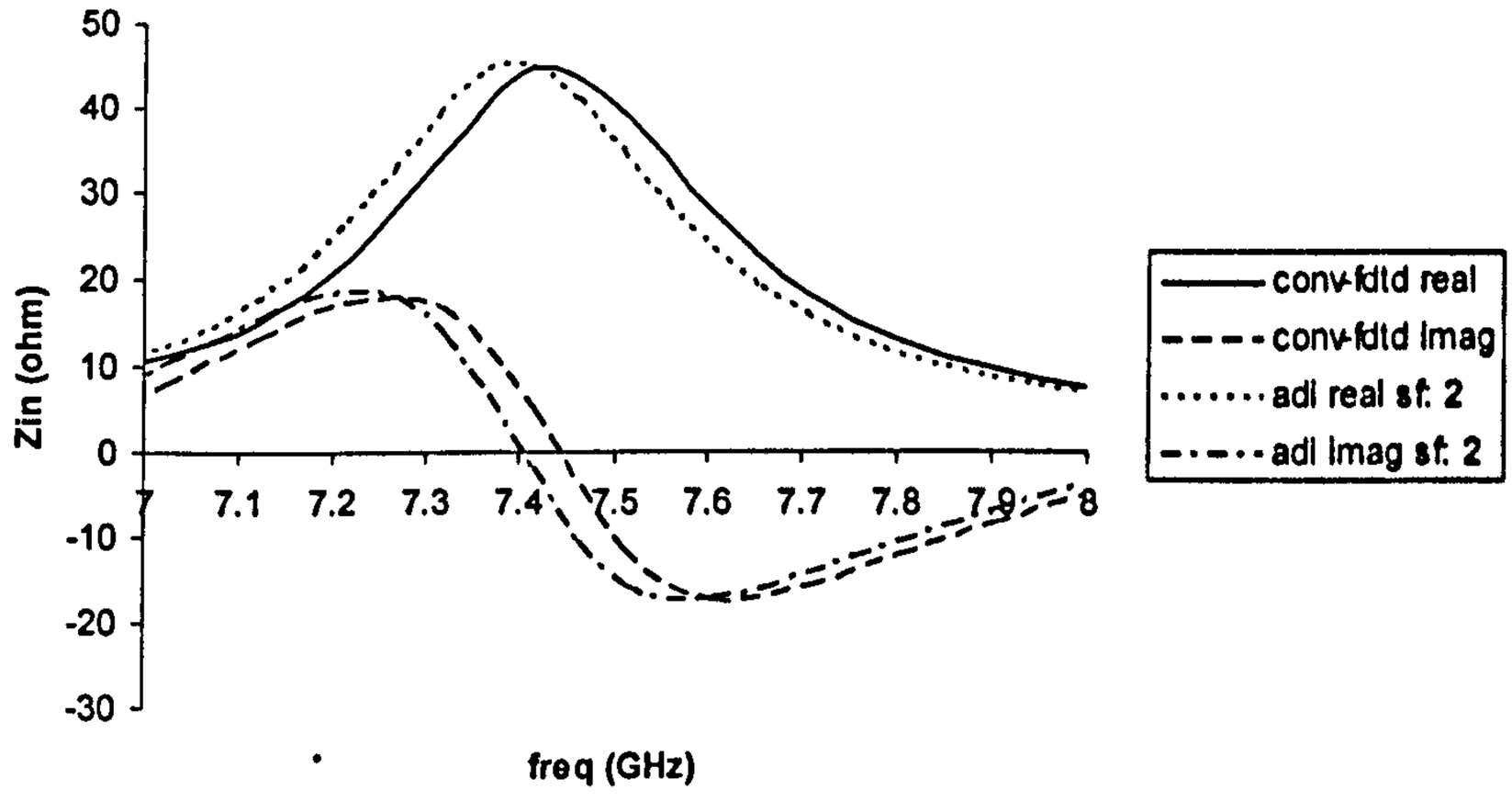

Fig.5.16 : Comparison between conventional FDTD and ADI-FDTD with stability factor 2 for real and imaginary parts of input impedance of the patch antenna

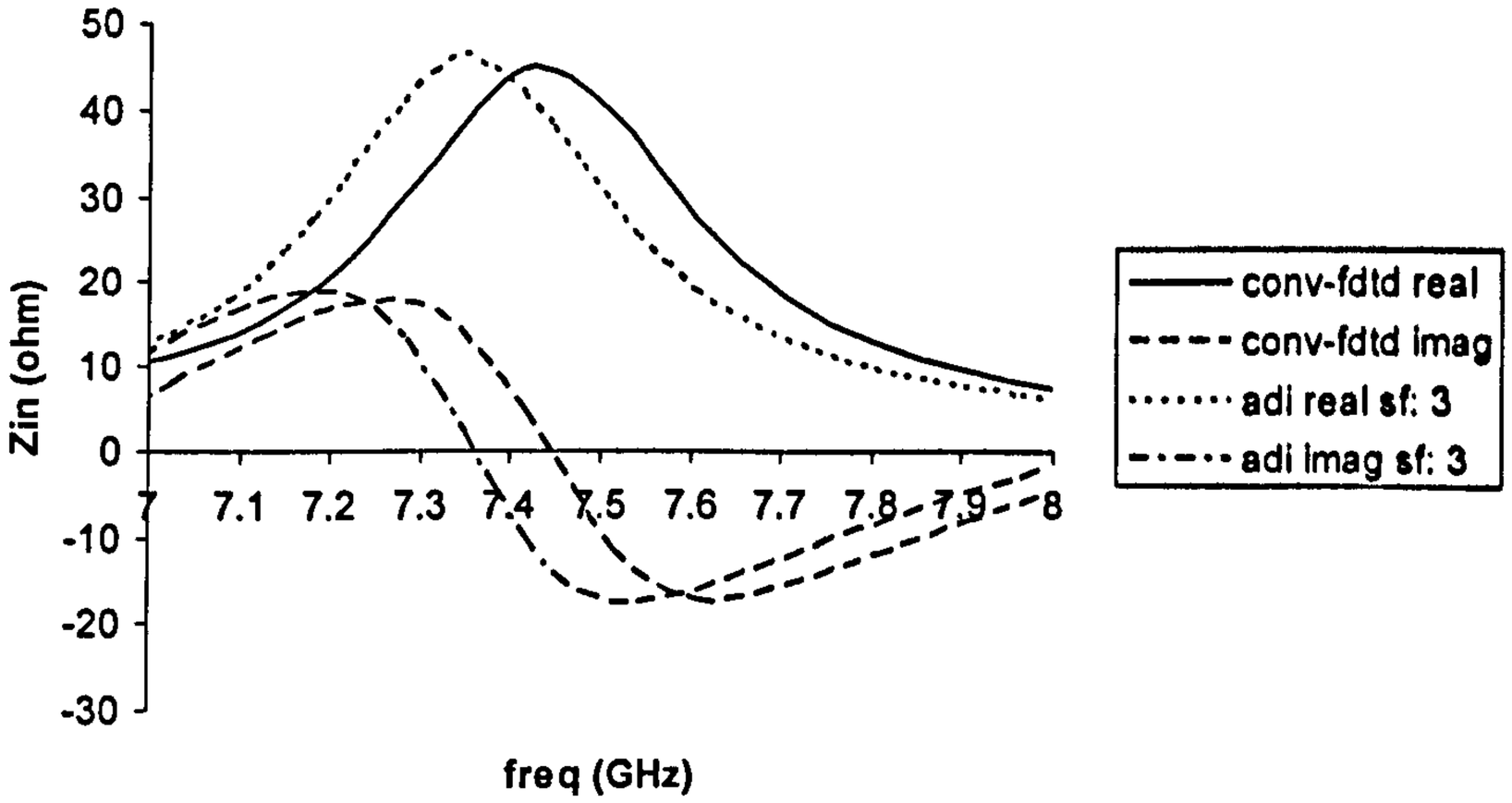

Fig.5.17 : Comparison between conventional FDTD and ADI-FDTD with stability factor 3 for real and imaginary parts of input impedance of the patch antenna

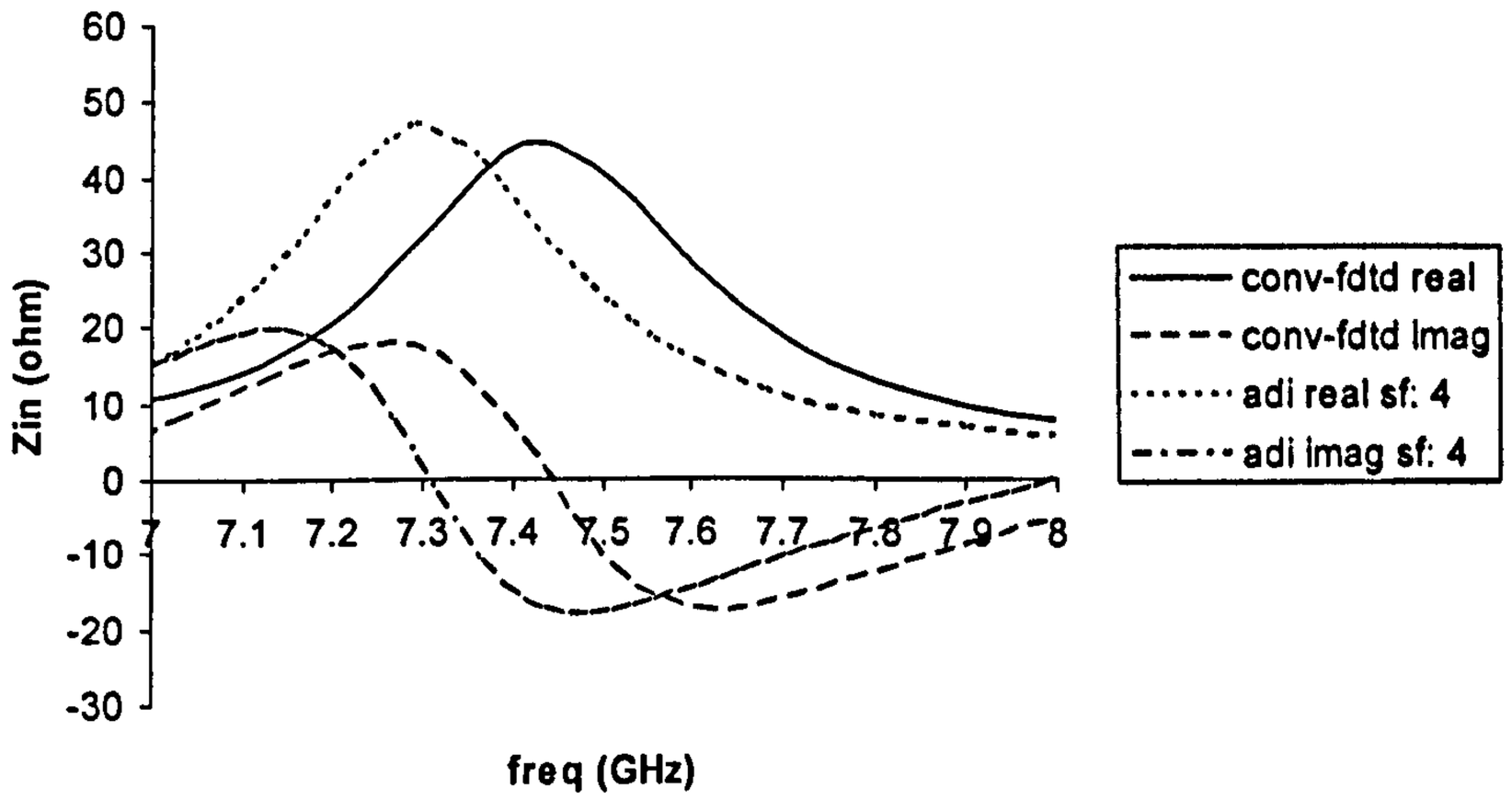

Fig.5.18 : Comparison between conventional FDTD and ADI-FDTD with stability factor 4 for real and imaginary parts of input impedance of the patch antenna

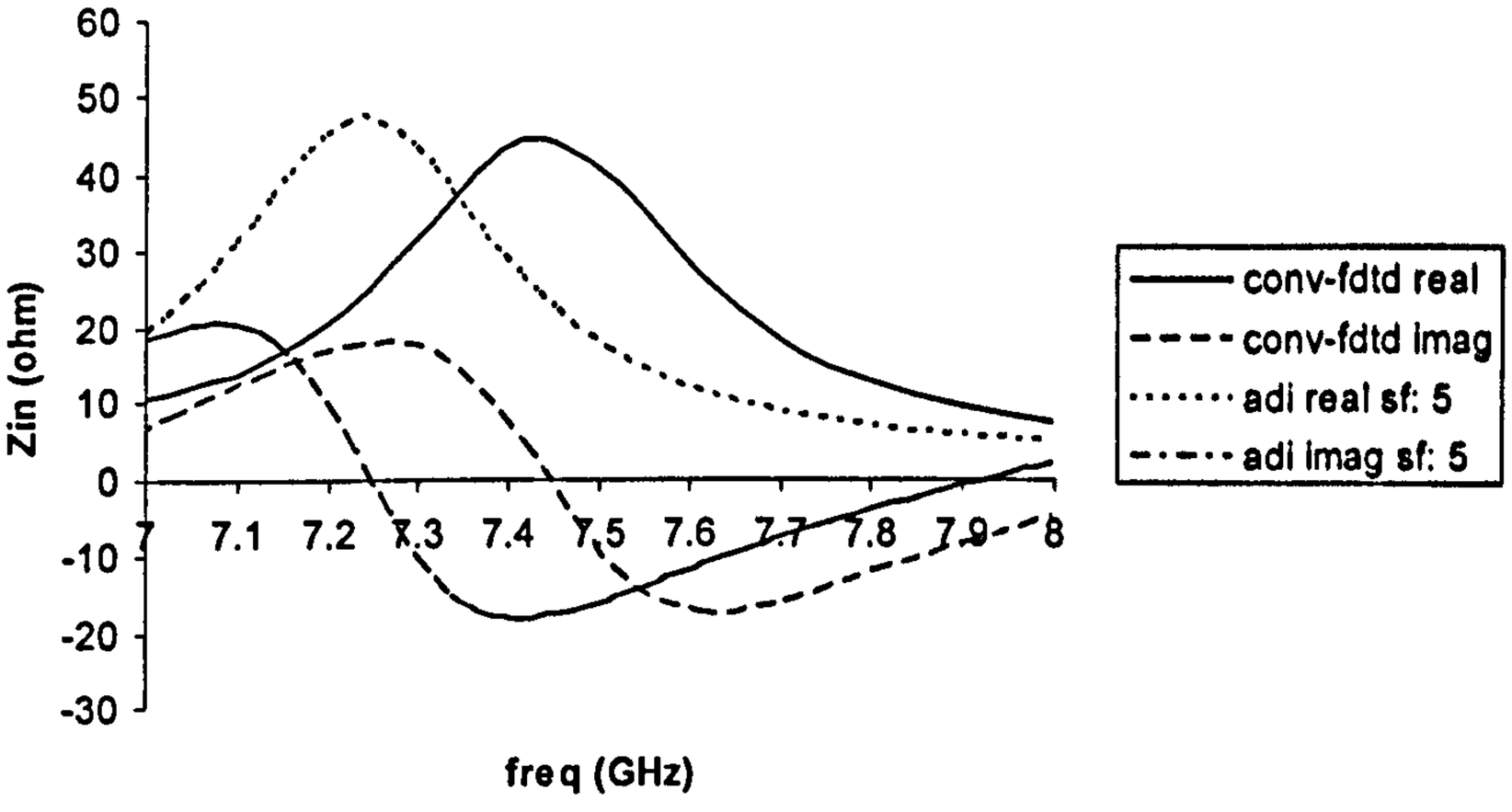

Fig.5.19 : Comparison between conventional FDTD and ADI-FDTD with stability factor 5 for real and imaginary parts of input impedance of the patch antenna

5.3.2 *Simulation of a line-fed rectangular microstrip patch with three parasitic patches*

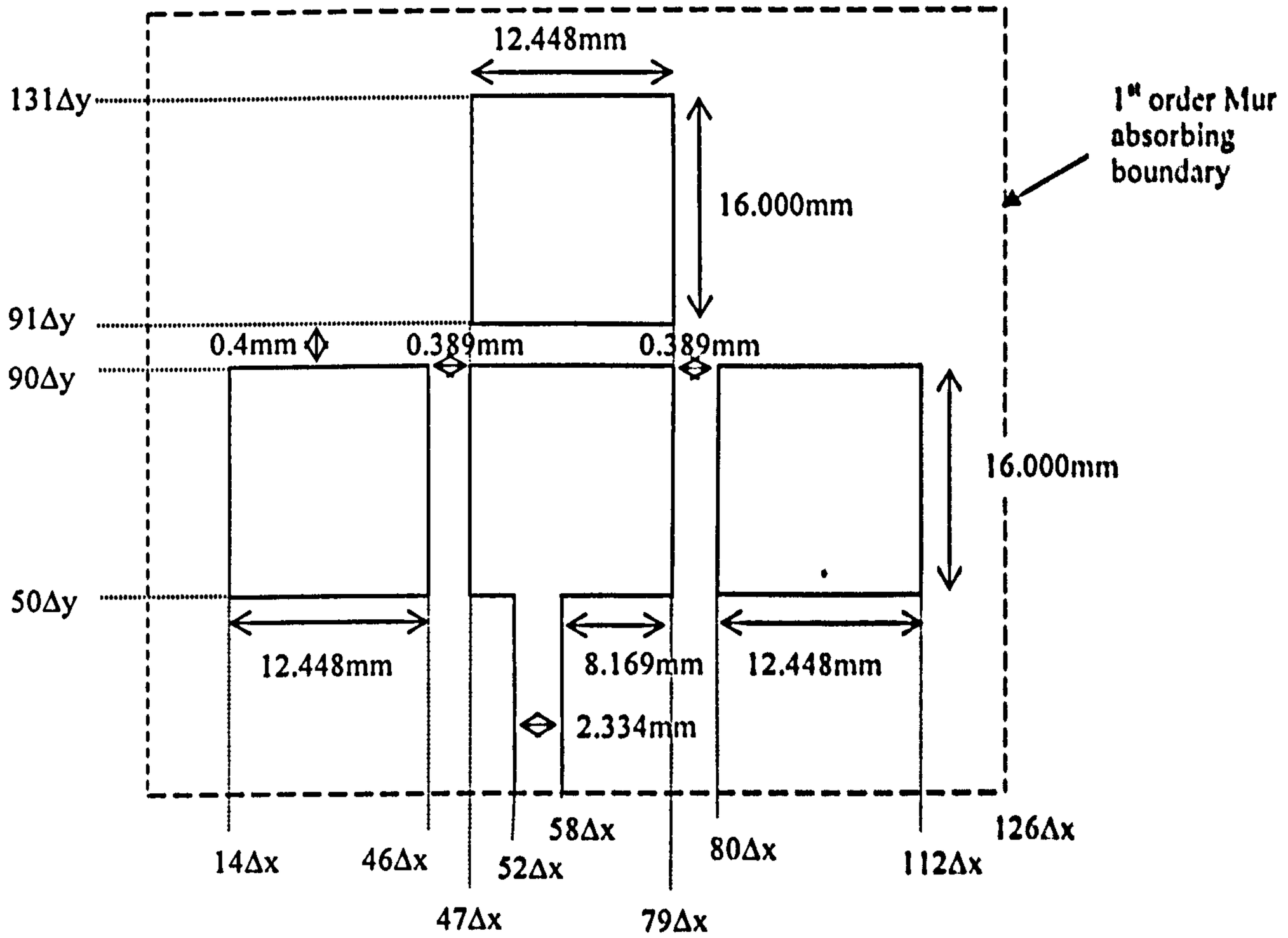

Fig.5.20 : Line-fed rectangular microstrip patch with three parasitic patches

By modelling the copper patch as a material with an electric conductivity of 5.8×10^7 S/m, we have been able to model the line-fed rectangular microstrip patch using the ADI-FDTD method without introducing instability or attenuation even when CFL stability criterion is not observed. In order to validate that this technique works on a relatively bigger electrical object, the line-fed rectangular patch is surrounded by three parasitic patches. The plan view of the structure is shown in Fig.5.20 above. The mesh parameters and excitation method are the same as that used in chapter 2. Figs. 5.21 – 5.24 show transient responses for this patch circuit.

5.3.2.1 Transient response

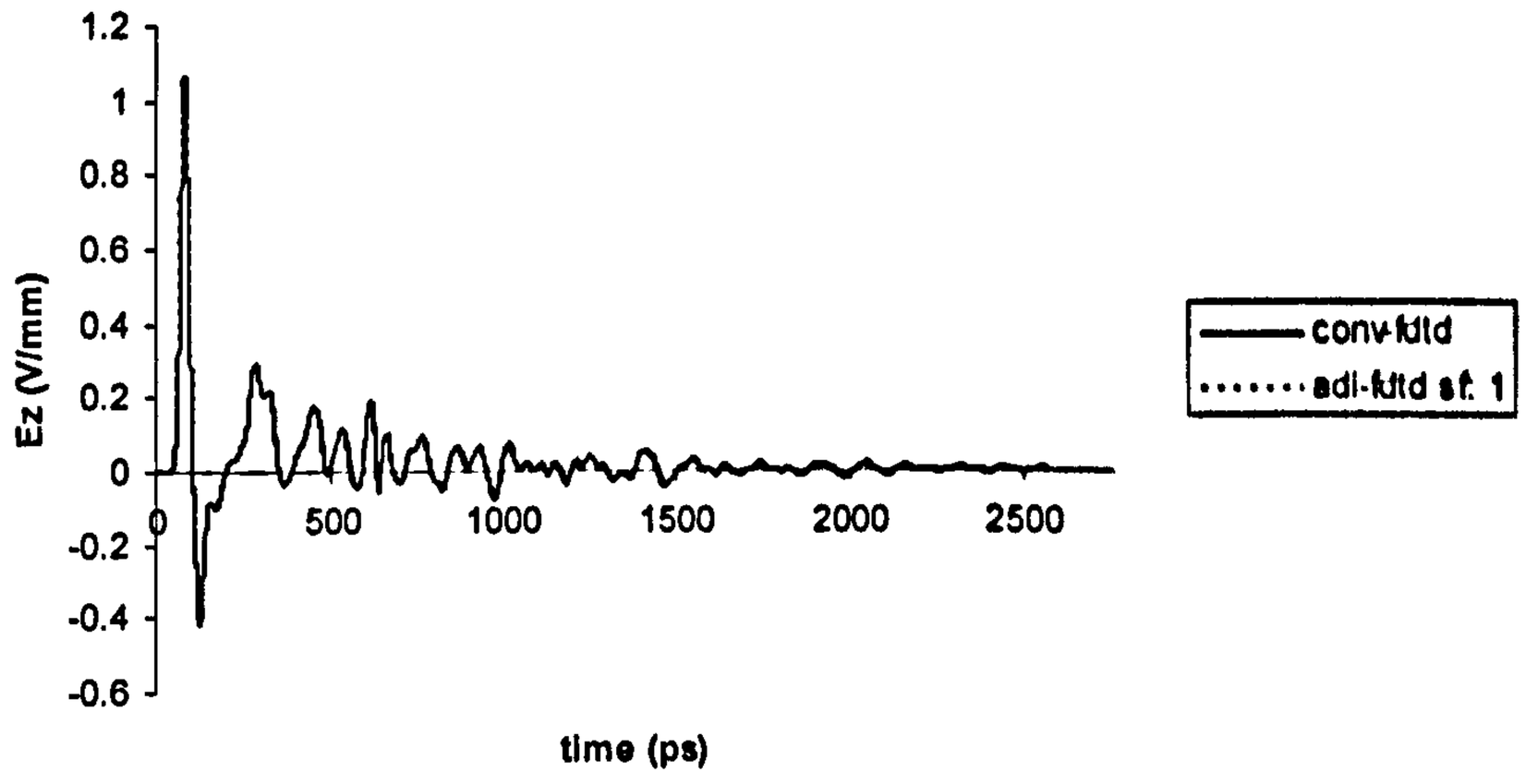

Fig. 5.21 : Comparison between conventional FDTD and ADI-FDTD with stability factor 1

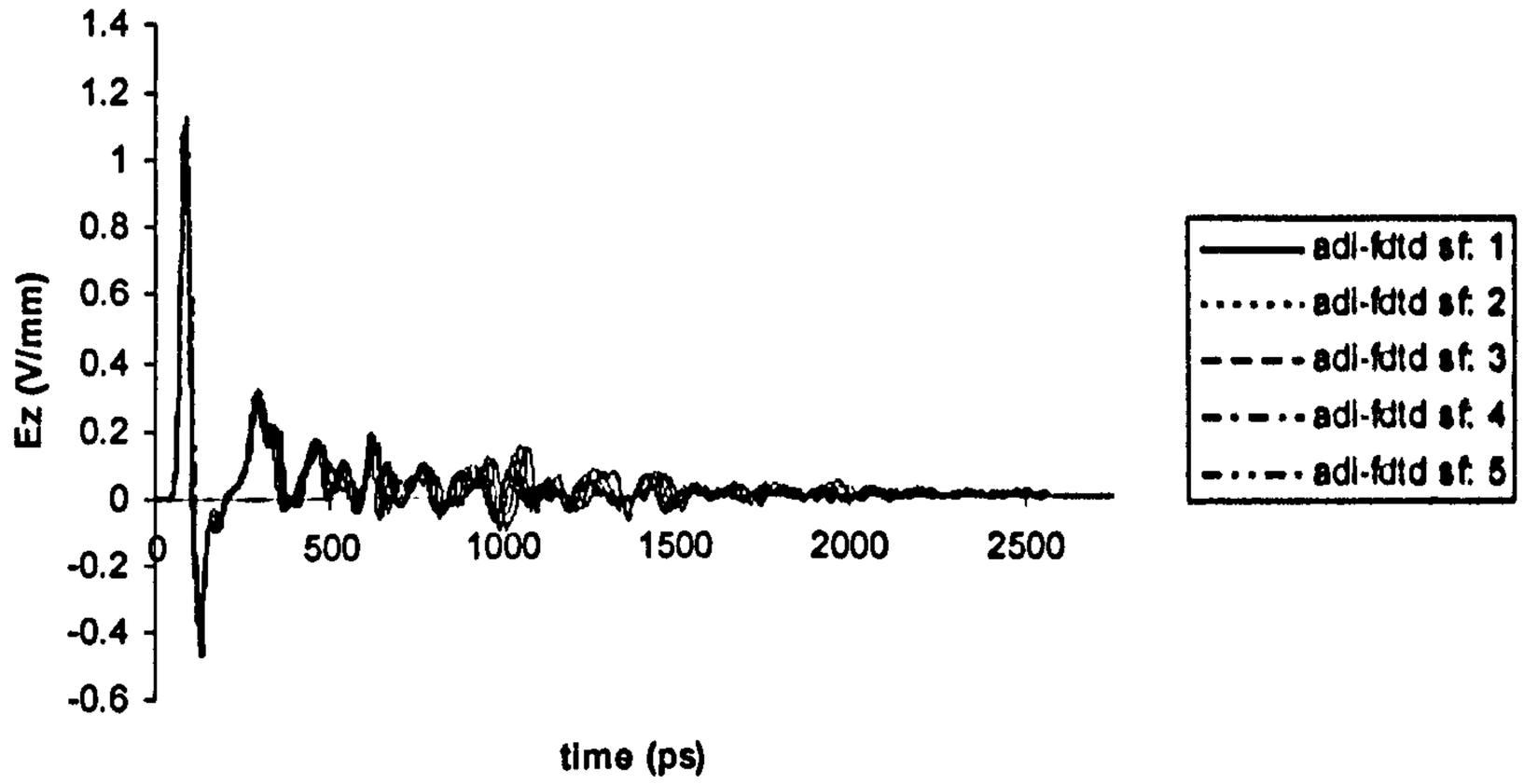

Fig. 5.22 : Comparison between ADI-FDTD with stability factors 1 to 5 in steps of 1

Fig. 5.22 shows comparison between ADI-FDTD with stability factors of 1 to 5. Again, the results are completely stable. This shows that the ADI-FDTD can be applied successfully on electrically large objects and the stability of the system is still maintained when the time step used in the algorithm is greater than the maximum allowable according to the CFL criterion. As the stability factor is increased and thus increasing the numerical time-step, the numerical dispersion becomes more significant as expected.

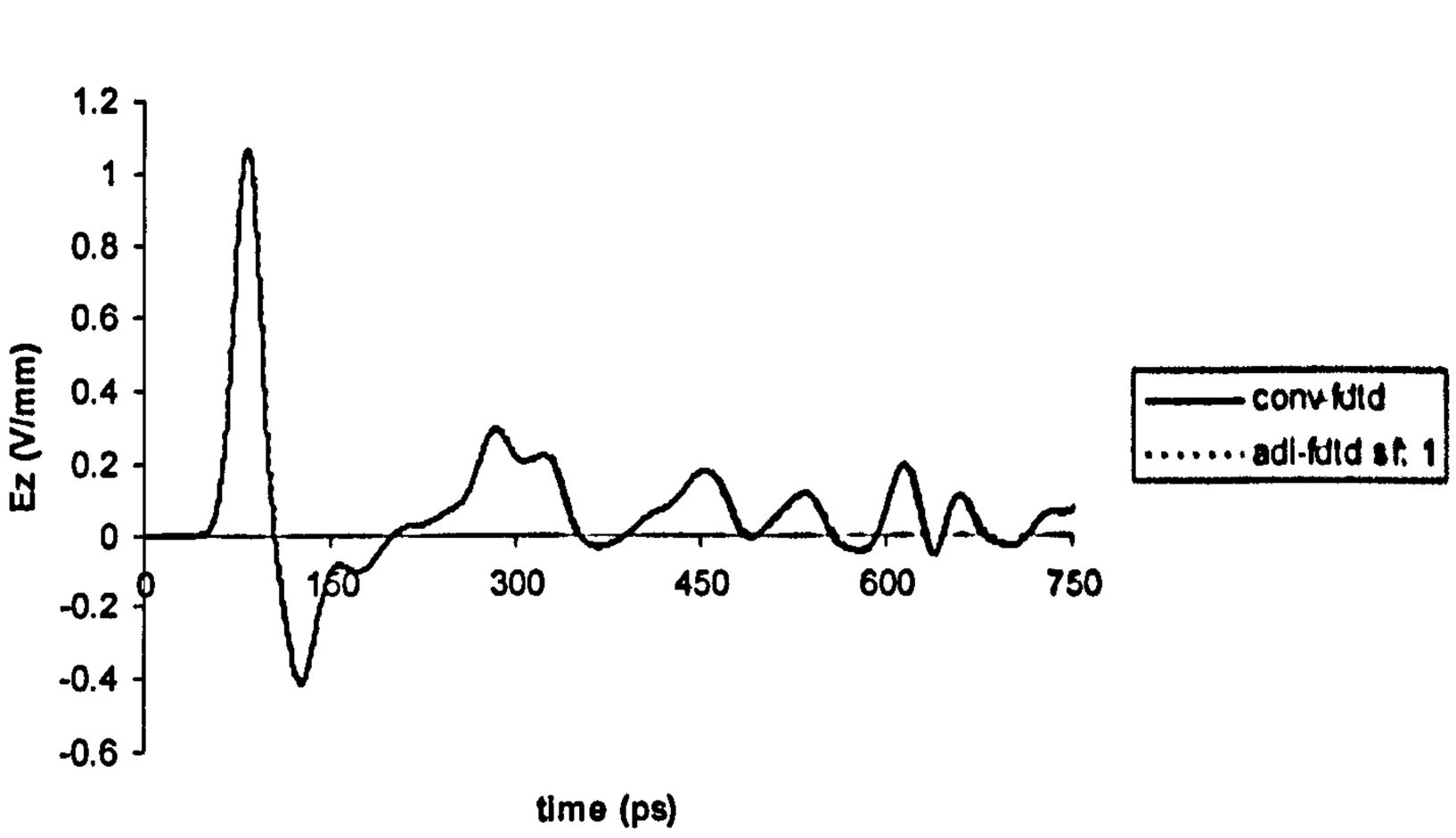

Fig.5.23 : Zoomed in comparison between conventional FDTD and ADI-FDTD with stability factor 1

Figs. 5.23 – 5.25 show the magnified view of the transient responses of the rectangular microstrip patch with three parasitic patches. From Fig. 5.25, it can be seen that the transient response starts to show significant inaccuracy in the result when the stability factor is increased beyond 3. This inaccuracy may be due to the fact that the dielectric gap separating the microstrip patches has been modelled with a single mesh width. The accuracy of the model and hence the result can be improved by increasing mesh resolution in the dielectric gap.

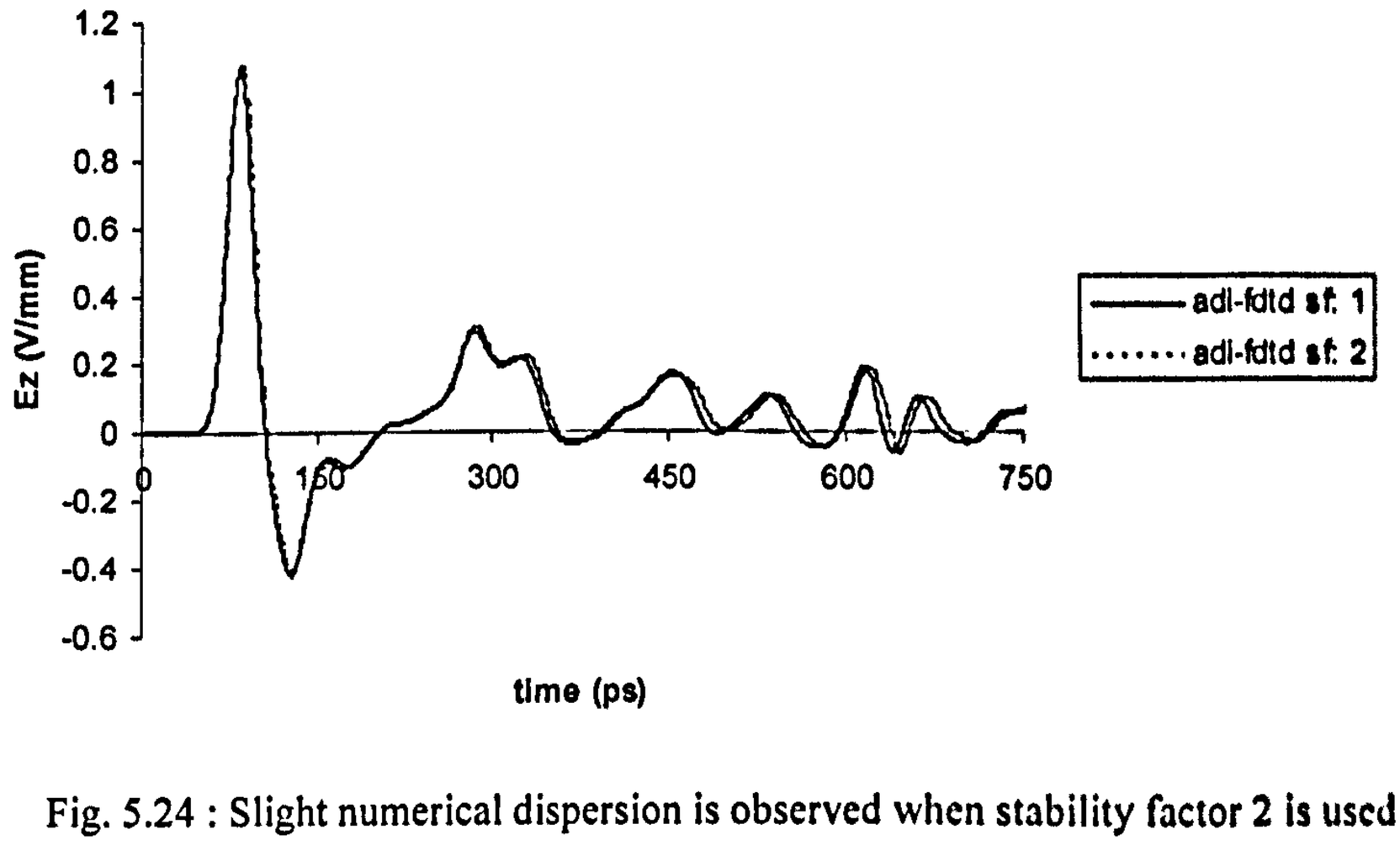

Fig. 5.24 : Slight numerical dispersion is observed when stability factor 2 is used in the ADI-FDTD

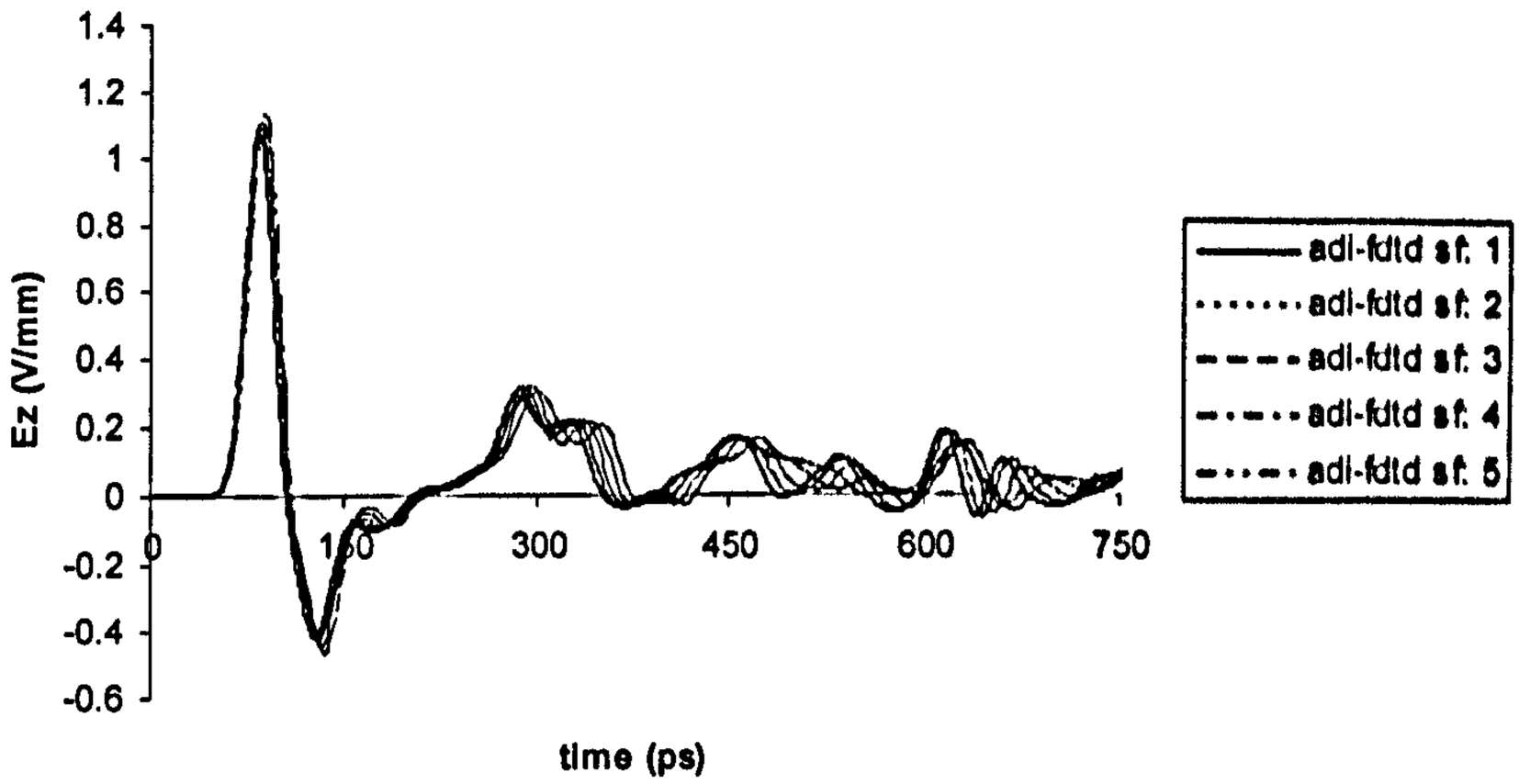

Fig. 5.25 : More significant numerical dispersion with stability factors greater than 3 and inaccuracy begins to show with stability factors beyond 3

5.3.2.2 Frequency response

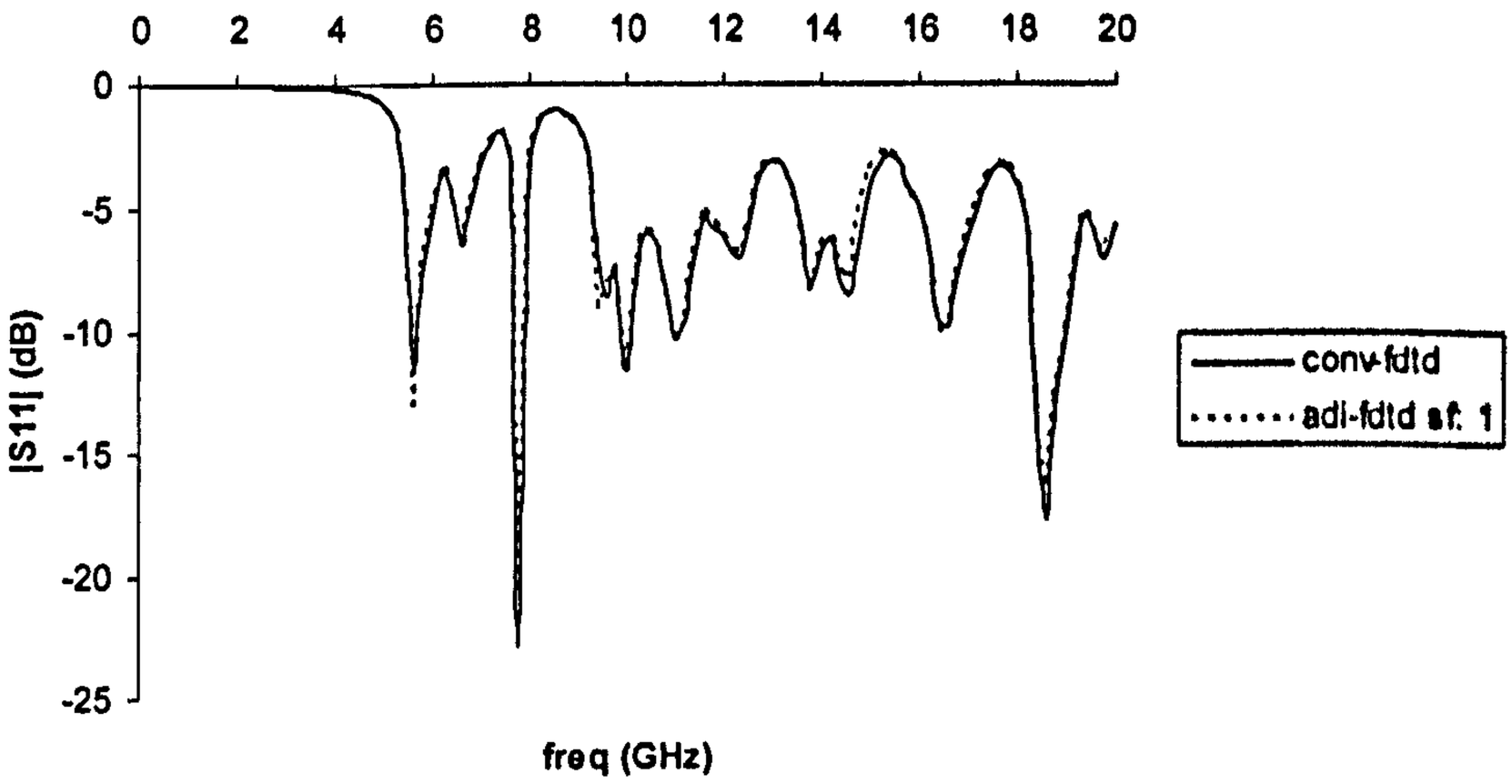

Fig. 5.26 : Comparison of conventional FDTD with ADI-FDTD with stability factor 1

Fig. 5.26 above shows the frequency responses from the conventional FDTD and ADI-FDTD with stability factor 1 agree almost perfectly with each other.

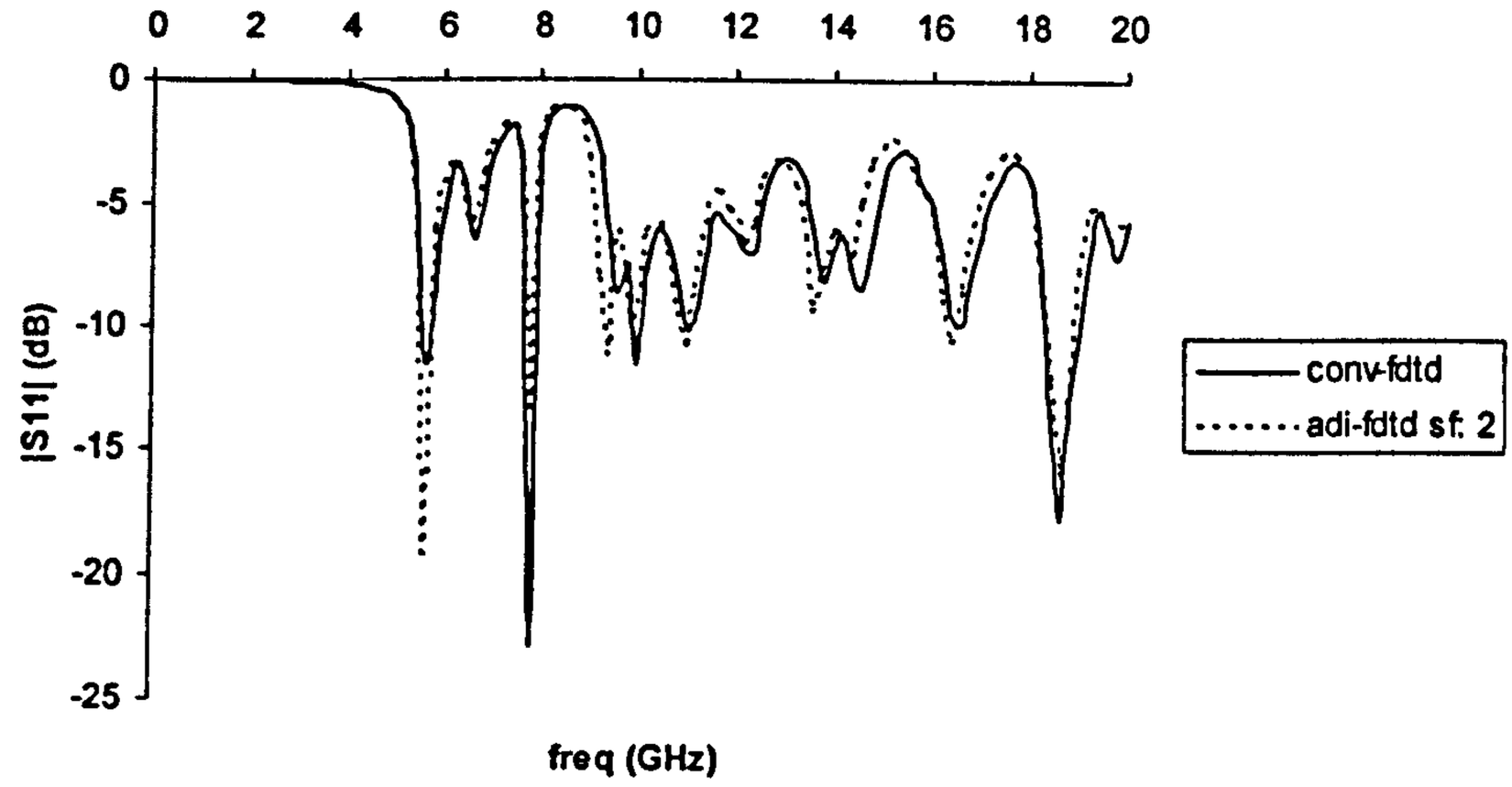

Fig. 5.27 : Comparison of conventional FDTD with ADI-FDTD with stability factor 2

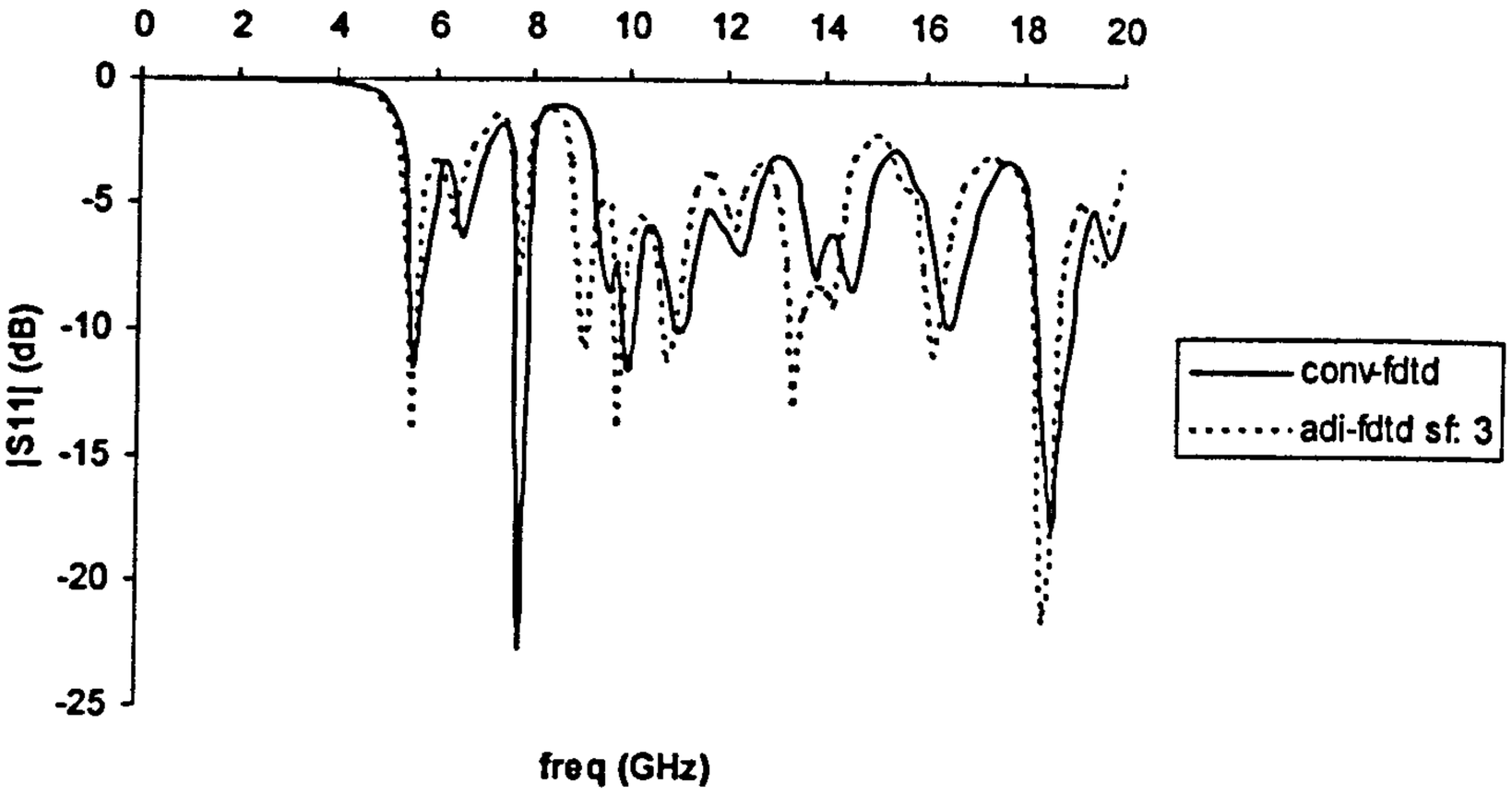

Fig. 5.28 : Comparison of conventional FDTD with ADI-FDTD with stability factor 3

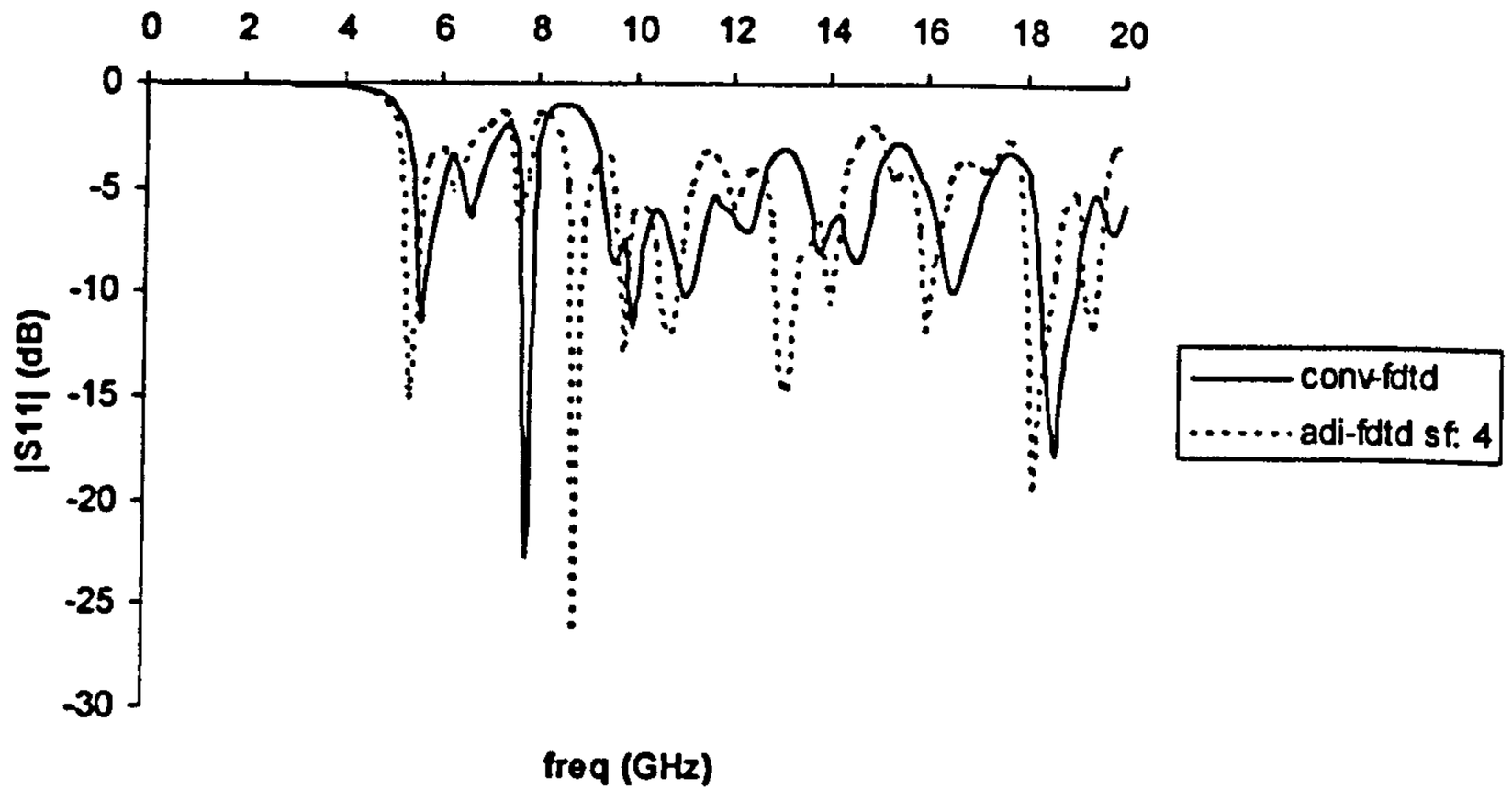

Fig. 5.29 : Comparison of conventional FDTD with ADI-FDTD with stability factor 4

As mentioned earlier, the inaccuracy in the results start to creep in when the stability factor is greater than 3. Fig. 5.28 shows that when stability factor 3 is used, the results suffer from only numerical dispersion due to the bigger time-step used. However, when stability factor of 4 is used, the result shown in Fig. 5.29, suffer from both numerical dispersion due to the increased time-step used and the inaccuracy of the model due to insufficient mesh resolution within the dielectric gap separating the main microstip patch and the three parasitic patches.

5.3.2.3 Input impedance

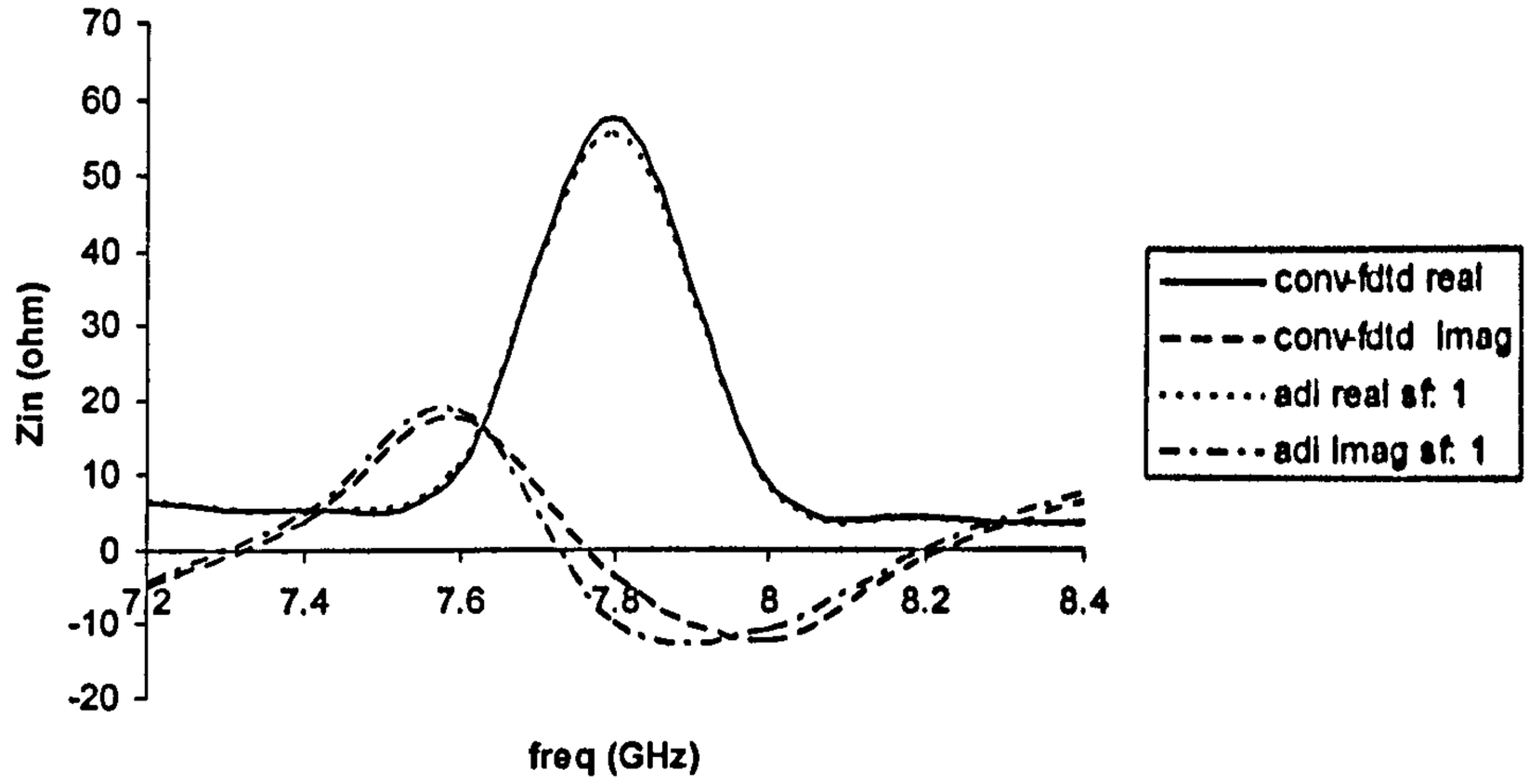

Fig. 5.30 : Comparison between conventional FDTD and ADI-FDTD with stability factor 1 for real and imaginary parts of input impedance for the line-fed rectangular microstrip patch with three parasitic patches

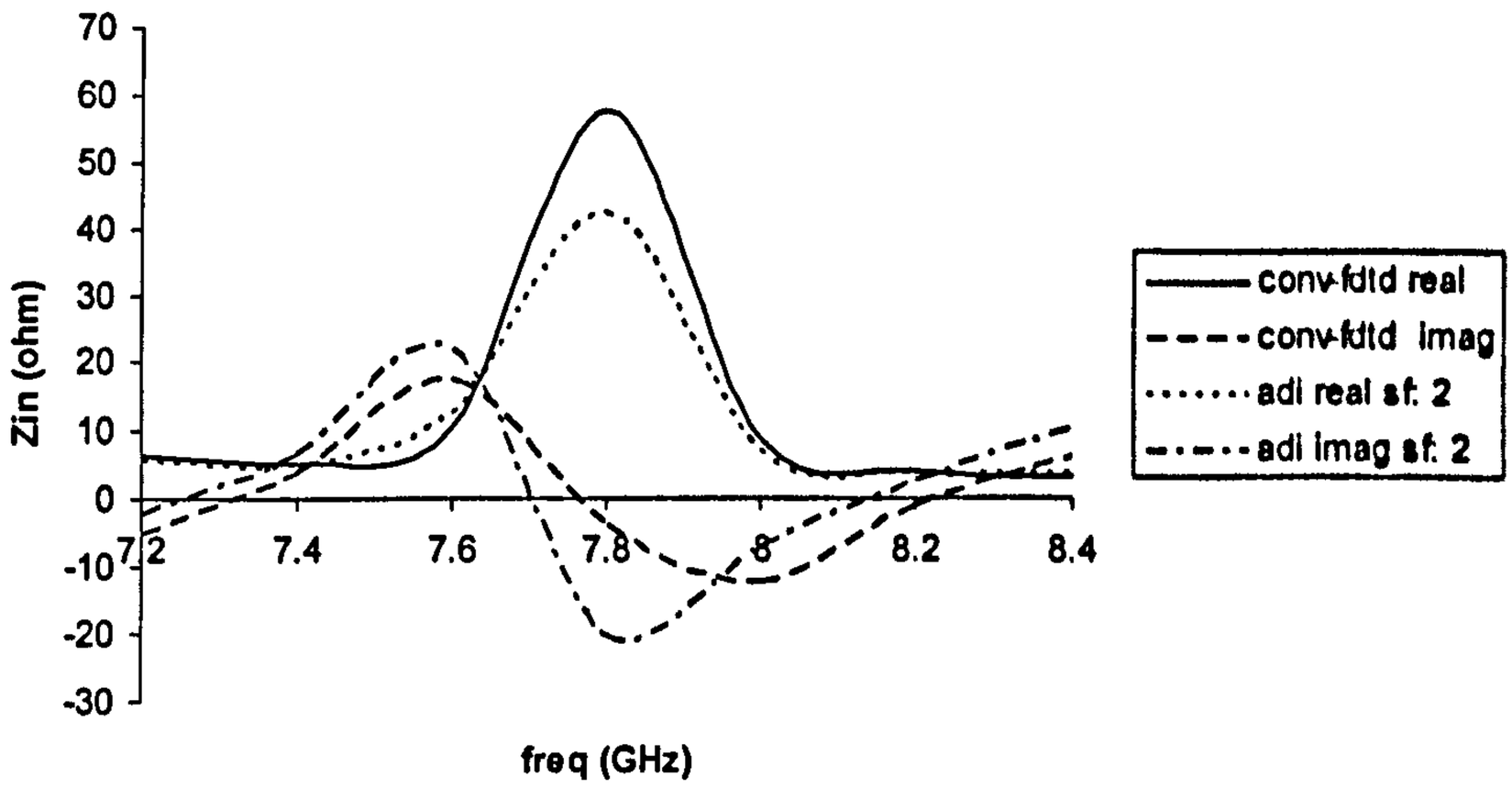

Fig. 5.31 : Comparison between conventional FDTD and ADI-FDTD with stability factor 2 for real and imaginary parts of input impedance for the line-fed rectangular microstrip patch with three parasitic patches

Again, the discrepancy in the amplitude of the input impedance plots shown in Fig. 5.31 is due to the insufficient mesh resolution in the dielectric gap between the patches.

5.4 Conclusion

It has been shown in this chapter that modelling the copper layer in ADI-FDTD as a layer of material with a finite electric conductivity taken as 5.8×10^7 S/m keeps the system completely stable even when the CFL stability criterion is violated. This is not true when the copper layer is modelled as a perfect electric conductor as discussed earlier in chapter 3.

Using this method of implementing the copper layer, the results for a line-fed microstrip rectangular patch show favourable comparison with published results and the results obtained from the conventional FDTD method. Tables of accuracy against stability factors used and the run-time comparison between the conventional FDTD and ADI-FDTD methods have also been presented.

To further validate the use of ADI-FDTD method on an electrically large object, the microstrip patch is modelled with three parasitic patches adjacent to its three edges. The results show stability when tested with stability factors of up to 8. As expected, increasing the stability factor increases the numerical dispersion error.

It has to be mentioned that the sole purpose of modelling this relatively large circuit is to validate the use of ADI-FDTD on electrically large objects. As a result, the gaps between the patches have been modelled using a single mesh width. This has introduced some errors into the results due to inaccurate modelling of the gaps. Nevertheless, the results are still stable with stability factors of up to 8.0.

In order to model small gaps accurately, a graded mesh should be employed in the computational domain where the mesh size is reduced gradually towards the gaps and is maintained small within the gaps. This forms part of the suggested further work.

As in any engineering feat, nothing comes free and in this ADI-FDTD case, there is a trade-off between accuracy and simulation run-time. ADI-FDTD allows us to violate the fundamental CFL stability criterion without causing instability in the system. By using the ADI-FDTD method instead of the conventional FDTD method, potentially the simulation run-time can be significantly reduced. However, increasing the time-step also reduces the accuracy of the simulation results. This accuracy is dependent on the structure being modelled. Therefore, for certain structures a significant reduction in simulation run-time will be possible whilst maintaining the accuracy within the required tolerable range. In addition to that, structures containing discontinuities can be modelled using fine mesh size without the constraint of using a correspondingly small time step in the simulation.

CHAPTER 6
CONCLUSION AND FURTHER WORK

6.1 Overall conclusion

The finite-difference time-domain method has been studied and applied in the Cartesian coordinate system for a three-dimensional rectangular microstrip structure. In order to remove the Courant-Friedrich-Levy stability criterion that governs the maximum time-step that can be used in the FDTD algorithm to maintain the stability of the system, the alternating-direction implicit method is investigated. The main contribution of this work has been the new method of simulating the copper layer on a microstrip in a three-dimensional Cartesian coordinate system in the ADI-FDTD scheme. This allows the application of the ADI-FDTD method to model any three-dimensional structure that consists of copper layers in the structure.

Although the ADI-FDTD method has been used in the literature, most analysis and application have been performed on simple three-dimensional cavities, in both homogeneous and inhomogeneous media [1.18] and [1.32]-[1.37]. Very often two-dimensional models have been used to verify the algorithm [1.28] and [1.29], when structures other than the free-space cavities were modelled, such as the parallel-plate waveguide model in [1.14], a two-dimensional model was used and a lossy dielectric with elcctric conductivity of 15.0 S/m was included in the model. On another occasion [1.38] a sheet of an infinite ground plane was modelled using an electric conductivity of 20.0 S/m and in [1.25], a monopole with a thin dielectric wall with electric conductivity of 4.0 S/m was modelled.

In [1.26], microstrip resonators and filters were modelled using the ADI-FDTD method in a graded mesh and a perfect electric conductor (PEC) boundary condition was applied on the microstrip layer. However, when a transmission line was modelled by implementing a perfect electric conductor boundary condition on the strip in the ADI-FDTD method as discussed in chapter 3 in this research work, the result was unstable. This phenomenon was later confirmed in [1.21] where it was reported that if the tri-diagonal solver in the literature [2.6] was used to solve the ADI-FDTD method when modelling a microstrip line, the result was not always stable. Subsequently, an alternative mathematical algorithm for solving the tri-diagonal matrix in the ADI-FDTD method was reported in [1.21].

For the first time, this research work has shown that by simulating the copper layer on the microstrip as a material with electric conductivity of 5.8×10^7 S/m (which is the electric conductivity of copper) in the three-dimensional ADI-FDTD scheme, the numerical results are always stable even when the tri-diagonal solver as proposed in [2.6] is used. A different tri-diagonal solver as reported in [1.21] is thus not required. It has been shown that the AD-FDTD method can be used to model realistic problems in engineering design without the need to put artificially high lossy material to maintain stability. In order to exploit the advantageous feature of the ADI-FDTD method, it is important that the ADI-FDTD method

can be successfully implemented not only on cavity structures but also on real practical three-dimensional structures that may consist of striplines and microstrips.

Another contribution of this research work is the proposed new modified ADI-FDTD method which introduces a factor *f* in the ADI-FDTD algorithm. Using this new method, microstrip lines can be simulated as perfect electric wall boundary where the tangential electric fields on the microstrip are set to zero and stability of the system is still maintained. Although the results from the modified ADI-FDTD method show a reduction in the amplitude, this technique is easy to implement and it is useful as a quick method to obtain accurate resonant frequency points.

The ADI-FDTD method has contributed enormously in the field of numerical electromagnetics. When in the past, the computational run-time is restricted indirectly by the CFL stability criterion, now with the advent of ADI-FDTD scheme, computational run-time can be significantly cut down to make each simulation a realistic, practical solution. However, nothing comes free. There is a trade-off between simulation run-time and accuracy of the simulation results. ADI-FDTD gives us the flexibility of using a bigger time-step than that allowed by the fundamental CFL stability criterion without causing instability in the system. By using the ADI-FDTD instead of the conventional FDTD method, potentially the simulation run-time can be reduced. But increasing the time-step also reduces the accuracy of the simulation results. This accuracy is dependent on the structure being modelled. Therefore, for certain structures a huge reduction in simulation run-time will be possible whilst maintaining the accuracy within the required tolerable range. Structures containing discontinuities can be modelled using fine mesh size without the constraint of using a correspondingly small time step in the simulation.

6.2 Further Work

6.2.1 Cylindrical coordinate system

The ADI-FDTD method can be extended to the cylindrical coordinate system to model three-dimensional cylindrical structure such as the probe-fed circular patch. As the diameter of the probe will be much smaller than the circular patch, the application of the ADI-FDTD in this structure means that the time-step used in the algorithm will not be restricted to the mesh size used to model the probe. Although, the application of ADI-FDTD on cylindrical coordinate system has recently been reported [1.31], there is yet to be any implementation of striplines or microstrips in the cylindrical coordinate system.

6.2.2 Microstrips with slots and notches

Now that there is a method of implementing copper layer in the microstrip that is not dependent on the accuracy of the tri-diagonal solver in the ADI-FDTD scheme, any three-dimensional structures with microstrips, such as stacked array of microstrip antennas can be modelled with narrow gaps, slots and notches where these discontinuities can be modelled with high spatial resolution by applying fine mesh size without the prohibitive cost in computational time.

6.2.3 Graded Mesh

In order to model small gaps, slots and notches accurately, higher mesh resolution is required around the vicinity of these discontinuities. To avoid having fine mesh throughout the whole computational domain, the mesh can be graded such that the mesh size gradually decreases as it approaches the discontinuities. Since in the ADI-FDTD method, the stability of the system no longer depends on the CFL criterion, the same time step within tolerable numerical dispersion, can be applied to the whole computational domain.

REFERENCES

[1] Papers

[1.1] F.A.Alhargan and S.R.Judah, "Reduced form of the Green's functions for disk and annular rings", IEEE Trans. Microwave Theory Tech., vol.39, no.3, pp.601-604, March 1991.

[1.2] P.B.Johns, and R.L.Beurle, "Numerical solution of 2-dimensional scattering problems using a transmission-line matrix", Proc. IEE, vol. 118, pp.1203-1208, 1971.

[1.3] W.J.R.Hoeffer, "The transmission-line matrix method – theory and applications", IEEE Trans. , vol. 33, pp. 882-892, 1985.

[1.4] K.S.Yee, "Numerical solution of initial boundary value problems involving Maxwell's equations in isotropic media, " IEEE Trans. Antennas Propagat., vol. AP-14, pp. 302-307, May 1966.

[1.5] D.M.Sheen, S.M.Ali, and M.D.Abouzahra, "Application of the three-dimensional finite-difference time-domain method to the analysis of planar microstrip circuits", IEEE Trans. Microwave Theory Tech., vol. 38, no. 7, pp. 849-857, July 1990.

[1.6] X.Zhang, and K.K.Mei, "Time-domain finite-difference approach to the calculation of the frequency-dependent characteristics of microstrip discontinuities", IEEE Trans. Microwave Theory Tech., vol. 36, no. 12, pp. 1775-1787, Dec. 1988.

[1.7] A.Taflove, and M.E.Brodwin, "Numerical solution of steady-state electromagnetic scattering problems using the time-dependent Maxwell's equations", IEEE Trans. Microwave Theory Tech., vol. 23, no. 8, pp. 623-630, Aug. 1975.

[1.8] P.Thoma, and T.Weiland, "A consistent subgridding scheme for the finite difference time domain method", International Journal of Numerical Modelling : Electronic Networks, Devices and Fields, vol. 9, pp. 359-374, 1996.

[1.9] M.Okoniewski, E.Okoniewska, and M.A.Stuchly, " Three-dimensional subgridding algorithm for FDTD", IEEE Trans. Antennas Propagat., vol 45, no.3, pp. 422-428, March 1997.

[1.10] S.S.Zivanovic, K.S.Yee, and K.K.Mei, "A subgridding method for the time-domain finite-difference method to solve Maxwell's equations", IEEE Trans. Microwave Theory Tech., vol. 39, no. 3, pp. 471-479, March 1991.

[1.11] I.S.Kim, and W.J.R.Hoefer, "A local refinement algorithm for the time-domain finite-difference method using Maxwell's curl equations", IEEE Trans. Microwave Theory Tech., vol. 38, no. 6, pp. 812-815, June 1990.

[1.12] D.T.Prescott, and N.V.Shuley, "A method of incorporating different sized cells into the finite-difference time-domain analysis technique", IEEE Trans. Microwave Theory Tech., vol. 2, no. 11, pp. 434-436, Nov. 1992.

[1.13] D.W.Peaceman, and H.H.Rachford, Jr., "The numerical solution of parabolic and elliptic differential equations", J. Soc. Indust. Appl. Math, vol. 3, no.1, pp. 28-41, March 1955.

[1.14] T.Namiki, "A new FDTD algorithm based on alternating-direction implicit method", IEEE Trans. Microwave Theory Tech., vol. 47, no. 10, pp. 2003-2007, Oct. 1999.

[1.15] B. Engquist, and A.Majda, "Absorbing boundary conditions for the numerical simulation of waves", Math. Comp., vol. 31, pp. 629-651, July 1977.

[1.16] G.Mur, "Absorbing boundary conditions for the finite-difference approximation of the time-domain electromagnetic-field equations", IEEE Trans. Electromagn. Compat., vol. 23 no. 4, pp. 377-382, Nov.1981.

[1.17] S.G.Garcia, T.Lee, and S.C.Hagness, "On the accuracy of the ADI-FDTD method", IEEE Antennas and Wireless Propagation Letters, vol. 1, no. 1, pp. 31-34, 2002.

[1.18] F.Zheng, Z.Chen, and J.Zhang, "Toward the development of a three-dimensional unconditionally stable finite-difference time-domain method", IEEE Trans. Microwave Theory Tech., vol. 48, no. 9, pp.1550-1558, Sept. 2000.

[1.19] A.P.Zhao, "Analysis of the numerical dispersion of the 2-D alternating-direction implicit FDTD method", IEEE Trans. Microwave Theory Tech., vol. 50, no. 4, pp.1156-1164, Apr. 2002.

[1.20] M.J.Chang, L.C.Chow, and W.S.Chang, "Improved alternating-direction implicit method for solving transient three-dimensional heat diffusion problems", Numerical Heat Transfer, Part B, vol. 19, pp. 69-84, 1991.

[1.21] A.P.Zhao, "Two special notes on the implementation of the unconditionally stable ADI-FDTD method", Microwave Opt Technol Lett, vol. 33, no. 4, pp. 273-277, May 2002.

[1.22] A.P.Zhao, "The influences of the time step on the numerical dispersion error of an unconditionally stable 3-D ADI-FDTD method : A simple and unified approach to determine the maximum allowable time step required by a desired numerical dispersion accuracy", Microwave Opt Technol Lett, vol. 35, no. 1, pp. 60-65, Oct. 2002.

[1.23] T.W.Lee, and S.Hagness, "Wave source conditions for the unconditionally stable ADI-FDTD method", IEEE AP-S Digest, vol. 4, pp. 142-145, July 2001.

[1.24] S.Garcia, T.Lee, and S.Hagness, "Accuracy limitations of the ADI-FDTD method due to truncation error", Proc. 18th ACES Conf., Monterey, CA, pp. 281-287, 2002.

[1.25] T.Namiki, "3-D ADI-FDTD Method – Uncondionally stable time-domain algorithm for solving full vector Maxwell's equations", IEEE Trans. Microwave Theory Tech., vol. 48, no. 10, pp.1743-1748, Oct. 2000.

[1.26] T.Namiki, and K.Ito, "Numerical simulation of microstrip resonators and filters using the ADI-FDTD method", IEEE Trans. Microwave Theory Tech., vol. 49, no. 4 pp. 665-670, Apr. 2001.

[1.27] T.Namiki, "Numerical simulation using ADI-FDTD method to estimate shielding effectiveness of thin conductive enclosures", IEEE Trans. Microwave Theory Tech., vol. 49, no. 6, pp. 1060-1066, June 2001.

[1.28] T.Namiki, K.Ito, "Investigation of numerical errors of the two-dimensional ADI-FDTD method", IEEE Trans. Microwave Theory Tech., vol. 48, no. 11, pp. 1950-1956, Nov. 2000.

[1.29] F.Zheng, Z.Chen, and J.Zhang, "A finite-difference time-domain method without the Courant stability conditions", IEEE Microwave Guided Wave Lett., vol. 9, no. 11, pp. 441-443, Nov. 1999.

[1.30] F.Zheng, and Z.Chen, "Numerical dispersion analysis of the uncondionally stable 3-D ADI-FDTD method", IEEE Trans. Microwave Theory Tech., vol. 49, no. 5, pp. 1006-1009, May 2001.

[1.31] C.Yuan, and Z.Chen, "A three-dimensional unconditionally stable ADI-FDTD method in the cylindrical coordinate system", IEEE Trans. Microwave Theory Tech., vol. 50, no. 10, pp. 2401-2405, Oct.2002.

[1.32] M.Darms, R.Schuhmann, H.Spachmann, and T.Weiland, "Dispersion and asymmetry effects of ADI-FDTD", IEEE Microwave and Wireless Components Lett., vol. 12, no.12, pp.491-493, Dec.2002.

[1.33] S.Wang, and F.L.Teixeira, "An efficient PML implementation for the ADI-FDTD method", IEEE Microwave and Wireless Components Lett., vol.13, no. 2, pp. 72-74, Feb.2003.

[1.34] G.Liu, and S.D.Gedney, "Perfectly matched layer media for an uncondionally stable three-dimensional ADI-FDTD method", IEEE Microwave and Guided Wave Lett., vol.10, no.7, pp.261-263, July 2000.

[1.35] A.P.Zhao, "Uniaxial perfectly matched layer media for an unconditionally stable 3-D ADI-FDTD method", IEEE Microwave and Wireless Components Lett., vol.12, no.12, pp. 497-499, Dec. 2002.

[1.36] G.Lazzi, "Unconditionally stable D-H FDTD formulation with anisotropic PML boundary conditions", IEEE Microwave and Wireless Components Lett., vol.11, no.4, pp. 149-151, Apr.2001.

[1.37] Z.Chen, and J.Zhang, "An unconditionally stable 3-D ADI-MRTD method free of the CFL stability condition", IEEE Microwave and Wireless Components Lett., vol.11, no.8, pp. 349-351, Aug.2001.

[1.38] T.Namiki, "Unconditionally stable FDTD algorithm for solving three-dimensional Maxwell's equations", 2000 IEEE MTT-S Int.Microwave Symp.Dig., pp.231-234, Boston, May 2000.

[1.39] J.P.Berenger, "A perfectly matched layer for the absorption of electromagnetic waves", J.Comput. Phys., vol. 114, pp. 185-200, Oct. 1994.

[1.40] I.Wolff, "Finite difference time-domain simulation of electromagnetic fields and microwave circuits", Int. Jour.of MIMICAE, vol. 5, no. 3 pp. 163-182, 1992.

[1.41] D.H.Choi, and W.J.R.Hoefer, "The finite-difference time-domain method and its application to eigenvalue problems", IEEE Trans.Microwave Theory Tech., vol. 34, no. 12, pp. 1464-1470, Dec.1986.

[1.42] X.Zhang, J.Fang, and K.K.Mei, "Calculations of the dispersive characteristics of microstrips by the time-domain finite difference method", IEEE Trans. Microwave Theory Tech., vol. 36, no. 2, pp. 263-267. Feb.1988.

[1.43] Z.Bi, K.Wu, C.Wu, and J.Litva, "A dispersive boundary condition for microstrip component analysis using the FD-TD method", IEEE Trans. Microwave Theory Tech., vol. 40, no. 4, pp. 774-777, Apr.1992.

[1.44] K.K.Mei, and J.Fang, "Superabsorption – a method to improve absorbing boundary condition", IEEE Trans. Microwave Theory Tech., vol. 40, no. 9, pp.1001-1010, Sept.1992.

[1.45] J.Fang, and D.Xeu, "Numerical errors in the computation of impedances by FDTD method and ways to eliminate them", IEEE Microwave and Guided Wave Lett., vol. 5, no. 1, pp. 6-8, Jan.1995.

[1.46] G.Zheng, and K.Chen, "The studies of cylindrical microstrip line with the FD-TD method in cylindrical coordinate system", Int.Journal of Infrared Millimeter Wave, vol. 13, no. 9, pp. 1421-1431, 1992.

[1.47] N.Dib, T.Weller, M.Scardelletti, and M.Imparato, "Analysis of cylindrical transmission lines the finite-difference time-domain method", IEEE Trans. Microwave Theory Tech., vol. 47, no. 4, pp.509-512, Apr. 1999

[1.48] S.C.Ow and S.R.Judah, "Three-dimensional FDTD based on modified alternating-direction implicit method", Proceedings of the 8th International Symposium on Microwave and Optical Technology, pp. 257-260, June 2001.

[2] Books

[2.1] K.C.Gupta, R.Garg, and R.Chadha, Computer-aided design of microwave circuits, Artech House, Dedham, MA, 1981.

[2.2] G.F.Roach, Greens Functions, Van Nostrand Reinhold Company, 1970.

[2.3] T.Itoh, Numerical techniques for microwave and millimeter-wave passive structure, Wiley, New York, 1989.

[2.4] G.D.Smith, Numerical solution of partial differential equations, Oxford University Press, London, 1965.

[2.5] A.Taflove, Computational Electrodynamics : The finite-difference time-domain method, Artech House, MA, 1995.

[2.6] W.H.Press, S.A.Teukolsky, W.T.Vetterling, and B.P.Flannery, Numerical recipes in C – the art of scientific computing, 2nd ed., Cambridge University Press, New York, 1992, pp. 50-51.

[2.7] W.F.Ames, Numerical methods for partial differential equations, New York : Academic, 1977.

[2.8] A.R.Mitchell, and D.F.Griffiths, The finite difference method in partial differential equations, Wiley, New York, 1980.

[2.9] A.Taflove, Advances in Computational Electrodynamics : The finite-difference time-domain method, Artech House, MA, 1998.

[2.10] W.C.Chew, Waves and Fields in Inhomogeneous Media, IEEE Press, NY, 1995.

[2.11] R.F.Harrington, Time-Harmonic Electromagnetic Fields, McGraw-Hill, 1961.

APPENDIX A1
2ND ORDER ACCURACY OF CENTRAL-DIFFERENCE APPROXIMATION

Consider a Taylor's series expansion of u (x_i , t) about the time instance t_n to the time instance $t_n + \Delta t/2$, keeping the space point fixed at x_i :

$$u\left(t_n+\frac{\Delta t}{2}\right)\Big|_{x_i} = u|_{x_i,t_n} + \frac{\Delta t}{2}\frac{\partial u}{\partial t}\Big|_{x_i,t_n} + \left(\frac{\Delta t}{2}\right)^2\frac{1}{2!}\frac{\partial^2 u}{\partial t^2}\Big|_{x_i,t_n} + \left(\frac{\Delta t}{2}\right)^3\frac{1}{3!}\frac{\partial^3 u}{\partial t^3}\Big|_{x_i,t_n} + \ldots. \quad \text{(A1.1)}$$

Now, the Taylor's series expansion of u (x_i , t) about the time instance t_n to the time instance $t_n - \Delta t/2$, keeping the space point fixed at x_i is :

$$u\left(t_n-\frac{\Delta t}{2}\right)\Big|_{x_i} = u|_{x_i,t_n} - \frac{\Delta t}{2}\frac{\partial u}{\partial t}\Big|_{x_i,t_n} + \left(\frac{\Delta t}{2}\right)^2\frac{1}{2!}\frac{\partial^2 u}{\partial t^2}\Big|_{x_i,t_n} - \left(\frac{\Delta t}{2}\right)^3\frac{1}{3!}\frac{\partial^3 u}{\partial t^3}\Big|_{x_i,t_n} + \ldots. \quad \text{(A1.2)}$$

(1) – (2) gives :

$$u\left(t_n+\frac{\Delta t}{2}\right)\Big|_{x_i} - u\left(t_n-\frac{\Delta t}{2}\right)\Big|_{x_i} = \Delta t\frac{\partial u}{\partial t}\Big|_{x_i,t_n} + \left(\frac{\Delta t}{2}\right)^3\frac{1}{3}\frac{\partial^3 u}{\partial t^3}\Big|_{x_i,t_n} + \ldots. \quad \text{(A1.3)}$$

Re-arranging (3), we get,

$$\begin{aligned}\frac{\partial u}{\partial t}\Big|_{x_i,t_n} &= \frac{u\left(t_n+\frac{\Delta t}{2}\right)\Big|_{x_i} - u\left(t_n-\frac{\Delta t}{2}\right)\Big|_{x_i} - \left(\frac{\Delta t}{2}\right)^3\frac{1}{3}\frac{\partial^3 u}{\partial t^3}\Big|_{x_i,t_n}}{\Delta t} \\ &= \frac{u\left(t_n+\frac{\Delta t}{2}\right)\Big|_{x_i} - u\left(t_n-\frac{\Delta t}{2}\right)\Big|_{x_i}}{\Delta t} - \left(\frac{\Delta t}{2}\right)^2\frac{1}{6}\frac{\partial^3 u}{\partial t^3}\Big|_{x_i,t_n}\end{aligned} \quad \text{(A1.4)}$$

Taking only the first RHS term of (4), the second term is the error term. Then,

$$\frac{\partial u}{\partial t}\Big|_{x_i,t_n} = \frac{u\left(t_n+\frac{\Delta t}{2}\right)\Big|_{x_i} - u\left(t_n-\frac{\Delta t}{2}\right)\Big|_{x_i}}{\Delta t} + O\left[(\Delta t)^2\right] \quad \text{(A1.5)}$$

where $O\left[(\Delta t)^2\right]$ is a shorthand notation for the remainder or error term, which approaches zero as the square of the time increment. Equation (5) is referred to as a 2nd order accurate, central-difference approximation to the first order time derivative of u.

APPENDIX B1
TRI-DIAGONAL MATRIX EQUATIONS FOR ADI-FDTD METHOD

Procedure 1

$$E_x^{n+1/2}(i+1/2,j-1,k) - E_x^{n+1/2}(i+1/2,j,k)\left[2+\left(\frac{\sqrt{\mu\varepsilon}\,\Delta y}{\Delta t}\right)^2\right] + E_x^{n+1/2}(i+1/2,j+1,k)$$

$$= -E_x^n(i+1/2,j,k)\left(\frac{\sqrt{\mu\varepsilon}\,\Delta y}{\Delta t}\right)^2 + \left(\frac{\Delta y}{\Delta x}\right)\left[E_y^n(i+1,j+1/2,k) - E_y^n(i,j+1/2,k) - E_y^n(i+1,j-1/2,k) + E_y^n(i,j-1/2,k)\right]$$

$$-\left(\frac{\mu\Delta y}{\Delta t}\right)\left[H_z^n(i+1/2,j+1/2,k) - H_z^n(i+1/2,j-1/2,k)\right] + \left(\frac{\mu\Delta y^2}{\Delta t\Delta z}\right)\left[H_y^n(i+1/2,j,k+1/2) - H_y^n(i+1/2,j,k-1/2)\right]$$

(B1.1)

$$E_y^{n+1/2}(i,j+1/2,k-1) - E_y^{n+1/2}(i,j+1/2,k)\left[2+\left(\frac{\sqrt{\mu\varepsilon}\,\Delta z}{\Delta t}\right)^2\right] + E_y^{n+1/2}(i,j+1/2,k+1)$$

$$= -E_y^n(i,j+1/2,k)\left(\frac{\sqrt{\mu\varepsilon}\,\Delta z}{\Delta t}\right)^2 + \left(\frac{\Delta z}{\Delta y}\right)\left[E_z^n(i,j+1,k+1/2) - E_z^n(i,j,k+1/2) - E_z^n(i,j+1,k-1/2) + E_z^n(i,j,k-1/2)\right]$$

$$-\left(\frac{\mu\Delta z}{\Delta t}\right)\left[H_x^n(i,j+1/2,k+1/2) - H_x^n(i,j+1/2,k-1/2)\right] + \left(\frac{\mu\Delta z^2}{\Delta t\Delta x}\right)\left[H_z^n(i+1/2,j+1/2,k) - H_z^n(i-1/2,j+1/2,k)\right]$$

(B1.2)

$$E_z^{n+1/2}(i-1,j,k+1/2) - E_z^{n+1/2}(i,j,k+1/2)\left[2+\left(\frac{\sqrt{\mu\varepsilon}\Delta x}{\Delta t}\right)^2\right] + E_z^{n+1/2}(i+1,j,k+1/2)$$

$$= -E_z^n(i,j,k+1/2)\left(\frac{\sqrt{\mu\varepsilon}\Delta x}{\Delta t}\right)^2 + \left(\frac{\Delta x}{\Delta z}\right)\left[E_x^n(i+1/2,j,k+1) - E_x^n(i+1/2,j,k) - E_x^n(i-1/2,j,k+1) + E_x^n(i-1/2,j,k)\right]$$

$$-\left(\frac{\mu\Delta x}{\Delta t}\right)\left[H_y^n(i+1/2,j,k+1/2) - H_y^n(i-1/2,j,k+1/2)\right] + \left(\frac{\mu\Delta x^2}{\Delta t\Delta y}\right)\left[H_x^n(i,j+1/2,k+1/2) - H_x^n(i,j-1/2,k+1/2)\right]$$

(B1.3)

Procedure 2

$$E_x^{n+1}(i+1/2,j,k-1) - E_x^{n+1}(i+1/2,j,k)\left[2+\left(\frac{\sqrt{\mu\varepsilon}\Delta z}{\Delta t}\right)^2\right] + E_x^{n+1}(i+1/2,j,k+1)$$

$$= -E_x^{n+1/2}(i+1/2,j,k)\left(\frac{\sqrt{\mu\varepsilon}\Delta z}{\Delta t}\right)^2 + \left(\frac{\Delta z}{\Delta x}\right)\left[E_z^{n+1/2}(i+1,j,k+1/2) - E_z^{n+1/2}(i,j,k+1/2) - E_z^{n+1/2}(i+1,j,k-1/2) + E_z^{n+1/2}(i,j,k-1/2)\right]$$

$$-\left(\frac{\mu\Delta z}{\Delta t}\right)\left[H_y^{n+1/2}(i+1/2,j,k+1/2) - H_y^{n+1/2}(i+1/2,j,k-1/2)\right] + \left(\frac{\mu\Delta z^2}{\Delta t\Delta y}\right)\left[H_z^{n+1/2}(i+1/2,j+1/2,k) - H_z^{n+1/2}(i+1/2,j-1/2,k)\right]$$

(B1.4)

$$E_y^{n+1}(i-1,j+1/2,k) - E_y^{n+1}(i,j+1/2,k)\left[2+\left(\frac{\sqrt{\mu\varepsilon}\Delta x}{\Delta t}\right)^2\right] + E_y^{n+1}(i+1,j+1/2,k)$$

$$= -E_y^{n+1/2}(i,j+1/2,k)\left(\frac{\sqrt{\mu\varepsilon}\Delta x}{\Delta t}\right)^2 + \left(\frac{\Delta x}{\Delta y}\right)\left[E_x^{n+1/2}(i+1/2,j+1,k) - E_x^{n+1/2}(i+1/2,j,k) - E_x^{n+1/2}(i-1/2,j+1,k) + E_x^{n+1/2}(i-1/2,j,k)\right]$$

$$-\left(\frac{\mu\Delta x}{\Delta t}\right)\left[H_z^{n+1/2}(i+1/2,j+1/2,k) - H_z^{n+1/2}(i-1/2,j+1/2,k)\right] + \left(\frac{\mu\Delta x^2}{\Delta t\Delta z}\right)\left[H_x^{n+1/2}(i,j+1/2,k+1/2) - H_x^{n+1/2}(i,j+1/2,k-1/2)\right]$$

(B1.5)

$$E_z^{n+1}(i,j-1,k+1/2) - E_z^{n+1}(i,j,k+1/2)\left[2+\left(\frac{\sqrt{\mu\varepsilon}\Delta y}{\Delta t}\right)^2\right] + E_z^{n+1}(i,j+1,k+1/2)$$

$$= -E_z^{n+1/2}(i+1/2,j,k)\left(\frac{\sqrt{\mu\varepsilon}\Delta y}{\Delta t}\right)^2 + \left(\frac{\Delta y}{\Delta z}\right)\left[E_y^{n+1/2}(i,j+1/2,k+1) - E_y^{n+1/2}(i,j+1/2,k) - E_y^{n+1/2}(i,j-1/2,k+1) + E_y^{n+1/2}(i,j-1/2,k)\right]$$

$$-\left(\frac{\mu\Delta y}{\Delta t}\right)\left[H_x^{n+1/2}(i,j+1/2,k+1/2) - H_x^{n+1/2}(i,j-1/2,k+1/2)\right] + \left(\frac{\mu\Delta y^2}{\Delta t\Delta x}\right)\left[H_y^{n+1/2}(i+1/2,j,k+1/2) - H_y^{n+1/2}(i-1/2,j,k+1/2)\right]$$

(B1.6)

APPENDIX B2
TRI-DIAGONAL MATRIX EQUATIONS FOR MODIFIED ADI-FDTD METHOD

Procedure 1

$$E_x^{n+1/2}(i+1/2,j-1,k) - E_x^{n+1/2}(i+1/2,j,k)\left[2+\left(\frac{\sqrt{\mu\varepsilon}\Delta y}{\Delta t}\right)^2\left(\frac{1}{(2-f)^2}\right)\right] + E_x^{n+1/2}(i+1/2,j+1,k)$$

$$= -E_x^n(i+1/2,j,k)\left(\frac{\sqrt{\mu\varepsilon}\Delta y}{\Delta t}\right)^2\left(\frac{1}{(2-f)^2}\right)$$

$$+\left(\frac{\Delta y}{\Delta x}\right)\left(\frac{f}{2-f}\right)\left[E_y^n(i+1,j+1/2,k) - E_y^n(i,j+1/2,k) - E_y^n(i+1,j-1/2,k) + E_y^n(i,j-1/2,k)\right]$$

$$-\left(\frac{\mu\Delta y}{\Delta t}\right)\left(\frac{1}{2-f}\right)\left[H_z^n(i+1/2,j+1/2,k) - H_z^n(i+1/2,j-1/2,k)\right]$$

$$+\left(\frac{\mu\Delta y^2}{\Delta t\Delta z}\right)\left(\frac{f}{(2-f)^2}\right)\left[H_y^n(i+1/2,j,k+1/2) - H_y^n(i+1/2,j,k-1/2)\right] \qquad \text{(B2.1)}$$

$$E_y^{n+1/2}(i,j+1/2,k-1) - E_y^{n+1/2}(i,j+1/2,k)\left[2+\left(\frac{\sqrt{\mu\varepsilon}\Delta z}{\Delta t}\right)^2\left(\frac{1}{(2-f)^2}\right)\right] + E_y^{n+1/2}(i,j+1/2,k+1)$$

$$= -E_y^n(i,j+1/2,k)\left(\frac{\sqrt{\mu\varepsilon}\Delta z}{\Delta t}\right)^2\left(\frac{1}{(2-f)^2}\right)$$

$$+\left(\frac{\Delta z}{\Delta y}\right)\left(\frac{f}{2-f}\right)\left[E_z^n(i,j+1,k+1/2) - E_z^n(i,j,k+1/2) - E_z^n(i,j+1,k-1/2) + E_z^n(i,j,k-1/2)\right]$$

$$-\left(\frac{\mu\Delta z}{\Delta t}\right)\left(\frac{1}{2-f}\right)\left[H_x^n(i,j+1/2,k+1/2) - H_x^{n+1/2}(i,j+1/2,k-1/2)\right]$$

$$+\left(\frac{\mu\Delta z^2}{\Delta t\Delta x}\right)\left(\frac{f}{(2-f)^2}\right)\left[H_z^n(i+1/2,j+1/2,k) - H_z^n(i-1/2,j+1/2,k)\right] \qquad \text{(B2.2)}$$

$$E_z^{n+1/2}(i-1,j,k+1/2) - E_z^{n+1/2}(i,j,k+1/2)\left[2+\left(\frac{\sqrt{\mu\varepsilon}\Delta x}{\Delta t}\right)^2\left(\frac{1}{(2-f)^2}\right)\right] + E_z^{n+1}(i+1,j,k+1/2)$$

$$= -E_z^n(i+1/2,j,k)\left(\frac{\sqrt{\mu\varepsilon}\Delta x}{\Delta t}\right)^2\left(\frac{1}{(2-f)^2}\right)$$

$$+\left(\frac{\Delta x}{\Delta z}\right)\left(\frac{f}{2-f}\right)\left[E_x^n(i+1/2,j,k+1) - E_x^n(i+1/2,j,k) - E_x^n(i-1/2,j,k+1) + E_x^n(i-1/2,j,k)\right]$$

$$-\left(\frac{\mu\Delta x}{\Delta t}\right)\left(\frac{1}{2-f}\right)\left[H_y^n(i+1/2,j,k+1/2) - H_y^n(i-1/2,j,k+1/2)\right]$$

$$+\left(\frac{\mu\Delta y^2}{\Delta t\Delta x}\right)\left(\frac{f}{(2-f)^2}\right)\left[H_x^n(i,j+1/2,k+1/2) - H_x^n(i,j-1/2,k+1/2)\right] \qquad \text{(B2.3)}$$

Procedure 2

$$E_x^{n+1}(i+1/2,j,k-1) - E_x^{n+1}(i+1/2,j,k)\left[2+\left(\frac{\sqrt{\mu\varepsilon}\Delta z}{\Delta t}\right)^2\left(\frac{1}{(2-f)^2}\right)\right] + E_x^{n+1}(i+1/2,j,k+1)$$

$$= -E_x^{n+1/2}(i+1/2,j,k)\left(\frac{\sqrt{\mu\varepsilon}\Delta z}{\Delta t}\right)^2\left(\frac{1}{(2-f)^2}\right)$$

$$+\left(\frac{\Delta z}{\Delta x}\right)\left(\frac{f}{2-f}\right)\left[E_z^{n+1/2}(i+1,j,k+1/2) - E_z^{n+1/2}(i,j,k+1/2) - E_z^{n+1/2}(i+1,j,k-1/2) + E_z^{n+1/2}(i,j,k-1/2)\right]$$

$$-\left(\frac{\mu\Delta z}{\Delta t}\right)\left(\frac{1}{2-f}\right)\left[H_y^{n+1/2}(i+1/2,j,k+1/2) - H_y^{n+1/2}(i+1/2,j,k-1/2)\right]$$

$$+\left(\frac{\mu\Delta z^2}{\Delta t\Delta y}\right)\left(\frac{f}{(2-f)^2}\right)\left[H_z^{n+1/2}(i+1/2,j+1/2,k) - H_z^{n+1/2}(i+1/2,j-1/2,k)\right] \qquad \text{(B2.4)}$$

$$E_y^{n+1}(i-1,j+1/2,k) - E_y^{n+1}(i,j+1/2,k)\left[2+\left(\frac{\sqrt{\mu\varepsilon}\Delta x}{\Delta t}\right)^2\left(\frac{1}{(2-f)^2}\right)\right] + E_y^{n+1}(i+1,j+1/2,k)$$

$$= -E_y^{n+1/2}(i,j+1/2,k)\left(\frac{\sqrt{\mu\varepsilon}\Delta x}{\Delta t}\right)^2\left(\frac{1}{(2-f)^2}\right)$$

$$+\left(\frac{\Delta x}{\Delta y}\right)\left(\frac{f}{2-f}\right)\left[E_x^{n+1/2}(i+1/2,j+1,k) - E_x^{n+1/2}(i+1/2,j,k) - E_x^{n+1/2}(i-1/2,j+1,k) + E_x^{n+1/2}(i-1/2,j,k)\right]$$

$$-\left(\frac{\mu\Delta x}{\Delta t}\right)\left(\frac{1}{2-f}\right)\left[H_z^{n+1/2}(i+1/2,j+1/2,k) - H_z^{n+1/2}(i-1/2,j+1/2,k)\right]$$

$$+\left(\frac{\mu\Delta x^2}{\Delta t\Delta z}\right)\left(\frac{f}{(2-f)^2}\right)\left[H_x^{n+1/2}(i,j+1/2,k+1/2) - H_x^{n+1/2}(i,j+1/2,k-1/2)\right] \qquad \text{(B2.5)}$$

$$E_z^{n+1}(i,j-1,k+1/2) - E_z^{n+1}(i,j,k+1/2)\left[2+\left(\frac{\sqrt{\mu\varepsilon}\Delta y}{\Delta t}\right)^2\left(\frac{1}{(2-f)^2}\right)\right] + E_z^{n+1}(i,j+1,k+1/2)$$

$$= -E_z^{n+1/2}(i+1/2,j,k)\left(\frac{\sqrt{\mu\varepsilon}\Delta y}{\Delta t}\right)^2\left(\frac{1}{(2-f)^2}\right)$$

$$+\left(\frac{\Delta y}{\Delta z}\right)\left(\frac{f}{2-f}\right)\left[E_y^{n+1/2}(i,j+1/2,k+1) - E_y^{n+1/2}(i,j+1/2,k) - E_y^{n+1/2}(i,j-1/2,k+1) + E_y^{n+1/2}(i,j-1/2,k)\right]$$

$$-\left(\frac{\mu\Delta y}{\Delta t}\right)\left(\frac{1}{2-f}\right)\left[H_x^{n+1/2}(i,j+1/2,k+1/2) - H_x^{n+1/2}(i,j-1/2,k+1/2)\right]$$

$$+\left(\frac{\mu\Delta y^2}{\Delta t\Delta x}\right)\left(\frac{f}{(2-f)^2}\right)\left[H_y^{n+1/2}(i+1/2,j,k+1/2) - H_y^{n+1/2}(i-1/2,j,k+1/2)\right] \qquad \text{(B2.6)}$$

APPENDIX B3
TRI-DIAGONAL MATRIX EQUATIONS FOR ADI-FDTD METHOD WITH ELECTRIC CONDUCTIVITY TERM

Procedure 1

$$E_x^{n+1/2}(i+1/2,j-1,k) - E_x^{n+1/2}(i+1/2,j,k)\left[2+\left(\frac{\sqrt{\mu\varepsilon}\Delta y}{\Delta t}\right)^2\left(1+\frac{\sigma(i+1/2,j,k)\ \Delta t}{4\varepsilon}\right)\right] + E_x^{n+1/2}(i+1/2,j+1,k)$$

$$= -E_x^n(i+1/2,j,k)\left(\frac{\sqrt{\mu\varepsilon}\Delta y}{\Delta t}\right)^2\left(1-\frac{\sigma(i+1/2,j,k)\ \Delta t}{4\varepsilon}\right)$$

$$+\left(\frac{\Delta y}{\Delta x}\right)\left[E_y^n(i+1,j+1/2,k) - E_y^n(ij+1/2,k) - E_y^n(i+1,j-1/2,k) + E_y^n(ij-1/2,k)\right]$$

$$-\left(\frac{\mu\Delta y}{\Delta t}\right)\left[H_z^n(i+1/2,j+1/2,k) - H_z^n(i+1/2,j-1/2,k)\right] + \left(\frac{\mu\Delta y^2}{\Delta t\Delta z}\right)\left[H_y^n(i+1/2,j,k+1/2) - H_y^n(i+1/2,j,k-1/2)\right]$$

(B2.1)

$$E_y^{n+1/2}(ij+1/2,k-1) - E_y^{n+1/2}(ij+1/2,k)\left[2+\left(\frac{\sqrt{\mu\varepsilon}\Delta z}{\Delta t}\right)^2\left(1+\frac{\sigma(ij+1/2,k)\ \Delta t}{4\varepsilon}\right)\right] + E_y^{n+1/2}(ij+1/2,k+1)$$

$$= -E_y^n(ij+1/2,k)\left(\frac{\sqrt{\mu\varepsilon}\Delta z}{\Delta t}\right)^2\left(1-\frac{\sigma(ij+1/2,k)\ \Delta t}{4\varepsilon}\right)$$

$$+\left(\frac{\Delta z}{\Delta y}\right)\left[E_z^n(ij+1,k+1/2) - E_z^n(ij,k+1/2) - E_z^n(ij+1,k-1/2) + E_z^n(ij,k-1/2)\right]$$

$$-\left(\frac{\mu\Delta z}{\Delta t}\right)\left[H_x^n(ij+1/2,k+1/2) - H_x^n(ij+1/2,k-1/2)\right] + \left(\frac{\mu\Delta z^2}{\Delta t\Delta x}\right)\left[H_z^n(i+1/2j+1/2,k) - H_z^n(i-1/2j+1/2,k)\right]$$

(B2.2)

$$E_z^{n+1/2}(i-1,j,k+1/2) - E_z^{n+1/2}(ij,k+1/2)\left[2+\left(\frac{\sqrt{\mu\varepsilon}\Delta x}{\Delta t}\right)^2\left(1+\frac{\sigma(ij,k+1/2)\ \Delta t}{4\varepsilon}\right)\right] + E_z^{n+1/2}(i+1,j,k+1/2)$$

$$= -E_z^n(ij,k+1/2)\left(\frac{\sqrt{\mu\varepsilon}\Delta x}{\Delta t}\right)^2\left(1-\frac{\sigma(ij,k+1/2)\,\Delta t}{4\varepsilon}\right)$$

$$+\left(\frac{\Delta x}{\Delta z}\right)\left[E_x^n(i+1/2j,k+1) - E_x^n(i+1/2j,k) - E_x^n(i-1/2j,k+1) + E_x^n(i-1/2j,k)\right]$$

$$-\left(\frac{\mu\Delta x}{\Delta t}\right)\left[H_y^n(i+1/2j,k+1/2) - H_y^n(i-1/2j,k+1/2)\right] + \left(\frac{\mu\Delta x^2}{\Delta t\Delta y}\right)\left[H_x^n(ij+1/2,k+1/2) - H_x^n(ij-1/2,k+1/2)\right]$$

(B2.3)

Procedure 2

$$E_x^{n+1}(i+1/2,j,k-1) - E_x^{n+1}(i+1/2,j,k)\left[2+\left(\frac{\sqrt{\mu\varepsilon}\Delta z}{\Delta t}\right)^2\left(1+\frac{\sigma(i+1/2,j,k)\,\Delta t}{4\varepsilon}\right)\right] + E_x^{n+1}(i+1/2,j,k+1)$$

$$= -E_x^{n+1/2}(i+1/2,j,k)\left(\frac{\sqrt{\mu\varepsilon}\Delta z}{\Delta t}\right)^2\left(1-\frac{\sigma(i+1/2,j,k)\,\Delta t}{4\varepsilon}\right)$$

$$+\left(\frac{\Delta z}{\Delta x}\right)\left[E_z^{n+1/2}(i+1,j,k+1/2) - E_z^{n+1/2}(i,j,k+1/2) - E_z^{n+1/2}(i+1,j,k-1/2) + E_z^{n+1/2}(i,j,k-1/2)\right]$$

$$-\left(\frac{\mu\Delta z}{\Delta t}\right)\left[H_y^{n+1/2}(i+1/2,j,k+1/2) - H_y^{n+1/2}(i+1/2,j,k-1/2)\right] + \left(\frac{\mu\Delta z^2}{\Delta t\Delta y}\right)\left[H_z^{n+1/2}(i+1/2,j+1/2,k) - H_z^{n+1/2}(i+1/2,j-1/2,k)\right]$$

(B2.4)

$$E_y^{n+1}(i-1,j+1/2,k) - E_y^{n+1}(i,j+1/2,k)\left[2+\left(\frac{\sqrt{\mu\varepsilon}\Delta x}{\Delta t}\right)^2\left(1+\frac{\sigma(i,j+1/2,k)\,\Delta t}{4\varepsilon}\right)\right] + E_y^{n+1}(i+1,j+1/2,k)$$

$$= -E_y^{n+1/2}(i,j+1/2,k)\left(\frac{\sqrt{\mu\varepsilon}\Delta x}{\Delta t}\right)^2\left(1-\frac{\sigma(i,j+1/2,k)\,\Delta t}{4\varepsilon}\right)$$

$$+\left(\frac{\Delta x}{\Delta y}\right)\left[E_x^{n+1/2}(i+1/2,j+1,k) - E_x^{n+1/2}(i+1/2,j,k) - E_x^{n+1/2}(i-1/2,j+1,k) + E_x^{n+1/2}(i-1/2,j,k)\right]$$

$$-\left(\frac{\mu\Delta x}{\Delta t}\right)\left[H_z^{n+1/2}(i+1/2,j+1/2,k) - H_z^{n+1/2}(i-1/2,j+1/2,k)\right] + \left(\frac{\mu\Delta x^2}{\Delta t\Delta z}\right)\left[H_x^{n+1/2}(i,j+1/2,k+1/2) - H_x^{n+1/2}(i,j+1/2,k-1/2)\right]$$

(B2.5)

$$E_z^{n+1}(i,j-1,k+1/2) - E_z^{n+1}(i,j,k+1/2)\left[2+\left(\frac{\sqrt{\mu\varepsilon}\Delta y}{\Delta t}\right)^2\left(1+\frac{\sigma(i,j+1/2,k)\,\Delta t}{4\varepsilon}\right)\right] + E_z^{n+1}(i,j+1,k+1/2)$$

$$= -E_z^{n+1/2}(i+1/2,j,k)\left(\frac{\sqrt{\mu\varepsilon}\Delta y}{\Delta t}\right)^2\left(1-\frac{\sigma(i,j+1/2,k)\,\Delta t}{4\varepsilon}\right)$$

$$+\left(\frac{\Delta y}{\Delta z}\right)\left[E_y^{n+1/2}(i,j+1/2,k+1) - E_y^{n+1/2}(i,j+1/2,k) - E_y^{n+1/2}(i,j-1/2,k+1) + E_y^{n+1/2}(i,j-1/2,k)\right]$$

$$-\left(\frac{\mu\Delta y}{\Delta t}\right)\left[H_x^{n+1/2}(i,j+1/2,k+1/2) - H_x^{n+1/2}(i,j-1/2,k+1/2)\right] + \left(\frac{\mu\Delta y^2}{\Delta t\Delta x}\right)\left[H_y^{n+1/2}(i+1/2,j,k+1/2) - H_y^{n+1/2}(i-1/2,j,k+1/2)\right]$$

(B2.6)

APPENDIX C1
GRAPHICAL ILLUSTRATION OF IMPLICIT/EXPLICIT ADI-FDTD METHOD

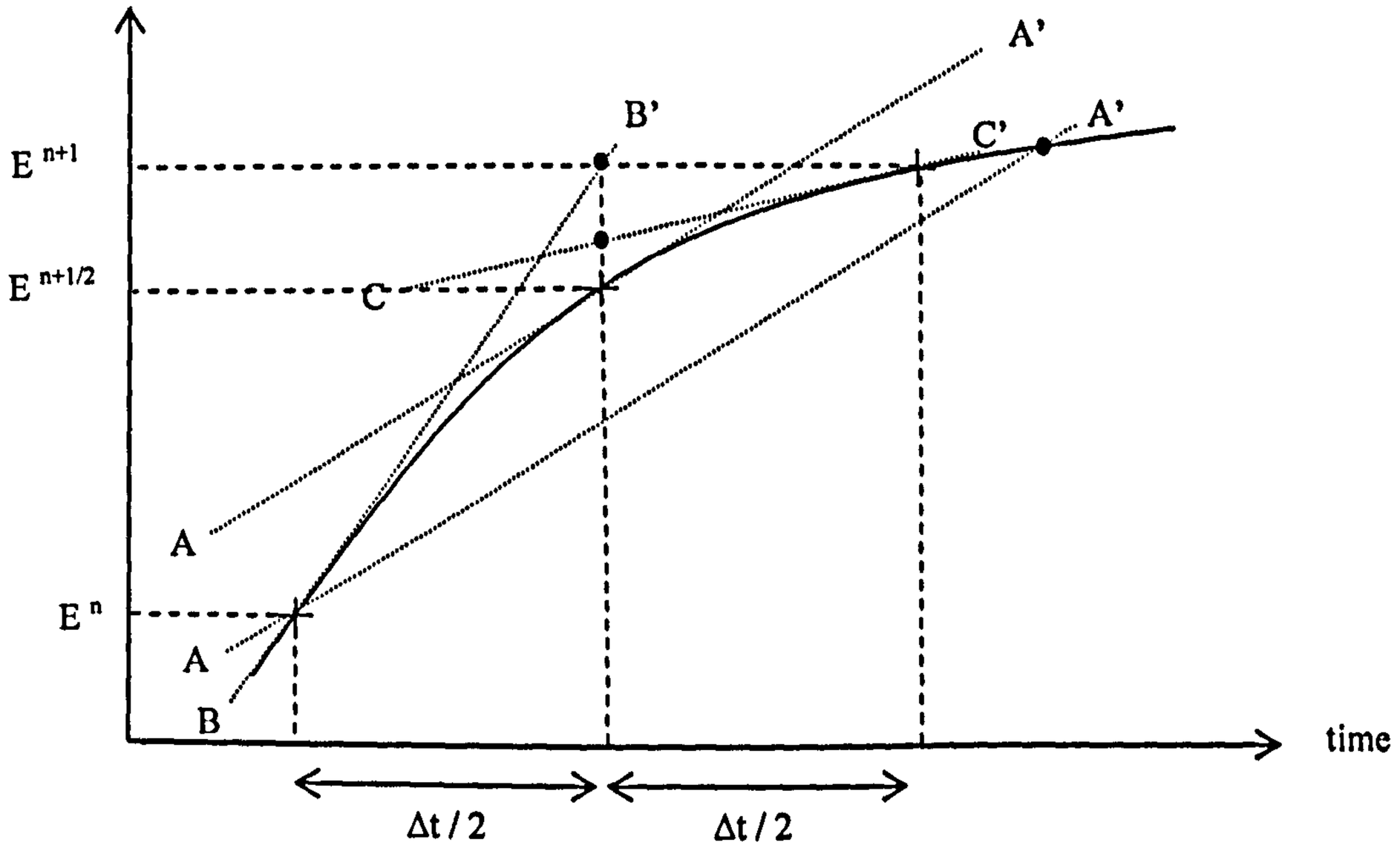

Fig. C1.1

Using an explicit method or 2nd order Runga-Kutta method to find electric field at time (n+1)Δt gives :

$$E^{n+1} = E^{n} + \Delta t \left.\frac{dE}{dt}\right|_{n+1/2} \qquad \text{(C1.1)}$$

where $\left.\frac{dE}{dt}\right|_{n+1/2}$ is the gradient at $E^{n+1/2}$ illustrated in Fig. C1.1 by the gradient of AA'

In electromagnetic fields,

$$\left.\frac{dE}{dt}\right|_{n+1/2} = \frac{1}{\varepsilon}\nabla \times H\Big|_{n+1/2} \qquad \text{(C1.2)}$$

Substituting (C1.2) into (C1.1), we get

$$E^{n+1} = E^{n} + \frac{\Delta t}{\varepsilon}\nabla \times H\Big|_{n+1/2} \qquad \text{(C1.3)}$$

(C1.3) is the form of the conventional FDTD *explicit* method.

Using an explicit method to find $E^{n+1/2}$ from E^n using forward difference gives :

$$E^{n+1/2} = E^n + \frac{\Delta t}{2} \left.\frac{dE}{dt}\right|_n \qquad \text{(C1.4)}$$

where $\left.\frac{dE}{dt}\right|_n$ is the gradient at E^n illustrated in Fig. C1.1 by the gradient of BB'.

Using an implicit method to find E^{n+1} from $E^{n+1/2}$ using backward difference gives :

$$E^{n+1/2} = E^{n+1} - \frac{\Delta t}{2} \left.\frac{dE}{dt}\right|_{n+1} \qquad \text{(C1.5)}$$

where $\left.\frac{dE}{dt}\right|_{n+1}$ is the gradient at E^{n+1} illustrated in Fig. C1.1 by the gradient of CC'.

Re-arranging (C1.5),

$$E^{n+1} = E^{n+1/2} + \frac{\Delta t}{2} \left.\frac{dE}{dt}\right|_{n+1} \qquad \text{(C1.6)}$$

Combining (C1.4) and (C1.6), we get

$$E^{n+1} = E^n + \frac{\Delta t}{2} \left.\frac{dE}{dt}\right|_n + \frac{\Delta t}{2} \left.\frac{dE}{dt}\right|_{n+1} \qquad \text{(C1.7)}$$

or expressing the time derivative of electric field in (C1.7) in terms of magnetic field gives us

$$E^{n+1} = E^n + \underbrace{\frac{\Delta t}{2\varepsilon} \nabla \times H\big|_n}_{\text{explicit term}} + \underbrace{\frac{\Delta t}{2\varepsilon} \nabla \times H\big|_{n+1}}_{\text{implicit term}} \qquad \text{(C1.8)}$$

(C1.8) is the form of the Crank-Nicolson FDTD *implicit* method.

Expanding (C1.8) for E_x term we get :

$$E_x^{n+1}(i+1/2,j,k) = E_x^n(i+1/2,j,k) + \frac{\Delta t}{2\varepsilon}\left\{\frac{H_z^n(i+1/2,j+1/2,k) - H_z^n(i+1/2,j-1/2,k)}{\Delta y}\,②\right.$$
$$\left. - \frac{H_y^n(i+1/2,j,k+1/2) - H_y^n(i+1/2,j,k-1/2)}{\Delta z}\,①\right\}$$
$$\frac{\Delta t}{2\varepsilon}\left\{\frac{H_z^{n+1}(i+1/2,j+1/2,k) - H_z^{n+1}(i+1/2,j-1/2,k)}{\Delta y}\,①\right.$$
$$\left. - \frac{H_y^{n+1}(i+1/2,j,k+1/2) - H_y^{n+1}(i+1/2,j,k-1/2)}{\Delta z}\,②\right\} \qquad \text{(C1.9)}$$

ADI-FDTD method is in a similar form to (C1.9) but splitting it into two separate procedures each for successive half time-step iteration. Procedure 1 & 2 are taken from RHS terms as shown in (C1.9). This results in the following terms for procedure 1 and 2 of the ADI-FDTD method, repeated here from (3.1a) and (3.4a) respectively.

$$E_x^{n+1/2}(i+1/2,j,k) = E_x^n(i+1/2,j,k) + \frac{\Delta t}{2\varepsilon}\left\{\frac{H_z^{n+1/2}(i+1/2,j+1/2,k) - H_z^{n+1/2}(i+1/2,j-1/2,k)}{\Delta y} - \frac{H_y^n(i+1/2,j,k+1/2) - H_y^n(i+1/2,j,k-1/2)}{\Delta z}\right\} \quad \text{(C1.10)}$$

$$E_x^{n+1}(i+1/2,j,k) = E_x^{n+1/2}(i+1/2,j,k) + \frac{\Delta t}{2\varepsilon}\left\{\frac{H_z^{n+1/2}(i+1/2,j+1/2,k) - H_z^{n+1/2}(i+1/2,j-1/2,k)}{\Delta y} - \frac{H_y^{n+1}(i+1/2,j,k+1/2) - H_y^{n+1}(i+1/2,j,k-1/2)}{\Delta z}\right\} \quad \text{(C1.11)}$$